Spring 5-4-2019

Monocyte Anti-Inflammatory Activity Is Dictated by Metabolic Status during Staphylococcus Aureus Biofilm Infection

Kelsey J. Yamada
University of Nebraska Medical Center

MONOCYTE ANTI-INFLAMMATORY ACTIVITY IS DICTATED BY METABOLIC STATUS DURING *STAPHYLOCOCCUS AUREUS* BIOFILM INFECTION

By

Kelsey J. Yamada

A DISSERTATION

Presented to the Faculty of

The Graduate College of the University of Nebraska Medical Center

In partial fulfillment of the requirements for the degree of

Doctor of Philosophy

Department of Pathology and Microbiology

Under the supervision of Professor Tammy Kielian, Ph.D.

University of Nebraska Medical Center

Omaha, NE

United States of America

January 2019

Supervisory Committee:

Paul D. Fey, Ph.D.	**Curtis W. Hartman, M.D.**
Geoffrey M. Thiele, Ph.D.	**Jessica Snowden M.D.**

Table of contents

Acknowledgements

I will begin by thanking my mentor Dr. Tammy Kielian, for her continued guidance, encouragement, and support throughout my graduate scientific training. I enrolled into the M.D./Ph.D. program here at the University of Nebraska Medical Center with the career goal of performing translational medical research that address questions that are encountered during clinical practice. Dr. Kielian provided me with unique opportunities to perform translational research and trained me to formulate scientific questions with an emphasis on its clinical significance and to also develop experimental approaches which allow me to address these questions. Dr. Kielian stands out for her enthusiasm for scientific research and success that comes from creativity, hard work, and the willingness to collaborate with others to investigate disease processes. Over the last two years, she has not only provided me with scientific knowledge, but has taught me a boundless set of professional and personal skills that will allow me to flourish in my future scientific research.

I would also like to thank my supervisory committee, Drs. Paul Fey, Curtis Hartman, Jessica Snowden, and Geoffery M. Thiele. They have been an instrumental part of the success of my projects, and academic development. In addition, I would like to thank Dr. Hartman for allowing me to join him in the operating room during his orthopedic surgeries as it has enhanced my clinical knowledge pertinent to my research.

In addition, I would like to thank my previous mentors who have helped to develop my scientific skills and shape my academic trajectory. My first laboratory advisor at Creighton University, Dr. Soochin Cho, introduced me to everything from proper laboratory bench practices, to presenting scientific research, to mentoring others. Dr. Cho's mentorship even continues today, where he mentors me in academic endeavors and, more importantly, life. Dr. Mark A. Freitag, who helped me to develop the ability to ask and answer scientific questions through the field of theoretical physical chemistry. Despite not being in the field of biomedical research, his mentorship has helped me remain persistent and realize that there are solutions to

every problem. Finally, Dr. Helene F. Rosenberg, Chief of Inflammation Immunobiology Section in the Laboratory of Allergic Diseases at the National Institute of Allergy and Infectious Diseases, who mentored me for two years as a post-baccalaureate. This experience was integral to my academic trajectory because Dr. Rosenberg gave me the opportunity to develop and manage my own project. Dr. Rosenberg also helped me to understand what it takes to be a successful physician scientist and taught me how to develop questions with clinical significance. More importantly, Dr. Rosenberg's caring and thoughtful nature has helped me develop personally. The sum of these experiences has been invaluable and is what led me to UNMC to seek out a career in biomedical research.

Next, I would like to thank members of Dr. Kielian's laboratory who I have had the pleasure of working alongside over the past two years. Amy Aldrich, Dr. Megan Bosch, Dr. Cortney Heim, and Dr. Brady Betten have been particularly instrumental in all of this work, helping with animal surgeries, and having the patience to teach me a considerable number of necessary laboratory skills that I did not have prior to my graduate training. In addition, their encouragement and willingness to help and provide a means of scientific discussion directly contributed to the success of my research. Thank you to Jessica Odvody for setting up a fool-proof system for continuity of our laboratory's Pfizer study. I would like to thank Rachel Fallet, for caring for the breeding colony, answering mouse-related questions, and allowing me to rely on her to coordinate the Pfizer study when I was pre-occupied by other experiments. I would also like to acknowledge many former members of Dr. Kielian's laboratory, Dr. Casey Gries, Dr. Tyler Scherr, Ms. Anna Staudacher, and Mrs. Debbie Vidlak for showing me the ropes when I first joined the lab and being a complete pleasure to work with throughout my graduate training.

I also owe a sincere thank you to several members of Dr. Kenneth Bayles, Dr. Tatiana Bronich, Dr. Paul Fey, Dr. Pankaj Singh, and Dr. Gwen Skar laboratories for their assistance on various projects and willingness to collaborate: Logan Bullock, Xinyuan (Ann) Xi, Dr. McKenzie Lehman, Chunyi Zhou, Dr. Kuldeep Attri, and Matthew Beaver. I would like to also acknowledge

the flow cytometry core facility, specifically Dr. Craig Semerad, Victoria Smith, and Sam Wall for their patience and assistance with many experiments. Finally, I would like to thank LabRat Design for the artwork presented in Figure 1.1 and 3.11.

Abbreviations

2-NBDG	2-(N-(7-Nitrobenz-2-oxa-1,3-diazol-4-yl)Amino)-2-Deoxyglucose
Ab	Antibody
ACME	Arginine catabolic mobile element
ADAM10	A disintegrin and metalloproteinase domain-containing protein 10
agr	Accessory gene regulator
AMP	Antimicrobial peptides
APC	Antigen presenting cells
ANOVA	Analysis of variance
Arg-1	Arginase-1
ATP	Adenosine triphosphate
BCA	Bicinchoninic acid
BHI	Brain-heart infusion
BMDMΦ	Bone marrow-derived macrophage
BODIPY C_{12}	4,4-Difluoro-5,7-Dimethyl-4-Bora-3a,4a-Diaza-s-Indacene-3-Dodecanoic Acid
Bp	Base pairs
c-kit	Stem cell factor

C3	Complement component 3
C5	Complement component 5
CA-MRSA	Community-associated Methicillin-resistant *Staphylococcus aureus*
CAUTI	Catheter associated urinary tract infection
CC#	Clonal complex
CCL	C-C chemokine ligand
CCR	C-C chemokine receptor
CD	Cluster of Differentiation
cDNA	complementary DNA
CFU	Colony forming units
CHIPS	*S. aureus* chemotaxis inhibitory proteins
CNS	Central nervous system
CO_2	Carbon Dioxide
CRBSI	Central venous catheter related blood stream infection
CVC	Central venous catheters
CXCL	C-X-C chemokine ligand
CXCR	C-X-C chemokine receptor
Cy5	Cyanine-5

DAMP	Damage associated molecular pattern
DDIT4	DNA-damage-inducible transcript 4
DFMO	Difluoromethylornithine
dH2O	Distilled water
DMEM	Dulbecco's Modified Eagle's Medium
DNA	Deoxyribonucleic acid
dNTP	Deoxyribonucleotide triphosphate
Eap	Extracellular adherence proteins
ECAR	Extracellular acidification rate
ECM	Extracellular matrix
EDTA	Ethylenediaminetetraacetic acid
Efb	Extracellular fibrinogen-binding protein
ELISA	Enzyme-linked immunosorbent assay
EtOH	Ethyl alcohol
FACS	Fluorescence-activated cell sorting
FBS	Fetal bovine serum
FCCP	Carbonilcyanide p-triflouromethoxyphenylhydrazone
Fc	Fragment, crystallizable

FITC	Fluorescein isothiocyanate
fl/fl	Flox/flox – dual flanking LoxP sites
G6P	Glucose-6-phosphate
GAPDH	Glyceraldehyde-3-phosphate dehydrogenase
G-CSF	Granulocyte colony stimulating factor
GFP	Green fluorescent protein
GLUT	Glucose transporter
GM-CSF	Granulocyte-macrophage colony stimulating factor
G-MDSC	Granulocytic myeloid-derived suppressor cell
HA	Healthcare associated
HBSS	Hank's balanced salt solution
HEPES	4-(2-hydroxyethyl)-1-piperazineethanesulfonic acid
HIF-1α	Hypoxia inducible factor 1 alpha
HIV	Human immunodeficiency virus
Hla	Alpha-toxin; alpha-hemolysin
HPLC/MS/MS	High-performance liquid chromatography tandem mass spectrometry
HRP	Horseradish peroxidase

H2O2	Hydrogen peroxide
Iba-1	Ionized calcium-binding adaptor molecule-1
ICAM	intercellular adhesion molecule
IDH	Isocitrate dehydrogenase
IFN	Interferon
Ig	Immunoglobulin
IL	Interleukin
iNOS	inducible nitric oxide synthase
i.p.	Intraperitoneal
i.v.	Intravenous
IVIS	*In Vivo* Imaging System
IRB	Institutional Review Board
IVIS	In vivo imaging system
JC-1	5,5',6,6'-Tetrachloro-1,1',3,3'-tetraethylbenzimidazolocarbocyanine iodide
KO	Knockout
K-wire	Kirschner wire
LAC	Los Angeles County

LC-MS/MS	Liquid Chromatography with tandem mass spectrometry).
L-glut	L-glutamine
LipA	lipoic acid synthase
L-NIL	N6-(1-Iminoethyl)-lysine, hydrochloride
LOD	Limit of detection
loxP	locus of x-over P
LPS	lipopolysaccharide
LTA	lipoteichoic acid
LukAB	Leukocidin AB
M1	Classically activated macrophage
M2	Alternatively activated macrophage
МΦ	Macrophage
mAb	Monoclonal antibody
M-CSF	Macrophage colony stimulating factor
MCP-1	Monocyte chemoattractant protein-1
MDSC	Myeloid-derived suppressor cell
$MgCl_2$	Magnesium chloride
MHC	Major histocompatibility complex

MIP	Macrophage inflammatory protein
M-MDSC	Monocytic myeloid-derived suppressor cell
MOI	Multiplicity of infection
MSCRAMM	Microbial Surface Components Recognizing Adhesive Matrix Molecules
MRSA	Methicillin-resistant *Staphylococcus aureus*
MSSA	Methicillin-sensitive *Staphylococcus aureus*
MyD88	Myeloid differentiation primary response gene 88
NADH	Nicotinamide adenine dinucleotide
NADPH	Nicotinamide adenine dinucleotide phosphate
NaOH	Sodium hydroxide
ND	Not detected
Ndusf4	NADH:ubiquinone oxidoreductase subunit S4
NET	Neutrophil extracellular trap
NF-κB	Nuclear factor kappa-light-chain-enhancer of activated B cells
NO	Nitric oxide
O.D.	Optical density
OCR	Oxygen consumption rate

ODC	Ornithine decarboxylase
OxPhos	Oxidative phosphorylation
P. aeruginosa	Pseudomonas aeruginosa
PAMP	Pathogen-associated molecular pattern
PAS	Polyethanol sulfonate
PBS	Phosphate-buffered saline
PCA	Principle component analysis
PCR	Polymerase chain reaction
PDH	Pyruvate dehydrogenase
PE	Phycoerythrin
PerCP	Peridinin-chlorophyll-protein complex
PFA	Paraformaldehyde
PFK	Phosphofructokinase
PGN	Peptidoglycan
PJI	Prosthetic joint infection
PMN	Polymorphonuclear cell
PPAR-α	Peroxisome proliferator-activated receptor-α
PPP	Pentose phosphate pathway

PRR	Pattern-recognition receptor
PSM	Phenol-soluble modulins
PVL	Panton-Valentine leukocidin
qRT-PCR	Quantitative real time-polymerase chain reaction
RANKL	Receptor activator of nuclear factor kappa-B ligand
RANTES	Regulated on activation normal T cell expressed and secreted
RIP	RNAIII inhibiting peptide
RNA	Ribonucleic acid
ROS	Reactive oxygen species
RPM	Rotations per minute
RPMI	Roswell Park Memorial Institute
RT	Reverse transcriptase
S. aureus	*Staphylococcus aureus*
s.c.	Subcutaneous
S. epidermidis	Staphylococcus epidermidis
SCC*mec*	Staphylococcal cassette chromosome *mec*
SD	Standard deviation
SDH	Succinate dehydrogenase

SpA	Staphylococcal protein A
SSTI	Skin and soft tissue infection
STAT3	Signal transducer and activator of transcription 3
STAT6	Signal transducer and activator of transcription 6
TCA	Tricarboxylic acid; citric acid
TCR	T cell receptor
Tfam	transcription factor A
TGF-β	Transforming growth factor beta
Th	T helper
THA	Total hip arthroplasty
TKA	Total knee arthroplasty
TLR	Toll-like receptor
TNF	Tumor necrosis factor
Tris-HCl	Tris (hydroxymethyl) aminomethane hydrochloride
TSST-1	Toxic shock syndrome toxin 1
Treg	Regulatory T cell
TSA	Trypticase soy agar
u-PFK2	Ubiquitous 6-phosphofructo-2-kinase/fructose bisphosphatase-2

USA	United States of America
VEGF	Vascular endothelial growth factor
VISA	Vancomycin-intermediate *Staphylococcus aureus*
VRSA	Vancomycin resistant *Staphylococcus aureus*
WT	Wild-type

List of Figures and Tables

University of Nebraska Medical Center

Omaha, Nebraska

United States of America

January 2019

MONOCYTE ANTI-INFLAMMATORY ACTIVITY IS DICTATED BY METABOLIC STATUS DURING *STAPHYLOCOCCUS AUREUS* BIOFILM INFECTION

Kelsey J. Yamada

University of Nebraska Medical Center, 2019

Omaha, NE

United States of America

Advisor: Tammy Kielian, Ph.D.

Abstract

Staphylococcus aureus biofilms represent a significant cause of morbidity and economic burden and are often associated with nosocomial infections, including medically implanted devices. In particular, prosthetic joint infections (PJIs) are a growing concern due to the continued increase in orthopedic procedures. Staphylococcal species cause >50% of all PJIs, while *S. aureus* represents the most invasive and associated with the most morbidity. *S. aureus*-associated biofilm infections are recalcitrant to antibiotic therapy, due to both the acquisition of genetic elements and metabolic dormancy. Furthermore, *S. aureus* biofilm infections remain chronic because they cannot be cleared by the immune system. Recent studies from our laboratory have demonstrated that *S. aureus* biofilms actively polarize the immune response associated with these infections to promote biofilm persistence. Specifically, biofilm infections are characterized by an influx of myeloid derived suppressor cells (MDSCs), paucity of T cells and neutrophils, and the polarization of anti-inflammatory monocytes. Augmentation of monocyte pro-inflammatory activity, either by adoptive transfer or MDSC depletion studies, promotes bacterial clearance, highlighting a critical role for monocyte/macrophage inflammatory polarization in dictating biofilm persistence. The inflammatory properties of leukocytes are linked to their metabolic activity, where anti-inflammatory macrophages primarily rely on oxidative phosphorylation (OxPhos), whereas pro-inflammatory macrophages utilize aerobic glycolysis. This suggests that biofilm-associated monocytes likely shift their metabolism to favor OxPhos over glycolysis. Therefore, we characterized the metabolic state of monocytes during *S. aureus* orthopedic implant infection and whether the metabolic reprogramming of monocytes would promote pro-inflammatory activity and biofilm clearance. Specifically, nanoparticle targeted delivery of oligomycin to inhibit monocyte ATP-synthase of the electron transport chain significantly altered monocyte metabolism and increased pro-inflammatory gene expression, which resulted in a significant reduction in *S. aureus* biofilm burdens. In addition, nanoparticle treatment acted synergistically with antibiotics to clear the biofilm infection, suggesting that targeting monocyte

metabolic activity may represent a novel therapeutic target during PJIs. Prior work from our laboratory suggested that arginase-1 (*Arg-1*) expression, a marker of anti-inflammatory polarized monocytes/macrophages, may also contribute to the inability of myeloid cells to clear *S. aureus* biofilms. Using a conditional knockout mouse model of myeloid *Arg-1*, we show that while myeloid-derived Arginase-1 does not influence *S. aureus* biofilm establishment and persistence, it does play a significant role in controlling planktonic *S. aureus* infection. Collectively, these studies reveal that monocyte metabolism is skewed towards OxPhos during the early stages of biofilm formation that limits pro-inflammatory activity, effectively facilitating biofilm establishment.

Chapter 1: Introduction

Modified from:

Yamada KJ, Kielian T: Biofilm-Leukocyte Cross-Talk: Impact on Immune Polarization and Immunometabolism. J Innate Immun 2018. doi: 10.1159/000492680

1) *Staphylococcus aureus* biofilm infection

a) Methicillin-resistant *Staphylococcus aureus* (MRSA)

Staphylococcus aureus (*S. aureus*) is a gram-positive bacterial pathogen that is found to permanently colonize the skin and nasal mucosa of approximately 30% of people worldwide while transiently associating with another 60% without causing infection (1-5). Nevertheless, *S. aureus* is regarded as a significant threat to human health, causing a range of diseases from superficial skin and soft tissue infections (SSTIs) to more invasive infections such as sepsis, osteomyelitis, or pneumonia (2, 3). Prior to the 1940s, *S. aureus* infections were routinely treated with antibiotics. However, staphylococci have the capacity to acquire antibiotic resistance determinants through horizontal transmission, which has been routinely observed following the introduction of new antimicrobial agents into clinical practice (6, 7). In addition, the common misuse and overuse of antibiotics has contributed to the ability of *S. aureus* to acquire resistance to several antibiotics by the 1960s. Today, *S. aureus* has gained resistance to nearly all antibiotics, including penicillin, erythromycin, and tetracyclines (6, 8, 9) giving rise to methicillin-resistant *S. aureus* (MRSA) strains (10, 11). Therefore, significant efforts have been made to improve clinical care by enhancing antimicrobial stewardship practices (12).

Due to the high pathogenic potential of *S. aureus*, the emergence of MRSA strains poses a significant challenge to the treatment of *S. aureus* infections. The defining feature of MRSA, over methicillin-susceptible *S. aureus* (MSSA), is the acquisition and insertion of staphylococcal cassette chromosome *mec* (SCC*mec*) (6, 7, 13, 14). While there are currently 11 SCC*mec* types, all of these mobile genetic elements carry the *mecA* gene which allows for broad-spectrum resistance to β-lactam antibiotics (5, 15-17). This is because the *mecA* gene encodes for the low-affinity penicillin-binding protein 2A (PBP2a), which β-lactam antibiotics are unable to inhibit at physiologic concentrations, leaving cell wall synthesis uninterrupted (15, 16).

The acquisition of the SCC*mec* mobile genetic element and emergence of MRSA strains has significantly complicated treatment of *S. aureus* infections (12-14, 18-21) and MRSA has

now become the most frequent cause of hospital-acquired infections (15, 16, 22, 23). Over the past three decades, MRSA infections have increased in incidence within healthy individuals who lack classic epidemiologic risk factors, such as hospital exposure or chronic disease, which are referred to as community-associated MRSA (CA-MRSA) infections (10, 15, 16, 22-24). Furthermore, both healthcare-(HA) and community-acquired MRSA isolates have attained resistance to non-methicillin antibiotics such as erythromycin (25), clindamycin (26), ciprofloxacin (27), and tetracycline (28). While glycopeptides, like vancomycin, are commonly used and effective against MRSA infections, clinical isolates have emerged that exhibit complete resistance to vancomycin (VRSA), or intermediate-resistance (VISA) which are only susceptible to extremely high vancomycin concentrations (29-31). While the prevalence of VRSA is currently relatively low (<5%), the continued use of vancomycin will likely cause VRSA strains to become more prevalent (2, 6, 32-34). MRSA infections are associated with significant morbidity and mortality rates ranging from 15-60%, which now account for greater than 50% of all nosocomial infection isolates (35). These increased infection rates ultimately result in an estimated 18,000 deaths and 80,000 invasive infections annually in the United States alone (36, 37).

As stated above, until recently, MRSA infections were primarily the result of healthcare-associated (HA-MRSA) infections, and affected hosts with compromised immune systems, chronically ill, or those who had implanted medical devices (5, 23, 38, 39). However, the incidence of CA-MRSA has continued to increase over the past decades to affect healthy individuals who lack the classic epidemiological risk factors (10, 15, 16, 22-24, 39). Populations who are at risk for CA-MRSA infection include intravenous (i.v.) drug users, prison inmates, athletes, residence in high-density populations, or those who come in contact with infected individuals (40-44). In addition, CA-MRSA is molecularly distinct from HA-MRSA. CA-MRSA more frequently harbors the smaller SCC*mec* IV, while HA-MRSA carries SCC*mec* II. CA-MRSA is often associated with increased virulence, relative to HA-MRSA, due to its expanded

repertoire of virulence genes, such as Panton-Valentine leukocidin (PVL) and staphylococcal enterotoxins (39, 42, 45, 46). In addition CA-MRSA can more robustly inhibit immune-mediated clearance through the expression of staphylokinase, staphylococcal complement inhibitor, and *S. aureus* chemotaxis inhibitory proteins (CHIPS) (47-49). Of note, these molecular determinants are species-specific, affecting human but not murine cells. Therefore, the emergence of CA-MRSA has represented a costly and increasingly deadly challenge for the treatment of *S. aureus* associated disease.

The Kielian laboratory utilizes a clonal complex 8 (CC8)/USA300 *S. aureus* clinical isolate that was isolated from an outbreak in the Los Angeles County (LAC) jail in 2000. The USA300 clade is the major cause of CA-MRSA infections in the US, Canada, and Europe (50-52). USA300 strains are more closely related to *S. aureus* lineages CC30/USA200 and CC1/USA400 as compared to CC5/USA100 and CC45/USA600, all of which frequently cause disease globally (53-55). In general, USA300 isolates belong to a single pulsed-field subtype – USA300-0114, indicating that the strain has become wide spread without acquiring significant genomic changes (23, 50-52, 56, 57). USA300-0114 is the primary strain responsible for most CA-MRSA infections in the US and predominantly carries the IVa SCC*mec* subtype, *spa* type YHGFMBQBLO, *msrA*-mediated macrolide resistance, and a number of virulence genes, including *lukS-PV/lukF-PV* (PVL), and *arcA* (arginine catabolic mobile element (ACME)) (45, 46, 57-59). In addition to its general stability and clinical prevalence, compared to isolates from the 1960s, the USA300 LAC strain is significantly more virulent, invasive, and able to resist immune-mediated killing (60, 61). To facilitate genetic manipulation, the USA300 LAC strain utilized in Dr. Kielian's laboratory was cured of the p01 (cryptic), p02 (confers tetracycline resistance), and p03 (confers lincosamide, macrolide, mupirocin, and streptogramin B resistance) plasmids, which is referred to as USA300 LAC13c (23, 56, 62). Unless otherwise noted, this strain was used in all of the publications and *in vitro* and *in vivo* experiments described in this dissertation, to strengthen the translational impact of our work.

b) Bacterial biofilms

Bacterial pathogens adapt to host tissues and immune defenses by shifting between planktonic and biofilm modes of growth (63-67). In general, a bacterial biofilm can be differentiated from planktonic infection by its association or attachment to a surface, which can be biotic or abiotic (67-71). For example, infections of native damaged heart valves or implanted medical devices are both classified as invasive biofilm infections. In contrast, skin and soft tissue infections and sepsis encourage planktonic bacterial growth over biofilm (68, 69, 72). Biofilms are multicellular communities of bacteria embedded in an extracellular matrix, which exhibit altered growth, metabolism, and gene expression relative to planktonic cells of the same species (67-69, 72-74). For example, biofilms are typically antibiotic tolerant compared to their planktonic counterparts, which show susceptibility (71). This is due to the metabolic heterogeneity of biofilms, which confers antibiotic tolerance, since most available antibiotics act on dividing, metabolically active cells by targeting cell wall and protein synthesis machinery. Therefore, most antibiotics are not effective against metabolically dormant cells in the biofilm, which are also called "persister" cells (68-70, 75).

The biofilm community is encased in an extracellular matrix (ECM) that supports the three-dimensional organization of bacteria, while providing protection from the environment, antimicrobial killing, and immune-mediated clearance (68-70, 75). Unlike the growth of planktonic bacteria in liquid culture, the spatial arrangements of bacteria within an anchored biofilm shape their microenvironment, from intercellular relationships to concentration gradients. The sum of these interactions influences bacterial growth rates, metabolism, gene expression, and general biological activities within the biofilm (68, 73, 75). Furthermore, biofilms elicit unique immune responses compared to planktonic infections, which will be discussed in the sections below (69, 76, 77). These attributes are typically not shared with planktonic infections, highlighting the distinctions between the two modes of bacterial growth.

Biofilm gradients

Biofilm growth is driven, in part, by adaptive changes in bacteria in response to environmental cues, which leads to the establishment of chemical gradients throughout its structure (67, 68, 72, 75). The formation and persistence of these gradients are influenced by diminished fluid flow within the biofilm, spatial relationships of bacteria, as well as rates of solute production, consumption, and diffusion (78, 79). Generalizations can be made concerning the direction of a concentration gradient for metabolic products and substrates based on Reaction-Diffusion theory (67, 79-81). For example, metabolites produced by the biofilm, such as carbon dioxide (CO_2) and acids, can quickly diffuse at the biofilm-fluid interface but do so at a slower rate in the interior, resulting in a CO_2 gradient, which is greatest at the biofilm core (67, 82). Conversely, the availability of metabolic substrates, such as glucose, oxygen, and other nutrients is generally greatest at the fluid-biofilm interface and are slowly depleted as they diffuse towards the center of the biofilm (79, 82). It also follows that the ability of antibiotics to penetrate a biofilm and reach an effective concentration is dependent on diffusion (82, 83). This provides an additional layer of protection to the "persister" cells at the center of the biofilm which already exhibit increased antibiotic resistance (68-70, 75). Furthermore, biofilms can maintain a zone of relative nutrient depletion and toxin accumulation that may affect leukocyte recruitment or invasion into the biofilm core (67). These multi-faceted and dynamic gradients ultimately provide a spectrum of unique microenvironments for biofilm-associated bacteria and the infiltrating leukocytes that encounter biofilm infections.

Biofilm physiology

Bacterial biofilms are known to display increased resistance to stress and display general differences in physiology compared to their planktonic counterparts (3, 60, 63, 74, 75, 84-87). Besides the chemical gradients described above, the intercellular relationships of biofilm-associated bacteria and how they influence quorum sensing-mediated gene regulation are unique

compared to planktonic organisms (73, 88-90). For example, transcriptomic analysis comparing biofilm and planktonic *S. aureus* (91) demonstrated global differences in gene expression that were clearly distinct between each mode of growth. Furthermore, small molecules like cyclic-di-GMP have been shown to play a role in promoting biofilm formation and growth (92, 93). In general, biofilms exhibit reduced metabolism adapted to microaerobic growth and favor the production of ECM components. These attributes endow biofilm tolerance to metal, oxidative, and antibiotic stress (94). In *S. aureus* biofilms, genes associated with responses to oxidative stress, metabolism, and toxin production are upregulated in biofilms relative to their planktonic counterparts (60, 91, 94-96). Some studies have shown that oxidative stress will also induce biofilm formation, or allow a biofilm to better resist oxidative stress (96). In addition, an abundance of small RNAs are differentially expressed between biofilm and planktonic growth, which suggests that post-transcriptional regulation is another means of physiologic regulation (91, 97). Proteomic analysis of secreted proteins demonstrated that 108 of 301 proteins (36%) were significantly enriched in *S. aureus* biofilms compared to planktonic cultures. This included proteases and toxins, such as alpha-toxin (Hla) and leukocidin AB (LukAB) (60). Analysis of >700 proteins from *P. aeruginosa* biofilms revealed that biofilm induced proteins could be grouped by their function and temporal relationship with biofilm developmental stages (74). Other studies have reported the induction of specific genes and proteins that coincide with progressive stages of biofilm development (74, 98). Furthermore, changes in gene expression patterns can contribute to biofilm topology. For example, *P. aeruginosa* can stochastically express type IV pili to induce elevated stalks at specific foci within a biofilm (99). In addition, stochastic expression of *S. aureus* nuclease during early biofilm growth has been implicated in biofilm establishment (88). Together, this highlights the differences in biofilm physiology and function compared to planktonic bacteria.

Biofilm extracellular matrix (ECM)

Although the extracellular matrix (ECM) is a dynamic structure, especially during the initial stages of biofilm development, this discussion will focus on the ECM components of a mature biofilm (67, 68). In general, the bacterial biofilm ECM is composed of extracellular DNA, polysaccharides, and proteins, where the contributions of each to biofilm structure continue to be studied. Prior work has shown that proteinase K treatment leads to the dispersal of *S. aureus* and *S. epidermidis* biofilms (100), but growth enhancement of *P. aeruginosa* biofilms (101). This suggests that the protein components of a staphylococcal biofilm likely have direct structural contributions, whereas the contribution of proteins to *P. aeruginosa* biofilms is more complex. Tetz *et al*. found that DNase I treatment of biofilms from several bacterial species, including *P. aeruginosa* and *S. aureus*, resulted in biofilm dispersal without affecting cell viability. They also found that DNase I treatment acted synergistically with antibiotics by promoting antibiotic penetration into the biofilm and subsequent killing of *S. aureus* biofilms (102). The clinical implications of this finding suggest that antibiotic efficacy may be increased by disrupting the biofilm structure.

The structural attributes of a biofilm promote adherence to biotic and abiotic surfaces while maintaining intercellular contacts. In addition, host-derived proteins can be exploited to facilitate biofilm establishment and maturation. For example, serum proteins including, fibronectin, fibrinogen, and collagen, rapidly coat foreign devices and are recognized by bacterial surface proteins, collectively referred to as Microbial Surface Components Recognizing Adhesive Matrix Molecules (MSCRAMMs), which facilitate bacterial adhesion and accumulation (103). In addition, host-derived soluble proteins or cell components released from necrotic eukaryotic cells can also be incorporated into the biofilm ECM. For example, *Pseudomonas* biofilm growth is enhanced by the incorporation of neutrophil components released via NETosis or toxin-mediated neutrophil necrosis (104).

Other ECM components do not directly contribute to the ECM biomass but instead regulate the complexity and topology of the biofilm structure. For example, bacteria release nucleases, proteases, and detergent-like molecules that remodel the ECM to form channels that facilitate nutrient diffusion to the deeper biofilm layers. *S. aureus* (87) and *P. aeruginosa* (75) produce detergent like molecules such as, phenol-soluble modulins (PSMs) and rhamnolipids, respectively, which influence biofilm structure and dissemination. These molecules are multi-functional and contribute to the repertoire of virulence factors that allow biofilms to escape immune-mediated clearance, which will be discussed in greater detail below.

c) Prosthetic joint- and catheter-associated biofilm infections

The risk of infection is increased by the presence of a foreign material, such as indwelling medical devices (69, 105-111), where bacteria usually establish biofilm infection (68, 69, 77, 110, 111). These infectious complications often occur during a narrow peri-operative window, with a small number of organisms needed to colonize the implant. *S. aureus* invasion at the surgical site and adherence to the indwelling device will then lead to the formation of a biofilm infection (69, 77, 112-114). The establishment of infection is likely aided by the small inoculum size that affords escape from immune detection and clearance (69, 114). Furthermore, infection establishment is likely promoted by trauma- or surgery-induced immune suppression, which is characterized by a local anti-inflammatory milieu, dampening antimicrobial responses and promoting biofilm growth (115, 116). However, in a few cases infecting pathogens can hematogenously seed indwelling medical devices during states of transient bacteremia (117-120). With the high asymptomatic colonization rates of staphylococcal species on the skin and nasopharynx, it is unsurprising that staphylococcal species are the most common etiologic agents of device-related infections (24, 107, 108, 110, 111, 120, 121), where *S. aureus* is the second most common cause of prosthetic joint infection (PJI) only behind *S. epidermidis* (110, 111, 122-124).

The number of orthopedic procedures, such as total knee (TKA) and total hip (THA) arthroplasties, continue to increase and are estimated to reach 572,000 and 3.48 million, respectively by 2030 (125, 126). A devastating complication following arthroplasty is infection, and the estimated incidence of prosthetic joint infections (PJIs) in the United States is 2.18% for all THAs and TKAs. The current standard-of-care for treating PJI is to surgically remove the infected device and fill the site with a temporary antibiotic-impregnated spacer to control the infection in combination with systemic antibiotics. Weeks to months later, depending on the time required to clear the infection, this is followed by a second surgery to replace the prosthesis. Throughout this entire process the patient has limited mobility, leaving them with significant morbidity and economic burden (107, 108, 111, 124). Patients diagnosed with PJI are prone to infection recurrence, with some studies reporting initial success rates as low as 77% (127) and an annual reinfection rate of up to 9% (128, 129).

Central venous catheters (CVC) and urinary catheters for vascular or bladder access, respectively are utilized commonly in clinical scenarios. While CVCs and urinary catheters are indispensable, they are often associated with a variety of complications. Central venous catheter-related blood stream infections (CRBSIs) account for 90% of all blood stream infections, 51% of which are due to staphylococcal species (117, 130). In addition, CRBSI carry a high rate of morbidity due to the virulent nature of *S. aureus*. In the U.S., catheter-associated urinary tract infections (CAUTIs) have an incidence of about 5 per 1000 catheter days (131, 132). Furthermore, studies have shown that catheterization promotes the colonization and infection by MRSA through the release of fibrinogen from the urothelium (133). Although *S. aureus* accounts for only about 2% of these cases, MRSA-related CAUTIs have a 4-fold greater chance of progressing to disseminated bacteremia, which carries significant mortality risks (133, 134). Like all biofilm infections, these catheter-related infections require both the removal of the infected device and concurrent antibiotic treatment (117).

d) Mouse models of biofilm infection

Currently, there are a limited number of animal models used to study the immune response to *S. aureus* biofilm infections. Two well-described models include orthopedic implant- and catheter-associated infection. These models have been used in various tissues to understand the host-pathogen interactions during a biofilm infection, and were utilized in this dissertation work.

In general, the orthopedic implant-associated biofilm infection model explores host-pathogen interactions under static conditions in close proximity to the bone marrow cavity (109). In this model, a titanium pin is inserted into the shaft of the femur through a channel drilled at the knee joint, which allows it to closely model a PJI following TKA. Furthermore, this model can be used to examine the rising incidence of implant-associated osteomyelitis, of which *S. aureus* is also a leading cause (135). This model was developed to accurately represent clinical disease, with special attention given to the materials used and bacterial inoculum. Since titanium alloys are the most commonly used material in THA and TKA, the Kielian laboratory utilizes a nickel-titanium alloy wire for their studies (136). The inoculating dose may also influence the course of infection because higher initial burdens can alter the immune response to promote biofilm formation. Furthermore, the 10^3 colony forming unit (cfu) inoculum used in this work more closely models clinical scenarios where small numbers of bacteria are sufficient for establishing infection (114, 137).

In contrast, the catheter-associated infection model allows host-pathogen interactions to be explored in a variety of tissues throughout the body, under dynamic or static conditions. Commonly used models include venous and CNS catheter-associated infection, in addition to the subcutaneous catheter-associated infection model routinely employed in Dr. Kielian's laboratory and a portion of this dissertation (138-143). Furthermore, a catheter based endocarditis model has been employed in rabbits (144). The subcutaneous catheter model does not recapitulate the sheer/dynamic forces that a biofilm experiences on a venous catheter, but advantages include the

use of a low infectious inoculum (10^3 CFU) compared to hematogenous models (~10^7 to 10^8 CFU) and a relatively straightforward device placement that is more high throughput compared to the orthopedic infection model (109, 138). Furthermore, the accessibility of the infected device is advantageous because it allows for real-time monitoring of infection by IVIS (139) and direct administration of treatments which are not limited by volume, compared to the small joint space in the orthopedic model (138).

Collectively these mouse models allow for the investigation of *S. aureus* biofilm-immune crosstalk that are clinically relevant (145, 146). Furthermore, they provide a better mechanistic understanding through the use of bacterial mutant strains and genetic knockout mice (60, 114, 138, 139, 146-149). Continued use of these models could help to identify critical determinants during PJIs or therapeutic targets that could clinically translate and reduce patient morbidity and mortality during *S. aureus* biofilm infection.

2) Immune evasion during *S. aureus* biofilm infection

Bacterial biofilms are able to subvert the host immune response by several mechanisms, which include interfering with humoral immunity, secreting toxins to impair recognition, and regulating the inflammatory status of recruited leukocytes. Furthermore, *S. aureus* is able to maintain biofilm infection in the host, even in the presence of a robust immune response. This suggests that *S. aureus* is able to evade innate and acquired immune responses, making it difficult to develop vaccine strategies for these infections. Indeed, several efforts towards vaccine development for *S. aureus* have failed, although multi-valent vaccine approaches are still being pursued (150-152). The failure to elicit an effective immune response results in a chronic *S. aureus* biofilm infection, which typically requires physical dissociation and removal of infected tissues/medical implants for treatment.

a) Evasion of innate immune recognition by pattern recognition receptors (PRRs)

Detection of invading bacterial pathogens requires recognition of pathogen-associated molecular patterns (PAMPs) which occurs through pattern recognition receptors (PRRs), including Toll-like receptors (TLRs) (153, 154). There are thirteen human TLRs and ten mouse TLRs currently identified (153, 154). Although they recognize a variety of ligands, they most commonly signal through MyD88 and NF-κB pathways, leading to the activation of inflammatory pathways and transcription and translation of pro-inflammatory cytokines and chemokines (155-158). In the case of *S. aureus*, TLR2 is critical to recognize extracellular peptidoglycan (PGN) and lipoproteins, while TLR9 detects the presence of unmethylated CpG motifs on bacterial DNA (159). TLR9 discriminates between self and non-self, since mammalian DNA is methylated at guanine residues. TLR-mediated recognition is critical for controlling planktonic *staphylococcal* infections, as MyD88- or TLR2-deficient animals demonstrated increased susceptibility to *S. aureus*-induced sepsis concomitant with decreased cytokine production (160-162). TLR9 recognition of unmethylated bacterial CpG-DNA has also been shown to stimulate an immune response from osteoblasts and dendritic cells (163, 164).

Bacterial cell death and lysis are essential processes during staphylococcal biofilm development and prior studies have shown that mutations in genes involved in autolysis, such as *atlA*, play a critical role in this process (96, 165-167). Furthermore, inhibition of autolysis with polyethanol sulfonate (PAS) significantly impacted biofilm structure and development (167, 168). Autolysis leads to the release of PAMPs, such as PGN and bacterial DNA, during biofilm growth. Although it would be expected that these PAMPs would trigger pro-inflammatory responses through TLR recognition, prior studies have shown that neither TLR2 nor TLR9 influence *S. aureus* biofilm growth *in vivo* (139, 169). In contrast, MyD88 signaling is critical for *S. aureus* biofilm containment, likely through the action of IL-1β, since biofilm burdens were higher in MyD88 and IL-1R KO mice (147, 169). In conclusion, while autolysis is essential to biofilm formation and liberates molecules that are capable of stimulating TLR-mediated signaling, TLRs

do not have a significant effect on the detection and response to *S. aureus* biofilms, despite being critical to controlling planktonic bacterial growth (139, 160-162, 169).

b) Toxin production

Many *S. aureus* toxins are regulated by quorum sensing mechanisms that are effectively enriched during biofilm growth, and can directly kill MΦs, neutrophils, and other leukocytes to inhibit immune recognition and microbicidal activity (54, 60, 170-173). Recently, our laboratory has shown that MΦ phagocytosis was inhibited following exposure to conditioned media from a wildtype *S. aureus* biofilm (60). Phagocytic activity was restored following proteinase K treatment, indicating that soluble proteins were partially responsible for inhibiting MΦ phagocytosis. In addition, conditioned medium from a *S. aureus* accessory gene regulator (*agr*) mutant biofilm was unable to inhibit MΦ phagocytosis, suggesting that the candidate protein(s) were regulated by quorum sensing. This work went on to demonstrate that the responsible proteins secreted from *S. aureus* biofilms that inhibit MΦ phagocytosis were the toxins, α-hemolysin (Hla) and leukocidin AB (LukAB) (60). Hla acts on red blood cells and leukocytes by binding ADAM10, causing protein oligimerization, pore-formation, and osmotic cell death (69, 171). Furthermore, Hla facilitates immune evasion within phagosomes, preventing the intracellular killing of phagocytosed bacteria (172). While LukAB has been shown to target and bind CD11b, to kill neutrophils (174, 175). A *S. aureus hla*/*lukAB* mutant displayed significantly reduced bacterial burdens and increased MΦ recruitment in the mouse orthopedic implant biofilm infection model compared to WT or the individual Δ*hla* or Δ*lukAB* mutants, demonstrating a complementary role for both toxins *in vivo* (60).

c) Evasion of humoral components of immunity

Established biofilms utilize several mechanisms to protect against humoral immune attack. The benefit of *S. aureus*-specific antibodies remains unclear since, previously infected

patients who have high circulating antibody levels can experience recurrent *S. aureus* infections (176, 177). Staphylococcal protein A (SpA) is a secreted protein that can bind the Fc or Fab portion of IgG or IgM (178, 179). Binding of the Fc domain by SpA prevents opsono-phagocytic killing, whereas Fab binding leads to clonal expansion of B cells (170, 180). Recent studies have shown that staphylococcal biofilms do not prevent the diffusion of humoral components into the biofilm, but instead their large biomass and antigen abundance, as compared to planktonic bacteria, dilutes targeting antibodies and interferes with opsono-phagocytosis (181). This is further supported by the finding that chronic *S. aureus* biofilm infections can induce antibodies against a biofilm antigen (SA0486,) without reducing bacterial burden (182).

Other humoral components, including complement and antimicrobial peptides (AMPs) are also targets of immune evasion during biofilm growth. Extracellular fibrinogen-binding protein (Efb) produced by *S. aureus* binds complement protein C3, to inhibit the classical and alternative pathways of complement. Specifically, Efb can inhibit complement-mediated opsono-phagocytosis by saturating C3 molecules and preventing coordinated C3 deposition and complement activation (183). AMPs, are amphipathic, positively charged molecules that disrupt microbial membranes and inhibit cellular processes (184). Currently, very few AMPs have shown efficacy against *S. aureus* biofilm development. However, a few AMPs like RNAIII inhibiting peptide (RIP) and cathelicidin were able to inhibit biofilm development (185, 186). However, most evidence suggests that leukocyte-derived AMPs are not sufficient to promote *S. aureus* biofilm clearance.

d) Immune polarization by biofilms

Previously, the complex biofilm matrix was believed to be the primary facilitator of immune evasion (76, 77). However, our laboratory and others have shown that *S. aureus* biofilms actively skew the immune response to an overall anti-inflammatory state (138, 139, 148, 187). This is evident by limited T cell and neutrophil recruitment, abundance of MDSCs, and

polarization of anti-inflammatory MΦs/monocytes at the site of *S. aureus* biofilm infections (138, 148, 188, 189). Although the immunomodulatory properties of *S. aureus* biofilms have not yet been fully elucidated, our laboratory has recently shown that one mechanism is through IL-10 production, as a result of MDSC recruitment (148). MDSCs are a heterogeneous population of myeloid progenitors that alter leukocyte activation, and MDSCs are well recognized for their immunosuppressive roles in chronic diseases, such as cancer, infections, and autoimmunity (190-195). We have also demonstrated that MDSCs are enriched in subjects with PJI compared to aseptic loosening, demonstrating the similarity between our mouse model and human disease (145, 146). Our laboratory has demonstrated that MDSCs are integral to *S. aureus* biofilm establishment and persistence as a result of their ability to polarize infiltrating MΦs towards an anti-inflammatory phenotype (146, 148, 187). Accordingly, our laboratory has shown that MDSC depletion augments MΦ pro-inflammatory activity, which translates into reduced biofilm burdens (189). Biofilm clearance is also facilitated by the adoptive transfer of pro-inflammatory MΦs at the site of biofilm infection (138). Together this highlights the importance of MDSC and monocyte/MΦ crosstalk in determining the outcome of *S. aureus* biofilm infection.

T cells

T-cell populations are limited in both mouse and human PJIs, as compared to tissues recovered from aseptic revisions where T-cell populations were abundant (114, 146, 148, 187). However, T-cells may play a role in preventing and controlling *S. aureus* infections, since HIV patients are more susceptible to MRSA infections and T-cell deficient mice are more susceptible to lethal challenge than immune-competent animals (196, 197). One mechanism whereby *S. aureus* can inhibit an effective T-cell response is to secrete some of its repertoire of 23 superantigens, including toxic shock syndrome toxin 1 (TSST-1) (173, 198, 199). Superantigens exert their actions by bypassing the classical pathway of antigen processing and presentation on MHCII molecules on antigen-presenting cells (APCs). Instead they directly bind to the MHCII

molecules of APCs and to T-cell receptor (TCR) without being processed, resulting in the activation up to 20% of T-cell populations (200, 201). The overstimulation and activation of non-specific T-cells can induce local depletion of IL-2 to limit the expansion of otherwise antigen-specific T-cells (200, 201). In addition, superantigen stimulation skews T-cells to a Th1 activation type, to drive non-specific cytokine production, which delays the development and expansion of *S. aureus* antibody producing B-cells (202). Of note, *S. aureus* superantigen action is mainly restricted to human MHC, which has prompted the development of transgenic mouse models which express human HLA (203-205).

Neutrophils

Neutrophils are an important part of the innate immune response during infection of bacterial pathogens like *S. aureus*. Neutrophils rapidly migrate to sites of inflammation, and are among the first responders to *S. aureus* infections, second only to resident macrophages (206-209). Neutrophils respond to chemokines, such as CXCL1 and CXCL2, which are produced in response to PAMPs, to direct their chemotaxis and extravasation from the vasculature (210-212). Specifically, *S. aureus* components, including lipoteichoic acid (LTA), PGN, and TSST-1, can elicit chemokine production from stromal cells and tissue MΦs to recruit neutrophils to the infection site (210-213). Neutrophils possess many of the PRRs that respond and recognize *S. aureus*-associated molecules. PRR engagement allows neutrophils to phagocytose *S. aureus* and activate pathways that increase their antimicrobial activity (210, 214, 215). Neutrophils are best known for their ability to produce large amounts of reactive oxygen species (ROS) and antimicrobial peptides, such as cathepsins and lysozyme (209, 216-218). In addition, neutrophils secrete pro-inflammatory cytokines and chemokines, including CXCL2, CXCL11, IL-1β, and TNF-α, to recruit and activate other immune effector cells (208, 210, 214, 215, 218).

However, *S. aureus* possesses several mechanisms to evade neutrophil detection and killing. Major *S. aureus* toxins, like Hla and leukocidins, induce pore formation and osmotic lysis

of numerous leukocytes, including neutrophils (60, 219). *S. aureus* produces chemotaxis inhibitory protein of staphylococci (CHIPS), which blocks chemotaxis by directly binding chemotactic receptors and inhibiting neutrophil recruitment (220-222). In addition, *S. aureus* produces extracellular adherence proteins (Eap), that bind and inhibit intercellular adhesion molecule (ICAM-1), which is a receptor on endothelial cells involved in leukocyte adhesion and diapedesis from the intravascular space (223, 224). *S. aureus* can also block phagocytosis with protein A, its capsule, or cause frustrated phagocytosis when growing as a biofilm. Finally, even when neutrophils reach the site of infection and phagocytize *S. aureus*, neutrophils undergo morphological changes that are consistent with cell necrosis (i.e. neutrophil extracellular trap (NET) formation) and are unable to effectively clear the infection (207, 225).

Myeloid derived suppressor cells (MDSCs)

Another mechanism of active immune polarization by *S. aureus* biofilms is the preferential accumulation of MDSCs ($CD45^{+}CD11b^{high}Ly6G^{high}Ly6C^{+}$). MDSCs are likely recruited and expanded at the site of biofilm infections, in part, due to the robust chemokine/cytokine milieu, which has been identified as a key signal for promoting MDSC activation and expansion (146, 148, 187, 189, 226). MDSCs are a heterogeneous population of immature myeloid progenitors, which in healthy individuals are transient and rapidly differentiate into mature granulocytes and MΦs. However, in chronic pathological conditions, such as cancers, infections, or autoimmune disorders, MDSCs are arrested in an immature state where they can suppress the immune system by interfering with leukocyte effector pathways (227-229). MDSCs constitute the majority of leukocytes present during a *S. aureus* biofilm infection; however their functional role and the mechanism by which *S. aureus* recruits is not well understood. Models of planktonic and biofilm *S. aureus* infections have shown that *S. aureus* actively expand/recruit populations of MDSCs (106, 146, 148, 187, 230, 231).

In general, MDSCs inhibit T cell expansion and activation using many mechanisms (229, 232). Previous studies have shown that MDSC expression of Arginase-1 (Arg-1), NADPH oxidase can inhibit T-cell activation via arginine depletion and reactive oxygen species (ROS) production, respectively (233-238). MDSCs can also express unidirectional importers that deplete cysteine from the microenvironment to inhibit T cell activation and function (239). Furthermore, MDSCs have been proposed to produce numerous mediators, including IL-1β, IL-6, IL-10, GM-CSF, M-CSF, stem cell factor (c-kit), TGF-β, and vascular endothelial growth factor (VEGF) to modulate leukocyte activation in addition to promoting further MDSC expansion (229, 232). During a *S. aureus* biofilm infection, many of these cytokines are abundant in the extracellular milieu, and the expression of genes such as *arg-1* and *iNOS* are upregulated in MDSCs (146, 148, 187). However, studies using inhibitors or knockout animals of Arg-1 or iNOS in *S. aureus* biofilm infections failed to show any detectable changes in bacterial burdens from the biofilm. However, mice deficient in *iNOS* or myeloid *arg*-1 had significantly higher bacterial burdens during planktonic *S. aureus* infections, suggesting that they are essential in controlling planktonic infection but are dispensable for biofilms (240, 241). Recent work has demonstrated that MDSCs are a primary source of IL-10 and maintain suppressive activity *ex vivo* (146, 148, 187). Biofilm-associated orthopedic implant infections in IL-10 knockout mice or following anti-Ly6G antibody depletion, resulted in a reduction of bacterial burdens and reprogramming of monocytes to a pro-inflammatory state (146, 148, 187). In support of this, our laboratory has shown that MDSCs are the primary source of IL-10 during *S. aureus* biofilm infection, which can block MΦ NF-κB activation and down-regulate cytokine expression (148). However, the lack of complete clearance of the biofilm suggests that the biofilm possess additional mechanism of immune inhibition.

Macrophages (MΦs)

MΦs are innate immune effector cells that are critical to defend against bacterial pathogens and scavenge cellular debris. While *S. aureus* employs a similar repertoire of immune evasion mechanisms towards MΦs as they do with neutrophils, MΦs have additional roles in the immune response. Neutrophils are known for their potent antibacterial activity and require constant influx to maintain their numbers due to their short lifespan (209, 214, 218, 225). In comparison, every tissue in the body has a resident MΦ population, which along with newly recruited MΦs play a key role in maintaining tissue homeostasis by eliminating waste and cell debris, secreting cytokines, and recycling nutrients to support the tissue microenvironment (242-248).

MΦs are derived from monocytes, which differentiate upon traversing the vascular endothelium into tissues (243, 249). At the time of infection, *S. aureus* first encounters tissue resident MΦs. Upon stimulation of TLRs and scavenger receptors, MΦs become activated and can expand by local proliferation as well as continued monocyte recruitment and differentiation (250-252). This is in stark contrast to neutrophils, which are not tissue resident cells and must be recruited by chemokines (210-212). MΦs can exhibit both pro- and anti-inflammatory properties, and are generally characterized based on gene expression signatures, cytokine production, and function. MΦ polarization is dynamic and ultimately determined by their microenvironment and cytokine milieu (244, 245, 252, 253). The concept of immune polarization originated from *in vitro* studies of MΦ activation, which led to the identification of M1 (classical) and M2 (alternative) states to describe pro-inflammatory versus anti-inflammatory attributes of MΦs, respectively (254). However, it is now well-recognized that *in vivo*, MΦ activation exists in a spectrum between pro- and anti-inflammatory states, which exhibits some degree of plasticity as a result of integrating pro-/anti-inflammatory signals. Here, we will discuss the immune polarization states of murine MΦs following exposure to biofilm or planktonic bacterial infections. Of note, there are important distinctions between murine and human MΦs in terms of

cytokines responsible for driving polarization states and effector molecules, such as inducible nitric oxide (iNOS), which is more robustly expressed in murine compared to human MΦs (254). For more detailed information on MΦ immune polarization states and corresponding metabolic effects, the reader is referred to several excellent reviews (255, 256).

S. aureus biofilm infections are characterized by anti-inflammatory monocytes/MΦs, MDSC expansion, and paucity of T cells in both humans and mouse models (106, 138, 146, 148, 187). Specifically, Iba-1 MΦs upregulated *arg-1* transcription, which is a marker of anti-inflammatory activity (138). In contrast, planktonic *S. aureus* infections are generally cleared by eliciting a robust pro-inflammatory response through the activation of MΦ PRRs, neutrophil recruitment, and T cell activation. MΦs associated with *S. aureus* biofilm infections are characterized by increased *arg-1* and decreased *iNOS* expression (138, 146, 148, 187). *In vitro* studies have shown that MΦs are capable of phagocytosing *S. aureus* from a disrupted, but not intact biofilm (104, 139). This suggests that the size of a biofilm likely represents a physical barrier, inducing a phenomenon known as "frustrated phagocytosis" (60, 85, 139) and the release of intracellular molecules from phagocytes that can lead to bystander toxicity of surrounding immune and stromal cells. In addition, MΦ immune effector mechanisms differ in their utility during biofilm and planktonic infections. Recent work presented in Chapter 4 of this dissertation, demonstrates that despite the importance of myeloid-derived Arg-1 in controlling *S. aureus* planktonic infection, *Arg-1* does not play a significant role during implant-associated biofilm infections (241). Hanke *et. al.* demonstrated that the MΦ activation state was critical for biofilm persistence. For example, as opposed to endogenous biofilm-associated MΦs, which do not exert any anti-bacterial activity, the adoptive transfer of activated pro-inflammatory MΦs into *S. aureus* biofilm infections *in vivo*, facilitated biofilm clearance. In addition, activated pro-inflammatory MΦs were able to infiltrate and phagocytose *S. aureus* biofilms *in vitro*, which was not observed with non-activated MΦs (138). Furthrmore, depletion of MDSCs with a Ly6G antibody significantly reduced biofilm burdens and increased the pro-inflammatory activity of

biofilm-associated monocytes. The ability of monocytes/MΦs to promote biofilm clearance in the absence of MDSC action was indirectly demonstrated using a Gr-1 antibody, which resulted in significantly increased *S. aureus* burdens, since effector Ly6C monocytes and by extension, mature MΦs, were also depleted. Taken together, these results support the conclusion that biofilm-mediated MDSC recruitment regulates, in part, the anti-inflammatory polarization of monocytes, effectively promoting biofilm persistence (187).

3) Immunometabolism

The field of immunometabolism focuses on intrinsic changes in leukocyte metabolism, which ultimately govern inflammatory phenotypes (256, 257). The link between metabolic alterations and cellular function was first reported by Otto Warburg, when he observed that proliferating tumor cells relied heavily on aerobic glycolysis (258, 259). It was also shown that aerobic glycolysis is a primary feature of pro-inflammatory MΦs and dendritic cells (256). This metabolic shift is necessary to increase carbon flux through the pentose-phosphate pathway and provide precursor molecules for anabolic processes and/or production of reactive oxygen species (256, 257, 260). In contrast, MΦs primarily rely on oxidative phosphorylation (OxPhos) to drive their anti-inflammatory activity, with fatty acid oxidation also playing a role. In MΦs, these metabolic switches are facilitated by global changes in gene expression. For example, pro-inflammatory MΦs express u-PFK2 (ubiquitous phosphofructokinase), a highly active PFK-2 isoform and down-regulate TCA cycle enzymes, facilitating intracellular accumulation of glucose, succinate, and citrate (256, 257). In the mouse, pro-inflammatory MΦs also generate nitric oxide through upregulation of iNOS, which directly inhibits OxPhos (256).

a) Biofilm factors influencing immunometabolism

Although biofilms are generally less metabolically active than planktonic bacteria, the sheer number of organisms allows the biofilm to establish metabolic gradients by depleting

glucose and oxygen from the surrounding microenvironment (261). Furthermore, host cell lysis can increase the abundance of metabolic enzymes, such as hexokinase and indoleamine-2,3-dioxygenase, which can deplete usable glucose and amino acids, respectively (262). Mammalian intracellular metabolic pathways are sensitively regulated by nutrient availability, including glucose, glutamine, and fatty acids. Local hypoxia and nutrient depletion from the microenvironment can reduce glycolytic rates in MΦs and promote anti-inflammatory polarization (255, 256). Local nutrient depletion likely results from contributions of both the biofilm and host cells, as it has been shown that neutrophils consume the majority of oxygen in cystic fibrosis patients that often have biofilm infection (104). Although immune shifts are possible during planktonic infections with highly metabolically active bacteria such as *Staphylococcus* spp., it is unlikely that planktonic infections can deplete nutrients as quickly as they are replenished in the host. Therefore, it is probable that the communal and relatively static nature of biofilms allow these metabolic gradients and zones of micronutrient depletion to persist over the course of infection, having a dramatic impact on leukocyte metabolism and inflammatory phenotypes.

In addition to nutrient depletion, bacteria can generate metabolites that can alter the activation and metabolism of host leukocytes. *S. aureus* is able to redirect its metabolism to acidify the local microenvironment to encourage the release of iron from transferrin (263). *S. aureus* lipoic acid synthase (*LipA*), blunts TLR activation by modifying the E2 subunit of the metabolic enzyme pyruvate dehydrogenase (PDH) (264). To date, all of the work studying the influence of *S. aureus* on host metabolism has used planktonic bacteria. Other bacterial biofilms have been shown to produce metabolites that can influence the metabolism of host cells. Biofilms collected from colon cancer patients show that polyamine synthesis from the host and polyamine acylation from the biofilm act synergistically to promote glycolytic activity and oncogenic transformation in colonic epithelial cells (265). Furthermore, the effects of planktonic *S. aureus*

on leukocyte metabolism may be amplified during biofilm growth, due to the nutrient and chemical gradients that are established during infection (67).

b) Effect of metabolism on leukocyte development and lifespan

OxPhos is more efficient than glycolysis in extracting energy from glucose. However, under conditions where glycolysis is enhanced, a concomitant increase in the pentose phosphate pathway (PPP) is generally observed to provide NADPH and ribose phosphate, which are required for biosynthesis, cell division, and other cellular functions (255, 256). An important aspect of immunity is controlling cellular life span, such as memory lymphocyte populations and terminally differentiated leukocytes responding to pathogens. Following the resolution of infection, the life span of these effector cells must be tightly regulated to prevent potential bystander pathology. Several studies have demonstrated that reliance on OxPhos metabolism supports leukocyte longevity. For example, anti-inflammatory MΦs that favor OxPhos have an increased life span, whereas pro-inflammatory MΦs, which rely more on glycolysis are shorter lived (255). This relationship is most pronounced in memory T cells, where long-lived resting T cells do not oxidize glucose but instead rely solely on fatty acid β-oxidation, whereas cytokine stimulation promotes glycolytic metabolism, with cells undergoing rapid apoptosis following cytokine withdrawal (255).

With regard to biofilms, recent studies have demonstrated that *S. aureus* biofilm-associated MΦs exhibit anti-inflammatory profiles, despite elevated pro-inflammatory cytokines in infected tissues (148, 187). Cytokine levels were significantly reduced during device-associated biofilm infection in MyD88-deficient mice; however, this resulted in increased bacterial burden and dissemination, since MΦs and neutrophils lacked major TLR effector pathways necessary for killing planktonic bacteria following biofilm dispersal (147). It is possible that elevated glycolysis-inducing cytokines could contribute to biofilm persistence by eliminating effector cells by apoptosis in combination with biofilm-derived lytic toxins until nutrients are

depleted, at which point newly recruited MΦs and neutrophils are unable to be activated; however, this remains speculative. Although cytokine-induced apoptosis of MΦs and neutrophils occur during planktonic infections, the static and chronic nature of biofilms facilitates continued cytokine accumulation, likely accounting for the robust cytokine milieu associated with *S. aureus* biofilm infections *in vivo* (106, 146, 148, 187).

c) Effect of metabolism on leukocyte function

TCA cycle defects in pro-inflammatory MΦs lead to the accumulation of TCA cycle intermediates, namely citrate and succinate (Figure 1.1). Accumulation of succinate promotes HIF-1α stabilization, epigenetic changes, and enhances IL-1β production through inhibition of α-ketoglutarate-dependent enzymes (255). Citrate can be used to generate itaconic acid, which is an anti-microbial metabolite that has been shown to inhibit the growth of planktonic *Salmonella enterica* and *Mycobacterium tuberculosis* (255). However, the antimicrobial actions of itaconic acid have not yet been explored in the context of biofilm infections. Furthermore, citrate is used as a precursor for nitric oxide, ROS, lipid, and prostaglandin production. Since biofilm-associated MΦs are anti-inflammatory in nature, it is likely that they primarily utilize OxPhos metabolism. This has recently been established in *S. aureus* orthopedic biofilm infection (Chapter 3), where infiltrating monocytes display significantly increased OxPhos and less glycolysis than monocytes isolated from sham animals (i.e. sterile orthopedic implants)

In summary, biofilms are communities of organisms encased in a complex extracellular matrix, which can colonize both biotic and abiotic surfaces. Biofilm infections are associated with significant morbidity and economic burden, since they are recalcitrant to antibiotic therapy and require physical removal and/or debridement of infected tissues for treatment. Biofilms can subvert the host immune response by preventing immune detection, toxin production, and polarizing monocytes/MΦs towards an anti-inflammatory state, which promotes biofilm persistence even in an immune competent host (Figure 1.1). Recent metabolic studies have shown

that immune cell function and metabolism are intimately related. In terms of bacterial infection, immunometabolism studies have primarily focused on MΦs and neutrophils responding to planktonic bacteria. Given the differences in inflammatory properties of MΦs and neutrophils responding to planktonic versus biofilm infections, future studies must also consider the metabolic properties of biofilm-associated immune cells, which is addressed in Chapter 3 of this dissertation.

Figure 1.1

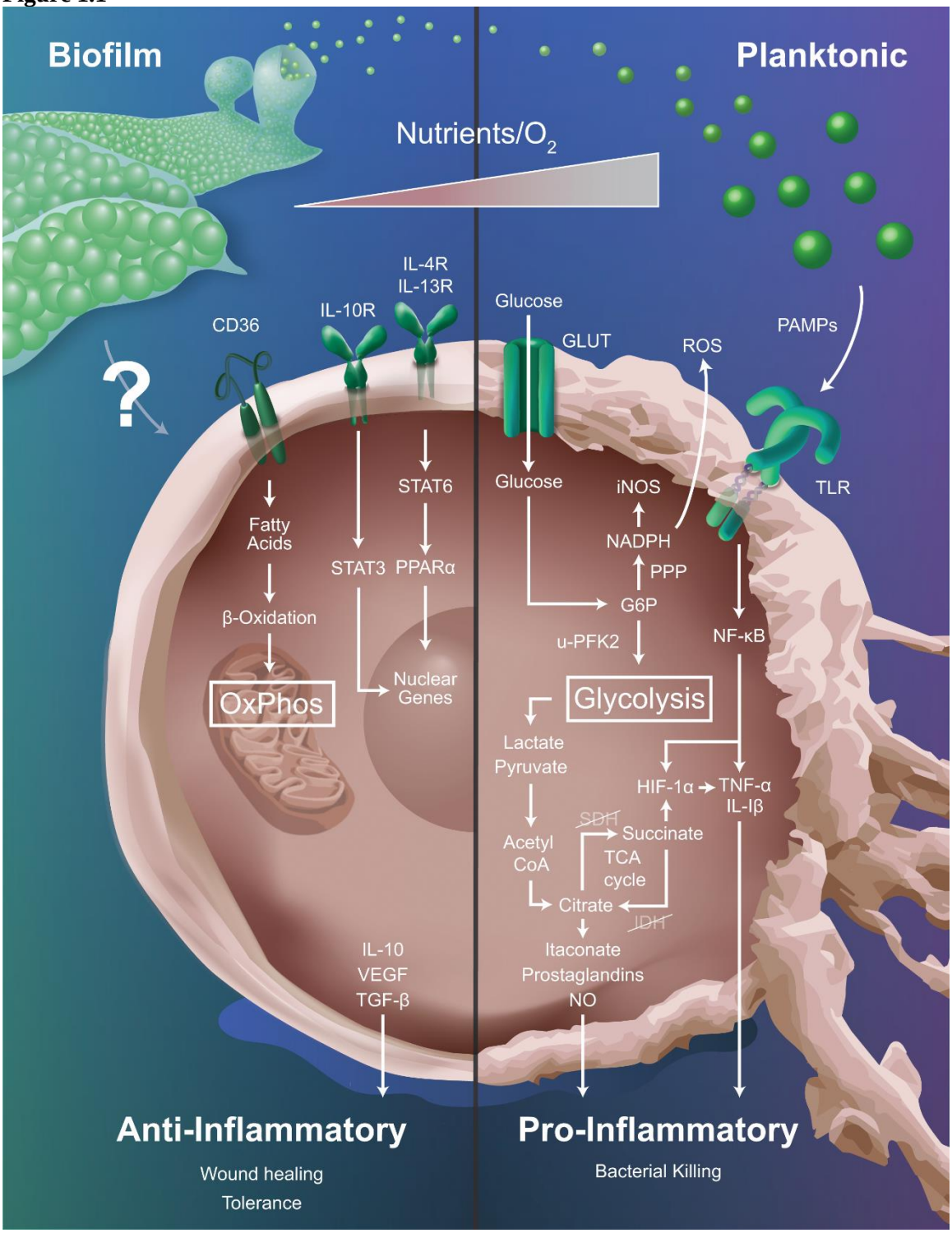

Metabolic profiles influence macrophage inflammatory status. Macrophages respond to planktonic infections via sensing of pathogen-associated molecular patterns (PAMPs) through Toll-like receptor (TLR) engagement. This favors aerobic glycolysis to provide TCA cycle

intermediates for anabolic processes required for pro-inflammatory effector mechanisms. In contrast, biofilm infections polarize macrophages towards an anti-inflammatory state and the biofilm-derived signals that drive this process are largely unknown (indicated by question mark). Since anti-inflammatory macrophages are typified by oxidative phosphorylation (OxPhos) it is predicted that biofilm infections will bias cells towards this metabolic pathway and several receptors associated with anti-inflammatory cytokines might be involved (i.e. CD36, IL-10R, IL-4R, and IL-13R). The metabolic gradients present in the tissue microenvironment (i.e. nutrients, oxygen) also influence the pro- versus anti-inflammatory profiles of macrophages that are intimately linked to their metabolic state. G6P, glucose-6-phosphate; GLUT, glucose transporter; HIF-1α, hypoxia inducible factor-alpha; IL-1β, IDH, isocitrate dehydrogenase; interleukin-1 beta; IL-4R, interleukin-4 receptor; IL-10, interleukin-10; IL-10R, interleukin-10 receptor; IL-13R, interleukin-13 receptor; iNOS, inducible nitric oxide synthase; NADPH, nicotinamide adenine dinucleotide phosphate; NF-κB, nuclear factor-kappa B; NO, nitric oxide; PPARα, peroxisome proliferator-activated receptor alpha; PPP, pentose phosphate pathway; ROS, reactive oxygen species; SDH, succinate dehydrogenase; STAT3, signal transducer and activator of transcription 3; STAT6, signal transducer and activator of transcription 6; TCA, tricarboxylic acid cycle; TGF-β, transforming growth factor-beta; TNF-α, tumor necrosis factor-alpha; uPFK2, ubiquitous 6-phosphofructo-2-kinase/fructose bisphosphatase 2; VEGF, vascular endothelial growth factor.

4) Overview of Dissertation

S. aureus biofilms are a major cause of chronic infections that cannot be cleared by the immune system partially due to their ability to resist many immune mechanisms of killing. In addition, prior studies from our laboratory have demonstrated that *S. aureus* biofilm infections subvert immune-mediated clearance mechanisms by actively skewing the host innate immune response towards an anti-inflammatory phenotype (138, 147, 187). Most notably, biofilms induce anti-inflammatory MΦ polarization, which contributes to biofilm establishment and persistence. Prior studies have also highlighted the importance of MΦ inflammatory state in dictating the outcome of *S. aureus* biofilm infection (138, 187). Specifically, MDSC depletion to remove the inhibition of MΦ activation, or adoptive transfer of pro-inflammatory MΦs promotes biofilm clearance (138, 187). The inflammatory properties of leukocytes are linked to their metabolic activity, where anti-inflammatory MΦs primarily rely on OxPhos, while pro-inflammatory MΦs utilize aerobic glycolysis. Therefore, we hypothesized that biofilm-associated monocytes/MΦs experience a metabolic shift to favor OxPhos over glycolysis, leading to anti-inflammatory polarization and *S. aureus* biofilm persistence.

During the course of my dissertation research, we have studied the metabolic properties of biofilm-associated monocytes, by targeting various aspects of metabolism in order to shift the immune response. First, we utilized a novel nanoparticle-mediated drug delivery system to specifically target monocyte metabolism and promote pro-inflammatory activation and biofilm clearance (Chapter 3). Indeed, we have demonstrated that this approach attenuated biofilm growth while highlighting the extensive nature of monocyte-MDSC crosstalk. However, preliminary studies with a more global genetic approach targeting myeloid cell metabolism resulted in an opposite outcome where bacterial burdens were elevated (Chapter 5). Comparing the disparate results from these approaches suggests that leukocyte metabolism is differentially regulated during *S. aureus* biofilm infection to dictate effector functions. Finally, we investigated the functional importance of Arg-1 during *S. aureus* biofilm infection using myeloid-conditional KO

mice, expecting it to be a key modulator of monocyte/MΦ polarization. While Arg-1 played a significant role in limiting the growth of planktonic *S. aureus in vivo*, it had no impact on *S. aureus* biofilm infection and did not act as a redundant mechanism to deplete arginine or produce polyamines. This was unexpected given the robust increase in *arg-1* expression in myeloid cells during *S. aureus* biofilm infection. The overarching theme of my dissertation research was to understand the role of monocyte metabolism during *S. aureus* biofilm infection. My results demonstrated that the metabolic activity of monocytes modulates their inflammatory phenotype and interactions other leukocytes during *S. aureus* biofilm infection. It also highlights the complexity of leukocyte crosstalk and contrasts the immune mechanisms involved during *S. aureus* biofilm vs. planktonic growth.

Chapter 2: Materials and Methods

1) Mouse strains

A breeding colony of C57BL/6 mice was established in Dr. Kielian's laboratory upon purchasing animals from the National Cancer Institute (Frederick, MD) or Jackson Laboratories (Bar Harbor, ME). Some animals were also ordered directly from Charles River Laboratories (Frederick, MD). These studies were performed in strict accordance with recommendations found in the Guide for the Care and Use of Laboratory Animals of the National Institutes of Health (NIH) and were reviewed by the Institutional Animal Care and Use Committee of the University of Nebraska Medical Center.

***Ndusf4*$^{fl/fl}$** mice were obtained from the laboratory of Phillip G. Morgan, M.D. (Seattle Children's Research Institute, Seattle WA). These conditional knockouts were generated by Richard Palmiter (University of Washington, Seattle, WA), by inserting *loxP* sites flanking exon 2 of the NADH dehydrogenase (ubiquinone) Fe-A protein 4 (*Ndusf4*) gene, which is a subunit of mitochondrial complex I. This line was backcrossed to C57BL/6 mice for ≥20 generations by Dr. Palmiter's laboratory, before donating to The Jackson Laboratory (Bar Harbor, ME, stock number 026963, B6.129S4-Ndufs4^{tm1Rpa}/J). While published reports suggest that homozygous floxed mice appear normal, our laboratory observed gross phenotypic differences (266, 267). This includes loose skin and nasal abnormalities.

***Arg-1*$^{fl/fl}$** mice were purchased from The Jackson Laboratory (Bar Harbor, ME, stock number 008817, C57BL/6-Arg1^{tm1Pmu}/J). A targeting vector containing PGK-Neomycin cassette was used to insert *loxP* sites flanking exons 7 and 8 of the *Arg-1* gene of C57BL/6 embryonic stem cells. These exons encode for two catalytic aspartic acid residues that are essential for gene activity. Chimeric males were back crossed to C57BL/6 mice for ≥11 generations. Homozygous animals display no phenotypic or functional impairments (268).

***LysM*^{Cre}** mice were purchased from The Jackson Laboratory (Bar Harbor, ME, stock number 004781, B6.129P2-Lyz2$^{tm1(cre)Ifo}$/J). A targeting vector containing *frt*-flanked neomycin cassette was used to insert a nuclear-localized Cre-recombinase into the first coding ATG of lysozyme 2 (*Lyz2*) gene. Chimeric mice were backcrossed to C57BL/6 mice for ≥6 generations. While gene activity is abolished in homozygotes, animals remain viable and fertile without displaying physical or behavioral abnormalities. These animals express Cre-recombinase in activity in cells of the myeloid lineage, including monocytes, MΦs, and granulocytes (269).

***Tie2*^{Cre}** mice were purchased from The Jackson Laboratory (Bar Harbor, ME, stock number 008863, B6.Cg-Tg(Tek-cre)1Ywa/J). *Cre* cDNA was inserted between the mouse *Tek* tyrosine kinase (*Tie2*) promoter and enhancer in fertilized oocytes of B6SJLF1 mice. Chimeric animals were backcrossed for ≥8 generations to C57BL/6 mice. These animals provide uniform expression of Cre-recombinase in endothelial cells and macrophages (270). Hemizygous mice are viable and fertile without displaying physical or behavioral abnormalities.

***Ndusf4*$^{fl/fl}$*;LysM*^{Cre}** mice were generated from breeding *Ndusf4*$^{fl/fl}$*LysM*^{null} female mice with ***Ndusf4*$^{fl/fl}$*LysM*^{Cre}** male mice.

***Arg-1*$^{fl/fl}$*;Tie2*^{Cre}** mice were generated from breeding *Arg-1*$^{fl/fl}$*Tie2*^{null} female mice with *Arg-1*$^{fl/fl}$*Tie2*^{Cre} male mice.

***Arg-1*$^{fl/fl}$*;LysM*^{Cre}** mice were generated from breeding *Arg-1*$^{fl/fl}$*LysM*^{null} female mice with *Arg-1*$^{fl/fl}$*LysM*^{Cre} male mice.

Mouse genotyping

Individual mouse genotypes were determined by PCR. Mice were ear tagged with 4-digit numerical identifiers, and tail samples (1-2mm) were collected from non-weaned mice at 4 weeks of age using sterile scissors. Tail samples were incubated with 250 μL of Alkaline Lysis Reagent

(25 mM NaOH, 0.2 mM EDTA) at 95°C for 1.5 – 3.0 h on a heat block. Following incubation on heat block, 250 µL Neutralization Reagent was added (40mM Tris-HCl), and samples were vortexed to disrupt tissues. DNA preparations were either immediately used in genotyping PCR reaction or stored at -20°C and thawed upon use. Following genotyping PCR reaction, samples were run on an ethidium bromide containing 1.7% agarose gel at 90 volts until bands could be resolved.

PCR Reaction (KAPA Taq PCR kit, KAPA Biosystems, Wilmington, MA):

10X buffer with loading dye -	1.2 µL → Final of 1X
$MgCl_2$ (25 mM) -	0.25 µL → Final of 0.52 µM
dNTPs (2.5 mM) -	1.0 µL → Final of 200 µM
Primers (20µM) -	0.6 µL → Final of 1.0 µM (each primer)
Taq (5 units/µL) -	0.05 µL → Final of 0.25 units in 12 µL
DNA preparation	1.0 µL
PCR grade water	To 12 µL (reactions with 2, 3, or 4 primers received 7.3, 6.7, or 6.1 µL respectively)

Touchdown PCR cycling:

PCR cycler

1. 94.0°C for 2:00
2. 94.0°C for 0:20
3. 65.0°C for 0:15
   →decrease temperature by 0.5°C per cycle
4. 68.0°C for 1:00
5. Return to step #2 for 10 cycles.
6. 94.0°C for 0:15
7. 60.0°C for 0:15
8. 72.0°C for 0:45
9. Return to step #6 for 30 cycles
10. 72.0°C for 2:00
11. 4.0°C for 00:00 (forever)

The following primers were used in the reactions:

Ndusf4-flox forward: AGTCAGCAACATTTGGCAGT
Ndusf4-flox reverse: GAGCTTGCCTAGGAGGAGGT

➔ 201bp = homozygous for wildtype allele
380bp = homozygous for floxed allele
201bp & 380 bp = heterozygote for floxed allele

Arg1-flox forward: TGCGAGTTCATGACTAAGGTT
Arg1-flox reverse: AAAGCTCAGGTGAATCGG

➔ 200bp = homozygous for wildtype allele
250bp = homozygous for floxed allele
200bp & 250bp = heterozygote for floxed allele

LysM-mutant: CCCAGAAATGCCAGATTACG
LysM-wildtype: TTACAGTCGGCCAGGCTGAC

LysM-common: CTTGGGCTGCCAGAATTTCTC
➔ 350bp = homozygous for wildtype allele
350bp & 700bp = positive for LysM (Homozygote LysM^{Cre} animals were not used)

Tie2-Cre forward: GCGGTCTGGCAGTAAAAACTATC
Tie2-Cre reverse: GTGAAACAGCATTGCTGTCACTT
Tie2-control forward: CTAGGCCACAGAATTGAAAGATCT
Tie2-control reverse: GTAGGTGGAAATTCTAGCATCATCC
➔ 300bp = Control band
~100bp = Cre – positive

2) Bacterial strains and microbiological techniques

Bacterial Strains

The USA300 LAC strain of *S. aureus* is a community-acquired methicillin-resistant (CA-MRSA) isolate previously provided by Dr. Frank DeLeo (National Institute of Allergy and Infectious Diseases Rocky Mountain Laboratories, Hamilton, MT). This strain was isolated from Los Angeles county (LAC) jail inmates with skin and soft tissue infection and was also responsible for the CA-MRSA outbreak of 2002 (62). This *S. aureus* strain contains two plasmids, p01 and p03 and the USA300 LAC 13c strain used in the Kielian laboratory has been cured of both plasmids (139). This will be referred to as USA300 LAC throughout the dissertation.

For *in vitro* imaging of biofilms, USA300 LAC was phage-transduced with the plasmid pCM29 to express GFP driven by the *sarA*P1 promoter (USA300 LAC-GFP), and plasmid expression was maintained with chloramphenicol selection (10 μg/ml) (271).

Bacterial storage

Bacterial strains were stored at -80°C in glycerol stocks, prepared from log-phase cultures propagated in brain-heart infusion broth (BHI, Fisher Scientific, Pittsburgh, PA) followed by centrifugation at 2,400 rpm for 10 min, 4°C. The pellet was resuspended in 10ml of ice-cold 1X PBS and washed by centrifugation at 2,400 rpm for 10 min, 4°C. After discarding the

supernatant, the pellet was resuspended in 25% glycerol in 1X PBS and this bacterial-glycerol suspension was aliquoted into appropriately labeled cryovials and stored at -80°C. This stock was used to prepare fresh bacterial streak plates before every experiment in an effort to avoid accumulating bacterial mutations by prolonged storage at 4°C.

In vitro S. aureus biofilms

Prior to each experiment, *S. aureus* was freshly streaked on a TSA plate supplemented with 5% sheep's blood (Remel) from a glycerol stock using a sterile flamed loop, and grown overnight. A single bacterial colony was selected from the plate and used to inoculate 2.0mL of complete biofilm media (RPMI 1640, 10% FBS, L-glutamine, HEPES, 10µg/mL chloramphenicol [only for GFP bacteria used in confocal experiments]) at 37°C, shaking at 250 rpm, overnight. Eight-well glass-chamber slides (ThermoScientific, Waltham, MA) or sterile 96-well plates, were coated with 20% human plasma in sterile carbonate-bicarbonate buffer (Sigma-Aldrich, St. Louis, MO) and incubated overnight at 4°C. Plasma-coating buffer was removed the following day. The O.D. of the overnight culture was measured (BioMate 3S Spectrophotometer, Thermo Scientific, Waltham, MA) at 600nm. Chamber slides were inoculated with bacteria diluted to an OD_{600} of 0.05 in 400µL of complete biofilm medium. Individual wells of a 96-well plate were inoculated with bacteria diluted to an OD_{600} of 0.05 in 200µL of complete biofilm medium. Following inoculation, biofilms were incubated at 37°C under static aerobic conditions for 4 days. Media changes were performed every 24 h by carefully removing ~35% volume from each well/chamber and adding 50% volume of fresh biofilm media to account for evaporation.

Preparation of bacteria for *in vivo* experiments

Prior to each experiment, *S. aureus* was freshly streaked on a TSA plate supplemented with 5% sheep's blood (Remel) from a glycerol stock using a sterile flamed loop, and grown overnight. A single colony was selected from the plate and used to inoculate 25 mL BHI in a 250 mL baffled

flask to maintain a 10:1 flask:volume ratio. The culture was incubated at 37°C with shaking at 250 rpm overnight (12-16 h). The OD_{600} was measured (BioMate 3S Spectrophotometer, Thermo Scientific, Waltham, MA) and 1.0 ml of the overnight culture was transferred into a 1.5 ml Eppendorf microcentrifuge tube and centrifuged at 14,000 rpm, 4°C for 10 min to pellet the bacteria. The supernatant was removed and the pellet was resuspended in 1.0 ml PBS and subsequently washed twice by centrifuging at 14,000 rpm for 5 min, 4°C. The washed overnight culture was resuspended in 1.0 mL PBS and estimated to be 5.0×10^9 CFU/mL based on several pilot study experiments.

The desired inoculum for prosthetic joint infections was 1.0×10^3 CFU in 2.0 µL (5.0×10^5 CFU/mL). This was prepared by performing serial dilutions on the washed overnight culture:

10^{-1} 1:10 dilution = 5.0×10^8 CFU/mL
10^{-2} 1:10 dilution = 5.0×10^7 CFU/mL
10^{-3} 1:10 dilution = 5.0×10^6 CFU/mL
10^{-4} 1:10 dilution = 5.0×10^5 CFU/mL

The desired inoculum for catheter associated infections was 1.0×10^3 CFU in 20 µL (5.0×10^4 CFU/mL). This was prepared by performing serial dilutions on the washed overnight culture:

10^{-1} 1:10 dilution = 5.0×10^8 CFU/mL
10^{-2} 1:10 dilution = 5.0×10^7 CFU/mL
10^{-3} 1:10 dilution = 5.0×10^6 CFU/mL
10^{-4} 1:10 dilution = 5.0×10^5 CFU/mL
10^{-5} 1:10 dilution = 5.0×10^4 CFU/mL

The desired inoculum for subcutaneous abscess infections was 1.0×10^7 CFU in 20 µL (5.0×10^8 CFU/mL). This was prepared by performing serial dilutions on the washed overnight culture:

10^{-1} 1:10 dilution = 5.0×10^8 CFU/mL

The exact number of bacteria (CFU/mL) from the overnight culture was determined following preparation of bacteria for infection by performing triplicate dilutions as shown below:

10^{-2} 10 µL of the 1.0 mL washed overnight culture in PBS
10^{-3} 10 µL of 10^{-2} dilution into 90 µL
10^{-4} 10 µL of 10^{-3} dilution into 90 µL
10^{-5} 10 µL of 10^{-4} dilution into 90 µL
10^{-6} 10 µL of 10^{-5} dilution into 90 µL
10^{-7} 10 µL of 10^{-6} dilution into 90 µL

10^{-8} 10 µL of 10^{-7} dilution into 90 µL
10^{-9} 10 µL of 10^{-8} dilution into 90 µL

10 µL of each of the dilutions were plated onto blood agar plates using track dilutions and counted the following day. The track with the largest number of resolvable colonies was counted to determine the actual CFU used for infection. For example:

Track of 10µL of 10^{-8} had 42 colonies
Original culture: $42 \times 10^8 = 4.2 \times 10^9$ CFU/mL
Prosthetic joint infection inoculum: $(4.2 \times 10^9$ CFU/mL) x (0.002 mL) x $(10^{-4}) = 8.4 \times 10^2$ CFU
Catheter associated inoculum: $(4.2 \times 10^9$ CFU/mL) x (0.020 mL) x $(10^{-5}) = 8.4 \times 10^2$ CFU
Subcutaneous abscess inoculum: $(4.2 \times 10^9$ CFU/mL) x (0.020 mL) x $(10^{-1}) = 8.4 \times 10^6$ CFU

3) Cell culture techniques

L929 Culture

Supernatant from L929 cells was used as a source of MΦ-colony stimulating factor (M-CSF) to expand mouse bone marrow-derived MΦs. L929 cells were obtained from ATCC (Manassas, VA) and immediately thawed and cultured in 25 mm^2 vented flask in L929 medium (RPMI-1640, containing 10% heat-inactivated FBS (Atlanta Biologicals, Atlanta, GA), 1% v/v HEPES (1 M stock, HyClone, South Logan, UT), 1% v/v Glutamine (200 mM stock, HyClone), antibiotic-antimycotic solution (10,000 IU/ml Penicillin, 10,000 µg/ml Streptomycin, 25 µg/ml Amphotericin B, final 1% v/v, Mediatech Inc., Manassas, VA)). Cells were grown at 37°C in a 5% CO_2 incubator until confluency. Cells were expanded and subcultured by scraping and re-seeded at a 1:20 density in 175mm^2 vented flasks. Upon reaching confluency, cells were subcultured once more by scraping and re-seeding into 8 - 175 mm^2 vented flasks. Two weeks after cells reached confluency, supernatants were harvested, filtered, and stored in 50 mL conical tubes at -80°C. A mouse M-CSF ELISA (vendor, location) revealed that L929 supernatants contained 20-40µg/mL M-CSF.

Primary mouse bone marrow-derived macrophage (BMDM) culture

Adult C57BL/6, *Ndusf4*$^{fl/fl}$;*LysM*^{null}, *Ndusf4*$^{fl/fl}$;*LysM*^{Cre}, *Arg-1*$^{fl/fl}$;*LysM*^{null}, *Arg-1*$^{fl/fl}$;*LysM*^{Cre}, *Arg-1*$^{fl/fl}$;*Tie2*^{null}, and *Arg-1*$^{fl/fl}$;*Tie2*^{Cre}, were euthanized with an overdose of inhaled isoflurane (Isothesia, VetUS, Dublin, OH) using a euthanasia chamber and cervical dislocation was performed as a secondary method to ensure death. The abdominal surface of the mouse was flooded with 70% EtOH, to prevent fur from contaminating specimens and a subcutaneous incision was made near the midline of the abdomen. Skin was separated from the peritoneum until all hind limbs were exposed and excess muscle was dissected away. Hind limbs were removed at the hip joint and immediately submerged in a petri dish containing 70% EtOH before being stored in 1X PBS on ice. Excess connective tissue and muscle was removed from the bone surface with Kimwipes and clean bones were placed in fresh 1X PBS.

At this point, the entire procedure was performed under aseptic conditions in a biological safety cabinet with sterile autoclaved instruments. The bone marrow was flushed from the bone into sterile RPMI-1640 serum-free medium, and washed once with sterile medium. The supernatant was aspirated and red blood cells were lysed by briefly adding 900 µL of sterile water immediately followed by the addition of 100 µL 10X PBS, and QS to 25 ml with sterile RPMI-1640. Cell debris was removed by filtering through a 40 µm cell strainer, and the filtered cell suspension was centrifuged at 1,200 rpm for 5 min, at 4°C. Cells were washed with medium, centrifuged, and counted using trypan blue (Lonza, Walkersville, Germany) on a hemocytometer. Cells were plated on 150 x 20 mm non-treated cell culture plates (USA scientific, Ocala, FL) at a density of 5.0 x 10^6 cells/plate, in 20 mL of media. BMDMΦ media was composed of RPMI-1640 containing 10% heat-inactivated FBS (Atlanta Biologicals, Atlanta, GA), 1% v/v HEPES (1 M stock, Hyclone, South Logan, UT), 1% v/v Glutamine (200 mM stock, HyClone), antibiotic-antimycotic solution (10,000 IU/ml Penicillin, 10,000 µg/ml Streptomycin, 25 µg/ml Amphotericin B, final 1% v/v, Mediatech Inc., Manassas, VA), 0.1% v/v 50 mM Beta-mercaptoethanol (Fisher Scientific, Pittsburgh, PA), and 5% conditioned medium from L929

fibroblasts (ATCC) as a source of M-CSF. Medium was replaced on cultures at days 3 and 5 after initial plating and cells were harvested on day 7 for experiments. Flow cytometric analyses revealed that > 99% of cells were macrophages based on CD11b and F4/80 staining after a 6-day culture period.

4) Confocal microscopy of *Ndusf4*$^{fl/fl}$;*LysM*^{Cre} MΦ-*S. aureus* biofilm co-cultures

GFP expressing *S. aureus* biofilms transduced with pCM29 (chloramphenicol) were grown for 4 days in 8-well borosilicate chambered cover glass slides (ThermoScientific) coated with 20% human plasma. Complete biofilm medium (RPMI 1640, 10% FBS, L-glutamine, HEPES, 10µg/mL chloramphenicol) was changed every 24 h. Our prior studies demonstrated that these growth conditions resulted in mature *S. aureus* biofilms based on the presence of tower structures and thickness (138, 139). Mature bone marrow-derived MΦs were labeled with CellTracker Blue (Molecular Probes, San Diego, CA) and added to the biofilm at $2x10^5$ per well, for an estimated MOI of 500:1 (bacteria:MΦ). MΦs were allowed to settle for 2 h prior to imaging. MΦ-biofilm interactions were visualized using a Zeiss laser scanning confocal microscope (LSM 710 META; Carl Zeiss, Oberkochen, Germany). Z-stacks were collected from beneath the glass slide extending to above the point where bacteria could no longer be detected. Three-dimensional images of biofilms and measurements to demonstrate biofilm thickness were performed using Zen 2012 software (Carl Zeiss).

5) Gentamicin protection assay

Bone marrow-derived MΦs from *Ndusf4*$^{fl/fl}$;*LysM*^{null} and *Ndusf4*$^{fl/fl}$;*LysM*^{Cre} mice were prepared as described above. On the day 6 *in vitro* (DIV), MΦs were harvested and re-plated in 96-well tissue culture plates at a density of $5.0x10^4$ MΦs/well and incubated at 37°C in a 5% CO_2 incubator overnight. Media was removed, and wells were rinsed with antibiotic-free biofilm medium twice, and inoculated with *S. aureus* at an MOI of 1, 10, or 100 ($5.0x10^4$ CFU, $5.0x10^5$ CFU, $5.0x10^6$

CFU, respectively), in 100μL. Plates were incubated at 37°C for 45 min. Medium was removed and replaced with biofilm medium containing 100μg/mL gentamicin, and incubated at 37°C for 30 min to kill extracellular bacteria. Following gentamicin treatment, medium was replaced with fresh biofilm medium containing 1.0μg/mL gentamicin. At 0, 2, 4, 6, 12, 24, 48, or 72 h following treatment with gentamicin, supernatants were collected and stored at -20°C. Adherent MΦs were lysed with 100μL of sterile H_2O for 10 min. Track dilutions of lysates were made and plated on TSA plates supplemented with 5% sheep blood. The tracks with the largest number of resolvable colonies were counted to determine the number of surviving intracellular bacteria.

6) Seahorse Biosciences Assay

The bio-energetic profiles of bone marrow-derived MΦs were assessed using a XF96 extracellular flux analyzer (Seahorse Biosciences, North Billerica, MA). Briefly, MΦs were seeded in XF96 plates at $5x10^4$ cells/well 24 h prior to assay, whereupon cells were treated with 10ng/mL rmIL-4, *S. aureus* PGN + IFN-γ (10μg/mL and 10ng/mL, respectively), or CTO (Cy5-labeled, tuftsin-conjugated, oligomycin) nanoparticles (1μg/mL) for 24 h at 37°C. One hour prior to assay, MΦs were incubated in bicarbonate-free DMEM (Sigma-Aldrich) supplemented with 2mM L-glutamine and 1mM pyruvate at 37°C without CO_2. Glucose was included at 10mM for mitochondrial stress tests. For mitochondrial stress tests, oxygen consumption rate (OCR) was measured following sequential exposure to oligomycin (1μM), carbonilcyanide *p*-triflouromethoxyphenylhydrazone (FCCP, 1μM), and rotenone (0.5μM) (all from Sigma-Aldrich). By sequentially blocking different steps of the electron transport chain, well-established algorithms were used to calculate basal and maximal respiration (272, 273). To measure glycolytic activity, MΦs were pre-incubated for 1 h in medium lacking sodium bicarbonate, serum, and glucose prior to initiating the assay to reduce intracellular glucose stores. Next, cells were sequentially exposed to glucose (10mM) and oligomycin (1μM; both from Sigma-Aldrich), whereupon extracellular acidification rate (ECAR) was measured. Total protein was quantified

from each well following Seahorse assays to confirm lack of differential MΦ toxicity to the metabolic inhibitors.

7) Mouse models of *S. aureus* infection

Subcutaneous *S. aureus* abscesses

Age- and sex-matched mice (8-10 weeks old) were used to examine the immune response to *S. aureus* subcutaneous abscess infection. *Arg-1*$^{fl/fl}$;*Tie-2*^{Cre} conditional KO and *Arg-1*$^{fl/fl}$;*Tie-2*^{null} control mice were weighed and anesthetized with ketamine/xylazine (100mg/kg and 5mg/kg, respectively) by intraperitoneal (i.p.) injection. Once anesthetized, the left flank was shaved using clippers, and the surgical site was cleaned and disinfected with povidone-iodine. Mice received subcutaneous injections of *S. aureus* (10^7 CFU in 20µL sterile PBS) using a 27-gauge x ½" needle. Eye ointment (LubriFresh™ P.M., Major Pharmaceuticals, Livonia, MI) was used for all mice before they were returned to clean cages and kept under heat lamps to maintain core body temperature until fully recovered from anesthesia. Cages were labeled with orange biohazard cards and monitored daily throughout the course of infection. Abscess sizes were measured daily with calipers (accuracy of 0.001", and repeatability of 0.0005", iGaging, Los Angeles, CA), throughout the course of infection.

Subcutaneous catheter-associated biofilm infection

Age- and sex-matched mice (8-10 weeks old) were used to examine the immune response to *S. aureus* subcutaneous catheter infection. *Arg-1*$^{fl/fl}$;*Tie-2*^{Cre} conditional KO and *Arg-1*$^{fl/fl}$;*Tie-2*^{null} control mice were weighed and anesthetized with ketamine/xylazine (100mg/kg and 5mg/kg, respectively) by intraperitoneal (i.p.) injection. Once anesthetized, the left flank was shaved using clippers, and the surgical site was cleaned and disinfected with povidone-iodine. Next, a small subcutaneous (s.c.) incision was made in the left flank and a blunt probe was used to create a pocket for the insertion of a sterile, 16-gauge Teflon coated intravenous catheter, 1 cm in length

(Exel International, St. Petersburg, FL). The incision was sealed using Vetbond Tissue Adhesive (3M, St. Paul, MN) and 10^3 CFU USA300 LAC in 20 µL of sterile PBS was injected through the skin, directly into the catheter lumen using a 27-gauge x ½" needle. Eye ointment (LubriFresh™ P.M., Major Pharmaceuticals, Livonia, MI) was used for all mice before they were returned to clean cages and kept under heat lamps to maintain core body temperature until fully recovered from anesthesia. Cages were labeled with orange biohazard cards and monitored daily throughout the course of infection.

***S. aureus* biofilm-associated orthopedic implant infection**

Age- and sex-matched mice (8-10 weeks old) were used to simulate infectious complications in patients following orthopedic implant placement. Animals were weighed and anesthetized with ketamine/xylazine (100 mg/kg and 5 mg/kg, respectively) by i.p. injection. Once anesthetized, right leg was shaved using clippers, and the surgical site was cleaned and disinfected with povidone-iodine. A medial incision was created through the quadriceps with lateral displacement of the patella tendon to access the distal femur. A burr hole was made in the femoral intercondylar notch through the intramedullary canal using a 26-gauge needle, whereupon a pre-cut 0.8-cm orthopedic-grade Kirschner wire (0.6mm diameter, Nitinol [nickel-titanium]; Custom Wire Technologies, Port Washington, WI) was inserted into the intramedullary canal, leaving ~1mm protruding into the joint space. The exposed wire surface was inoculated with 10^3 CFU of *S. aureus* USA300 LAC in 2µL of sterile PBS. The quadriceps-patellar complex was reduced to the midline and the fascia was sutured with 6-0 metric absorbable sutures before the skin of the surgical site was closed with 6-0 metric nylon sutures (both from Covidien, Mansfield, MA). Animals received s.c. Buprenex (0.1mg/kg; Reckitt Benckiser, Hull, U.K.) for pain relief, and returned to clean cages under a heat lamp to ensure maintenance of core body temperature until fully recovered from anesthesia. Cages were labeled with orange biohazard cards and monitored

daily. A second dose of Buprenex was administered 24 h after surgery and after this interval, all mice exhibited normal ambulation and no discernable pain behaviors.

8) Nanoparticle synthesis and characterization

Polymeric nanoparticles based on an amphiphilic block copolymer of poly(ethylene glycol)-*b*-poly(L-glutamic acid) (PEG-b-PGA) with pendant phenylalanine functionalities were synthetized as previously described (274, 275). Briefly, PEG-*b*-PGA (Alamanda Polymers, Inc., Madison, AL; block lengths were 114 and 150 repeating units for PEG and PGA, respectively) was first modified with L-phenylalanine methyl ester via carbodiimide chemistry. The degree of grafting was 50% as determined by ^{1}H-NMR analysis. Polymeric micelles were then prepared by mixing the solution of copolymer in dimethylformamide with water (1: 1 v/v) following dialysis against water for 48 h. The formed micelles were cross-linked using 1,2-ethylenediamine in the presence of 1-(3-dimethylaminopropyl)-3-ethylcarbodiimide hydrochloride (EDC) with a targeted cross-link density of 20% (based on the molar ratio of cross-linker to carboxylic groups of the GA residues). Tuftsin peptide with a cysteine residue at the C-terminus (TKPRC) was synthesized on an automated solid-phase Liberty microwave peptide synthesizer (CEM, Matthews, NC) employing standard Fmoc chemistry using a Rink Amide resin (Nova Biochem). Sample purification (≥ 95%) was performed on a Phenomenex (Torrance, CA) Jupiter 10 μm Proteo 250 × 4.6 mm C12 column using a water (0.1% formic acid)–acetonitrile (0.1% formic acid) gradient. HPLC/MS analyses were performed on a Waters (Milford, MA) e2695 system equipped with a Waters 2489 absorption detector and a Waters Q-Tof Micro electrospray ionization mass spectrometer.

Tuftsin targeting moieties were conjugated to nanoparticles via a heterobifunctional maleimide-PEG-amine linker (MAL-PEG-NH_2, 7.5 kDa, JenKem Technology, Plane TX). First, MAL-PEG-NH_2 (0.27 μmol, 0.15 eq with respect to the amount of carboxylic groups) was conjugated to the free carboxyl groups (1.75 μmol) of EDC-activated nanoparticles. Resulting

constructs were purified using repeated ultrafiltration (MWCO 30,000, Millipore) at 2200 rpm for 15 min (3 washes). Purified peptide (0.31 μmol) was subsequently reacted with MAL-PEG functionalized nanoparticles in PBS at pH 7 for 2 h. Unreacted MAL groups were quenched by β-mercaptoethanol and targeted nanoparticles were purified by dialysis against distilled water using a dialysis membrane (MWCO 3500 Da). The amount of peptide conjugated on the surface of the nanoparticles was 126.3 ± 6.3 μg per mg of polymer (n=3) as determined by a BCA protein assay. Oligomycin-loaded nanoparticles were prepared by adding an ethanol solution of oligomycin (2 mg/mL) dropwise into the aqueous dispersion of tuftsin-coated nanoparticles (1 mg/mL) and mixed overnight at RT in an open-air system to allow for the slow evaporation of ethanol. The residual ethanol was then removed at reduced pressure. Unincorporated oligomycin was removed by filtration with 0.8 μm syringe filters (Thermo Scientific). Oligomycin content was determined by HPLC analysis under isocratic conditions using an Agilent 1200 HPLC system with a diode array detector set at 226 nm (276). A Nucleosil C18 column was used as stationary phase (250 mm × 4.6 mm), and the mobile phase was comprised of an acetonitrile/water mixture (80/20, v/v) applied at a flow rate of 1 mL/min. The resulting nanoparticles had an average hydrodynamic diameter of approximately 80 nm (ζ-potential = -8.4 mV) and were characterized by narrow size distributions using dynamic light scattering (Zetasizer Nano ZS, Malvern Instruments Ltd., Worcestershire, UK). The loading capacity of tuftsin-coated nanoparticles for oligomycin was 5.2 ± 0.9 % (w/w). Finally, fluorescently labelled non-modified (C), tuftsin-coated empty (CT) and tuftsin-oligomycin-loaded (CTO) nanoparticles were synthesized by adding Cy5 amine (Lumiprobe Corporation, Hunt Valley, MD) in DMSO to the aqueous dispersion of nanoparticles (equivalent to 0.16% of carboxylic groups in nanoparticles) in the presence of EDC and the mixture was incubated for 4 h in the dark. Unbound dye was removed by dialysis and fluorescence emission spectra of labelled nanoparticles were characterized using a FluoroMax-4 spectrofluorometer (HORIBA Scientific). Oligomycin release from CTO nanoparticles was determined using a PBS dialysis method with a 3.5 kDa membrane

cutoff. The kinetics of oligomycin release was determined by HPLC and concentrations are expressed as a percentage of the total oligomycin available vs. time. Over 90% of oligomycin was released from CTO nanoparticles within a 24 h period at physiological pH (Supplemental Figure 3.1).

9) *In vivo* drug administration

Nanoparticles

Animals were placed in an induction chamber without restraint and anesthetized with 2.5% isoflurane. A total of 10μg control (C or CT) or oligomycin (CTO) nanoparticles were administered by a single intra-articular injection (in 10μL of PBS) at either day 3 or 7 post-infection. Nanoparticle injection and length of retention was evaluated in the same cohort of mice using an *In Vivo* Imaging System (IVIS Spectrum; PerkinElmer, Waltham, MA) under isoflurane anesthesia, with excitation and emission wavelengths of 640nm and 680nm, respectively.

Antibiotics

Mice received daily systemic antibiotic treatments by i.p. injections (25 mg/kg/day rifampin and 5 mg/kg/day daptomycin) dissolved in 100 μL sterile PBS with a 26-gauge x 5/8 needle. In some experiments, 100 ng or 50 ng oligomycin (in 10 μL of PBS) was directly injected into the knee joint to assess antibiotic effects.

ROS, iNOS, and ODC inhibitors

Mice received i.p. injections of apocynin (6 mg/kg/day), N6-(1-iminoethyl)-L-lysine (L-NIL; 40 mg/kg/day), α-difluoromethylornithine (DFMO; 50 mg/kg/day), or vehicle beginning at 5 h prior to *S. aureus* infection. All small molecule inhibitors were administered i.p. once daily until sacrifice at 3 or 7 days post-infection (DPI).

10) Recovery of abscess- or implant-associated tissues for *S. aureus* enumeration

Recovery of subcutaneous abscess tissues

Animals were sacrificed by an overdose of inhaled isoflurane, followed by cervical dislocation. The surgical site was flooded with 70% ethanol to prevent potential sample contamination with skin microflora. The subcutaneous abscesses were excised, weighed, and collected in 0.5 mL of homogenization buffer (sterile PBS supplemented with a Complete™ protease inhibitor cocktail tablet (Roche Diagnostics, Indianapolis, IN)) on ice. Tissues were dissociated using the blunt end of a 3.0 mL syringe. An aliquot was filtered through a 35 μm filter (BD Falcon, Bedford, MA) and analyzed by flow cytometric analysis as described below. A second aliquot was centrifuged at 14,000 rpm for 10 min and the supernatants were transferred to a new 1.5mL centrifuge tube and stored at -80°C until Milliplex analysis. A final aliquot of homogenate was serially diluted and plated on TSA plates supplemented with 5% sheep blood to determine bacterial counts. Bacterial titers were expressed as Log_{10} (CFU/g wet tissue weight).

Recovery of subcutaneous catheters and surrounding tissues

Animals were sacrificed using an overdose of inhaled isoflurane, followed by cervical dislocation. The surgical site was flooded with 70% ethanol to prevent potential sample contamination with skin microflora. The section of the flank containing the catheter and associated tissue was removed, whereupon the catheter was separated from the surrounding host tissue, weighed, and placed in 0.5 mL of homogenization buffer (sterile PBS supplemented with a Complete™ protease inhibitor cocktail tablet (Roche Diagnostics, Indianapolis, IN)) on ice. Catheters were sonicated for 5 min on ice while catheter-associated tissues were dissociated using the blunt end of a 3.0 mL syringe. An aliquot was filtered through a 35 μm filter (BD Falcon, Bedford, MA) and analyzed by flow cytometric analysis as described below. A second aliquot was centrifuged at 14,000 rpm for 10 min and the supernatants were transferred to a new 1.5mL centrifuge tube and stored at -80°C until Milliplex analysis. A final aliquot of homogenate was

serially diluted and plated on TSA plates supplemented with 5% sheep blood to determine bacterial counts. Bacterial titers were expressed as Log_{10} (CFU/ml) for catheters or Log_{10} (cfu/g wet tissue weight) for catheter-associated tissues.

Recovery of orthopedic implant and surrounding tissues

Animals were sacrificed by an overdose of inhaled isoflurane, followed by cervical dislocation. The surgical site was flooded with 70% ethanol to prevent potential sample contamination with skin microflora. An incision was made in the skin of the right leg so that the skin could be carefully removed. The subcutaneous tissue overlying the patellar tendon was excised, weighed, and placed in 0.5 mL of homogenization buffer (sterile PBS supplemented with a Complete™ protease inhibitor cocktail tablet (Roche Diagnostics, Indianapolis, IN)) on ice. The tissue was dissociated with the blunt end of a 3.0 mL syringe. An aliquot was filtered through a 35 μm filter (BD Falcon, Bedford, MA) and analyzed by flow cytometric analysis as described below. A second aliquot was centrifuged at 14,000 rpm for 10 min and the supernatant was stored at -80°C until Milliplex analysis. A final aliquot of homogenate was serial diluted and plated on TSA plates supplemented with 5% sheep blood to determine bacterial counts. The tibia and fibula were transected distal to the knee joint, and the femur was disarticulated at the hip joint and removed. The remaining muscle and tendon tissues were removed from the bones using Kimwipes. The knee joint was separated from the femur to allow for collection of the titanium implant into 0.2 mL sterile PBS on ice, followed by vortexing at 2,000 rpm for 10 min to dislodge bacteria adherent to the implant. The knee joint and femur were weighed and placed into 0.5 mL homogenization buffer before being homogenized with a Polytron homogenizer at the highest setting for approximately 20 sec. Serial dilutions of the homogenates from the knee, femur, and implant were plated on TSA plates supplemented with 5% sheep blood to determine bacterial counts. Bacterial titers were expressed as Log_{10} (cfu/g wet tissue weight) for implant-associated tissue, knee joint, and femur, or Log_{10} (CFU/ml) for implant-associated titers. The remaining

homogenates from the knee and femurs were centrifuged at 14,000 rpm for 10 min and the supernatants were transferred to new 1.5mL centrifuge tubes and stored at -80°C until Milliplex analysis.

11) Western blot for arginase-1

MΦs were expanded from the bone marrow of *Arg-1*$^{fl/fl}$;*Tie-2*^{Cre} MΦ conditional KO, *Arg-1*$^{fl/fl}$;*LysM*^{Cre} myeloid conditional KO, and *Arg-1*$^{fl/fl}$;*Tie-2*^{null} control mice. At day *in vitro* 6, MΦs were harvested, re-plated, and treated with 10 ng/mL recombinant mouse (rm)IL-4 (BioLegend, San Diego, CA) for 24 h, whereupon cellular extracts were prepared with RIPA buffer (1% Triton-X, 0.1% SDS, supplemented with a Complete™ protease cocktail, Roche Diagnostics). Blots were probed with an anti-Arg-1 antibody (goat anti-mouse 1:200, sc-271430, Santa Cruz Biotechnology) followed by a rabbit anti-goat IgG-HRP (Abcam, Cambridge, MA).

12) Arginase assay

Arginase activity was measured in MΦs expanded from *Arg-1*$^{fl/fl}$;*Tie-2*^{Cre} conditional KO, *Arg-1*$^{fl/fl}$;*LysM*^{Cre}, and *Arg-1*$^{fl/fl}$;*Tie-2*^{null} control mice following stimulation with 10 ng/mL rmIL-4. To determine arginase activity in MΦs and MDSCs recovered from *S. aureus* catheter-associated biofilm infections, MΦs and MDSCs were isolated by FACS. Following isolation of *in vitro* stimulated or *ex vivo* isolated MΦs and MDSCs, cells were lysed in 100 µL of lysis buffer (10 mM Tris-HCl, pH 7.4, 1.0 µM pepstatin A, 1.0 µM leupeptin, 0.4% Triton X-100). Arginase activity assays were performed using an Arginase Activity Assay Kit (Sigma-Aldrich, St. Louis, MO) according to the manufacturer's instructions. Arginase activity was reported as units/L.

13) Hydroxyproline assay

To determine the relative collagen content in *S. aureus* catheter-associated tissues, hydroxyproline assays were performed using a Hydroxyproline Assay Kit (Sigma Aldrich).

Briefly, samples were prepared by homogenizing 10mg of infected tissue in 100µL of water, transferred to a pressure-tight vial with 100µL of 12M hydrochloric acid, and hydrolyzed at 120°C for 3 h. A total of 10-50µL per sample was transferred to a 96-well plate and evaporated at 60°C. Following the addition of reaction buffer the plate was read at 570nm using an iMark Microplate Absorbance Reader (Bio-Rad, Hercules, CA). Results were calculated based on a standard curve, and reported as µg hydroxyproline/mg tissue

14) Metabolomic analysis

Monocytes and MDSCs were recovered by FACS from animals with *S. aureus* orthopedic implant infection that received CT or CTO nanoparticles and polar metabolites were extracted. Briefly, monocytes and MDSCs were lysed using an 80% methanol/water mixture pre-chilled to -80°C. Cellular debris was removed by centrifugation at 13,000 rpm for 5 min at 4°C, whereupon supernatants containing metabolite extracts were collected and dried at room temperature using a speed vacuum concentrator (Eppendorf, Hamburg, Germany). Samples were resuspended in a 50% methanol/water mixture and analyzed using LC-MS/MS (Liquid Chromatography with tandem mass spectrometry). A single reaction monitoring (SRM) LC-MS/MS method was used with positive/negative ion polarity switching on a Xevo TQ-S mass spectrometer as described previously (277). The metabolite peak areas were calculated using MassLynx 4.1 (Waters Inc.) and normalized to the respective cell counts of each sample. The resultant peak areas were subjected to relative quantification analyses by utilizing MetaboAnalyst 3.0 (www.metaboanalyst.ca). Fold-change values of metabolites were expressed as CTO relative to CT treated mice. Individual values exhibited a normal distribution and outliers were identified by Grubb's test, followed by a Student's *t*-test to determine significance. Principal component analysis, heat map, and pathway impact analysis were also performed using MetaboAnalyst 3.0 software.

15) Flow cytometry

Flow cytometric analysis was used to characterize leukocyte infiltrates in inflamed subcutaneous tissues from abscesses or soft tissues surrounding subcutaneous catheter or orthopedic implants during *S. aureus* biofilm infection. Animals were sacrificed with an overdose of inhaled isoflurane and tissues were excised as previously described and placed in 500 µl FACS buffer (2% FBS in PBS) on ice. Tissues were dissociated with the blunt end of a plunger from a 3.0 mL syringe, and passed through a 35 µm filter (BD Falcon, Bedford, MA). Following removal of an aliquot for bacterial quantitation and Milliplex analysis, the filtrate was washed with FACS buffer and cells were collected by centrifugation (1,200rpm, 5 min, and 4°C). RBCs were lysed using BD Pharm Lyse (BD Biosciences, San Diego, CA) for 5 min at room temperature. After lysis, cells were washed with FACS buffer and resuspended in 250 µL FACS buffer supplemented with 2 µL Fc-block (TruStain FcX, BioLegend, San Diego, CA) for 5 min at 4°C to minimize nonspecific antibody binding. Compensation and isotype controls were made by pooling 50 µL of each sample to identify gating thresholds and assess the degree of nonspecific staining. The remaining 200µL was divided into two wells of a round-bottom 96-well plate to assess innate and adaptive leukocyte infiltrates using the panels described below. To exclude dead cells from analysis, cells were stained with Live/Dead Fixable Blue Dead Cell Stain (Invitrogen, Eugene, OR).

<u>General innate immune panel</u>:
CD45-APC
Ly6G-PE
Ly6C-PerCP-Cy5.5
F4/80-PE-Cy7
CD11b-FITC

<u>Innate immune panel for nanoparticle experiments</u>:
CD45-PacBlue
Ly6G-PE
Ly6C-PerCP-Cy5.5
F4/80-PE-Cy7
CD11b-FITC
Nanoparticle-APC (not an antibody)

General adaptive immune panel:
CD45-PE-Cy7
CD3-APC
CD4-PacBlue
CD8a-FITC
γδ-TCR-PE

Adaptive immune panel for nanoparticle experiments:
CD45-PE-Cy7
CD3-PE
CD4-PacBlue
CD8a-FITC
Nanoparticle-APC (not an antibody)

All fluorochrome-conjugated antibodies were purchased from BioLegend (San Diego, CA). For individual samples, 10,000-100,000 events were analyzed using BD FACSDiva software with cell populations expressed as percentage of total viable $CD45^+$ leukocytes.

JC-1, BODIPY C_{12}, and 2-NBDG staining

Staining with JC-1 (5,5',6,6'-Tetrachloro-1,1',3,3'-tetraethylbenzimidazolocarbocyanine iodide), BODIPY-12C (4,4-Difluoro-5,7-Dimethyl-4-Bora-3a,4a-Diaza-s-Indacene-3-Dodecanoic Acid), and 2-NBDG (2-(N-(7-Nitrobenz-2-oxa-1,3-diazol-4-yl)Amino)-2-Deoxyglucose) were used to assess the metabolic activity of leukocytes from the inflamed subcutaneous tissues surrounding orthopedic implants during *S. aureus* biofilm infection. Tissues were homogenized in 1.0 mL of PBS and passed through a 35 μm filter (BD Falcon). Unwashed cells were divided into three tubes and incubated with either JC-1 (100 ng/mL), BODIPY-12C (200 ng/mL), or 2NBDG (10 μM) for 30 minutes at 37ºC. Single stain controls, with or without FCCP treatment were made from pooled aliquots of each sample. Cells were washed with FACS buffer and resuspended in 250 μL FACS buffer supplemented with 2 μL Fc-block (TruStain FcX, BioLegend, San Diego, CA) for 5 min at 4°C to minimize nonspecific antibody binding. Cells were stained in a 96-well round bottom plate to assess innate leukocyte infiltrates using the panel described below. To exclude dead cells from analysis, cells were stained with Live/Dead Fixable Blue Dead Cell Stain (Invitrogen, Eugene, OR).

General innate immune panel:
CD45-APC
Ly6G-PacBlue
Ly6C-PerCP-Cy5.5
F4/80-PE-Cy7
CD11b-AF700

All fluorochrome-conjugated antibodies were purchased from BioLegend (San Diego, CA). For individual samples, 10,000-100,000 events were analyzed using BD FACSDiva software. Oxidative Phosphorylation activity (JC-1) was expressed as the ratio of the number of green to red cells of a specific cell population. B-oxidation (BODIPY C_{12}) and glycolytic (2-NBDG) activity was expressed as the percent of a specific cell population.

16) RNA isolation and real-time quantitative polymerase chain reaction (RT-qPCR)

Gene expression analysis of *in vitro* bone marrow derived MΦs

MΦs were expanded from the bone marrow of C57BL/6 mice as described above. At day *in vitro* 6, MΦs were harvested and seeded at $5x10^4$ cells/well in a 96-well plate. Following a 24 h adherence period, MΦs were treated with 10 ng/mL recombinant mouse (rm)IL-4 (BioLegend, San Diego, CA) ± various concentrations of oligomycin (Sigma-Aldrich, St. Louis, MO) for 4 h at 37°C, whereupon a Cells-to-Ct kit (ThermoFisher Scientific, Waltham, MA) was used to isolate RNA and synthesize cDNA for TaqMan qPCR (ThermoFisher Scientific). qPCR was performed using TaqMan primer/probe sets for Arg-1, TNF-α, and GAPDH (Glyceraldehyde 3-phosphate dehydrogenase). Gene expression levels were normalized to GAPDH expression and are presented as the fold-induction ($2^{-\Delta\Delta Ct}$) value relative to untreated MΦs.

Gene expression analysis of FACS-purified leukocytes from *Arg-1*$^{fl/fl}$ animals

Viable monocytes ($CD45^+Ly6G^-Ly6C^+F4/80^{\pm}$) or MDSCs ($CD45^+Ly6G^{high}Ly6C^+F4/80^-$) were purified from *S. aureus*-infected tissues by FACS on a FACSAria (BD Biosciences), whereupon total RNA was isolated using the cells-to-Ct TaqMan gene expression kit (ThermoFisher).

Reverse transcription (RT) and pre-amplification reactions were conducted according to the manufacturer's instructions using a Bio-Rad CFX Connect™ thermocycler. TaqMan primer/probe mixes (Applied Biosystems, Foster City, CA) for Arg-1, iNOS, and GAPDH were used to evaluate monocyte and MDSC gene expression. Gene expression levels of monocytes and MDSCs from *Arg-1*$^{fl/fl}$;*Tie2*^{Cre} animals were normalized to GAPDH and are presented as the fold-induction ($2^{-\Delta\Delta Ct}$) value relative to monocytes and MDSCs isolated from *Arg-1*$^{fl/fl}$;*Tie2*^{null} animals.

Gene expression analysis of FACS-purified leukocytes from nanoparticle treated animals

Viable monocytes ($CD45^+Ly6G^-Ly6C^+F4/80^-$) and MDSCs ($CD45^+Ly6G^+Ly6C^+CD11b^{high}F4/80^-$) from the soft tissue surrounding the infected knee were sorted by FACS on a FACSAria (BD Biosciences), whereupon RNA was immediately isolated on spin columns using an RNeasy Plus Micro Kit (QIAGEN, Hilden, Germany). cDNA was synthesized using the iScript™ cDNA Synthesis Kit (Bio-Rad, Hercules, CA). Pre-amplification reactions were conducted according to the manufacturer's instructions using a Bio-Rad CFX Connect™ thermocycler. Pre-amplified cDNA samples were diluted 1:2 in PCR molecular grade water and RT-qPCR was performed using TaqMan primer/probe mixes (Applied Biosystems, Foster City, CA) for the following genes: Arg-1, IL-10, IL-4, triggering receptor expressed on myeloid cells 2 (Trem2), hypoxia-inducible factor-alpha (HIF1-α), inducible nitric oxide synthase (iNOS), TNF-α, and Trem1. The housekeeping gene GAPDH was used to normalize expression levels. Primer/probe sets were optimized to PCR cycling conditions (95°C, 10 min; 95°C, 15 s; 60°C, 1 min – 40 cycles of steps 2 and 3). The cycle threshold for a particular gene in monocytes and macrophages was normalized to GAPDH cycle threshold to calculate the ΔCt value. The ΔΔCt value was derived by comparing the ΔCt values of monocytes and MDSCs from CTO treated animals to the ΔCt values of monocytes and MDSCs from CT treated animals to determine fold induction ($2^{-\Delta\Delta Ct}$).

17) Statistics

Significant differences between experimental groups were determined by an unpaired two-tailed Student *t*-test or a one-way ANOVA with Bonferroni's multiple comparisons using GraphPad Prism 6 (GraphPad Software, La Jolla, CA). For all analysis $p < 0.05$ was considered statistically significant.

Chapter 3: Metabolic reprogramming promotes monocytes pro-inflammatory activity and *Staphylococcus aureus* biofilm clearance

Publication (in resubmission):

Yamada KJ, Xi X, Attri KS, Zhang W, Singh PK, Bronich TK, Kielian T. 2018. Nanoparticle targeting of monocyte metabolism to treat *Staphylococcus aureus* prosthetic joint infection. ***J. Immunol.***, in revision.

Abstract

Biofilm-associated prosthetic joint infections (PJIs) cause significant morbidity due to their recalcitrance to immune-mediated clearance and antibiotics, with *Staphylococcus aureus* (*S. aureus*) among the most prevalent pathogens. Our previous studies demonstrated that *S. aureus* biofilm-associated monocytes are polarized to an anti-inflammatory phenotype and the adoptive transfer of pro-inflammatory macrophages attenuated biofilm burden, highlighting the critical role of monocyte/macrophage polarization in dictating biofilm persistence. The inflammatory properties of leukocytes are linked to their metabolic state, where anti-inflammatory macrophages primarily rely on oxidative phosphorylation (OxPhos) and pro-inflammatory macrophages utilize aerobic glycolysis. Here we demonstrate that biofilm-associated monocytes exhibit a metabolic bias favoring OxPhos and less glycolysis to facilitate their anti-inflammatory activity and biofilm persistence. To shift monocyte metabolism *in vivo* and reprogram cells to a pro-inflammatory state, a novel nanoparticle approach was utilized to deliver the OxPhos inhibitor oligomycin to monocytes. Using a mouse model of *S. aureus* PJI, >85% of oligomycin nanoparticles were internalized by monocytes, which significantly reduced *S. aureus* biofilm burden by altering metabolism and promoting the pro-inflammatory properties of infiltrating monocytes as revealed by metabolomics and RT-qPCR, respectively. Injection of oligomycin alone had no effect on monocyte metabolism or biofilm burdens, establishing that intracellular delivery of oligomycin is required to reprogram monocyte metabolic activity and oligomycin lacks antibacterial activity against *S. aureus* biofilms. Remarkably, monocyte metabolic reprogramming with oligomycin nanoparticles was effective at clearing established biofilms in combination with systemic antibiotics. These findings suggest that metabolic reprogramming of biofilm-associated monocytes may represent a novel therapeutic approach for PJI.

Introduction

The frequency of orthopedic procedures, such as total knee and total hip arthroplasty (TKA and THA, respectively), continues to increase and is predicted to reach an annual rate in the United States by 2030 of 572,000 and 3.48 million, respectively (125, 126). Although most surgeries are successful, devices may fail following prosthetic joint infection (PJI), a complication that can cause sustained disability and increased health care costs attributable to prolonged antibiotic treatment and multiple surgeries. The estimated annual incidence of prosthetic joint infection (PJI) in the United States is 2.18% for all THAs and TKAs; however, the infection rate following revision surgery is even higher (i.e. 3.2-5.6% for both THA and TKAs). The current standard-of-care for PJIs includes removal of the infected hardware, placement of an antibiotic-impregnated polymethylmethacrylate spacer for 4-6 weeks until the infection has resolved, followed by a second surgery to insert a new prosthesis. This demonstrates the importance of developing novel therapeutic approaches to treat biofilm-associated infections without requiring multiple surgical interventions (107, 108, 110, 111, 124).

Staphylococcus aureus (*S. aureus*) is a leading cause of PJI that is characterized by biofilm formation (111), and with the increased prevalence of methicillin-resistant *S. aureus* (MRSA) this pathogen has become an even greater therapeutic challenge (10). Biofilm infections persist despite antibiotic therapy due, in part, to decreased metabolic activity of biofilm-associated bacteria and evasion of the immune response (86, 111, 278). Our laboratory was the first to demonstrate that *S. aureus* biofilms skew the host immune response towards an anti-inflammatory state (139). This is evident by the polarization of anti-inflammatory monocytes/macrophages (MΦs) and abundance of myeloid-derived suppressor cells (MDSCs) (138, 148, 188, 189). MDSCs are a heterogeneous population of immature myeloid progenitors with the capacity to differentiate into mature granulocytes or MΦs given the appropriate environmental cues (227-229, 232). However, during chronic pathological conditions, such as cancer, infection, or autoimmune disorders, MDSCs are often arrested in an immature state where

they can inhibit T cell activation and monocyte/MΦ pro-inflammatory properties (227-229). We have demonstrated that MDSCs are integral to *S. aureus* biofilm establishment and persistence and polarize infiltrating monocytes towards an anti-inflammatory phenotype (146, 148, 189). These effects are mediated, in part, via IL-10 production by MDSCs, which can block NF-κB activation in monocytes and MΦs and down-regulate cytokine expression (106, 148, 189). In addition, MDSC depletion augmented monocyte pro-inflammatory activity, which translated into reduced biofilm burden (148, 189). Biofilm clearance is also facilitated by the adoptive transfer of pro-inflammatory MΦs at the site of biofilm infection (138). Therefore, the immune polarization state of monocytes and MΦs plays a key role in dictating biofilm persistence and this is influenced, in part, by MDSC-derived factors.

Recent studies have shown that the inflammatory phenotype of MΦs is intimately tied to their metabolic state. For example, anti-inflammatory MΦs rely primarily on oxidative phosphorylation (OxPhos) to drive their suppressive activity (256, 257, 260, 279). However, upon exposure to pro-inflammatory stimuli, MΦs favor aerobic glycolysis (256, 257, 260, 279-281). *In vitro* studies have shown that MΦ metabolic switches are facilitated by global changes in gene expression. Pro-inflammatory MΦs express the highly active PFK-2 isoform, u-PFK2 (ubiquitous phosphofructokinase) and down-regulate TCA cycle enzymes, promoting intracellular accumulation of glucose, succinate, and citrate (256, 260). In contrast, anti-inflammatory MΦs express the less active PFK-2 isoform PFKB1 and upregulate CD36 to facilitate triglyceride uptake to fuel the TCA cycle (256, 260, 282, 283). Of note, monocytes outnumber MΦs in our mouse PJI model and we have shown that monocytes are also polarized toward an anti-inflammatory state during *S. aureus* biofilm infection (106, 146, 148, 189). However, it is not known whether these anti-inflammatory monocytes can be metabolically reprogrammed to induce pro-inflammatory activity and biofilm clearance.

Monocyte metabolism and inflammatory phenotypes exist within a spectrum and shift in response to environmental stimuli. Here we show that monocytes infiltrating *S. aureus* biofilms

shift their metabolism towards OxPhos, and away from glycolysis. To demonstrate that the metabolic profile of biofilm-associated monocytes can be modified to promote their pro-inflammatory activity, we utilized novel cell-targeted nanoparticles containing the OxPhos inhibitor, oligomycin (284). Nanoparticles were conjugated with tuftsin, a tetrapeptide derived from the Fc domain of the IgG heavy chain, to target FcR-mediated uptake in monocytes (285, 286). *In vivo*, Cy5-labeled oligomycin nanoparticles were preferentially internalized by monocytes, with minimal uptake by MDSCs or neutrophils. Using a mouse model of *S. aureus* PJI, oligomycin nanoparticles inhibited monocyte OxPhos activity and shifted cells to a pro-inflammatory state concomitant with increased neutrophil and monocyte recruitment, resulting in significant reductions in *S. aureus* burden. Remarkably, combined treatment with oligomycin nanoparticles and systemic antibiotics reduced the titer of established biofilms below the limit of detection, a finding that to our knowledge has never been achieved for a mature biofilm *in vivo*. Collectively, monocyte metabolic reprogramming could represent a novel therapeutic avenue for circumventing the two-stage revision protocol for patients with PJI by treating an infected implant *in situ* and alleviating a second surgery, which would represent a significant reduction in patient morbidity.

Results

S. aureus biofilm infection promotes a shift towards OxPhos metabolism in monocytes.

Previous work from our laboratory has shown that *S. aureus* biofilms promote monocyte anti-inflammatory activity (146, 148, 187). To determine whether this anti-inflammatory bias is associated with a metabolic shift favoring OxPhos over glycolysis, the metabolic profiles of monocytes associated with *S. aureus* infected vs. sterile orthopedic implants were compared. OxPhos metabolism was evaluated with the bi-potential dye JC-1, which fluoresces red in mitochondria with large membrane potentials and green in depolarized mitochondria. Therefore, cells exhibiting increased OxPhos activity display a larger green:red ratio (287). OxPhos was significantly increased in monocytes recovered *S. aureus* biofilm infection compared to sterile implants at later time points (i.e. days 5-7; Fig. 3.1A), which our prior studies have demonstrated coincides with biofilm maturation as measured by antibiotic tolerance (226). Interestingly, monocyte OxPhos activity was significantly reduced during the first two days of infection (Fig. 3.1A), which may reflect an initial pro-inflammatory response that transforms over time to an anti-inflammatory state. Glycolysis was evaluated by the uptake of the fluorescent glucose analog 2-NBDG (288), which revealed significant and persistent reductions in glycolytic activity in *S. aureus* biofilm-associated monocytes compared to sterile implants (Fig. 3.1B). Collectively, increased OxPhos concomitant with reduced glycolysis in biofilm-associated monocytes corresponds with their known anti-inflammatory properties (256, 289, 290).

Figure 3.1

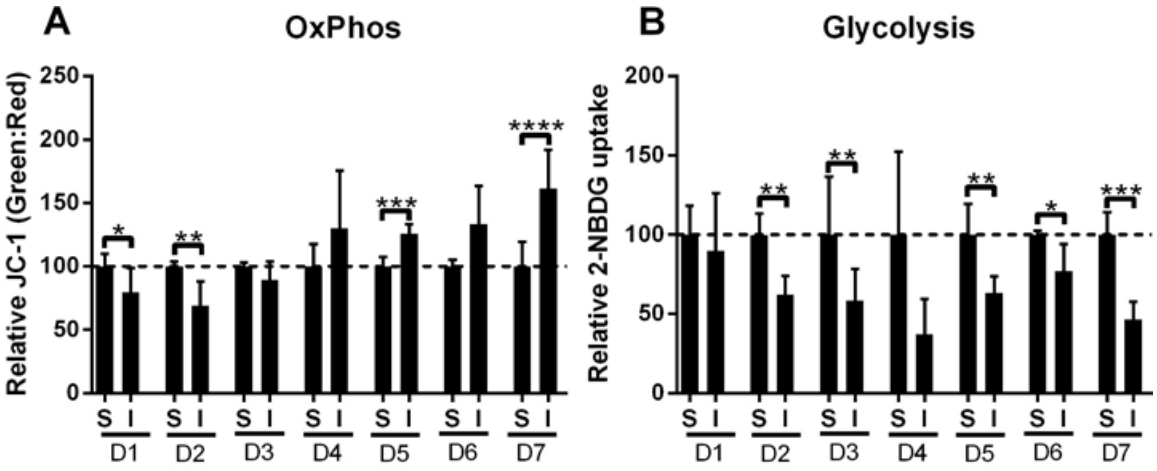

***S. aureus* biofilm infection promotes a shift towards OxPhos metabolism in monocytes.** Leukocytes associated with tissues surrounding the knee joint of mice with *S. aureus*-infected (I) or sterile (S) orthopedic implants were collected at the indicated time points (days 1-7), whereupon cells were stained with (**A**) the bi-potential dye JC-1 or (**B**) 2-NBDG as measures of OxPhos and glycolysis, respectively, and analyzed by flow cytometry. (**A**) OxPhos was calculated as the ratio of green:red monocytes ($CD11b^{high}Ly6G^{-}Ly6C^{+}F4/80^{-}$) following JC-1 staining and is reported as a percentage relative to animals receiving sterile implants. (**B**) Glycolytic activity is reported as the percentage of monocytes that were 2-NBDG^{+} relative to mice with sterile implants. Data are presented as the mean ± SD (n = 5-10 animals/group) combined from two independent experiments (*, $p < 0.05$; **, $p < 0.01$; ***, $p < 0.001$; ****, $p < 0.0001$; students *t*-test).

Inhibition of OxPhos by oligomycin promotes MΦ pro-inflammatory activity.

Since biofilm-associated monocytes displayed an OxPhos bias, we explored whether this could be attenuated to promote their pro-inflammatory activity. Oligomycin inactivates mitochondrial ATP synthase of the electron transport chain to inhibit OxPhos (284, 291-293). Prior work has demonstrated that oligomycin shifts MΦs towards aerobic glycolysis, which coincides with pro-inflammatory gene expression (284). To establish the efficacy of oligomycin in MΦ metabolic reprogramming and inflammatory capacity, mouse bone marrow-derived MΦs were treated with IL-4 in the presence/absence of oligomycin. Oligomycin decreased arginase-1 (Fig. 3.2A) and increased TNF-α expression (Fig. 3.2B) in a dose-dependent manner, hallmark genes of anti- and pro-inflammatory MΦs, respectively (138, 189, 260, 280). Total protein levels were similar between MΦs $\pm$ oligomycin treatment, indicating that alterations in gene expression were not the result of differences in cell numbers (Fig. 3.2C).

Figure 3.2

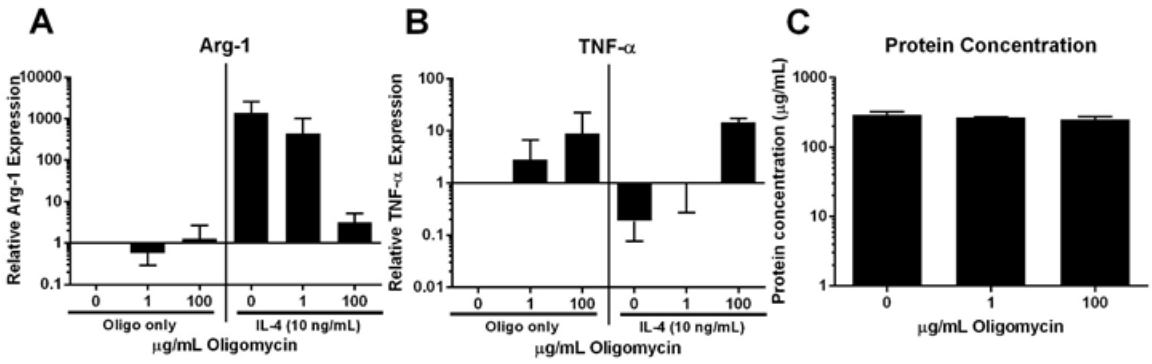

Inhibition of OxPhos by oligomycin favors MΦ pro-inflammatory activity. Bone marrow-derived MΦs were treated with IL-4 (10 ng/mL) ± various concentrations of oligomycin for 4 h, whereupon RNA was isolated for RT-qPCR analysis. (**A**) Arg-1 and (**B**) TNF-α expression was calculated after normalization to GAPDH and is presented as the fold-change relative to unstimulated MΦs. (**C**) Protein concentrations following oligomycin treatment confirming equivalent cell numbers between treatment groups. Data is presented as the mean ± SD (n = 4-6) combined from two independent experiments.

Oligomycin nanoparticles shift MΦ metabolism.

Given the ability of oligomycin to promote MΦ pro-inflammatory activity, we designed a nanoparticle delivery approach using tuftsin as a targeting moiety, to deliver oligomycin to biofilm-associated monocytes *in vivo* to enhance their pro-inflammatory activity and promote biofilm clearance. Tuftsin is a peptide derived from the Fc portion of IgG, which has been shown to facilitate nanoparticle internalization by MΦs through its interaction with Fc receptors (285, 294). Previous studies have utilized tuftsin-conjugated nanoparticles to deliver a variety of biomolecules to monocytes and MΦs in the context of arthritis, HIV, and other inflammatory diseases (285, 286, 294, 295). We utilized three nanoparticle types, namely Cy5 (C), Cy5/Tuftsin (CT), and Cy5/Tuftsin/Oligomycin (CTO), where the former two represented control formulations and all three harbored the Cy5 fluorochrome to identify nanoparticle localization *in vivo* (Table 3.1). Although oligomycin has been shown to affect MΦ respiratory capacity by inhibiting mitochondrial ATP synthase (284), to our knowledge no studies have examined the efficacy of oligomycin in a nanoparticle formulation. To establish the effects of oligomycin nanoparticles on MΦ metabolism, bone marrow-derived MΦs were treated with prototypical anti-inflammatory (IL-4) or pro-inflammatory (peptidoglycan (PGN) + IFN-γ) stimuli or CTO nanoparticles for 24 h, whereupon OxPhos and glycolytic status was examined using Seahorse Bioscience assays (Fig. 3.3). Oligomycin nanoparticles (CTO) significantly reduced MΦ basal and maximal respiratory rates compared to untreated and IL-4-stimulated cells (Fig. 3.3A, C, and D), which coincided with significantly higher glycolytic rates (Fig. 3.3B and E). The metabolic profile of CTO treated MΦs was most similar to pro-inflammatory MΦs polarized with IFN-γ + PGN, suggesting that oligomycin nanoparticles are capable of re-programming MΦ metabolism.

Table 3.1 Nanoparticle features

Abbreviations	Composition	Description
C	Cy5	fluorochrome
CT	Cy5/Tuftsin	fluorochrome + targeting
CTO	Cy5/Tuftsin/Oligomycin	fluorochrome + targeting + ETC inhibitor

Figure 3.3

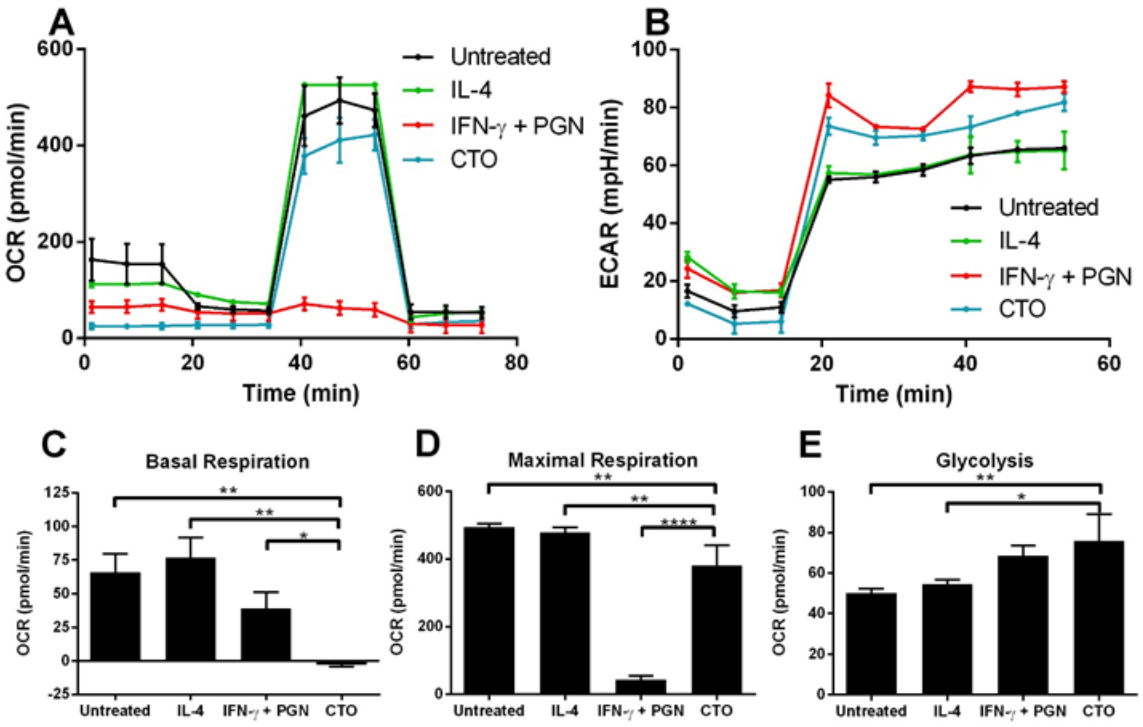

Oligomycin nanoparticles shift MΦ metabolism towards glycolysis. Bone marrow-derived MΦs were treated with IL-4 (10 ng/mL), peptidoglycan (PGN) + IFN-γ (10 μg/mL and 10 ng/mL, respectively), or Cy5/Tuftsin/Oligomycin (CTO) nanoparticles (1 μg/mL) for 24 h, whereupon Seahorse Bioscience assays were performed to assess (**A**) OxPhos and (**B**) glycolysis. (**C**) Basal and (**D**) maximal respiration, and (**E**) glycolytic rates were calculated using well-defined algorithms. Data is presented as the mean ± SD (n = 3). (*, $p < 0.05$; **, $p < 0.01$; ****, $p < 0.0001$; One-way ANOVA).

Tuftsin-conjugated nanoparticles are preferentially internalized by monocytes during S. aureus PJI.

As mentioned earlier, monocytes outnumber MΦs in our mouse PJI model (146, 148, 187, 226); therefore, to determine whether tuftsin-conjugated nanoparticles are targeted to monocytes *in vivo* during *S. aureus* PJI, mice received a single intra-articular injection of C or CT nanoparticles at day 7 post-infection, a time point corresponding to biofilm establishment (146, 148, 187, 226). Mice were sacrificed at 1, 2, or 3 days post-injection to evaluate Cy5 signal stability (Fig. 3.4A). IVIS imaging demonstrated nanoparticle retention in the joint at day 3 post-injection with signals detected out to day 12, suggesting that nanoparticles may act as a depot for continued action (Fig. 3.4B and Supplemental Fig. 3.2, respectively). Flow cytometry revealed that >85% of all $Cy5^+$ cells were monocytes ($CD45^+Ly6G^-Ly6C^+F4/80^-$), whereas minimal uptake was detected in MDSCs or neutrophils (Fig. 3.4C). Importantly, uptake of tuftsin-conjugated (CT) nanoparticles by biofilm-associated monocytes was significantly higher compared to non-coated (C) nanoparticles, where at 24 h after injection, approximately 15% of biofilm-associated monocytes were $Cy5^+$, which steadily declined to < 3.5% by 72 h post-injection (Fig. 3.4D). Collectively, these data demonstrate that tuftsin conjugation confers a high degree of specificity in targeting nanoparticles to monocytes and augments nanoparticle uptake.

Figure 3.4

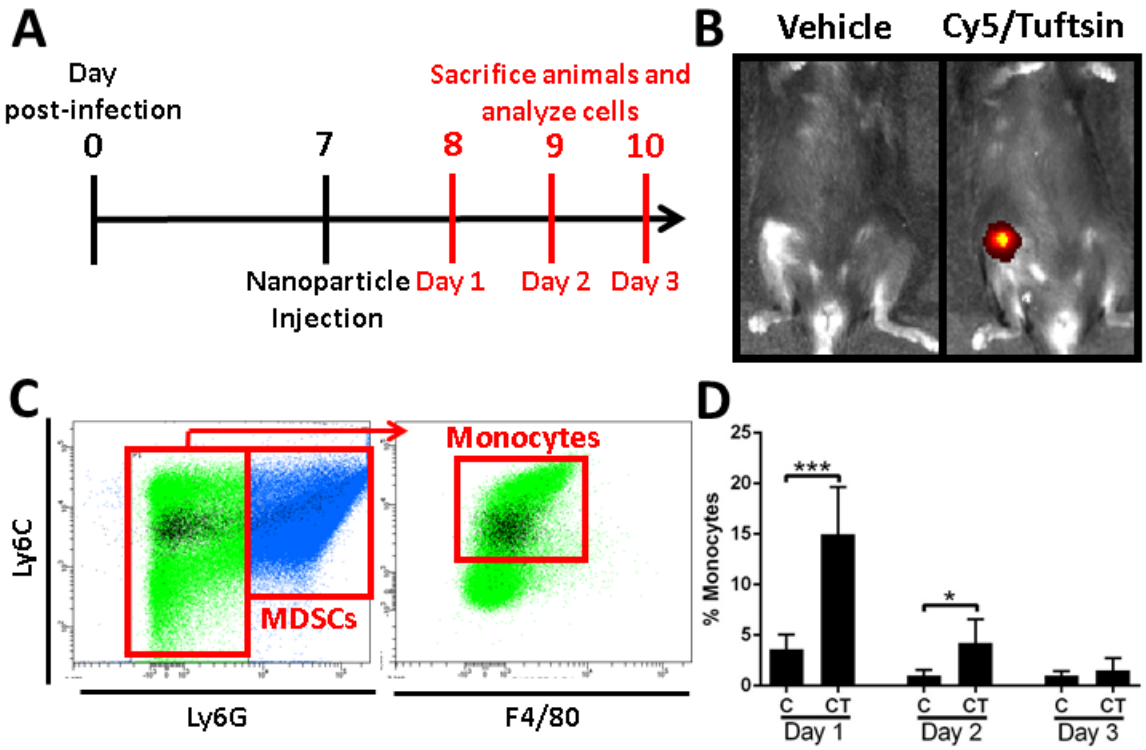

Preferential nanoparticle uptake by monocytes during PJI. (**A**) C57BL/6 mice received a single intra-articular injection of Cy5 (C) or Cy5/Tuftsin (CT) nanoparticles (10 µg) at day 7 post-infection and were analyzed on three consecutive days. (**B**) IVIS imaging of CT labeled nanoparticles in the infected joint at day 3 with representative flow plots (**C**). Left panel shows all $CD45^+$ cells and the right panel depicts $Ly6G^-Ly6C^+$ gated cells, where $Cy5^+$ monocytes ($Ly6G^-Ly6C^+F4/80^-$) are highlighted in black. (**D**) Mice receiving C or CT nanoparticles were sacrificed at 1-3 days following nanoparticle treatment, whereupon $Cy5^+$ monocytes were quantified by flow cytometry. Data is presented as the mean ± SD (n = 4-5 mice/time point). (*, $p < 0.05$; ***, $p < 0.001$; Student's *t*-test).

Oligomycin-containing nanoparticles re-program biofilm-associated monocytes towards a pro-inflammatory phenotype in vivo.

To determine whether the selective uptake of CTO nanoparticles by monocytes *in vivo* translated into metabolic re-programming, metabolomics was performed. For these studies, mice received a single intra-articular injection of CT or CTO nanoparticles at day 7 post-infection and were sacrificed 3 days later, whereupon polar metabolites were isolated from FACS-purified monocytes ($CD11b^{high}Ly6C^{+}Ly6G^{-}$ $F4/80^{-}$) and analyzed by LC-MS/MS. This interval was selected because our earlier studies determined that CTO nanoparticles had no impact on bacterial burden at day 3 post-injection (Supplemental Fig. 3.3), ensuring that any differences in monocyte activation reflected effects of CTO nanoparticles rather than alterations in bacterial abundance, which was significantly altered by day 7 (Supplemental Fig. 3.3). All biofilm-associated monocytes were analyzed, since $Cy5^{+}$ monocytes were less frequent at 3 days following nanoparticle injection (Fig. 3.4D), which precluded FACS enrichment. Principle component analysis (PCA) using unsupervised hierarchical clustering revealed distinct metabolic patterns of monocytes recovered from CT and CTO treated mice (Fig. 3.5A and B). Pathway impact analysis of differentially expressed metabolites revealed that arginine, proline, and branched chain amino acid metabolism were most significantly impacted (Fig. 3.5C). Despite these significant pathway changes, analysis of individual metabolites only identified a few significant differences, most notably decreased NAD^{+} levels in monocytes recovered from CTO treated animals (Table 3.2), indicative of OxPhos inhibition by oligomycin. To examine whether the shift in monocyte metabolism in response to oligomycin translated into enhanced pro-inflammatory properties, RT-qPCR was performed on FACS-purified monocytes using a panel of pro- and anti-inflammatory genes. Monocytes isolated from CTO treated mice displayed increased pro-inflammatory (HIF-1α, iNOS, TNF-α, and Trem1) concomitant with reduced anti-inflammatory (arginase-1, IL-10, IL-4, and Trem2) mediators compared to monocytes exposed to control (CT) nanoparticles (Fig. 3.6). The magnitude of metabolic and inflammatory mediator changes elicited by oligomycin

nanoparticles were likely modest because <5% of recovered monocytes were $Cy5^+$ (Fig. 3.4D), which further emphasizes the significance of these findings. Earlier intervals following nanoparticle injection were not examined to allow sufficient time for oligomycin to metabolically re-program monocyte metabolism following nanoparticle uptake. Collectively, these results establish that targeting oligomycin to monocytes using tuftsin nanoparticles induces a metabolic shift that promotes their pro-inflammatory properties.

Figure 3.5

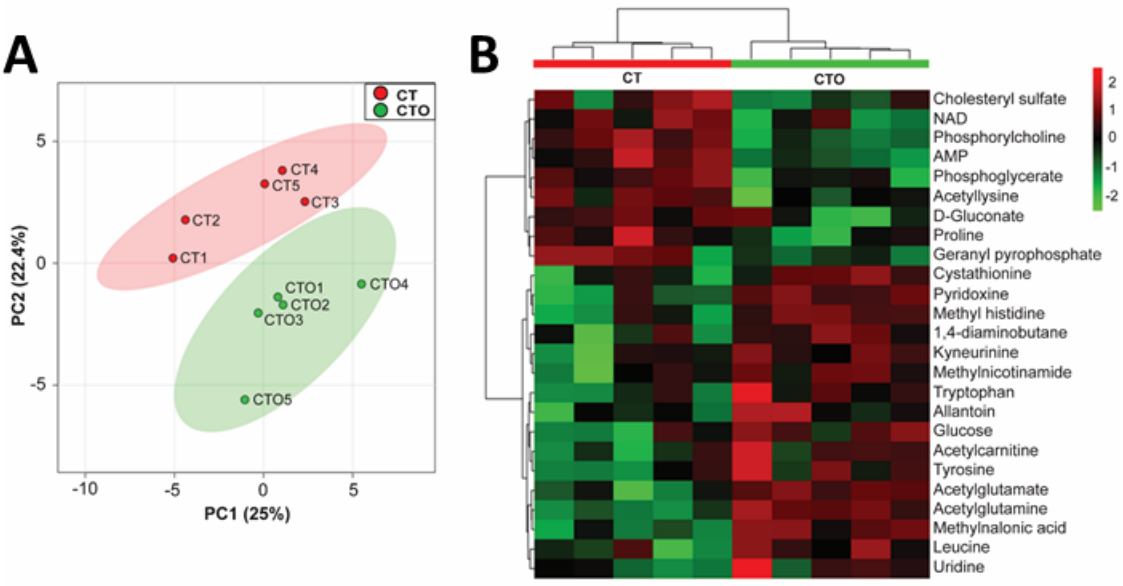

C

CTO regulated pathways in monocytes	Trend	*p*-value
Arginine and Proline Metabolism	↓	0.0134
Valine, Leucine & Isoleucine Metabolism	↓	0.0113

Oligomycin-containing nanoparticles induce a metabolic shift in biofilm-associated monocytes *in vivo*. C57BL/6 mice received a single intra-articular injection of Cy5/Tuftsin (CT) or Cy5/Tuftsin/Oligomycin (CTO) nanoparticles (10 μg) at day 7 post-infection (n = 5 mice/treatment group). Mice were sacrificed 3 days following nanoparticle injection and monocytes ($CD11b^{high}Ly6G^{-}Ly6C^{+}F4/80^{-}$) were recovered from each individual animal by FACS, whereupon intracellular metabolites were isolated for analysis by HPLC-MS/MS. (**A**) A principle component analysis (PCA) plot was generated using an algorithm in MetaboAnalyst with mean intensities and pareto scaling distribution. Ellipses represent a 95% confidence interval of the normal distribution for each cluster. (**B**) The heat-map depicts the top 25 metabolite differences in monocytes recovered from CTO and CT treated mice. The color key indicates $\log_2$-fold changes of normalized-mean peak intensities for metabolites in monocytes from CTO treated animals normalized to the CT nanoparticle treated group. (**C**) Identification of the most significantly

altered pathways in monocytes isolated from CTO treated animals as determined by pathway impact analysis.

Table 3.2. Intracellular metabolites from CT and CTO treated MDSCs and monocytes*

	MDSCs				Monocytes			
	CT	CTO	Fold Δ	P-value	CT	CTO	Fold Δ	P-value
NADH	230.96	987.24	4.27	**0.0001**				
AMP	28448.06	30887.49	1.09	0.4732	8049.87	3738.80	0.46	**0.0131**
phosphorylcholine	54710.35	42805.98	0.78	0.0887	59220.23	23283.73	0.39	**0.0039**
phosphoglycerate	3675.21	2552.41	0.69	**0.0087**	2094.56	693.79	0.33	**0.0230**
amino octanoic acid	359348.45	214208.79	0.60	**0.0150**	198258.16	166393.41	0.84	0.5679
octulose monophosphate	1251.47	652.06	0.52	**0.0072**	1056.36	1375.83	1.30	0.1732
hexose phosphate	4513.27	1978.78	0.44	**0.0060**	1261.01	1041.04	0.83	0.5358
methyl-oxo-pentanoate	4295.21	1879.28	0.44	0.1140	3283.94	1856.03	0.57	**0.0493**
proline	14840.42	6255.23	0.42	**0.0219**	36241.89	17299.73	0.48	0.0600
argininosuccinate	13556.30	5689.39	0.42	**0.0224**	13053.01	9895.81	0.76	0.3789
acetylcarnitine	4737020.76	1980968.73	0.42	**0.0074**	2705159.57	2617356.63	0.97	0.9108
glycerophosphocholine	224161.08	92877.93	0.41	**0.0001**	284310.52	258921.43	0.91	0.7302
malate	6270.01	2564.13	0.41	**0.0005**	6923.16	7305.33	1.06	0.8244
biotin	22832.65	8173.01	0.36	**0.0016**	38784.23	25758.81	0.66	0.2101
carbamoyl aspartate	15839.22	5539.75	0.35	**0.0001**	17379.64	11672.62	0.67	0.2083
1,4-diaminobutane	1669.81	575.51	0.34	**0.0086**	1991.87	2058.02	1.03	0.9245
aspartate	43571.45	14625.59	0.34	**0.0041**	39461.81	30715.02	0.78	0.3703
acetyl ornithine	427325.21	141033.61	0.33	**0.0061**	369919.76	329268.98	0.89	0.6792
arginine	654825.55	215629.05	0.33	**0.0089**	537270.27	496236.71	0.92	0.7618
geranyl pyrophosphate	4059.84	1297.46	0.32	**0.0076**	3787.62	2600.52	0.69	0.2682
thiamine	12741.25	3979.46	0.31	**0.0003**	18692.29	13920.87	0.74	0.2821
phenyl acetylglutamine	47370.51	14792.02	0.31	**0.0060**	44993.63	30845.69	0.69	0.3015
pipecolic acid	96831.86	300066.48	0.31	**0.0000**	1346786.74	1164982.29	0.87	0.5991
inosine	4503.24	1373.42	0.30	**0.0010**	2542.28	1834.50	0.72	0.3929
methylnicotinamide	15618.70	4716.50	0.30	**0.0175**	11210.60	10691.12	0.95	0.8729
methionine sulfoxide	14441.79	4322.62	0.30	**0.0287**	16613.50	16020.02	0.96	0.9054
acetylserine	304852.03	90174.14	0.30	**0.0000**	420870.73	361506.78	0.86	0.6131
dimethyglycine	596357.10	176288.74	0.30	**0.0003**	680422.89	576081.09	0.85	0.5455
mesaconic acid	3138832.39	902198.18	0.29	**0.0029**	2613194.80	2171897.97	0.83	0.4744
itaconic acid	418700.34	120019.94	0.29	**0.0028**	377928.56	302611.59	0.80	0.3956
pyrophosphate	344093.90	97693.23	0.28	**0.0021**	234661.09	211191.49	0.90	0.6907

Table 3.2 (cont.). Intracellular metabolites from CT and CTO treated MDSCs and monocytes*

	MDSCs				Monocytes			
	CT	CTO	Fold Δ	P-value	CT	CTO	Fold Δ	P-value
leucine	595958.48	168025.76	0.28	**0.0004**	681946.44	619007.47	0.91	0.7277
spermidine	1068.74	297.65	0.28	**0.0219**	2486.46	1862.20	0.75	0.3961
glutamine	46272.09	12879.45	0.28	**0.0009**	56231.97	47633.94	0.85	0.6012
metanephrine	17549.15	4814.09	0.27	**0.0022**	19088.25	17776.91	0.93	0.8259
betaine	46961.12	12616.09	0.27	**0.0050**	28747.46	23328.76	0.81	0.5316
7-methylguanosine	17752.88	4763.33	0.27	**0.0000**	27813.06	24382.54	0.88	0.6404
citrate	1792491.13	472481.58	0.26	**0.0036**	1282441.02	1265529.03	0.99	0.9590
creatinine	858105.55	224150.40	0.26	**0.0000**	1283060.49	1050524.89	0.82	0.5022
lysine	412700.45	106913.54	0.26	**0.0002**	515826.83	448887.04	0.87	0.6085
indole	463265.15	116725.17	0.25	**0.0002**	470724.70	339231.95	0.72	0.3317
hypoxanthine	324937.56	80617.09	0.25	**0.0000**	487605.85	391813.14	0.80	0.4420
carnitine	143660.50	35568.69	0.25	**0.0078**	206066.04	133416.41	0.65	0.1979
lactate	10938.99	2690.17	0.25	**0.0006**	16907.24	12507.33	0.74	0.2566
ornithine	145540.65	35614.43	0.24	**0.0001**	137901.12	127836.07	0.93	0.7911
choline	2217322.04	531963.86	0.24	**0.0055**	2020691.48	1739095.78	0.86	0.5847
amino isobutyrate	12290.65	2921.84	0.24	**0.0002**	10622.32	9508.84	0.90	0.6461
acetyl glutamate	61562.01	14549.64	0.24	**0.0001**	65764.10	70330.71	1.07	0.8062
phenylpropiolic acid	890.53	198.35	0.22	**0.0012**	816.78	786.69	0.96	0.9399
cystathionine	3953.59	876.94	0.22	**0.0401**	2903.78	2815.83	0.97	0.9045
glutamate	1222459.00	269634.98	0.22	**0.0056**	1260582.55	1048365.28	0.83	0.5155
2-hydroxygluterate	1178.11	258.93	0.22	**0.0292**	551.86	684.59	1.24	0.5719
creatine	2184525.87	477143.44	0.22	**0.0075**	1924037.06	1500330.74	0.78	0.3511
betaine aldehyde	11707.97	2537.86	0.22	**0.0104**	9938.89	8862.38	0.89	0.7446
cholesteryl sulfate	17872.15	3857.99	0.22	**0.0117**	18794.03	12592.39	0.67	0.2539
anthranilate	3867.51	824.43	0.21	**0.0124**	3144.91	1898.86	0.60	0.3293
methyl histidine	117630.38	24551.32	0.21	**0.0097**	106123.92	110072.95	1.04	0.8923
succinate	5187.26	1071.83	0.21	**0.0056**	5581.73	4892.55	0.88	0.6752
aconitate	3470.42	701.06	0.20	**0.0011**	4137.89	4142.85	1.00	0.9971
pyridoxine	892902.77	171808.98	0.19	**0.0081**	729019.37	778520.79	1.07	0.8037
tyrosine	151214.76	29057.79	0.19	**0.0070**	130431.15	123118.45	0.94	0.8476
1-methyladenosine	31864.27	6109.45	0.19	**0.0000**	37126.74	33451.71	0.90	0.7631

Table 3.2 (cont.). Intracellular metabolites from CT and CTO treated MDSCs and monocytes*

	MDSCs				Monocytes			
	CT	CTO	Fold Δ	P-value	CT	CTO	Fold Δ	P-value
methylcysteine	162442.78	30426.18	0.19	**0.0071**	141086.24	127112.91	0.90	0.7304
tryptophan	179625.10	33535.58	0.19	**0.0046**	133199.94	137709.31	1.03	0.9210
glucose	42435.23	7658.38	0.18	**0.0028**	33657.50	32159.00	0.96	0.8825
Ng,NG-dimethyl-L-arginine	311055.15	56018.05	0.18	**0.0049**	305985.17	265305.75	0.87	0.6235
D-gluconate	5531.46	977.45	0.18	**0.0037**	5885.43	4126.70	0.70	0.3181
acetylglutamine	1991829.48	351228.24	0.18	**0.0062**	1653195.62	1708981.37	1.03	0.9040
myo-inositol	82324.23	14296.03	0.17	**0.0054**	63890.10	59667.70	0.93	0.7999
xanthosine	55213.12	9201.99	0.17	**0.0000**	74332.18	65463.52	0.88	0.7029
allantoin	8097.74	1299.27	0.16	**0.0006**	7292.10	8242.82	1.13	0.7087
valine	30293.38	4833.61	0.16	**0.0056**	31134.19	26913.39	0.86	0.6077
kyneurinine	12216.08	1884.32	0.15	**0.0054**	7923.02	10551.98	1.33	0.4320
nicotinamide	148691.12	22747.25	0.15	**0.0013**	92465.86	106831.39	1.16	0.7327
pantothenate	103332.69	15649.02	0.15	**0.0093**	94030.70	86732.95	0.92	0.7991
methylmalonic acid	8013.86	1210.10	0.15	**0.0104**	5162.45	6284.79	1.22	0.5080
acetyllysine	10319.45	1532.13	0.15	**0.0092**	11230.10	7776.12	0.69	0.2379
cytidine	300405.65	43954.29	0.15	**0.0082**	221483.90	166574.21	0.75	0.3849
xanthurenic acid	3490.77	490.47	0.14	**0.0125**	4869.40	5399.37	1.11	0.7607
hypoxanthine	3681.43	448.85	0.12	**0.0185**	4291.35	3793.19	0.88	0.6975
2-dehydro-D-gluconate	3741.68	417.12	0.11	**0.0088**	3126.74	2136.40	0.68	0.3685
beta hydroxybutyrate	993.14	44.63	0.04	**0.0157**	550.54	375.74	0.68	0.5021

***Fold-change values are expressed as CTO relative to CT.**

Figure 3.6

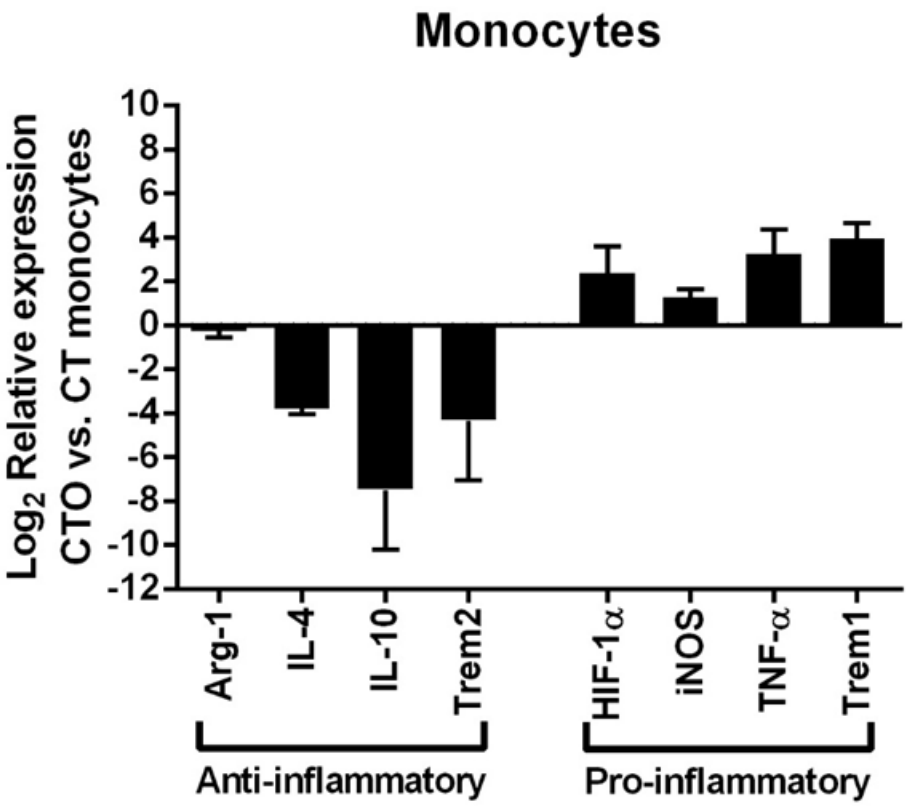

Oligomycin-containing nanoparticles polarize monocytes towards a pro-inflammatory phenotype *in vivo*. C57BL/6 mice received a single intra-articular injection of Cy5/Tuftsin (CT) or Cy5/Tuftsin/Oligomycin (CTO) nanoparticles (10 μg) at day 7 post-infection (n = 5 mice/treatment group). Mice were sacrificed 3 days following nanoparticle injection and monocytes ($CD11b^{high}Ly6G^{-}Ly6C^{+}F4/80^{-}$) were sorted from pooled samples (n = 5) by FACS, whereupon RNA was immediately isolated for RT-qPCR. Gene expression levels in monocytes recovered from CTO-treated animals were calculated after normalizing signals to GAPDH and are presented as the fold-change relative to monocytes isolated from mice receiving CT (control) nanoparticles. Data is presented as the mean ± SD (n = 3) combined from three independent experiments.

***Monocyte targeted oligomycin nanoparticles induce metabolomic and gene expression changes in MDSCs, indicative of cellular crosstalk*.**

Prior studies have identified a significant role for MDSCs in promoting monocyte anti-inflammatory activity during *S. aureus* orthopedic biofilm infection (146, 148, 189). Although <0.01% of MDSCs internalized tufstin nanoparticles (Fig. 3.4C), we were interested in determining the degree of cross-talk between metabolically altered monocytes and MDSCs. MDSCs ($CD11b^{high}Ly6C^{+}Ly6G^{+}F4/80^{-}$) were purified from CT and CTO treated animals, whereupon metabolomics and inflammatory gene expression were examined. Remarkably, although nanoparticle uptake was negligible in MDSCs, their metabolic profile was dramatically affected by CTO treatment (Fig. 3.7A and B), with the number of significant differentially expressed metabolites far outnumbering those for monocytes (Table 3.2). Metabolic pathway analysis revealed significant increases in glutathione, nicotinamide, taurine, and purine metabolism, whereas arginine, glutamine, and cyclic chain amino acids were significantly reduced (Fig. 3.7C). In contrast, RT-qPCR analysis was less straightforward, since anti-/pro-inflammatory mediator expression in MDSCs following CTO nanoparticle treatment did not display a discernable gene expression pattern consistent with a specific function (Fig. 3.7D). These results are the first to demonstrate that metabolic re-programming of monocytes can impact MDSC metabolism, which supports our earlier work of MDSC-monocyte crosstalk (146, 148, 189).

Figure 3.7

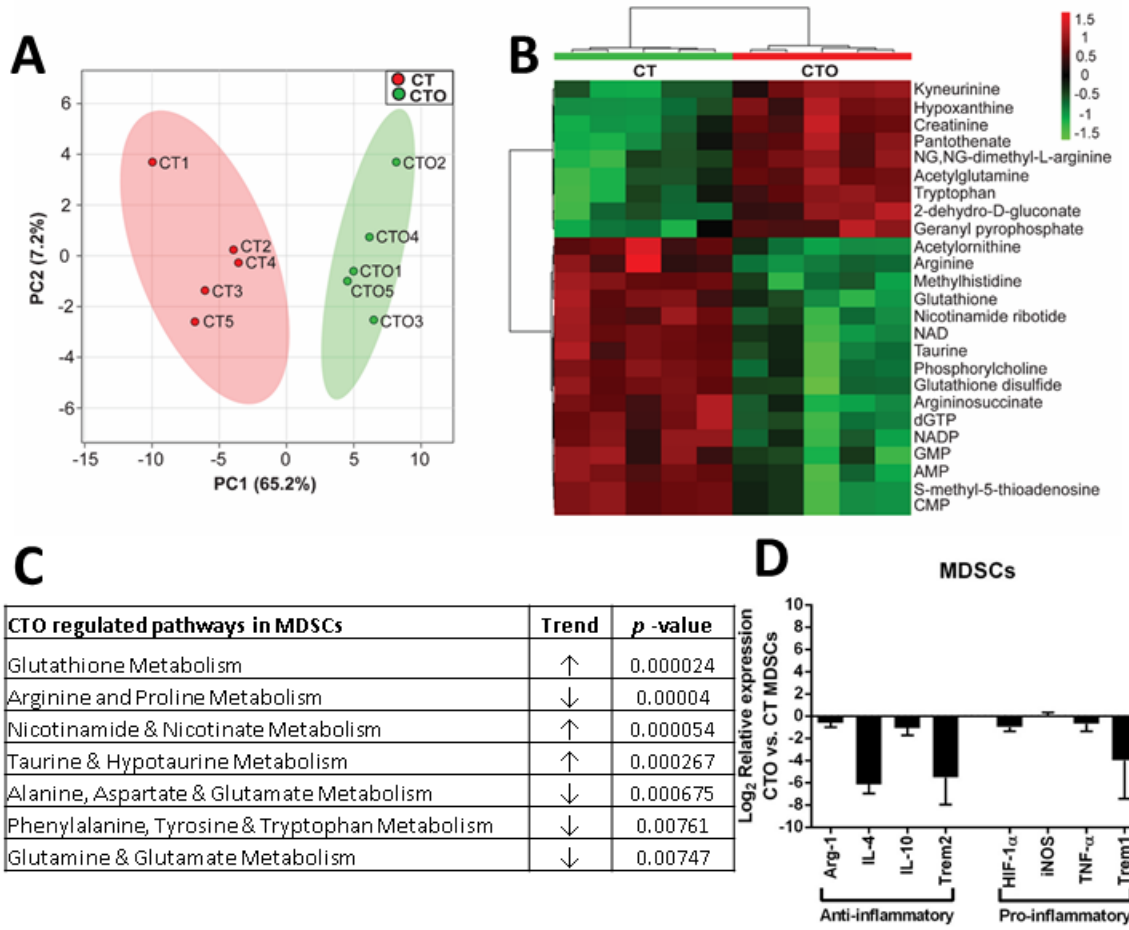

CTO regulated pathways in MDSCs	Trend	*p* -value
Glutathione Metabolism	↑	0.000024
Arginine and Proline Metabolism	↓	0.00004
Nicotinamide & Nicotinate Metabolism	↑	0.000054
Taurine & Hypotaurine Metabolism	↑	0.000267
Alanine, Aspartate & Glutamate Metabolism	↓	0.000675
Phenylalanine, Tyrosine & Tryptophan Metabolism	↓	0.00761
Glutamine & Glutamate Metabolism	↓	0.00747

Oligomycin-containing nanoparticles targeted to monocytes induce metabolomic and gene expression changes in MDSCs. C57BL/6 mice received a single intra-articular injection of Cy5/Tuftsin (CT) or Cy5/Tuftsin/Oligomycin (CTO) nanoparticles (10 μg) at day 7 post-infection (n = 5 mice/treatment group). Mice were sacrificed 3 days following nanoparticle injection and MDSCs ($CD11b^{high}Ly6G^{+}Ly6C^{+}F4/80^{-}$) were recovered from each individual animal by FACS, whereupon intracellular metabolites were isolated for analysis by HPLC-MS/MS. (**A**) A principle component analysis (PCA) plot was generated using an algorithm in MetaboAnalyst with mean intensities and pareto scaling distribution. Ellipses represent a 95% confidence interval of the normal distribution for each cluster. (**B**) The heat-map depicts the top 25 metabolite differences in MDSCs recovered from CTO and CT treated mice. The color key indicates $\log_2$-fold changes of

normalized-mean peak intensities for metabolites in MDSCs from CTO treated animals normalized to the CT nanoparticle treated group. (**C**) Identification of the most significantly altered pathways in MDSCs isolated from CTO treated animals as determined by pathway impact analysis. (**D**) MDSCs were sorted from pooled samples (n = 5 mice/group), whereupon RNA was immediately isolated for RT-qPCR. Gene expression levels in MDSCs recovered from CTO-treated animals were calculated after normalizing signals to GAPDH and are presented as the fold-change relative to MDSCs isolated from mice receiving CT (control) nanoparticles. Data shown as the mean ± SD (n = 3), combined from three independent experiments.

Nanoparticle-mediated delivery of oligomycin to monocytes attenuates established S. aureus PJI.

We next examined whether the observed metabolic re-programming and pro-inflammatory properties of biofilm-associated monocytes following oligomycin nanoparticle administration would impact biofilm clearance during *S. aureus* PJI. Two treatment paradigms were designed to examine the effect of monocyte metabolic re-programming during acute tissue infection versus an established biofilm (days 3 and 7 post-infection, respectively). Mice received a single intra-articular injection of control (C and CT) or oligomycin (CTO) nanoparticles on either day 3 (Supplemental Fig. 3.4) or day 7 post-infection (Fig. 3.8), whereupon bacterial burden and leukocyte infiltrates were examined over a 28 day period. In both settings, bacterial burdens were significantly reduced in the soft tissue, joint, femur, and implant between 7 and 28 days following nanoparticle injection (Supplemental Fig. 3.4 and Fig. 3.8, B-E). Interestingly, despite the reductions in bacterial titers at day 7 with CTO nanoparticles in both treatment paradigms, no significant differences in MDSC ($CD11b^{high}Ly6C^{+}Ly6G^{+}F4/80^{-}$), PMN ($CD11b^{low}Ly6C^{+}Ly6G^{+}F4/80^{-}$), monocyte ($CD11b^{high}Ly6C^{+}Ly6G^{-}F4/80^{-}$), or MΦ ($CD11b^{high}Ly6C^{-}Ly6G^{-}F4/80^{+}$) infiltrates were observed (Supplemental Fig. 3.4 and Fig. 3.8, F-I). However, at later time points (i.e. days 14 to 28 after nanoparticle treatment) mice receiving CTO nanoparticles had significantly fewer MDSCs concomitant with increased PMN, monocyte, and MΦ infiltrates, reflective of a more pro-inflammatory milieu (Fig. 3.8 and Supplemental Fig. 3.4, F-I).

To establish that the ability of oligomycin nanoparticles to attenuate *S. aureus* biofilm burdens resulted from monocyte metabolic reprogramming rather than direct antibacterial activity, mice were treated with free oligomycin only, empty nanoparticles (CT) with free oligomycin (not loaded), or oligomycin loaded nanoparticles (CTO). Free oligomycin was administered at a dose that was equivalent to the nanoparticle formulation (100 ng). Only CTO nanoparticles led to significant reductions in monocyte OxPhos activity, as revealed by JC-1

staining (Fig. 3.9A and C). This was independent of bacterial burdens, since CTO nanoparticles reduced monocyte OxPhos as early as day 3 post-treatment when no differences in biofilm titers were observed (Fig. 3.9B). Overall, no changes in glycolytic activity were observed with CTO nanoparticles (Fig. 3.9A and C); however, the reductions in OxPhos support a net glycolytic bias in monocytes following CTO treatment, which agrees with their enhanced pro-inflammatory activity (Fig. 3.6). Importantly, no changes in monocyte OxPhos or biofilm burdens were observed in animals treated with free oligomycin or CT nanoparticles + free oligomycin (not loaded) at either 3 or 7 days after intra-articular injection (Fig. 3.9). Furthermore, oligomycin delivery by direct intra-articular injection into the infected joint in either one bolus or two sequential doses also had no effect on bacterial burdens (Supplemental Figure 3.5). Finally, oligomycin displayed no bactericidal activity against *S. aureus* during early biofilm formation or mature biofilms *in vitro* (Supplemental Figure 3.6), which agrees with prior reports demonstrating that oligomycin does not possess any direct anti-bacterial activity against *S. aureus* (296, 297). Collectively, these results establish that the anti-biofilm effects of oligomycin are dependent on targeted intracellular delivery to monocytes and their subsequent metabolic re-programming to elicit pro-inflammatory activity, and not as an antibiotic.

Figure 3.8

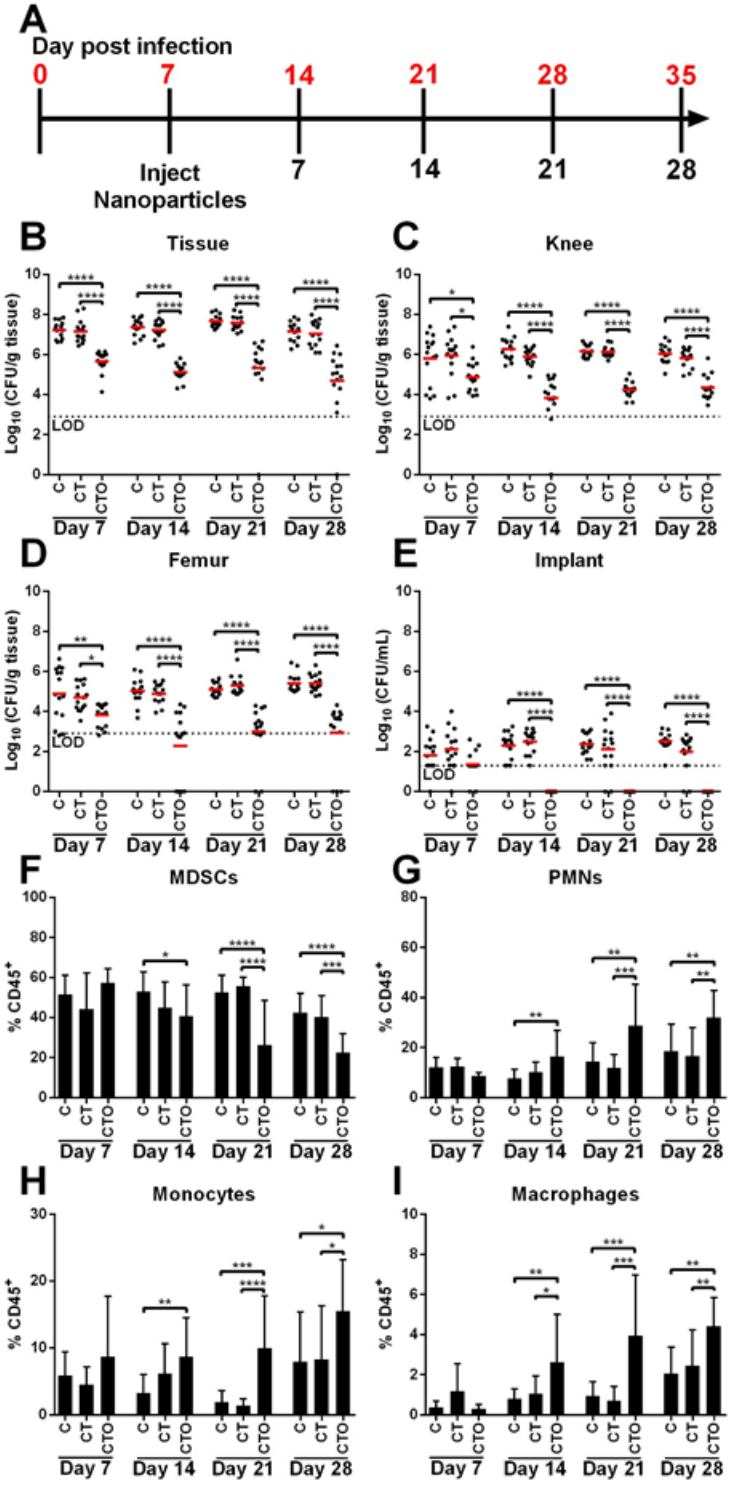

Nanoparticle-mediated delivery of oligomycin to monocytes reduces established biofilm infection. (**A**) C57BL/6 mice received a single intra-articular injection of Cy5 (C), Cy5/Tuftsin

(CT), or Cy5/Tuftsin/Oligomycin (CTO) nanoparticles at day 7 post-infection, and were analyzed at 7, 14, 21, or 28 days following nanoparticle treatment. Bacterial burdens were quantified in the (**B**) surrounding soft tissue, (**C**) knee, (**D**) femur, and (**E**) implant, where the red and dotted lines represent the mean and limit of detection (LOD), respectively. Infiltrating leukocytes were analyzed by flow cytometry and (**F**) MDSCs, (**G**) PMNs, (**H**) monocytes, and (**I**) MΦs are reported as the mean percentage of live $CD45^+$ leukocytes ± SD. Results are combined from three independent experiments (n = 15 mice/group/time point). (*, $p < 0.05$; **, $p < 0.01$; ***, $p < 0.001$; ****, $p < 0.0001$; One-way ANOVA).

Figure 3.9

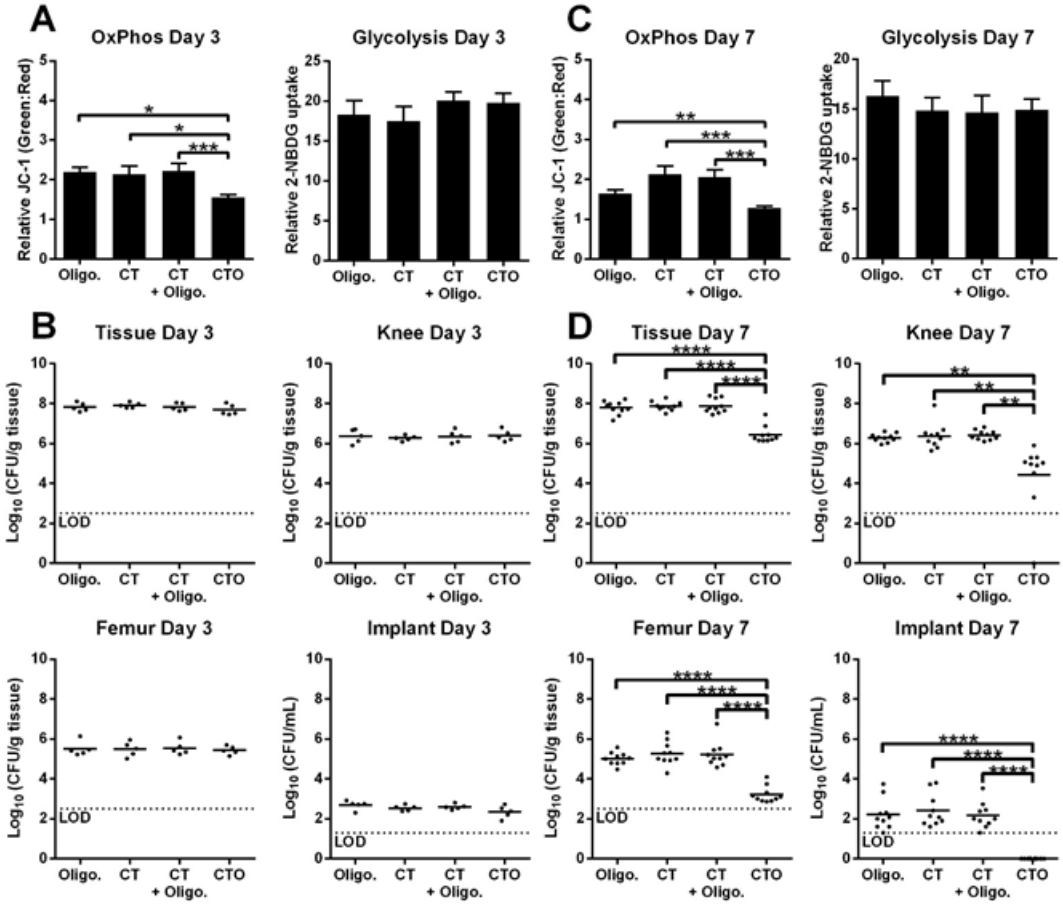

Nanoparticle-mediated delivery of oligomycin attenuates OxPhos metabolism in biofilm-associated monocytes. C57BL/6 mice received a single intra-articular injection of free oligomycin only, empty nanoparticles (CT), empty nanoparticles (CT) with free oligomycin (not loaded), or oligomycin loaded nanoparticles (CTO) at day 7 post-infection, and were analyzed at day 3 (**A, B**) or 7 (**C, D**) after treatment. (**A, C**) OxPhos was calculated as the ratio of green:red monocytes ($CD11b^{high}Ly6G^{-}Ly6C^{+}F4/80^{-}$) following JC-1 staining and glycolytic activity was calculated as the % of $2\text{-}NBDG^{+}$ monocytes. (**B, D**) Bacterial burdens were assessed in the surrounding soft tissue, knee, femur, and implant, where the dotted lines represent the limit of detection (LOD). (*, $p < 0.05$; **, $p < 0.01$; ***, $p < 0.001$; ****, $p < 0.0001$; One-way ANOVA).

Synergistic action of oligomycin nanoparticles and systemic antibiotics to clear established S. aureus biofilm infection.

Based on the finding that oligomycin nanoparticles transformed the biofilm milieu by promoting monocyte pro-inflammatory activity and effector leukocyte recruitment, we envisioned that residual bacteria may have less biofilm characteristics and increased susceptibility to systemic antibiotic treatment. To address this possibility, mice received CT or CTO nanoparticles on day 7 post-infection, whereupon systemic antibiotics (25 mg/kg/day rifampin and 5 mg/kg/day daptomycin) were administered 7 days later for a one week duration after which mice were sacrificed (corresponding to day 21 post-infection). Remarkably, bacterial burdens were largely below the limit of detection in animals that received CTO nanoparticles and antibiotics, whereas bacteria remained in the tissue and knee of mice treated with control CT nanoparticles and antibiotics or CTO nanoparticles alone (Fig. 3.10, A-D). These changes were reflected by significant reductions in MDSCs and increased monocyte and macrophage recruitment (Fig. 3.10, E-H), which our results show are reprogrammed towards a pro-inflammatory phenotype by intracellular oligomycin delivery (Fig. 3.6). To our knowledge, this is the first demonstration of an approach capable of clearing an established biofilm infection, which was achieved through the combined action of modulating monocyte metabolism to transform *S. aureus* biofilm susceptibility to antibiotics.

Figure 3.10

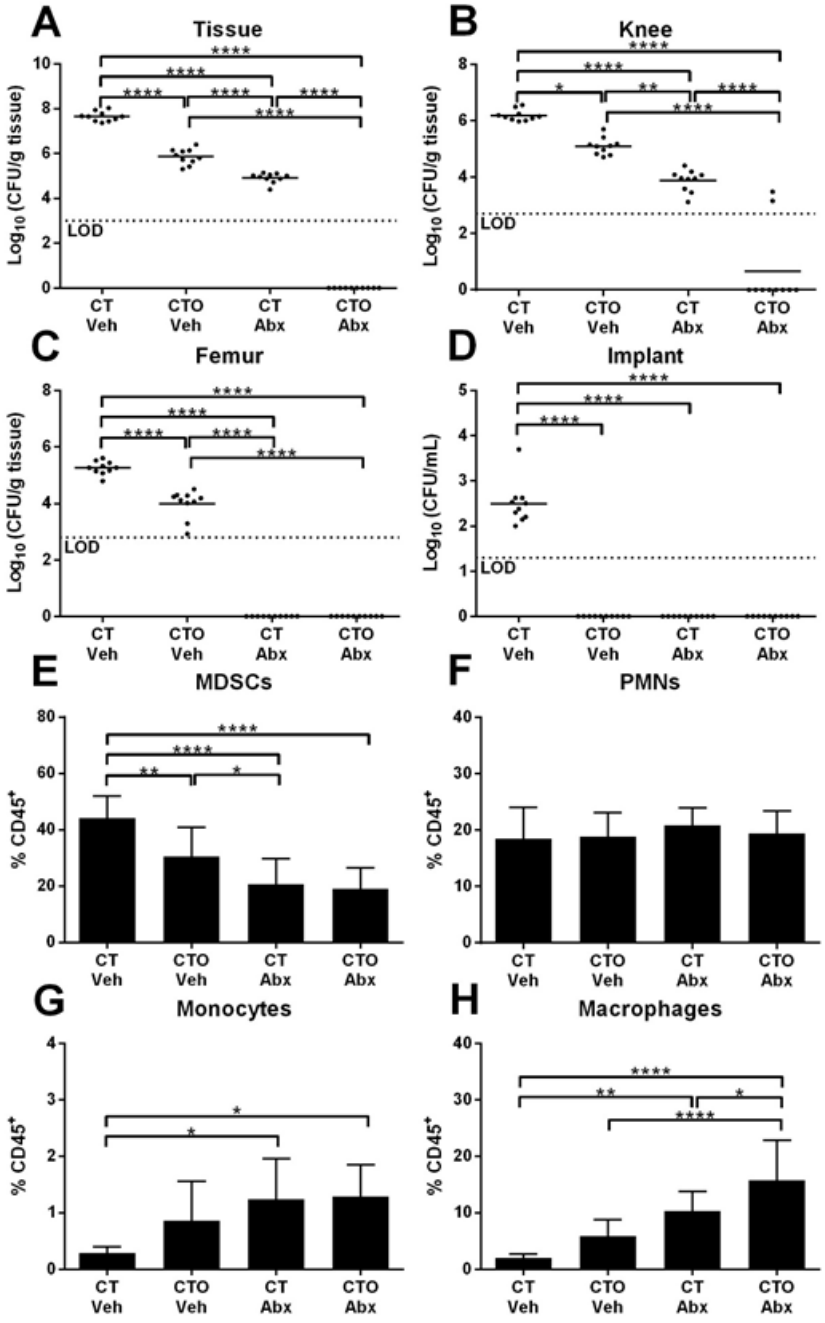

Monocyte metabolic reprogramming with oligomycin-containing nanoparticles synergizes with antibiotics to clear established *S. aureus* biofilm infection. C57BL/6 mice received a single intra-articular injection of Cy5/Tuftsin (CT) or Cy5/Tuftsin/Oligomycin (CTO) nanoparticles (10 μg) at day 7 post-infection. Seven days later, animals received daily i.p. injections of antibiotics (25 mg/kg/day rifampin and 5 mg/kg/day daptomycin) or vehicle for one

week, whereupon mice were sacrificed at day 21 post-infection. Bacterial burdens were quantified from the (**A**) surrounding soft tissue, (**B**) knee, (**C**) femur, and (**D**) implant, where the dotted line represents the limit of detection (LOD). Infiltrating leukocytes were analyzed by flow cytometry and (**E**) MDSCs, (**F**) PMNs, (**G**) monocytes, and (**H**) MΦs are reported as the mean ± SD percentage of live $CD45^+$ leukocytes. Results are combined from two independent experiments (n = 7-10 mice/group/time point). (*, $p < 0.05$; **, $p < 0.01$; ***, $p < 0.001$; ****, $p < 0.0001$; One-way ANOVA).

Figure 3.11

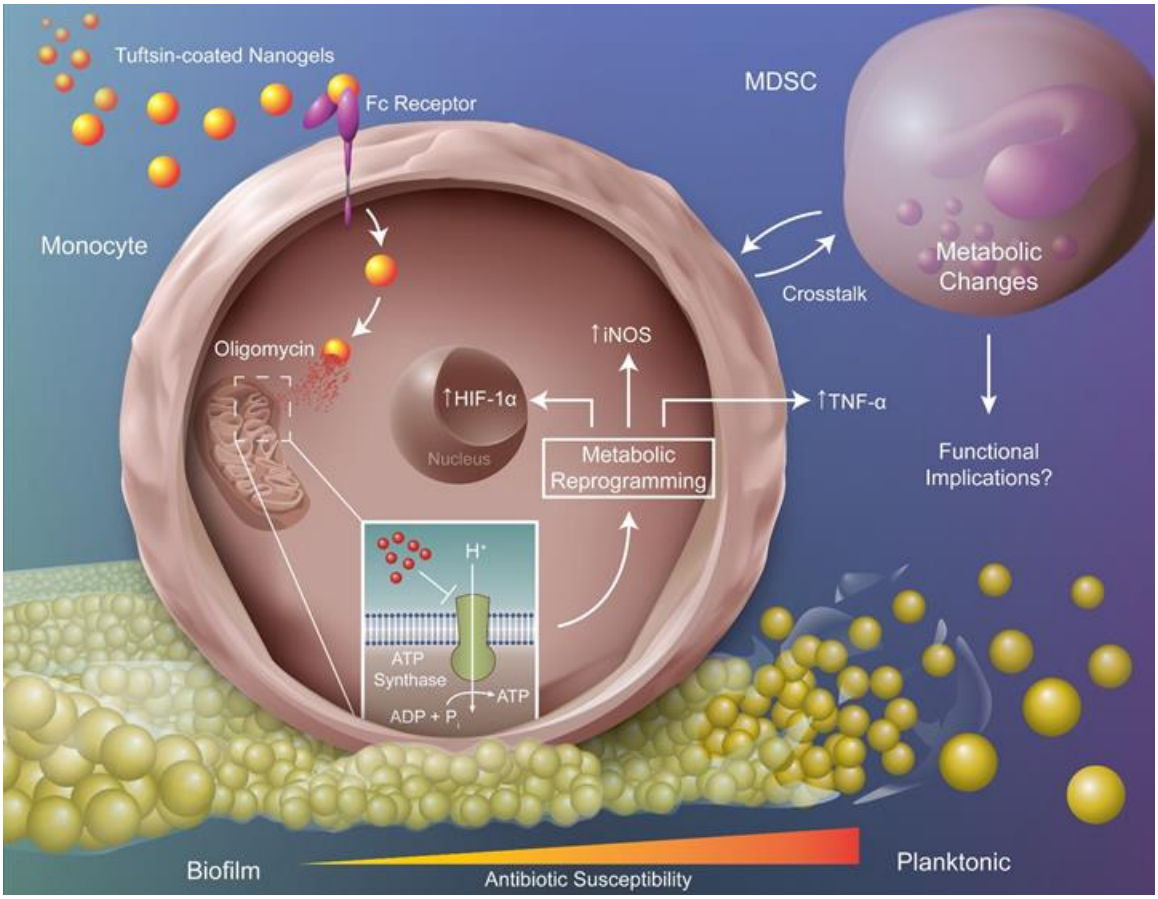

Metabolic reprogramming of monocytes promotes pro-inflammatory properties, MDSC crosstalk, and *S. aureus* biofilm dispersal. Nanoparticles containing the ATP synthase inhibitor oligomycin are targeted to Fc-receptor positive monocytes with tuftsin. Upon internalization, oligomycin inhibits ATP-synthase of the mitochondrial electron transport chain and induces metabolic reprogramming to shift monocyte metabolism and promote pro-inflammatory gene expression. Metabolically reprogrammed monocytes also influence MDSC metabolism and gene expression. Collectively, these changes promote biofilm clearance and a shift towards planktonic growth, as evident by increased antibiotic susceptibility and clearance of established biofilm infection. ADP, adenosine diphosphate; ATP, adenosine triphosphate; Fc-Receptor, fragment crystallizable region receptor; HIF-1α, hypoxia-inducible factor 1-alpha; iNOS, inducible nitric oxide synthase; MDSC, myeloid-derived suppressor cell; P_i, inorganic phosphate.

Supplemental Figure S3.1

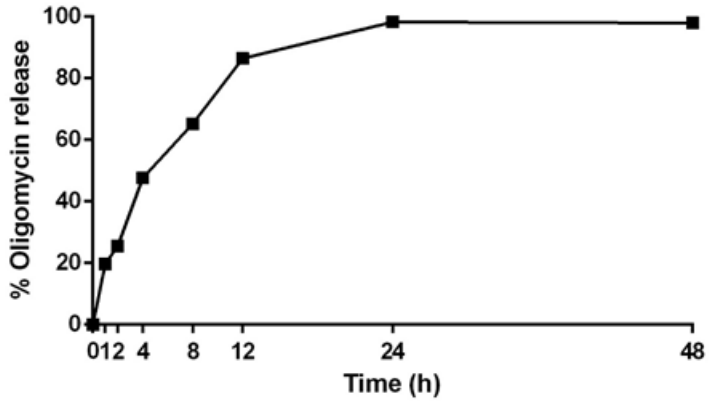

Kinetics of oligomycin release from tuftsin-modified nanoparticles. Oligomycin release from Cy5-tuftsin-oligomycin (CTO) nanoparticles was determined using a PBS dialysis method with a 3.5 kDa membrane cutoff. The kinetics of oligomycin release were determined by HPLC and concentrations are expressed as a percentage of the total oligomycin available vs. time (in hours; h).

Supplemental Figure S3.2

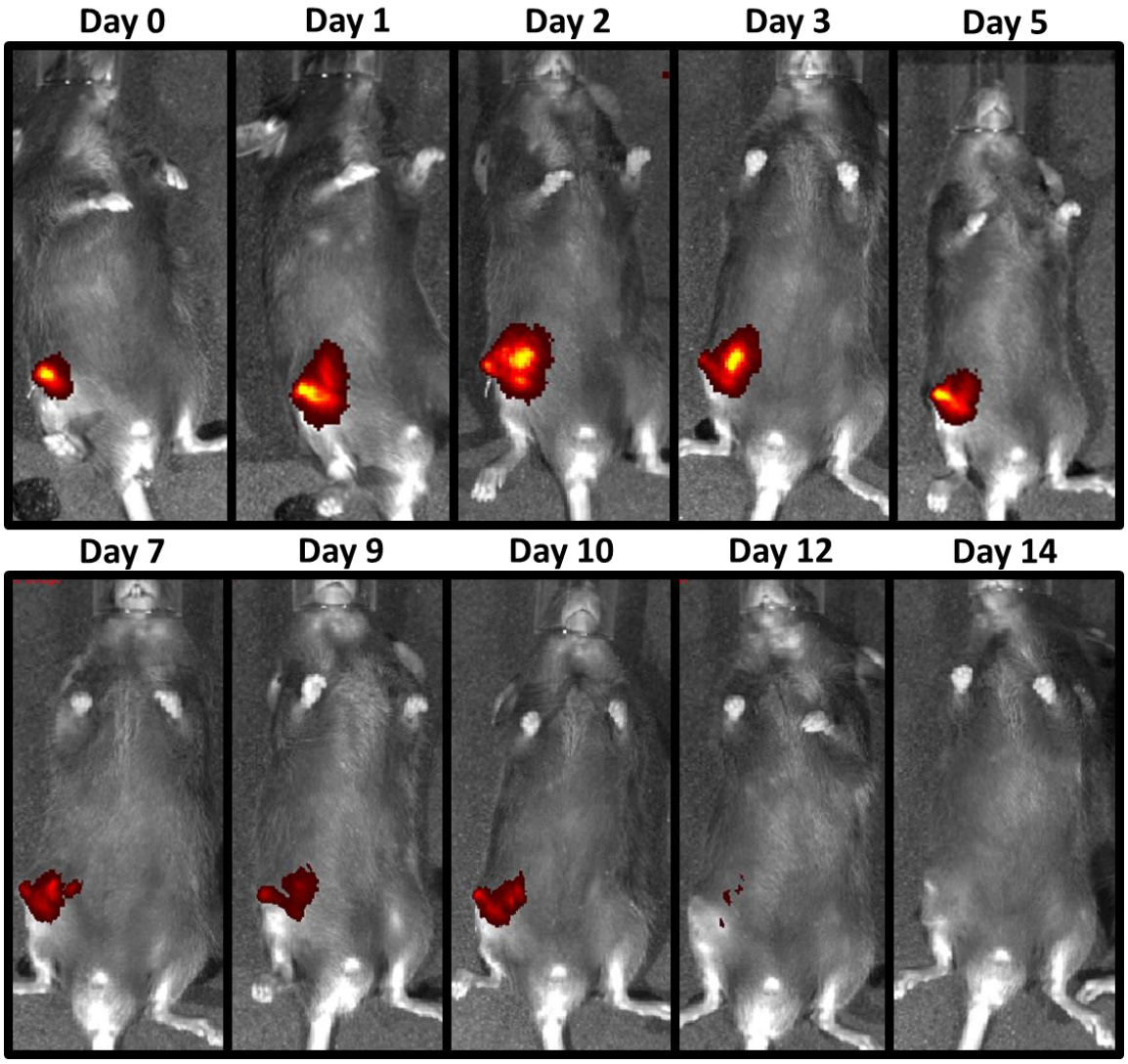

Longevity of nanoparticle retention at the site of *S. aureus* biofilm infection. C57BL/6 mice received a single intra-articular injection of Cy5 labeled nanoparticles at day 3 post-infection, whereupon the same animal was imaged over a two-week period to demonstrate the extent of nanoparticle retention and distribution. Results are representative of 5 individual mice.

Supplemental Figure S3.3

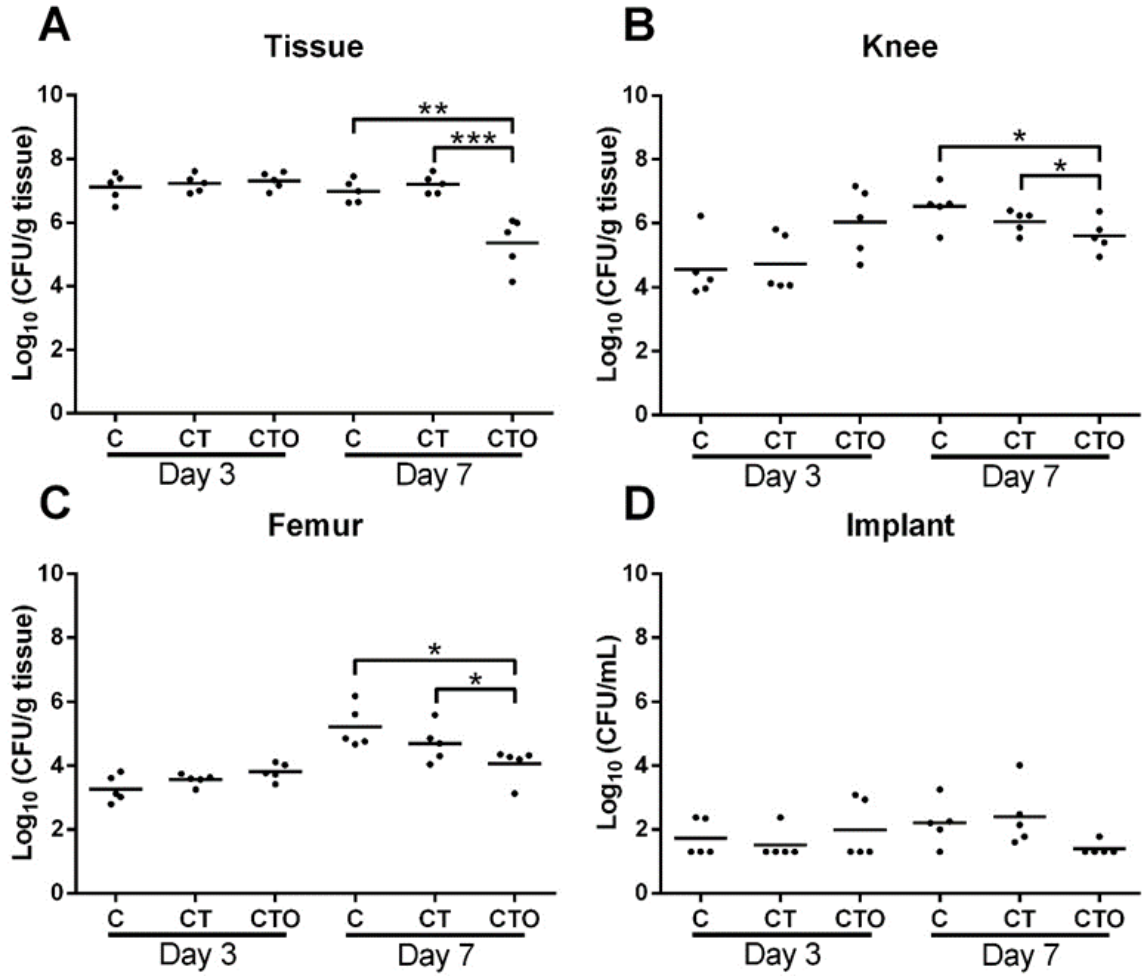

Oligomycin-containing nanoparticles do not significantly affect *S. aureus* biofilm burdens until 7 days post-infection. C57BL/6 mice received a single intra-articular injection of Cy5 (C), Cy5/Tuftsin (CT), or Cy5/Tuftsin/Oligomycin (CTO) nanoparticles at day 7 post-infection, whereupon animals were sacrificed 3 or 7 days following nanoparticle treatment. Bacterial burdens were quantified from the (**A**) surrounding soft tissue, (**B**) knee, (**C**) femur, and (**D**) implant. Results are from one experiment (n = 5 mice/group/time point). (*, $p < 0.05$; **, $p < 0.01$; ***, $p < 0.001$; One-way ANOVA).

Supplemental Figure S3.4

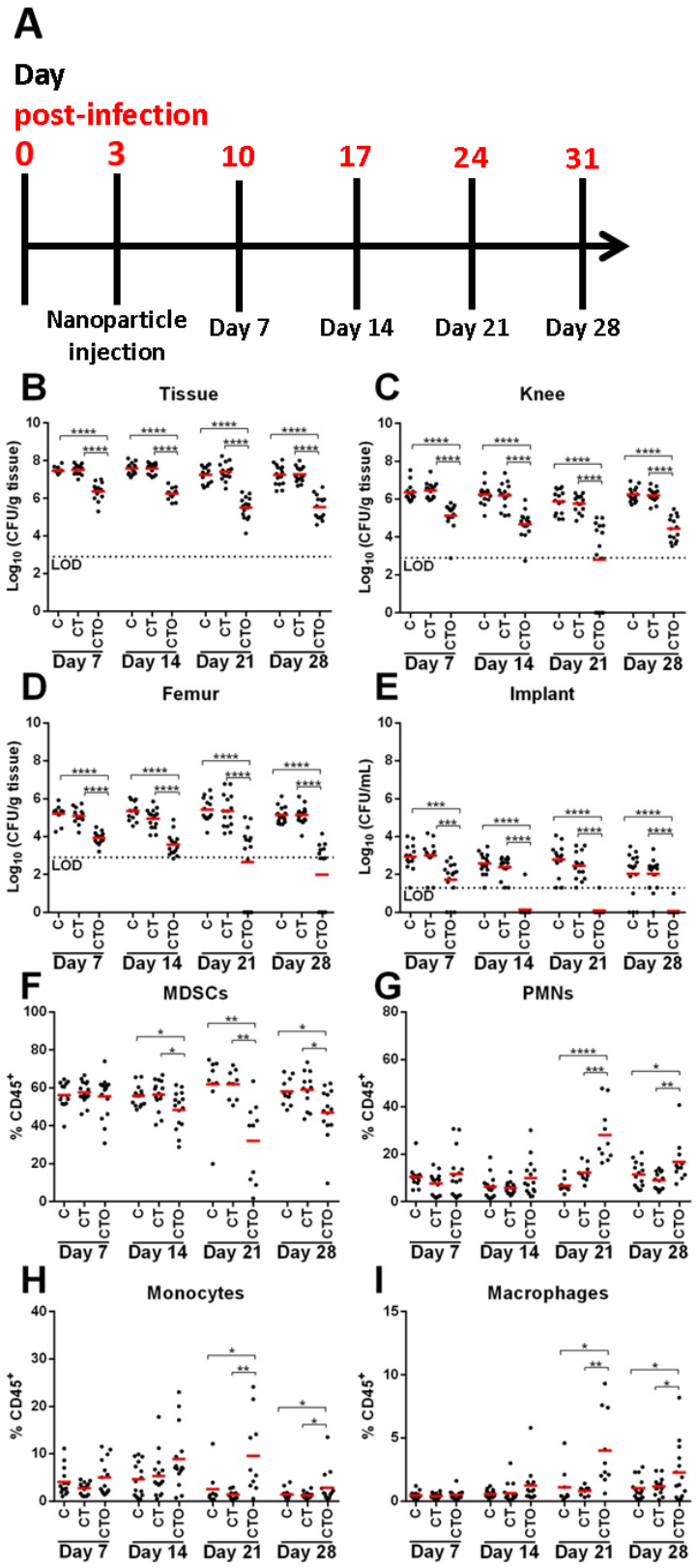

Nanoparticle-mediated delivery of oligomycin 3 days post-infection to monocytes reduces biofilm burden. (**A**) C57BL/6 mice received a single intra-articular injection of Cy5 (C), Cy5/Tuftsin (CT), or Cy5/Tuftsin/Oligomycin (CTO) nanoparticles at day 3 post-infection, and were analyzed at 7, 14, 21, or 28 days following nanoparticle treatment. Bacterial burdens were quantified in the (**B**) surrounding soft tissue, (**C**) knee, (**D**) femur, and (**E**) implant, where the red and dotted lines represent the mean and limit of detection (LOD), respectively. Infiltrating leukocytes were analyzed by flow cytometry and (**F**) MDSCs, (**G**) PMNs, (**H**) monocytes, and (**I**) MΦs are reported as the mean (red line) percentage of live $CD45^+$ leukocytes. Results are combined from three independent experiments (n = 15 mice/group/time point). (*, $p < 0.05$; **, $p < 0.01$; ***, $p < 0.001$; ****, $p < 0.0001$; One-way ANOVA).

Supplemental Figure S3.5

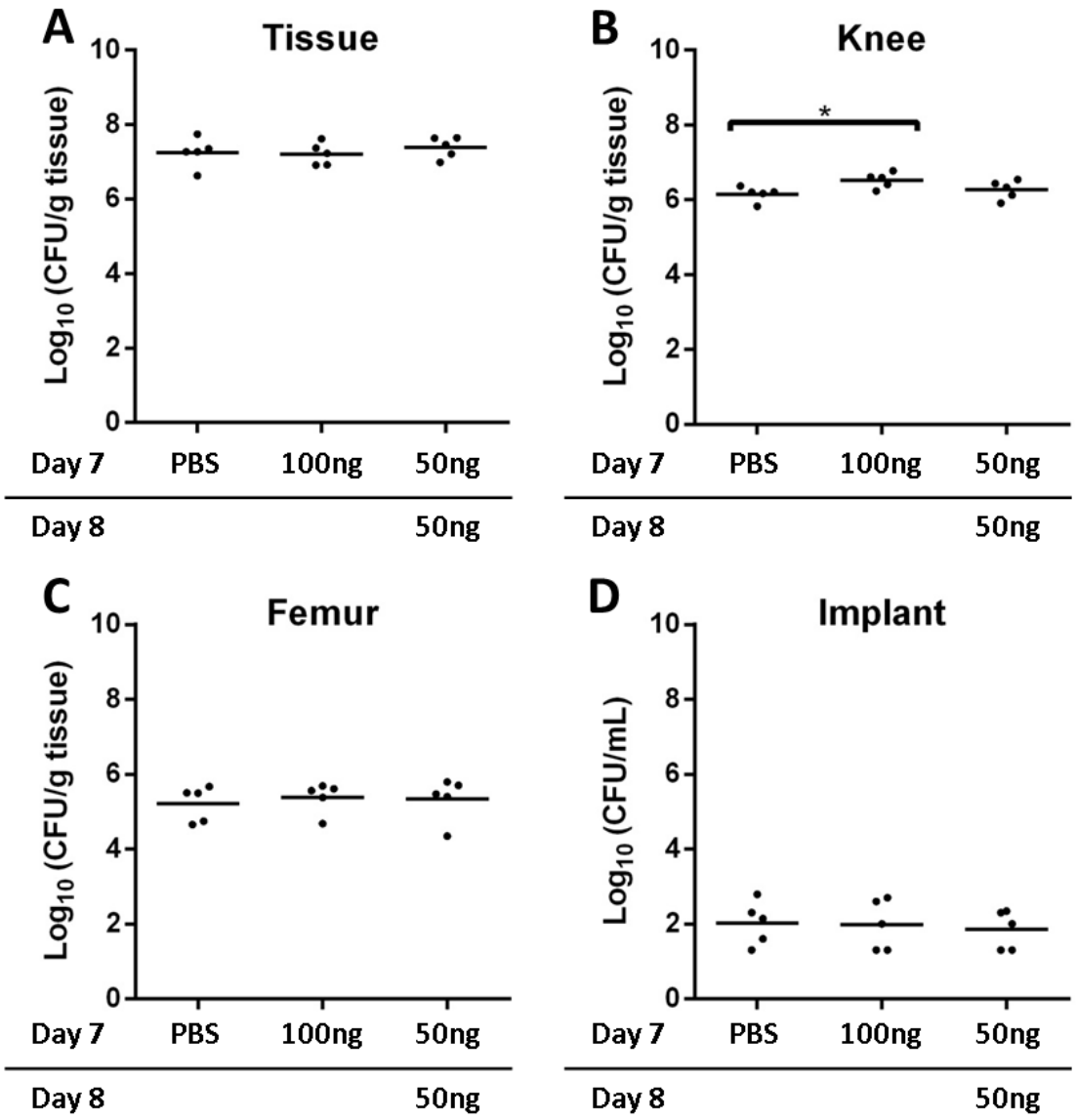

Oligomycin does not directly affect *S. aureus* biofilm bacterial burdens. C57BL/6 mice received intra-articular injections of oligomycin at 7 day post-infection (100 ng), or two sequential doses at days 7 & 8 post-infection (50 ng/day), or vehicle (PBS) and were sacrificed at day 14 post-infection. Bacterial burdens were quantified from the (**A**) surrounding soft tissue, (**B**) knee, (**C**) femur, and (**D**) implant. Results are from one experiment (n = 5 mice/group/time point). (*, $p < 0.05$; One-way ANOVA).

Supplemental Figure S3.6

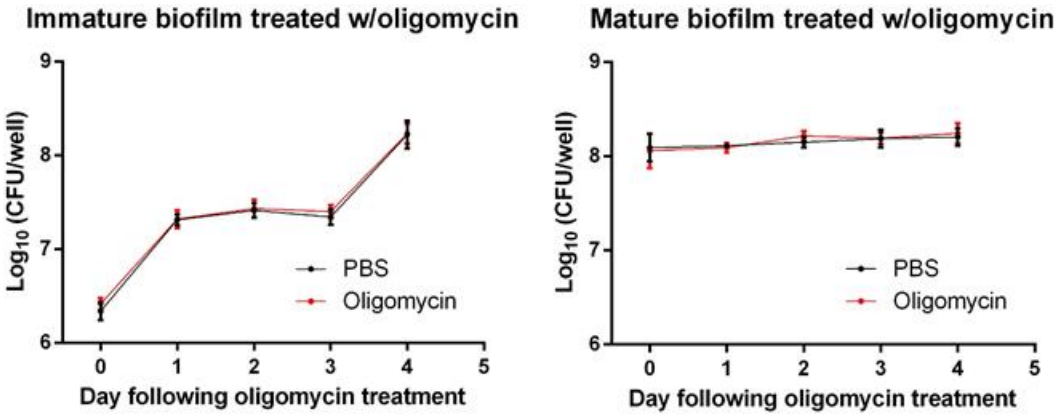

Oligomycin has no antibacterial activity against *S. aureus* during early or established biofilm growth. *S. aureus* biofilm formation was assessed in 96-well plates + oligomycin treatment. Oligomycin (10 µg/mL) was added to (**A**) planktonic *S. aureus* at time 0 or (**B**) mature biofilms for 4 days to determine effects on bacterial growth at the indicated time points following oligomycin treatment. Cultures were replenished daily with fresh medium containing oligomycin. Results are presented as Log_{10} colony forming units (CFU) per well (mean $\pm$ SD).

Discussion

Approximately one million knee and hip arthroplasties are performed in the United States annually, with PJIs representing the most common complication (110, 111, 122-126). These infections are associated with significant morbidity and medical expenses, since the current standard-of-care requires multiple surgical interventions over a period of months, during which patient mobility is limited (107, 108, 110, 111, 124). *S. aureus* is the second most common cause of PJI behind *S. epidermidis* (110, 111, 122-124) and biofilms cannot typically be cleared by antibiotics without removing the prosthesis, since the metabolic dormancy of biofilm-associated bacteria decreases their antibiotic susceptibility (86, 88, 110, 111). Further compounding this issue is the ability of *S. aureus* to promote an anti-inflammatory milieu typified by the polarization of anti-inflammatory monocytes and abundance of MDSC infiltrates (138, 146, 148, 188, 189). Monocytes can be a key effector cell during PJI in a permissive microenvironment, such as during MDSC depletion, where their pro-inflammatory activity is augmented leading to reduced biofilm burden (138, 148, 189). This study is the first to demonstrate that biofilm-associated monocytes are metabolically skewed towards OxPhos to support their anti-inflammatory properties. Interestingly, monocyte OxPhos activity was significantly lower during the first two days of *S. aureus* infection compared to sterile implants, whereas cells transitioned to favor OxPhos at later stages (i.e. days 5-7). These findings coincide with the kinetics of biofilm development *in vivo*, where our prior studies have shown that biofilm maturation is evident by day 7 post-infection as revealed by antibiotic tolerance (226). By extension, the early reduction in OxPhos activity suggests that monocytes may initially exhibit pro-inflammatory properties but transition to an anti-inflammatory phenotype that we have characterized with mature biofilms (146, 148, 187, 226). This potential early pro-inflammatory activity may explain the conundrum of heightened pro-inflammatory mediator production at the site of biofilm infection, which has no impact on the intrinsic anti-inflammatory properties of biofilm-associated leukocytes or biofilm burdens (146, 148, 187, 226). Furthermore, this study is the first to demonstrate that biofilm-

associated monocytes can be metabolically reprogrammed to inhibit OxPhos, transforming cells into a pro-inflammatory state capable of attenuating established *S. aureus* biofilms. Importantly, we provide several lines of evidence demonstrating that oligomycin lacks direct antimicrobial activity against *S. aureus*, including the failure of free oligomycin to alter biofilm burdens *in vitro* or *in vivo*. Furthermore, oligomycin needed to be loaded into nanoparticles to inhibit monocyte OxPhos, demonstrating the requirement for intracellular delivery.

Prior studies have shown that oligomycin promotes MΦ pro-inflammatory activity by inhibiting ATP synthase and OxPhos (284). We selected oligomycin over other metabolic inhibitors because it is less potent and would dampen but not completely block OxPhos, whereas stronger inhibitors, such as rotenone, are extremely toxic and have been shown to inhibit MΦ viability and function (298-301). Furthermore, a nanoparticle-directed method was preferred *in vivo* because of potential toxicity associated with a non-targeted systemic delivery approach (292, 293, 299, 300). In this study, nanoparticles were conjugated with tuftsin to facilitate FcR-mediated uptake in monocytes (285, 286, 294), which are the most abundant mononuclear phagocyte population during *S. aureus* PJI (106, 146, 148, 189). Although other FcR^+ cells infiltrate *S. aureus* biofilms, they are either of low abundance (i.e. PMNs) or express less FcR (i.e. MDSCs) compared to monocytes (302). We established that the tuftsin modification enhanced nanoparticle uptake by monocytes approximately 4-fold compared to non-conjugated nanoparticles.

Importantly, oligomycin nanoparticles were capable of metabolically re-programming biofilm-associated monocytes, which coincided with their polarization to a pro-inflammatory state, typified by increased pro- and reduced anti-inflammatory gene expression. These effects were remarkable given the finding that <5% of monocytes displayed direct evidence of nanoparticle uptake (i.e. $Cy5^+$) at the time of analysis. However, it is also possible that a greater number of monocytes had internalized nanoparticles but were no longer $Cy5^+$, since fluorescence is likely quenched in the phagosome as has been reported for other fluorochromes (303).

Metabolic pathway analysis of significantly downregulated metabolites showed that arginine, proline, and branched chain amino acid metabolism were most significantly altered in monocytes isolated from CTO treated mice. Decreased amino acid abundance may reflect increased protein synthesis to satisfy the need for metabolic intermediates during immune activation (289, 290, 304). Citrate and succinate accumulation was expected due to a glycolytic shift induced by oligomycin treatment and block in TCA cycle enzymes; however, both were less abundant in CTO monocytes (256, 289, 290, 305). Glucose and glucose-6-phosphate were also decreased in CTO monocytes, which prior *in vitro* studies showed were increased in pro-inflammatory MΦs (306). Nevertheless, secondary metabolites of the TCA cycle, such as aconitate and 2-hydroxyglutarate, were increased in CTO monocytes (260, 306-310), indicating an inhibition of the TCA cycle that supports a glycolytic bias. The endogenous macrophage activator uric acid and its metabolite, allantoin, were also more abundant in CTO monocytes (311, 312) as were methyl-malonic acid and uridine, consistent with prior *in vitro* studies of LPS stimulated monocytes with potent pro-inflammatory properties (313).

Although these metabolite patterns do not follow the strict definition of glycolytic or OxPhos metabolism that has been described *in vitro* (304, 314), we convincingly demonstrated that oligomycin nanoparticles induced a metabolic shift in biofilm-associated monocytes *in vivo* as reflected by significantly lower levels of OxPhos activity, suggesting a net shift towards glycolysis. It is important to recognize that the metabolomic signatures defined for pro- vs. anti-inflammatory MΦs are based on *in vitro* studies, where cells are polarized to activation extremes (304, 314). *In vivo,* monocytes/MΦs receive a complex array of signals and exist in a spectrum of activation states, with phenotypic and metabolic plasticity (249, 250, 252, 254, 315). Therefore, it is not unexpected that the metabolic profile of biofilm-associated monocytes possessed attributes of both OxPhos and glycolysis, which may be further explained by the milder OxPhos inhibitory activity of oligomycin as discussed earlier (284, 316). Importantly, transformation of biofilm-associated monocytes to a pro-inflammatory state following oligomycin nanoparticle treatment

was confirmed by RT-qPCR, where monocytes recovered from CTO treated animals displayed increased pro- and reduced anti-inflammatory gene expression as compared to monocytes from mice receiving CT control nanoparticles. These changes in monocyte metabolism and pro-inflammatory activity were independent of bacterial burden, which was equivalent between animals receiving oligomycin and control nanoparticles at day 3 post-treatment, and increased monocyte pro-inflammatory activity is likely responsible for the reduction in *S. aureus* titers from day 7 onward. Furthermore, monocyte OxPhos was unaffected following treatment with free oligomycin, establishing the requirement for intracellular delivery, which was facilitated by tuftsin-modified nanoparticles. This study is the first demonstration of the utility of nanoparticle-directed metabolic re-programming to modulate monocyte activation *in vivo* in the context of biofilm-associated infection.

An unexpected finding in this study was that biofilm-associated MDSCs displayed marked alterations in their metabolome, despite that fact that <0.01% cells exhibited evidence of nanoparticle uptake. To our knowledge, this is the first demonstration of monocyte-MDSC metabolic crosstalk during biofilm infection (Fig. 3.11), which supports our earlier observations where MDSC depletion led to enhanced monocyte pro-inflammatory activity (146, 148, 189). Metabolic pathway analysis revealed that MDSCs recovered from CTO treated mice had significant increases in glutathione, nicotinamide, taurine, and purine metabolism, whereas arginine, glutamine, negatively charged, and cyclic chain amino acids were down-regulated. It is difficult to predict the impact of these metabolic changes, since few studies have explored MDSC metabolism, especially *in vivo*; however, this metabolic signature would generally be consistent with a glycolytic preference. Similar to monocytes, a decrease in amino acids likely corresponds to an increase in protein synthesis or need for metabolic intermediates (289, 290, 304). An increase in GSH/GSSH has been shown to prime T cells for glycolytic metabolism and Th1 pro-inflammatory activity (317, 318) and the increase in NADH/NAD^+ (2.489-fold higher in MDSCs recovered from CTO compared to CT treated mice) corresponds to a reduction in electron

transport chain activity (314, 319). While elevated NADH/NAD^+ should increase lactic acid fermentation and lactate production, intracellular lactate levels were 4-fold lower in MDSCs from CTO treated animals. One potential explanation to account for this finding is that lactate is exported from the cell by monocarboxylate transporters (MCTs), which are enhanced following immune activation (260).

Major challenges pertaining to PJI treatment are the inability to clear infection without removing the prosthesis and preventing infection recurrence. Based on our findings that oligomycin nanoparticles augmented monocyte pro-inflammatory activity, we examined how this impacted biofilm burden. Remarkably, *S. aureus* titers were significantly reduced in mice receiving oligomycin nanoparticles out to 28 days post-injection. This was accompanied with a reduction in MDSCs concomitant with increased monocyte, PMN, and MΦ infiltrates, which were likely responsible for biofilm clearance. These findings are significant for several reasons. First, only a single injection of CTO nanoparticles was required reflecting sustained action, which is a desirable feature for potential therapeutic interventions. Second, nanoparticle treatment was not initiated until a mature biofilm was established (i.e. day 7 post-infection), which represents the most challenging treatment scenario. Third, combined treatment with CTO nanoparticles and systemic antibiotics reduced infectious burden to below the limit of detection. We propose that the shift in monocyte pro-inflammatory activity by oligomycin promotes biofilm disruption and transforms metabolically dormant biofilm-associated bacteria into a planktonic mode of growth, which is more susceptible to antibiotic action (Fig. 3.11). To our knowledge, this is the first demonstration of an *in vivo* approach that is capable of clearing established biofilms without removal of the infected implant.

Understanding the complex and dynamic interactions between *S. aureus* biofilm and the host immune response is critical to developing novel therapeutic approaches to reduce the morbidity associated with PJI. This study is the first to demonstrate that biofilm-associated monocytes can be metabolically reprogrammed using a novel nanoparticle targeted approach to

promote their pro-inflammatory properties, which results in biofilm clearance. A similar strategy might represent a therapeutic for PJI by modulating host immunity to facilitate the transition from biofilm to planktonic growth, which can be resolved by systemic antibiotic treatment and alleviate the need for removal of the infected prosthesis, resulting in less patient morbidity.

Chapter 4: Arginase-1 expression in myeloid cells regulates S. aureus planktonic but not biofilm infection

Publication:

Yamada KJ, Heim CE, Aldrich AL, Gries CM, Staudacher AG, Kielian T. 2018. Arginase-1 expression in myeloid cells regulates *Staphylococcus aureus* planktonic but not biofilm infection. Infect Immun 86:e00206-18. https://doi.org/10.1128/IAI.00206-18.

Abstract

S. aureus is a leading cause of device-associated biofilm infections, which represent a serious health care concern based on their chronicity and antibiotic resistance. We previously reported that *S. aureus* biofilms preferentially recruit myeloid-derived suppressor cells (MDSCs), which promote monocyte and macrophage anti-inflammatory properties. This is associated with increased myeloid arginase-1 (Arg-1) expression, which has been linked to anti-inflammatory and pro-fibrotic activity that are observed during *S. aureus* biofilm infections. To determine whether MDSCs and macrophages utilize Arg-1 to promote biofilm infection, Arg-1 was deleted in myeloid cells using *Tie-2*^{Cre} mice. Despite Arg-1 expression in biofilm-associated myeloid cells, bacterial burdens and leukocyte infiltrates were similar between wild type (WT) and *Arg-1*$^{fl/fl}$;*Tie-2*^{Cre} conditional knockout (KO) mice from days 3 to 14 post-infection in both orthopedic implant and catheter-associated biofilm models. However, inducible nitric oxide synthase (iNOS) expression was dramatically elevated in biofilm-associated MDSCs from *Arg-1*$^{fl/fl}$;*Tie-2*^{Cre} animals, suggesting a potential Arg-1-independent compensatory mechanism for MDSC-mediated immunomodulation. Treatment of *Arg-1*$^{fl/fl}$;*Tie-2*^{Cre} mice with the iNOS inhibitor N6-(1-Iminoethyl)-lysine, hydrochloride (L-NIL) had no effect on biofilm burdens or immune infiltrates, whereas treatment of WT mice with the Arg-1/ornithine decarboxylase inhibitor difluoromethylornithine (DFMO) increased bacterial titers, but only in the surrounding soft tissues that possess planktonic attributes. A role for myeloid-derived Arg-1 in regulating planktonic infection was confirmed using a subcutaneous abscess model, where *S. aureus* burdens were significantly increased in *Arg-1*$^{fl/fl}$;*Tie-2*^{Cre} compared to WT mice. Collectively, these results indicate that the effects of myeloid Arg-1 are context-dependent and are manifest during planktonic, but not biofilm infection.

Introduction

S. aureus is a leading cause of community-acquired and nosocomial infections in humans (24, 36, 37, 110, 111, 320, 321), and the presence of foreign materials increases infection risk due to the ability of *S. aureus* to form biofilms (24, 120, 121). Biofilms are heterogeneous bacterial communities that are difficult to eradicate based on their chronicity and recalcitrance to antibiotic therapy (24, 120, 121). In addition, previous work from our laboratory has shown that *S. aureus* biofilms actively skew the host immune response toward an anti-inflammatory phenotype that is characterized by the preferential recruitment of myeloid-derived suppressor cells (MDSCs) and anti-inflammatory monocytes and macrophages, whereas neutrophils and T cell infiltrates are minimal (138, 139, 146, 148, 187, 188). MDSCs recruited to the site of biofilm infection express IL-10, which is one contributing mechanism of immune suppression (148). In addition, biofilm-associated MDSCs and macrophages upregulate arginase-1 (Arg-1) expression, suggesting that Arg-1 could further potentiate the anti-inflammatory and pro-fibrotic cellular responses that are favored during *S. aureus* biofilm infections (138, 147, 189).

Arg-1 catalyzes the hydrolysis of arginine to ornithine and urea (322). During an immune response, myeloid-derived Arg-1 is an important enzyme involved in the regulation of arginine availability (322-326), and previous studies have demonstrated that myeloid-derived Arg-1 can inhibit pro-inflammatory immune responses (268, 322, 327-330). Arginine is a substrate for both Arg-1 and inducible nitric oxide synthase (iNOS), which are characteristic markers for anti- and pro-inflammatory macrophages, respectively (268, 331-333). In myeloid cells, ornithine generation by Arg-1 is used for proline or polyamine synthesis through ornithine decarboxylase (ODC), which promotes fibrosis by collagen formation (322). A previous study demonstrated the importance of host-derived polyamines for *S. aureus* clearance and wound healing in a subcutaneous abscess model that represents planktonic infection (149); however, a role for Arg-1 action in the context of biofilms has not yet been explored. Of note, biofilm infections are often encompassed by a fibrotic response, which coincides with robust Arg-1 expression (10, 15, 16).

Arg-1 activity also inhibits NO-mediated killing of pathogens by macrophages, since arginine is the primary substrate for iNOS (331-333). Furthermore, extracellular arginine depletion leads to reduced CD3ζ chain expression and the inability to augment cyclin D3 and cdk4, which leads to T cell hypo-responsiveness and cell cycle arrest, respectively (323-327, 329, 334). However, the effects of MDSC Arg-1 on inhibiting T cell proliferation may be context-dependent, as some studies have not demonstrated a role for the enzyme (335, 336). Previous work has demonstrated that myeloid-derived Arg-1 expression has a pathologic role in several cancers, Alzheimer's disease, and bacterial and helminth infections, establishing it as a key enzyme in dictating disease pathogenesis and immune outcomes (268, 322, 337, 338). Therefore, elevated Arg-1 expression by MDSCs and/or macrophages could participate in preventing an effective immune response to *S. aureus* biofilm infection through the depletion of extracellular arginine and suppression of pro-inflammatory responses.

The objective of this study was to examine the functional role of myeloid-derived Arg-1 in promoting device-associated *S. aureus* biofilm infection. Using a conditional knockout (KO) mouse to delete Arg-1 in myeloid cells (*Arg-1*$^{fl/fl}$;*Tie-2*^{Cre}) (268, 339) we established that Arg-1 expression was significantly reduced in myeloid cells *in vitro* and in MDSCs and macrophages isolated from *S. aureus* biofilm infections *ex vivo*. Utilizing two device-associated *S. aureus* biofilm infection models, we found that bacterial burdens were not dramatically different between wild type (WT) and *Arg-1*$^{fl/fl}$;*Tie-2*^{Cre} myeloid conditional KO mice. Further investigation showed that MDSCs from *Arg-1*$^{fl/fl}$;*Tie-2*^{Cre} conditional KO animals upregulated iNOS expression, suggesting a possible compensatory mechanism for arginine depletion and immunomodulation. However, treatment of *Arg-1*$^{fl/fl}$;*Tie-2*^{Cre} mice with a small molecule inhibitor of iNOS did not affect *S. aureus* biofilm burdens or leukocyte infiltrates. Additive effects were also not observed when mice were treated with a small molecule inhibitor of nicotinamide adenine dinucleotide phosphate (NADPH) oxidase. However, in the orthopedic implant model treatment of WT mice with the arginase and ODC inhibitor DFMO increased bacterial titers, but only in the surrounding

soft tissue that possesses some planktonic attributes and not in the joint or femur that model biofilm growth. Indeed, a role for myeloid-derived Arg-1 in regulating planktonic infection was confirmed using a subcutaneous abscess model, where *S. aureus* burdens were significantly increased in *Arg-1*$^{fl/fl}$;*Tie-2*^{Cre} compared to WT mice. Collectively, these results demonstrate that myeloid-derived Arg-1 controls *S. aureus* growth during planktonic, but not biofilm growth *in vivo*. By extension, the lack of Arg-1 involvement during biofilm formation represents another immune-evasion mechanism leading to infection persistence.

Results

Arginase-1 expression and enzyme activity are significantly reduced in myeloid cells from Arg-1 conditional KO mice. Arginase-1 is a marker of anti-inflammatory macrophages and inhibits inflammatory responses through depletion of available arginine stores (260, 268, 322, 326, 337, 340). Our laboratory previously reported increased Arg-1 expression in MDSCs, monocytes, and macrophages infiltrating tissues surrounding a *S. aureus* biofilm infection (138, 146-148, 187). Although MDSC depletion improved biofilm clearance by enhancing monocyte pro-inflammatory activity (148, 187), the mechanism of action and whether Arg-1 was involved remained unclear. This was an important issue to address, since Arg-1 activity has been implicated in several types of cancers, Alzheimer's disease, and infection (268, 322, 337, 338). In the current study, we used two mouse models of device-associated *S. aureus* biofilm infection to determine the role of myeloid-derived Arg-1 in shaping leukocyte infiltrates and promoting biofilm persistence. Prior reports have demonstrated that LysM-driven expression of Cre-recombinase is inefficient at flox-mediated Arg-1 deletion (268, 270). This was confirmed in the current study, where significant Arg-1 activity remained in *Arg-1*$^{fl/fl}$;*LysM*^{Cre} macrophages compared to wild type cells (Figure S4.1). As an alternative approach, we utilized *Arg-1*$^{fl/fl}$;*Tie-2*^{Cre} mice, which have been shown to efficiently delete Arg-1 from myeloid cells (268). We first confirmed efficient Arg-1 deletion in myeloid cells from *Arg-1*$^{fl/fl}$;*Tie-2*^{Cre} conditional KO mice. Both Arg-1 expression and enzyme activity were significantly increased in wild type *Arg-1*$^{fl/fl}$;*Tie-2*^{null} macrophages in response to IL-4 (Figure 4.1A and B). In contrast, bone marrow-derived macrophages from *Arg-1*$^{fl/fl}$;*Tie-2*^{Cre} mice displayed significant decreases in Arg-1 expression and activity relative to *Arg-1*$^{fl/fl}$;*Tie-2*^{null} control cells, both at baseline and following IL-4 treatment, confirming effective gene deletion (Figure 4.1A and 4.1B). Arginase activity in *Arg-1*$^{fl/fl}$;*Tie-2*^{Cre} macrophages may result from mitochondrial Arg-2 expression that can also catalyze the substrate used for the arginase assay (341).

Figure 4.1

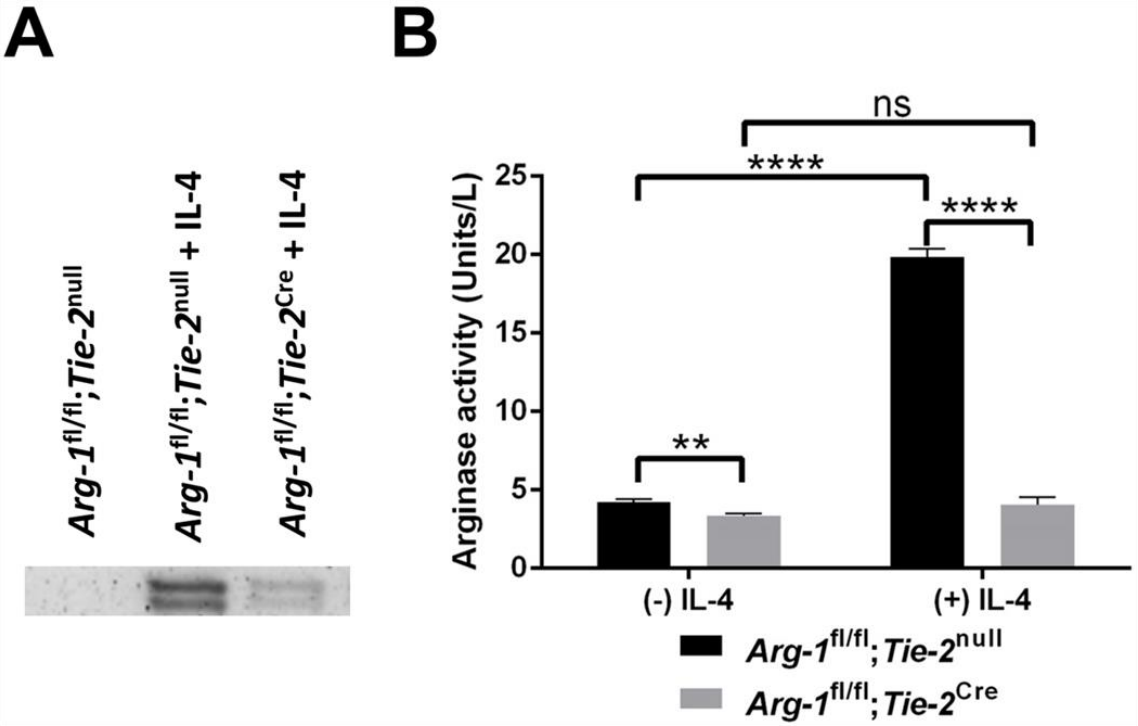

Arginase-1 expression and enzymatic activity are significantly reduced in *Arg-1*$^{fl/fl}$;*Tie-2*^{Cre} bone marrow-derived macrophages. Bone marrow-derived macrophages were unstimulated or treated with rmIL-4 (10ng/mL) for 24 h, whereupon whole cell protein extracts (20 µg) were used for Western blot (**A**) and arginase activity (**B**) assays. Arginase activity in whole cell extracts was measured by the amount of enzyme that converted 1.0 µmol of L-arginine to ornithine and urea per minute. **, p <0.01; ****, p < 0.0001; one-way ANOVA with Bonferroni's multiple comparison (ns, not significant).

Myeloid-derived arginase-1 does not dramatically affect S. aureus device-associated biofilm infection. Based on our *in vitro* studies demonstrating that Arg-1 activity was significantly reduced in *Arg-1*$^{fl/fl}$;*Tie-2*^{Cre} conditional KO macrophages, we next examined the role of Arg-1 in the establishment and persistence of *S. aureus* biofilms using two infection models. The first was orthopedic implant-associated biofilm infection, which our laboratory has shown is dominated by MDSCs that express Arg-1 and monocytes polarized towards an anti-inflammatory state (146, 148, 187). No differences in biofilm burdens or leukocyte infiltrates were observed between *Arg-1*$^{fl/fl}$;*Tie-2*^{Cre} conditional KO and *Arg-1*$^{fl/fl}$;*Tie-2*^{null} mice over the two-week infection period (Figure 4.2). We next examined a mouse model of catheter-associated biofilm infection, which is typified by a more robust macrophage infiltrate, fibrotic response, and Arg-1 expression compared to the orthopedic implant model (138, 139). Although MDSC infiltrates and bacterial burdens were significantly increased in catheter-associated tissues of *Arg-1*$^{fl/fl}$;*Tie-2*^{Cre} conditional KO mice at day 10 post-infection (Figure 4.3), this did not dramatically alter biofilm growth at later time points (days 14-28; data not shown). No significant differences in arginase activity were observed in either tissue or femur homogenates from WT and *Arg-1*$^{fl/fl}$;*Tie-2*^{Cre} mice in the orthopedic implant model (Figure S4.2). This is likely because fibroblasts and other stromal cells outnumber myeloid cells in these compartments and contribute to the arginase pool at the site of infection. In addition, we did not observe any dramatic alterations in tissue integrity or collagen content as determined by H&E and trichrome staining, respectively (data not shown). As a quantitative means to assess collagen formation, a hydroxyproline assay was performed. Although hydroxyproline levels were elevated at day 3 post-infection in *Arg-1*$^{fl/fl}$;*Tie-2*^{Cre} mice in the catheter-associated infection model (Figure S4.3) this was not observed at later time points, which confirmed the similarities in collagen levels between the two strains. Collectively, these results indicate that although Arg-1 expression is increased at the site of *S. aureus* biofilm infection, the enzyme itself in myeloid cells is not critical for regulating biofilm growth.

Figure 4.2

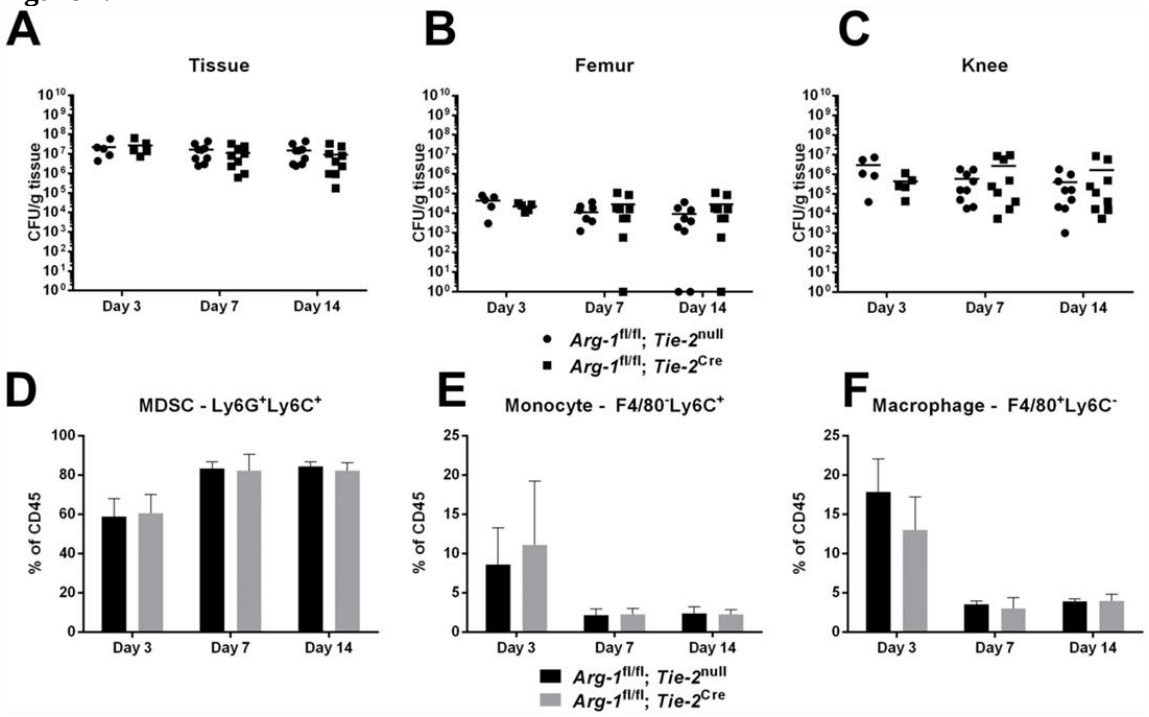

Arginase-1 expression in myeloid cells does not influence *S. aureus* orthopedic implant infection. A titanium orthopedic implant was placed in the femur of *Arg-1*$^{fl/fl}$;*Tie-2*^{null} (WT) and *Arg-1*$^{fl/fl}$;*Tie-2*^{Cre} mice and inoculated with 10^3 CFU *S. aureus* LAC. (**A-C**) Tissue surrounding the infected implant, femur, and knee joint was collected at the indicated intervals post-infection to quantify bacterial burdens. (**D-F**) Infiltrating leukocyte populations in implant-associated tissues were evaluated by flow cytometry. Results are representative of two independent experiments.

Figure 4.3

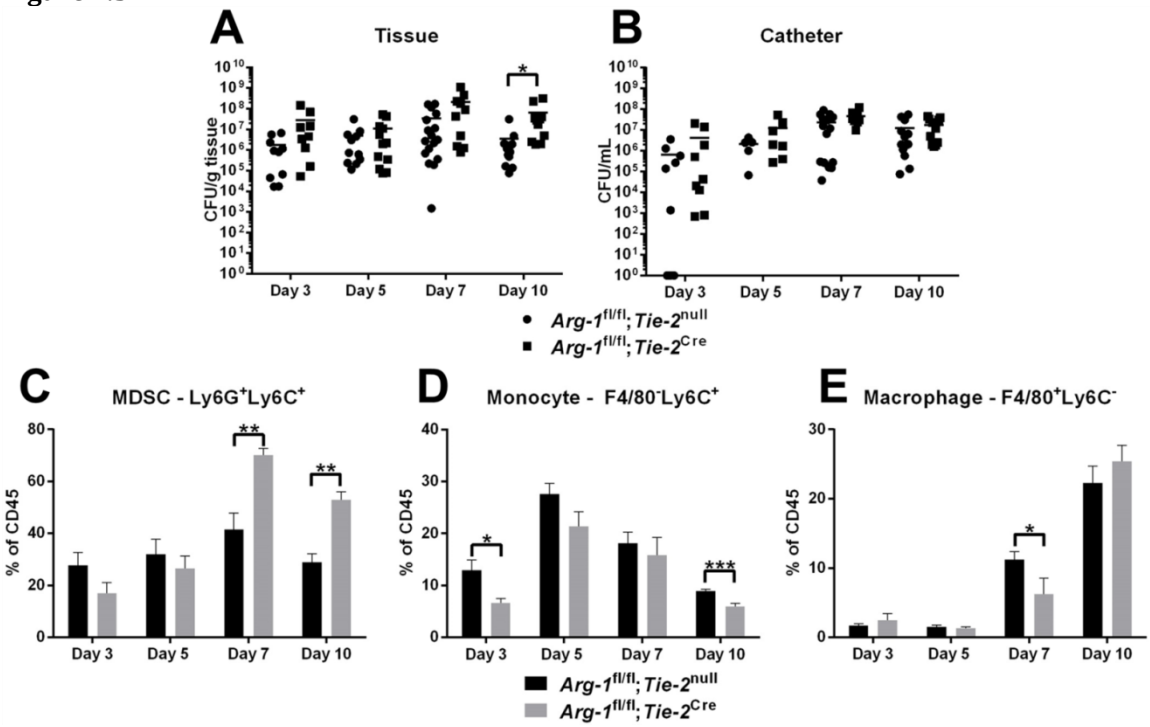

Arginase-1 in myeloid cells does not dramatically affect *S. aureus* catheter-associated biofilm infection. Catheter-associated infections were established in *Arg-1*$^{fl/fl}$;*Tie-2*^{null} (WT) and *Arg-1*$^{fl/fl}$;*Tie-2*^{Cre} mice following challenge with 10^3 CFU of *S. aureus* LAC. Animals were sacrificed at the indicated intervals post-infection, whereupon bacterial burdens in the surrounding tissue (**A**) and catheter (**B**) were determined and infiltrating leukocyte populations evaluated by flow cytometry (**C-E**). Results are representative of three independent experiments *, $p < 0.05$; **, $p < 0.01$; ***, $p < 0.001$; unpaired 2-tailed Student's *t*-test.

iNOS expression is increased in biofilm-associated MDSCs from Arg-1$^{fl/fl}$;Tie-2^{Cre} conditional KO mice. To establish that the overall lack of differences between *Arg-1*$^{fl/fl}$;*Tie-2*^{Cre} myeloid conditional KO and *Arg-1*$^{fl/fl}$;*Tie-2*^{null} mice in both the catheter and orthopedic implant infection models were not due to inefficient Arg-1 deletion *in vivo*, Arg-1 expression was examined in myeloid cells recovered from the site of infection. Both MDSCs ($CD45^+Ly6G^{high}Ly6C^+$) and monocytes ($CD45^+Ly6G^-Ly6C^+$) were isolated by FACS from *Arg-1*$^{fl/fl}$;*Tie-2*^{Cre} and *Arg-1*$^{fl/fl}$;*Tie-2*^{null} control mice at days 7 and 14 post-infection, whereupon Arg-1 expression and activity were assessed by RT-qPCR and enzymatic assays, respectively (Figure 4.4). As expected, Arg-1 expression and activity were dramatically reduced in macrophages and MDSCs from *Arg-1*$^{fl/fl}$;*Tie-2*^{Cre} conditional KO mice compared to *Arg-1*$^{fl/fl}$;*Tie-2*^{null} controls in the catheter-associated infection model at day 7 and 14 (Figure 4.4A). Because myeloid conditional Arg-1 deletion was verified in this model, this analysis was not repeated in the orthopedic implant biofilm model. Interestingly, MDSCs from *Arg-1*$^{fl/fl}$;*Tie-2*^{Cre} myeloid conditional KO mice showed a dramatic increase in iNOS expression (Figure 4.4A). Since prior studies from our laboratory have revealed a critical role for MDSCs in attenuating monocyte/macrophage pro-inflammatory activity and promoting biofilm persistence (12, 14), this suggested that a potential compensatory mechanism for arginine depletion may exist via upregulation of iNOS by MDSCs in the absence of Arg-1.

Figure 4.4

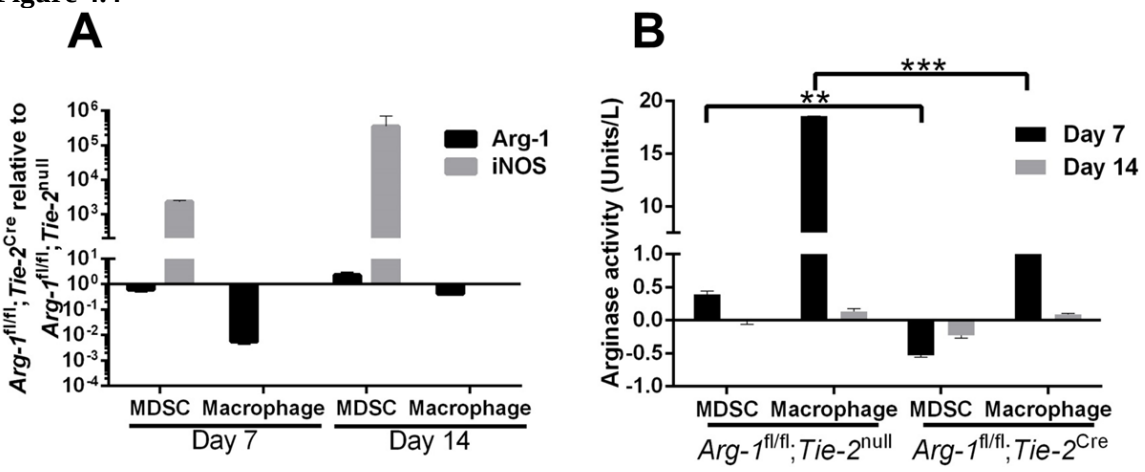

MDSCs and macrophages from *Arg-1*$^{fl/fl}$;*Tie-2*^{Cre} mice express limited arginase-1 *in vivo*. Catheter-associated infections were established in *Arg-1*$^{fl/fl}$;*Tie-2*^{null} (WT) and *Arg-1*$^{fl/fl}$;*Tie-2*^{Cre} mice following challenge with 10^3 CFU of *S. aureus* LAC. Animals were sacrificed at days 7 and 14 post-infection, whereupon MDSCs ($CD45^+Ly6G^{high}Ly6C^+$) and monocytes ($CD45^+Ly6G^-Ly6C^+$) were isolated by FACS for (**A**) RT-qPCR quantification of Arg-1 and iNOS expression and (**B**) arginase activity assay. Results are representative of two independent experiments. **, $p < 0.01$; ***, $p < 0.001$; unpaired 2-tailed Student's *t*-test.

iNOS or reactive oxygen species do not compensate for arginase-1 deficiency in myeloid cells. Given the observed increase in iNOS expression in MDSCs from Arg-1 myeloid conditional KO mice, we treated *Arg-1*$^{fl/fl}$;*Tie-2*^{Cre} animals with N6-(1-iminoethyl)-L-lysine (L-NIL), a small molecule inhibitor with selectivity for iNOS (cytokine-inducible) over nNOS (neuronal) and eNOS (endothelial) (342). Both *Arg-1*$^{fl/fl}$;*Tie-2*^{Cre} myeloid conditional KO and *Arg-1*$^{fl/fl}$;*Tie-2*^{null} control mice received daily administration of L-NIL or vehicle in the *S. aureus* orthopedic implant model. No differences in bacterial burdens from the knee, surrounding soft tissue, or femur, or leukocyte infiltrates were observed with L-NIL treatment (Figure 4.5A-C and data not shown), suggesting that the observed increase in iNOS expression by MDSCs does not compensate for reduced myeloid Arg-1. We next examined the potential role of NADPH oxidase as a redundant pathway for Arg-1 in modulating biofilm persistence, since ROS production by MDSCs has also been implicated in modulating their suppressive activity (229, 232). *Arg-1*$^{fl/fl}$;*Tie-2*^{Cre} myeloid conditional KO and *Arg-1*$^{fl/fl}$;*Tie-2*^{null} control mice were treated with the small molecule NADPH oxidase inhibitor apocynin, which also revealed no role in limiting the establishment or persistence of orthopedic implant-associated biofilm infection (Figure 4.5A-C).

Figure 4.5

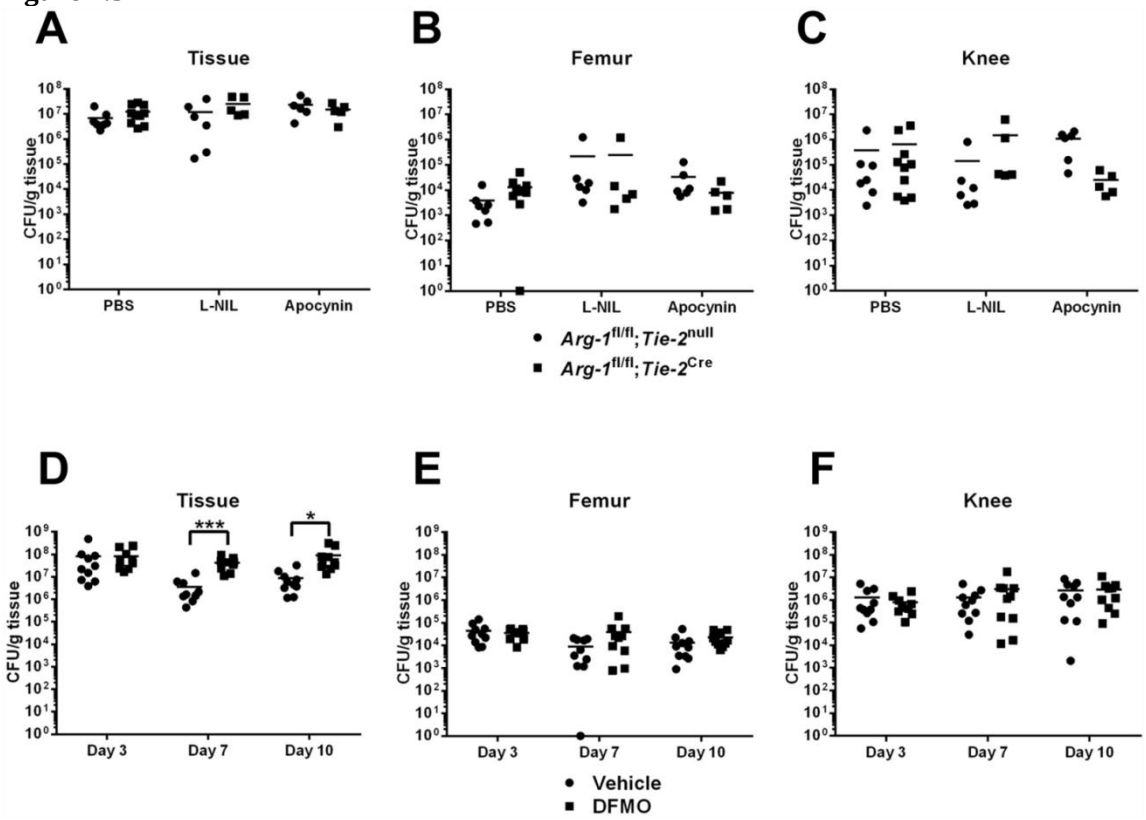

iNOS or reactive oxygen species do not compensate for arginase-1 deficiency in myeloid cells. *S. aureus* orthopedic implant infections were established in (**A-C**) *Arg-1*$^{fl/fl}$;*Tie-2*^{null} (WT), *Arg-1*$^{fl/fl}$;*Tie-2*^{Cre} or (**D-F**) C57BL/6 mice, whereupon animals received daily treatments of (**A-C**) apocynin (6 mg/kg) and L-NIL (40 mg/kg), or (D-F) DFMO (50 mg/kg) beginning at 5 h prior to infection. Bacterial burdens were quantified in (**A, D**) surrounding soft tissues, (**B, E**) femur, and (**C, F**) knee joint at the indicated time points post-infection. *, $p < 0.05$;***, $p < 0.001$; unpaired 2-tailed Student's *t*-test.

Inhibition of polyamine synthesis promotes bacterial growth in tissues surrounding biofilm infections. Although our results suggested that myeloid Arg-1 deletion had minimal effects on biofilm development, we treated WT mice with difluoromethylornithine (DFMO), a small molecule inhibitor of both arginase and ornithine decarboxylase (ODC), in the orthopedic implant infection model to examine the potential redundancy of ODC during *S. aureus* biofilm infection. Interestingly, bacterial burdens were increased at days 7 and 10 post-infection with DFMO treatment, but were only manifest in the soft tissue surrounding the biofilm infection site (Figure 4.5D). This finding agrees with an earlier report showing that polyamines are critical for anti-staphylococcal responses and resolution of skin abscesses following DFMO treatment (149). Importantly, our study advances this finding by identifying myeloid cells as a critical source of Arg-1 during subcutaneous *S. aureus* abscess formation, since bacterial burdens were significantly increased in abscesses from *Arg-1*$^{fl/fl}$;*Tie-2*^{Cre} compared to WT mice (Figure 4.6A). No gross differences in abscess size or dermatonecrosis were observed between *Arg-1*$^{fl/fl}$;*Tie-2*^{Cre} myeloid conditional KO and *Arg-1*$^{fl/fl}$;*Tie-2*^{null} control mice (Figure 4.6B and data not shown). We did not explore the effects of DFMO on MDSC function since our data demonstrated that myeloid-derived Arg-1 does not play a major role during *S. aureus* biofilm formation. Collectively, these results demonstrate that myeloid-derived Arg-1 controls *S. aureus* growth during planktonic, but not biofilm growth *in vivo*.

Figure 4.6

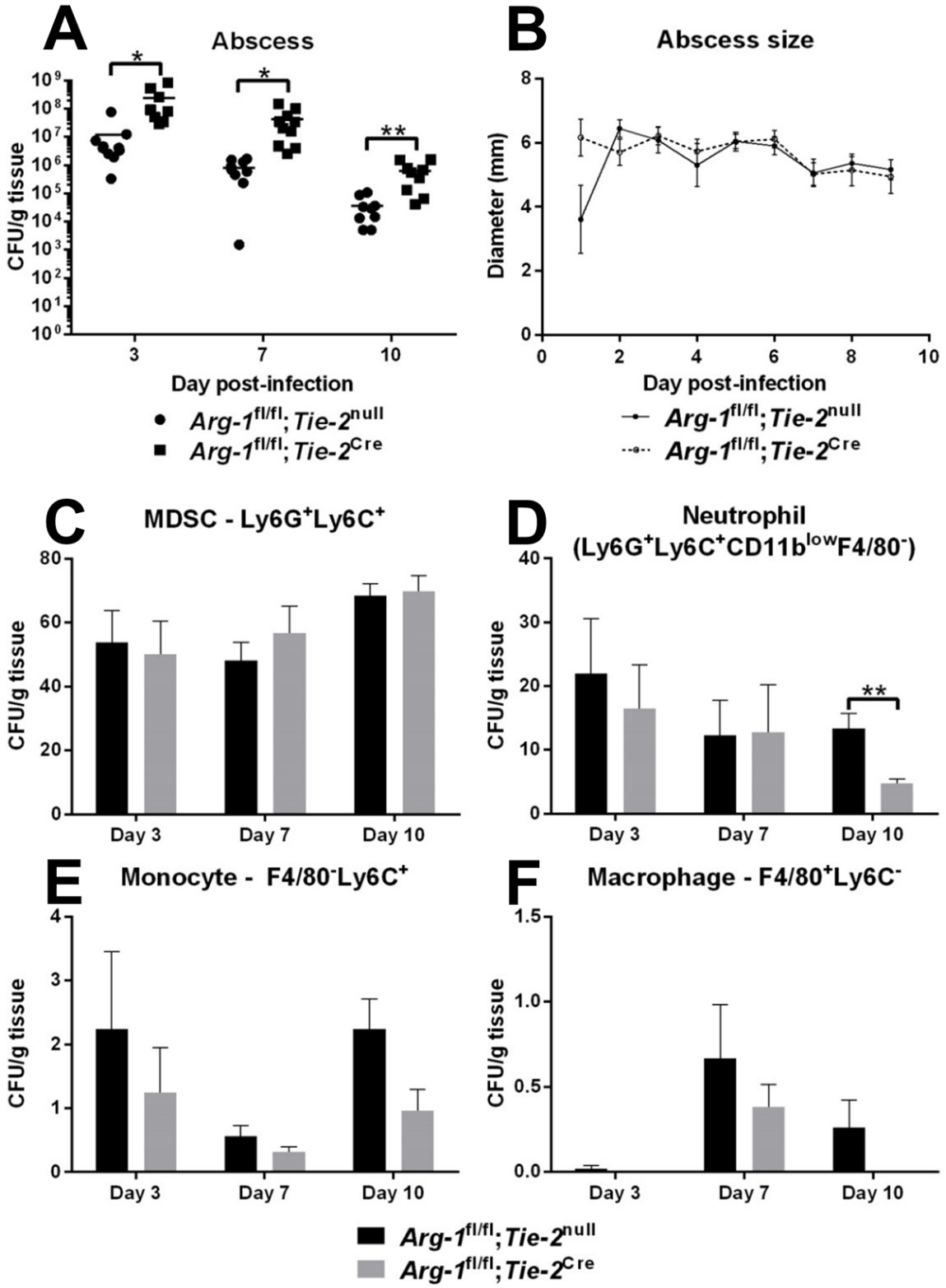
A
Abscess
CFU/g tissue
Day post-infection
Arg-1fl/fl;Tie-2null
Arg-1fl/fl;Tie-2Cre
B
Abscess size
Diameter (mm)
Day post-infection
Arg-1fl/fl;Tie-2null
Arg-1fl/fl;Tie-2Cre
C
MDSC - Ly6G+Ly6C+
CFU/g tissue
Day 3
Day 7
Day 10
D
Neutrophil
(Ly6G+Ly6C+CD11blowF4/80-)
CFU/g tissue
Day 3
Day 7
Day 10
E
Monocyte - F4/80-Ly6C+
CFU/g tissue
Day 3
Day 7
Day 10
F
Macrophage - F4/80+Ly6C-
CFU/g tissue
Day 3
Day 7
Day 10
Arg-1fl/fl;Tie-2null
Arg-1fl/fl;Tie-2Cre

Myeloid-derived arginase-1 contributes to *S. aureus* clearance during subcutaneous abscess infection. Subcutaneous abscesses were established in *Arg-1*$^{fl/fl}$;*Tie-2*^{null} (WT) and *Arg-1*$^{fl/fl}$;*Tie-2*^{Cre} mice following inoculation with 10^7 CFU *S. aureus* LAC. Animals were sacrificed at days 3, 7, and 10 post-infection, whereupon abscess-associated bacterial burdens (**A**) and leukocyte infiltrates (**C-F**) were determined. (**B**) Abscess sizes were monitored throughout the course of infection with calipers. Results are representative of two independent experiments. *, $p < 0.05$; **, $p < 0.01$; unpaired 2-tailed Student's *t*-test.

Supplemental Figure S4.1

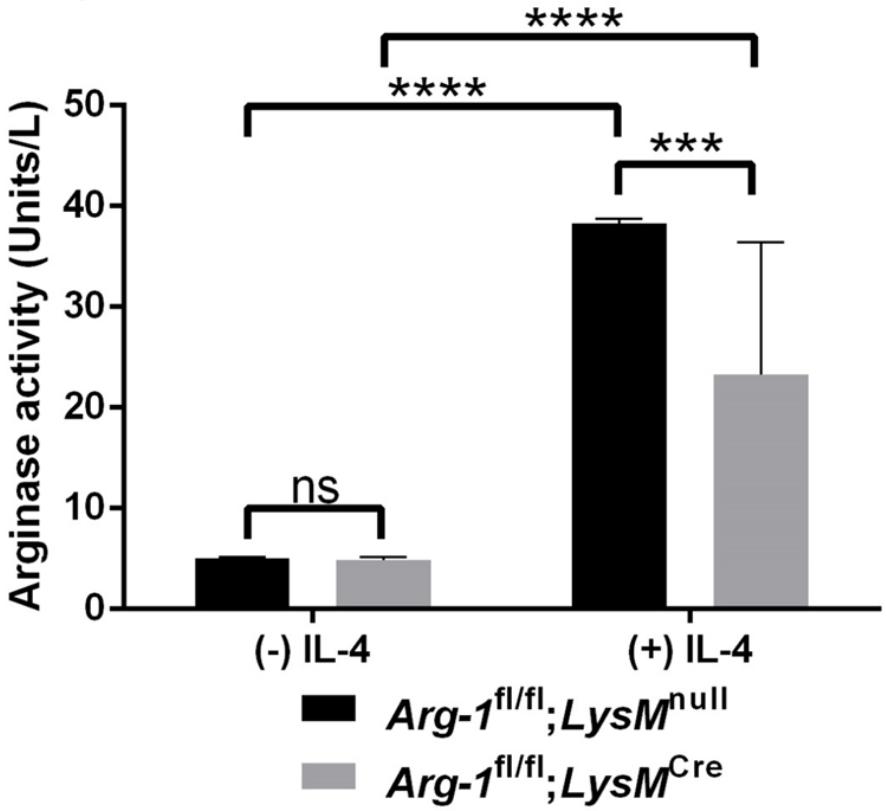

***LysM*^{Cre} is not efficient at reducing arginase activity in bone marrow-derived macrophages.** Bone marrow-derived macrophages were unstimulated or treated with rmIL-4 (10ng/mL) for 24 h, whereupon arginase activity in whole cell extracts (20 µg) was measured by the amount of enzyme that converted 1.0 µmol of L-arginine to ornithine and urea per minute. **, $p < 0.01$; ***, $p < 0.001$; ****, $p < 0.0001$; one-way ANOVA with Bonferroni's multiple comparison (ns, not significant).

Supplemental Figure S4.2

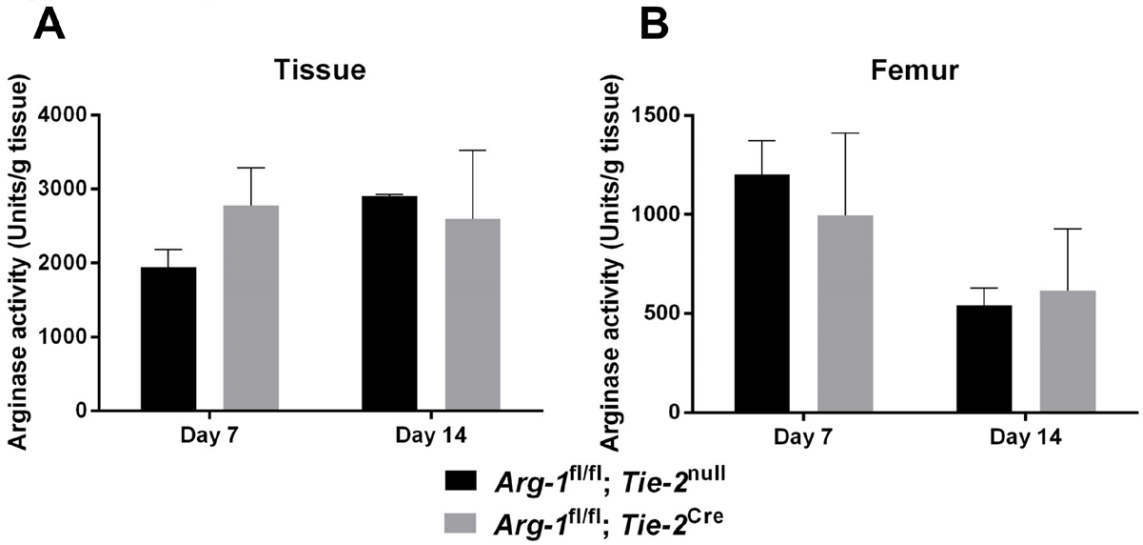

Arginase activity in whole tissue homogenates is similar between *Arg-1*$^{fl/fl}$;*Tie-2*^{Cre} and *Arg-1*$^{fl/fl}$;*Tie-2*^{null} mice. Cell-free homogenates from *Arg-1*$^{fl/fl}$;*Tie-2*^{Cre} conditional KO and *Arg-1*$^{fl/fl}$;*Tie-2*^{null} mice were prepared at days 7 or 14 post-infection in the orthopedic implant model for arginase activity assays. Arginase activity in whole cell extracts from the tissue (**A**) and femur (**B**) was determined by the amount of enzyme that converted 1.0 µmol of L-arginine to ornithine and urea per minute. Results are representative of three independent experiments.

Supplemental Figure S4.3

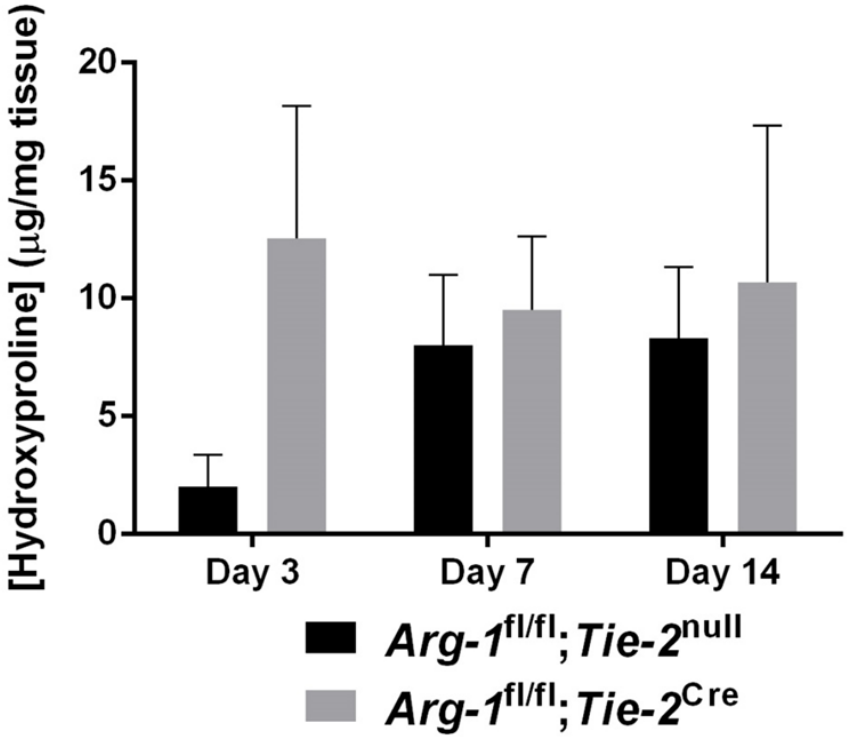

Myeloid derived Arg-1 activity does not play a significant role in collagen deposition during *S. aureus* catheter-associated infection. The soft tissues surrounding *S. aureus* infected catheters from *Arg-1*$^{fl/fl}$;*Tie-2*^{Cre} conditional KO and *Arg-1*$^{fl/fl}$;*Tie-2*^{null} mice were collected at day 3, 7, or 14 post-infection for hydroxyproline assays. Hydroxyproline content was measured by colorimetric assay, with results reported as μg of hydroxyproline per mg of tissue. Results are representative of two independent experiments.

Discussion

Our laboratory has demonstrated that MDSCs are preferentially recruited to *S. aureus* biofilm infections, where they inhibit monocyte pro-inflammatory activity to promote infection persistence (138, 139, 146-148, 187). MDSCs are the primary source of IL-10 during biofilm infection and prior studies have established that antibody-mediated depletion of MDSCs and IL-10 deficiency both result in reduced *S. aureus* biofilm burdens (138, 147, 148, 187). However, bacteria still remain in implant-associated tissues in both of these scenarios, indicating the existence of additional immunosuppressive mechanisms. Previous reports have shown that MDSCs and macrophages inhibit innate and adaptive immune responses through extracellular arginine depletion by Arg-1 (235, 327, 329). Our recent study revealed that Arg-1 expression was increased in MDSCs during *S. aureus* orthopedic implant biofilm infection and macrophages surrounding biofilm infected catheters dramatically upregulate Arg-1 (138, 148, 187, 188). Furthermore, host polyamine synthesis is important for controlling *S. aureus* growth in non-biofilm infection models, such as sepsis and subcutaneous abscesses (149). Arg-1 also plays a critical role in models of cancer, Alzheimer's disease, and infection, due to its immune suppressive properties (268, 322, 337, 338). Based on these observations, we sought to determine whether myeloid-derived Arg-1 facilitates *S. aureus* biofilm persistence, which could represent a viable treatment strategy since the enzyme is currently being explored as a therapeutic target in Alzheimer's disease (337).

Despite efficient depletion of myeloid-derived arginase activity from *Arg-1*$^{fl/fl}$;*Tie-2*^{Cre} mice, minimal differences in bacterial burdens or leukocyte infiltrates were observed in two distinct device-associated *S. aureus* biofilm infection models. MDSCs are the primary leukocyte infiltrate in both orthopedic implant and catheter-associated biofilm infection, whereas few T cells and neutrophils are present. However, one important distinction is that macrophage infiltrates are more abundant in catheter-associated infections compared to the orthopedic implant model (138, 146, 148, 187). The finding that leukocyte infiltrates were similar in *Arg-1*$^{fl/fl}$;*Tie-2*^{Cre} myeloid

conditional KO and *Arg-1*$^{fl/fl}$;*Tie-2*^{null} control mice in both models supports previous reports that Arg-1 activity regulates cellular activation rather than differential leukocyte recruitment (268, 322, 327, 328, 330). However, cellular activation status was not examined in the current study since no dramatic differences in biofilm titers were observed.

Interestingly, a marked increase in iNOS expression was observed in MDSCs from *Arg-1*$^{fl/fl}$;*Tie-2*^{Cre} myeloid conditional KO animals at both 7- and 14-days following infection. A previous study reported a similar phenomenon, where deletion of macrophage Arg-1 potentiated NO production by increasing arginine availability (268). To determine whether this increase in iNOS expression could compensate for myeloid-targeted Arg-1 depletion, *Arg-1*$^{fl/fl}$;*Tie-2*^{Cre} mice were treated with L-NIL, a small molecule inhibitor of iNOS. L-NIL had no effect on biofilm burdens or leukocyte infiltrates in *Arg-1*$^{fl/fl}$;*Tie-2*^{Cre} myeloid conditional KO mice, indicating that increased iNOS expression is not a significant compensatory mechanism for promoting biofilm persistence. In addition, unpublished data from our laboratory using iNOS KO mice has demonstrated that iNOS does not play a role in *S. aureus* biofilm infections. In contrast, McInnes *et al.* reported increased bacterial burdens and mortality during *S. aureus* septic arthritis in iNOS KO mice (240), identifying a distinction between biofilm and planktonic infection. In addition, the current study demonstrates that NADPH does not impact biofilm growth, since apocynin treatment had no effect on *S. aureus* burdens. This differs from a recent study by Sun *et al.* using NADPH-oxidase deficient mice, which revealed a critical role for ROS in controlling *S. aureus* pneumonia (343). Therefore, our study has revealed novel distinctions between *S. aureus* biofilm and planktonic infections, since iNOS and NADPH-oxidase do not affect biofilm formation but do regulate host immunity to planktonic infection.

As another potential point of redundancy, we examined whether ODC contributes to *S. aureus* persistence during biofilm infection, since a prior report revealed a critical role for polyamine synthesis in controlling *S. aureus* growth in a mouse skin abscess model (149). Interestingly, treatment of WT animals with the arginase/ODC inhibitor DFMO increased

bacterial burdens in the soft tissue surrounding infected orthopedic implants at days 7 and 10 post-infection, whereas no changes in bacterial titers were observed in the knee joint, femur, or implant. The selectivity of DFMO action in the tissue is reminiscent of our findings with the catheter-associated infection model, where *S. aureus* burdens were elevated in *Arg-1*$^{fl/fl}$;*Tie-2*^{Cre} conditional KO mice at day 10 post-infection in the surrounding soft tissues, which possess planktonic attributes since bacteria have dispersed from the catheter surface. To further demonstrate the importance of Arg-1 in the context of planktonic infection, we took advantage of a subcutaneous abscess model, where a role for polyamines in controlling bacterial growth has been previously shown (149). Importantly, our study advances this finding by identifying myeloid cells as a critical source of Arg-1 during subcutaneous *S. aureus* abscess formation, since bacterial burdens were significantly increased in abscesses from *Arg-1*$^{fl/fl}$;*Tie-2*^{Cre} compared to WT mice. Collectively, these results demonstrate that myeloid-derived Arg-1 activity and polyamine synthesis controls *S. aureus* growth during planktonic, but not biofilm growth *in vivo*.

The complete repertoire of mechanisms used by MDSCs to inhibit immune function and promote *S. aureus* biofilm establishment and persistence is still unknown. Previous studies from our laboratory have implicated a role for both IL-12 and IL-10 in the indirect recruitment and immunosuppressive function of MDSCs, respectively (146, 148). In cancer models, myeloid-derived Arg-1 has been shown to provide two complementary functions. First, depletion of extracellular arginine stores modulates the immune response by decreasing NO production, synthesis of arginine-containing proteins, and T cell activation (302, 322, 332, 333). Second, arginine metabolism provides precursor molecules for collagen and polyamine synthesis, which leads to fibrotic tissue deposition, vascular remodeling, and direct antibacterial actions (149, 260, 327, 331-333). Although prior work suggested that myeloid Arg-1 might be important for promoting *S. aureus* biofilm infection (146, 148, 187), this study demonstrates that myeloid Arg-1 does not directly influence the immune response to *S. aureus* biofilm infections or induce a compensatory increase in arginine flux towards RNI/ROS production. However, these

observations do not provide a specific mechanism by which this occurs. Namely, it does not rule out potential effects of Arg-1 on arginine bioavailability to support *S. aureus* growth and fitness *in vivo*. For example, previous studies have demonstrated that *S. aureus* growth and virulence is dependent on exogenous arginine or arginine biosynthesis via proline (344). Alternatively, *S. aureus* biofilm induction of Arg-1 expression in non-myeloid cells, such as fibroblasts or other mesenchymal cells, could over-ride any potential contribution of myeloid-derived Arg-1 activity during *S. aureus* biofilm infection. This would require crossing *Arg-1*$^{fl/fl}$ with a Cre line directed by the type I collagen promoter Col1a2 to target gene deletion in fibroblasts (345). Furthermore, mitochondrial Arg-2 released from dead or dying cells could also contribute to the overall pool of arginase enzyme activity (341). Additional studies are needed to address these possibilities; however, this study demonstrates that myeloid-derived Arg-1 has minimal effects on *S. aureus* biofilm growth, but instead plays a unique role in controlling *S. aureus* planktonic infections.

Chapter 5: Discussion and Future Directions

Key Findings and Conclusions

The innate immune system is the first line of defense against invading bacterial pathogens. Specifically, MΦs are a key component of the initial response to pathogens, as they are resident in all tissues, able to directly kill bacterial pathogens, and function as antigen presenting cells to effectively link the innate and adaptive immune systems. However, the ability of *S. aureus* to form biofilm has endowed it with sophisticated subversion strategies to actively inhibit immune-mediated clearance mechanisms. *S. aureus* biofilm infections actively polarize the innate immune response to promote biofilm establishment and persistence, which is evident by the influx of MDSCs, paucity of neutrophils and T cells, and the polarization of anti-inflammatory MΦs, all of which play a role in the chronicity of *S. aureus* biofilm infections (145, 146, 148, 187, 226).

Our laboratory has previously determined that the polarization of anti-inflammatory monocytes/MΦs plays a critical role in promoting *S. aureus* biofilm persistence. It is known that MΦs recruited to the site of *S. aureus* biofilm infections will quickly acquire anti-inflammatory properties and are subject to toxin-mediated death (139). However, adoptive transfer of *in vitro*-derived pro-inflammatory MΦs into a catheter-associated *S. aureus* biofilm infection inhibits biofilm formation and promotes clearance. Our laboratory has also shown that the cytokine milieu produced by biofilm-associated MDSCs polarizes monocytes to become anti-inflammatory (146, 148, 187, 226). Depletion of MDSCs and neutrophils with α-Ly6G antibody (1A8) transformed monocytes to a pro-inflammatory state, resulting in reduced biofilm burdens. Depletion of monocytes and MΦs in addition to MDSCs and neutrophils with α-GR-1 antibody increased bacterial burdens and worsened the infection, indirectly demonstrating that monocytes and MΦs are an essential effector cell population to control the *S. aureus* biofilm bacterial burdens (187).

My dissertation work was centered on elucidating the relationship between leukocyte metabolism and inflammatory function. The field of immunometabolism focuses on understanding the link between intrinsic changes in leukocyte metabolism and how it governs,

and is governed by, leukocyte inflammatory phenotype. It has been shown that pro-inflammatory MΦs and dendritic cells shift their metabolism towards aerobic glycolysis in order to provide the necessary carbon flux through the pentose phosphate pathway and provide precursor molecules for anabolic processes and/or production of reactive oxygen species (256, 257, 260). In contrast, anti-inflammatory MΦs primarily rely on OxPhos to drive their activity, with fatty acid oxidation also playing a role (256, 289, 290). In MΦs, these metabolic switches are facilitated by global changes in gene expression that will ultimately lead to a shift in metabolism, carbon consumption, metabolite accumulation, and overall leukocyte phenotype and inflammatory activity.

We demonstrated that leukocyte metabolism, specifically monocyte metabolism, can be targeted to ultimately promote clearance of the biofilm (Chapter 3). By designing nanoparticle formulations containing the ATP synthase inhibitor, oligomycin to specifically target Fc-receptor positive monocytes, we were able to dictate the outcome of biofilm infection. Monocytes isolated from nanoparticle treated animals displayed an altered intracellular metabolome as compared to control monocytes. In addition, they exhibited shifts in gene expression that were consistent with the profile of a pro-inflammatory monocyte. These metabolic and transcriptional changes translated to sustained decreases in bacterial burdens. Metabolomic and RT-qPCR analysis of MDSC populations showed significant changes in the intracellular metabolome and transcriptional profile despite showing no evidence of nanoparticle uptake. While MDSCs are known to direct the activity and function of other leukocytes, this finding highlights the dynamic crosstalk that occurs between activated monocytes and MDSCs. Previous work from our laboratory revealed that *S. aureus* biofilms cannot be cleared with any treatment regimen, including antibiotics (146, 148, 187). Surprisingly, nanoparticle administration acted synergistically with antibiotic treatment to clear the infection. Together this suggests that targeting monocyte metabolism can polarize monocytes to change the biofilm structure and milieu to allow for antibiotic-mediated clearance of the infection.

We investigated Arg-1 in the myeloid compartment to determine whether the metabolic enzyme plays a role in promoting biofilm persistence. During *S. aureus* biofilm infection, MDSCs and MΦs significantly upregulate Arg-1 expression, which catalyzes the conversion of arginine to ornithine and urea and ultimately regulates the availability of arginine. However, using *Arg-1*$^{fl/fl}$;*Tie2*^{Cre} conditional knockout animals, we found that myeloid Arg-1 does not play a critical role in biofilm establishment or persistence in either the *S. aureus* catheter or implant biofilm models. While Arg-1 was effectively deleted in *Arg-1*$^{fl/fl}$;*Tie2*^{Cre} MΦs, bacterial burdens were unchanged. Although *Arg-1*$^{fl/fl}$;*Tie2*^{Cre} conditional knockout animals did display a compensatory increase in iNOS expression, small molecule inhibitors of iNOS, NADPH oxidase, or ornithine decarboxylase did not alter the outcome of infection. This indicates that arginine availability does not dramatically influence *S. aureus* biofilm infection. Instead, we found that myeloid-derived Arg-1 does play an important role in controlling planktonic *S. aureus*, since *Arg-1*$^{fl/fl}$;*Tie2*^{Cre} animals had significantly higher bacterial burdens, although this did not translate into changes in dermatonecrosis or abscess size. This is supported by prior studies that demonstrate a role for arginine availability for polyamine synthesis in controlling *S. aureus* growth (149).

In summary, this work has advanced our understanding of the relationship between leukocyte metabolism and inflammatory phenotype in the context of *S. aureus* biofilm-associated infections. Furthermore, these studies also highlight the dynamic host-pathogen interactions in addition to the host-host interactions that occur in these complex infections. This emphasizes the challenges that are faced when treating, or trying to prevent *S. aureus* biofilm infections. However, it opens up a previously unexplored area of research in the context of leukocyte metabolism during *S. aureus* biofilm infections. The method of targeting effector leukocyte metabolism may ultimately lead to the development of novel therapeutic options for *S. aureus*-associated biofilm infections and other chronic diseases.

Future Directions

Genetic approach to targeting MΦ metabolism

Our work has demonstrated that nanoparticle-mediated delivery of metabolic inhibitors can promote monocyte polarization and clearance of *S. aureus* biofilms. As a complementary approach to regulate leukocyte metabolism during *S. aureus* biofilm infections, we have initiated studies with a transgenic mouse that possesses a targeted deletion in the electron transport chain. Nuclear encoded ubiquinone oxidoreductase iron-sulfur protein 4 (*Ndusf4*) is a non-catalytic subunit of complex I of the electron transport chain. Deletion of the *Ndusf4* gene results in decreased OxPhos activity, with a corresponding increase in glycolysis (266, 346, 347). Previous studies have utilized *Tie2* (receptor tyrosine kinase *Tek*)-driven Cre-recombinase expression to conditionally delete *Ndusf4* in MΦs (266, 348). Here we utilized *LysM*-driven Cre-recombinase expression to conditionally knockout *Ndusf4* in MΦs and monocytes, in addition to other myeloid cell populations (i.e. MDSCs and PMNs) (269). We hypothesized that these animals would display a similar phenotype during infection as mice treated with nanoparticles. Specifically, we predicted that inhibiting the electron transport chain and OxPhos activity in myeloid cells would enhance their pro-inflammatory activity and lead to biofilm clearance. The fact that *Ndusf4* is deleted in multiple myeloid populations will be important to consider when comparing these results with monocyte-directed nanoparticles.

Ndusf4$^{fl/fl}$ animals were kindly provided by Dr. Phillip G. Morgan (Seattle Children's Research Institute, Seattle WA) and crossed with *LysM*-driven Cre-recombinase animals. Preliminary studies measuring the metabolic activity of *Ndusf4*$^{fl/fl}$;*LysM*^{Cre} bone marrow-derived MΦs using Seahorse XF96 metabolic assays, showed that these MΦs have decreased OxPhos and increased glycolytic activity as expected (Figure 5.1). Specifically, *Ndusf4*$^{fl/fl}$;*LysM*^{Cre} MΦs had significantly less respiratory capacity due to the electron transport chain defect (Figure 5.1A and 5.1C). In addition, *Ndusf4*$^{fl/fl}$;*LysM*^{Cre} MΦs showed increased glycolytic activity Compared to

Ndusf4$^{fl/fl}$;*LysM*^{null} control MΦs, indicating that *Ndusf4*$^{fl/fl}$;*LysM*^{Cre} MΦs experienced a glycolytic shift in their metabolism (Figure 5.1D and 5.1E).

Previous work from our laboratory has shown that MΦs are unable to infiltrate an intact biofilm *in vitro* (60, 138, 139). Based on the fact that the loss of *Ndusf4* in MΦs pushed their metabolic activity towards glycolysis, we hypothesized that these cells should display a skewed phenotype towards pro-inflammatory activity and therefore be able to kill and infiltrate a *S. aureus* biofilm. To investigate this possibility, *Ndusf4*$^{fl/fl}$;*LysM*^{null} and *Ndusf4*$^{fl/fl}$;*LysM*^{Cre} MΦs were co-cultured *in vitro* with *S. aureus* biofilms at different stages of growth (Figure 5.2). We show that bacterial burdens in the biofilm increase over a 4 day period, indicating that upon co-culture, MΦs will encounter different bacterial numbers based on biofilm maturity (Figure 5.2). When MΦs were co-cultured with planktonic bacteria, no differences in bacterial titers were evident between wildtype and *Ndusf4*-deficient MΦs throughout a 4 day interval (Figure 5.2B). Similarly, biofilm burdens were indistinguishable when wildtype and *Ndusf4* deficient MΦs were incubated with biofilms of various levels of maturity (Figure 5.2C–F). Furthermore, confocal microscopy revealed similar invasion patterns of *Ndusf4*$^{fl/fl}$;*LysM*^{null} or *Ndusf4*$^{fl/fl}$;*LysM*^{Cre} MΦs into *S. aureus* biofilms (Figure 5.3).

Since the large numbers of bacteria in a biofilm may overshadow potential differences in MΦ bactericidal activity, gentamicin protection assays were performed to determine whether *Ndusf4*-deficient MΦs were better able to phagocytose and kill planktonic *S. aureus* (Figure 5.4). Modest differences were observed between wildtype and *Ndusf4*-KO MΦs during acute intervals and were MOI-dependent, which might reflect differences in phagocytic activity. At higher MOIs, intracellular *S. aureus* burdens were significantly reduced in *Ndusf4*-KO MΦs at 24 and 48 h suggesting that indeed, these MΦs possess greater bactericidal activity (Figure 5.4A-B).

Based on our *in vitro* data showing that *Ndusf4*-KO MΦs were more glycolytic (Figure 5.1) and better able to kill intracellular *S. aureus* (Figure 5.4), we next examined the role of myeloid metabolism in the establishment and persistence of a *S. aureus* orthopedic implant

biofilm infection. Our laboratory has shown that this infection model is dominated by MDSC infiltrates, which play a key role in directing the polarization of anti-inflammatory monocytes and MΦs. Monocyte and MΦ anti-inflammatory polarization is associated with a bias towards OxPhos metabolism (146, 148, 187, 226). We predicted that inhibiting the electron transport chain and OxPhos activity in myeloid cells by *Ndusf4* deletion would enhance their pro-inflammatory activity and lead to biofilm clearance. Surprisingly, despite the increased glycolytic activity in *Ndusf4*-KO MΦs *in vitro*, bacterial burdens were significantly higher in the infected soft tissues of *Ndusf4*$^{fl/fl}$;*LysM*^{Cre} conditional KO animals compared to *Ndusf4*$^{fl/fl}$;*LysM*^{null} controls (Figure 5.5A). In contrast, bacterial burdens in the knee joint, femur, and implant were relatively unaffected (Figure 5.5B-D). Although titers were significantly increased in the femur of *Ndusf4*$^{fl/fl}$;*LysM*^{Cre} conditional KO mice at 7 days post-infection, this was transient and not observed at later time points (Day 14 and 28). In general, leukocyte infiltrates were not significantly affected over the 28 day infection interval (Figure 5.5E-H). However, in a few instances MDSCs were significantly reduced concomitant with increased monocyte and MΦ populations in *Ndusf4*$^{fl/fl}$;*LysM*^{Cre} conditional KO mice. Collectively, these results indicate that although MΦs from *Ndusf4*$^{fl/fl}$;*LysM*^{Cre} animals are more glycolytic and better able to kill intracellular planktonic *S. aureus* the broader deletion of *Ndusf4* from all myeloid populations does not translate to a reduction in bacterial burdens *in vivo*.

Finally, we compared the ability *Ndusf4*$^{fl/fl}$;*LysM*^{Cre} and *Ndusf4*$^{fl/fl}$;*LysM*^{null} mice to control *S. aureus* abscess infection, to determine if a distinctions would be observed compared to biofilm growth (Figure 5.6). While subcutaneous *S. aureus* abscesses elicit a large MDSC infiltrate, the infection is generally cleared by the immune system and is not chronic, unlike biofilm (241, 349). Similar to what was seen during orthopedic implant biofilm infection, *Ndusf4*$^{fl/fl}$;*LysM*^{Cre} mice had significantly higher bacterial burdens (Figure 5.6A), in addition to larger abscesses (Figure 5.6B) and increased dermatonecrosis (Figure 5.6C). No significant differences in leukocyte infiltrates were observed (Figure 5.6).The increase in bacterial burdens in *Ndusf4*$^{fl/fl}$;*LysM*^{Cre} mice

could suggest that the metabolic state of monocytes/MΦs in these animals is influenced by the lack of *Ndusf4* in other myeloid cells that were also targeted (350).

MΦ/monocyte-specific *Ndusf4* conditional knockout

Conditional knockout mouse models allow for the deletion of a gene at a specific time or in specific tissues by controlling the timing and expression of Cre-recombinase. This strategy allowed us to specifically delete Arg-1, where the germline knockout is lethal, in MΦ (Tie2) (339) and myeloid (LysM) populations (Chapter 4) (269). We initiated our metabolic studies using LysM-driven Cre expression to delete *Ndusf4*, where LysM is expressed in all myeloid cells and not monocyte/MΦ-specific. Therefore, in *Ndusf4*$^{fl/fl}$;*LysM*^{Cre} mice the *Ndusf4* gene is deleted in monocytes, neutrophils, and MDSCs. Prior studies from our laboratory have shown that the specificity between targeting monocytes, MDSCs and neutrophils is important (187). Therefore, a clean, monocyte/-specific, conditional knockout is necessary because of the influence of MDSCs on other immune cells. Previous studies have shown that glycolysis in MDSCs promotes their expansion and arrests their maturation, maintaining suppressive activity (351). Therefore, while *Ndusf4*$^{fl/fl}$;*LysM*^{Cre} monocytes are more glycolytic *in vitro* this effect is possibly mitigated *in vivo* by the expanded/activated MDSC population. In addition, LysM expression isn't observed in all mononuclear phagocytes, and can vary between mice (268, 270). Therefore, future studies should be performed with *Ndusf4*$^{fl/fl}$;*Tie2*^{Cre} mice, which more specifically targets monocytes/MΦs over other myeloid populations. If bacterial burdens are reduced in infected *Ndusf4*$^{fl/fl}$;*Tie2*^{Cre} mice, this would confirm the modulatory effects of monocyte metabolism in addition to suggesting an opposing effect of MDSC metabolism in dictating *S. aureus* biofilm infection outcome.

Alternative floxed mouse models

Ndusf4$^{fl/fl}$ mice were utilized in our work to inactivate OxPhos because prior studies have shown that they are viable in another bacterial infection model (266). Other floxed animals, such as *Tfam*$^{fl/fl}$ (transcription factor A) which is a transcriptional regulator required for synthesis of ETC genes, have significant viability issues and often develop cancers (352). Although previous

work noted no changes in MΦ survival, viability could likely be affected once glycolytic metabolism is accelerated (255, 256, 266, 290). Alternative floxed animals could be utilized in the future that target complex II or depress ATP-synthase activity. However, to our knowledge there are not any currently available transgenic mouse models fitting these specifications.

In addition, it is worth noting that floxed animals may contain background mutations that affect phenotypes. Pertinent to this dissertation work, *Ndusf4*$^{fl/fl}$ mice had been reportedly backcrossed to C57BL/6 mice for > 20 generations, yet both *Ndusf4*$^{fl/fl}$;*LysM*^{Cre} and *Ndusf4*$^{fl/fl}$;*LysM*^{null} control animals exhibited gross changes in their snout morphology compared to standard C57BL/6 mice. In addition, their skin was loose and very pliable. Integument defects were previously noted in *Ndusf4* complete knockout animals, but had not been reported in the conditional knockout animals (266). This may partially explain biofilm clearance at later time points in the knee joint, femur, and implant of both *Ndusf4*$^{fl/fl}$;*LysM*^{Cre} and for *Ndusf4*$^{fl/fl}$;*LysM*^{null} control mice, which is not observed in C57BL/6 or other mouse strains utilized by our laboratory (146, 148, 187, 226).

Figure 5.1

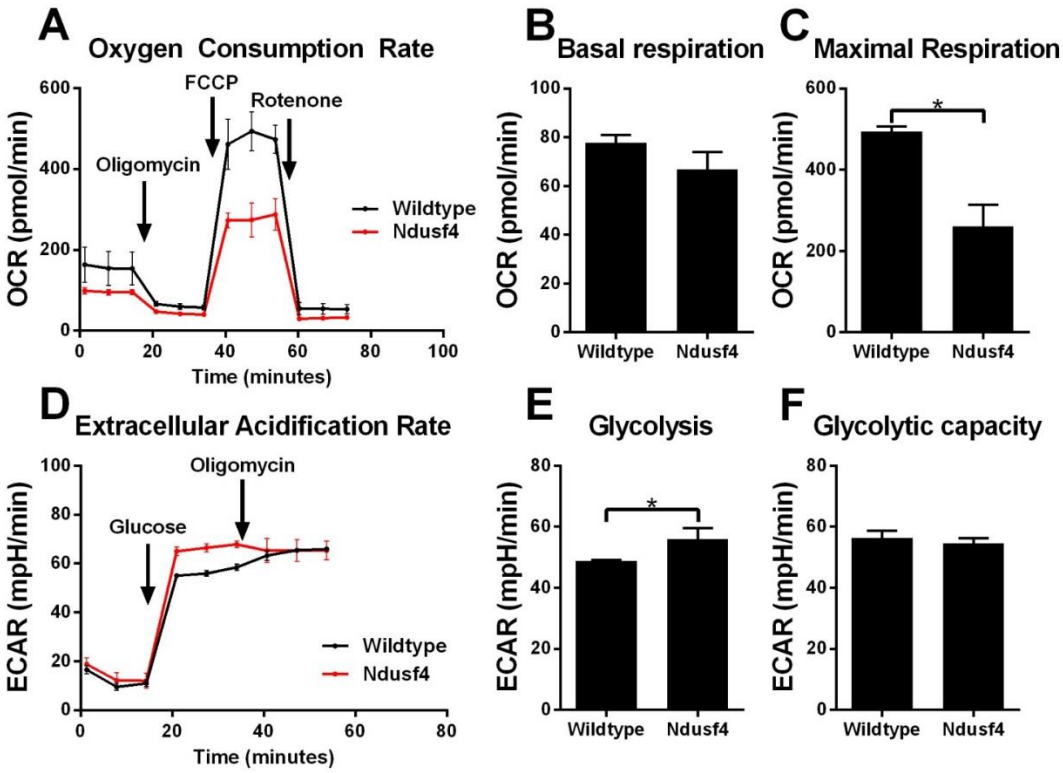

***Ndusf4* deletion in MΦs induces a shift in metabolism towards glycolysis.** Bone marrow-derived MΦs from *Ndusf4*$^{fl/fl}$;*LysM*^{null} and *Ndusf4*$^{fl/fl}$;*LysM*^{Cre} mice were harvested and plated for 24 h in a Seahorse XF96 culture plate, whereupon Seahorse Bioscience assays were performed to assess (**A**) OxPhos and (**D**) glycolysis. (**B**) Basal respiration, (**C**) maximal respiration, (**E**) glycolytic, and (**F**) glycolytic capacity were calculated using well-defined algorithms. Data is presented as the mean (n=3). (*, $p < 0.05$; Student's *t*-test.).

Figure 5.2

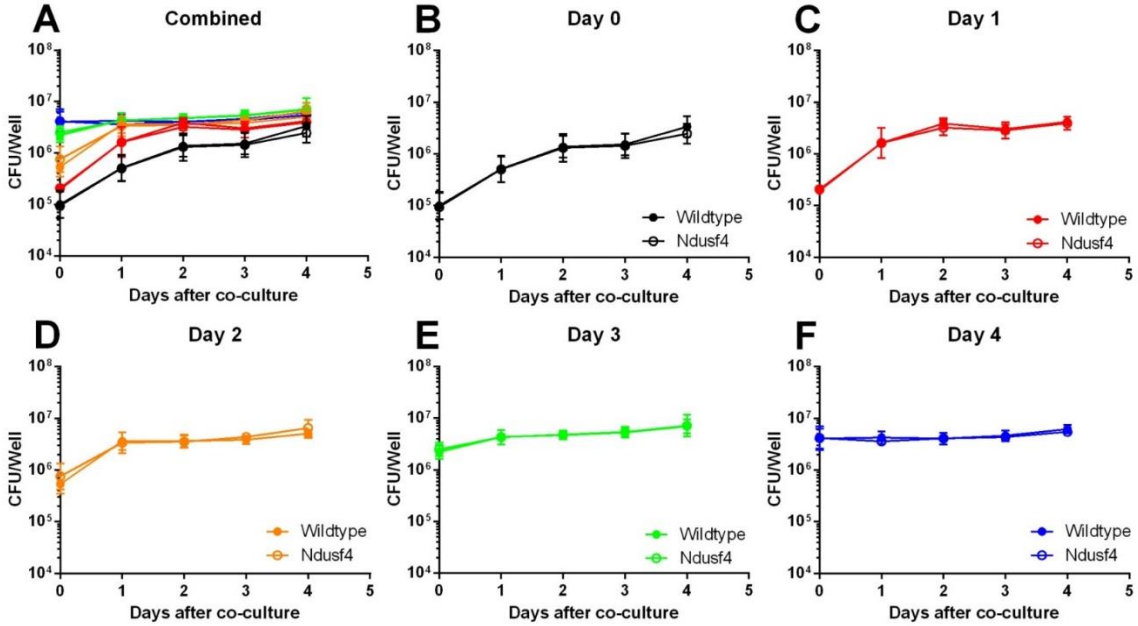

Co-culture of *Ndusf4*$^{fl/fl}$;*LysM*^{Cre} MΦs with *S. aureus* biofilms of various maturation states.

(**A**) Bone marrow-derived MΦs from *Ndusf4*$^{fl/fl}$;*LysM*^{null} and *Ndusf4*$^{fl/fl}$;*LysM*^{Cre} mice were co-cultured with planktonic bacteria (**B**, Day 0, black) or biofilms of varying maturity levels (**C**, Day 1, red; **D**, Day 2, orange; **E**, Day 3 , green; **F**, Day 4, blue). Remaining bacterial burdens following MΦs addition were enumerated daily for 4 consecutive days. Data is presented as the mean ± SD (n = 9 combined from 3 experiments).

Figure 5.3

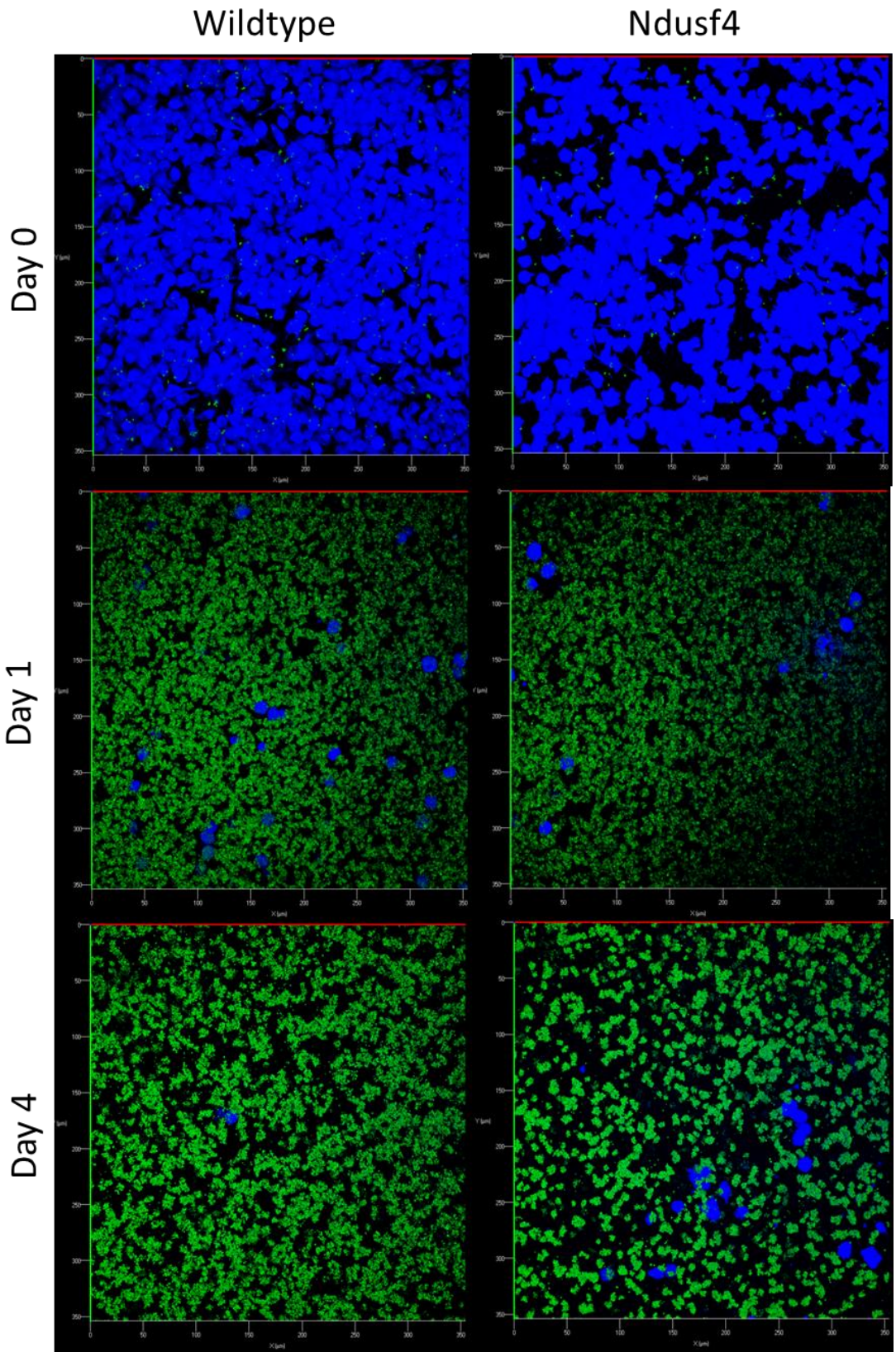

Confocal imaging of *Ndusf4*$^{fl/fl}$;*LysM*^{Cre} MΦ-*S. aureus* biofilm co-cultures. Bone marrow-derived MΦs from *Ndusf4*$^{fl/fl}$;*LysM*^{null} (wildtype, left) and *Ndusf4*$^{fl/fl}$;*LysM*^{Cre} (*Ndusf4*, right) mice were stained with CellTracker Blue and co-cultured with GFP expressing *S. aureus* biofilms that were 0, 1, or 4 days old at the beginning of the co-culture period. Figures show representative images of a 3D top-down view of the biofilm-MΦ co-culture.

Figure 5.4

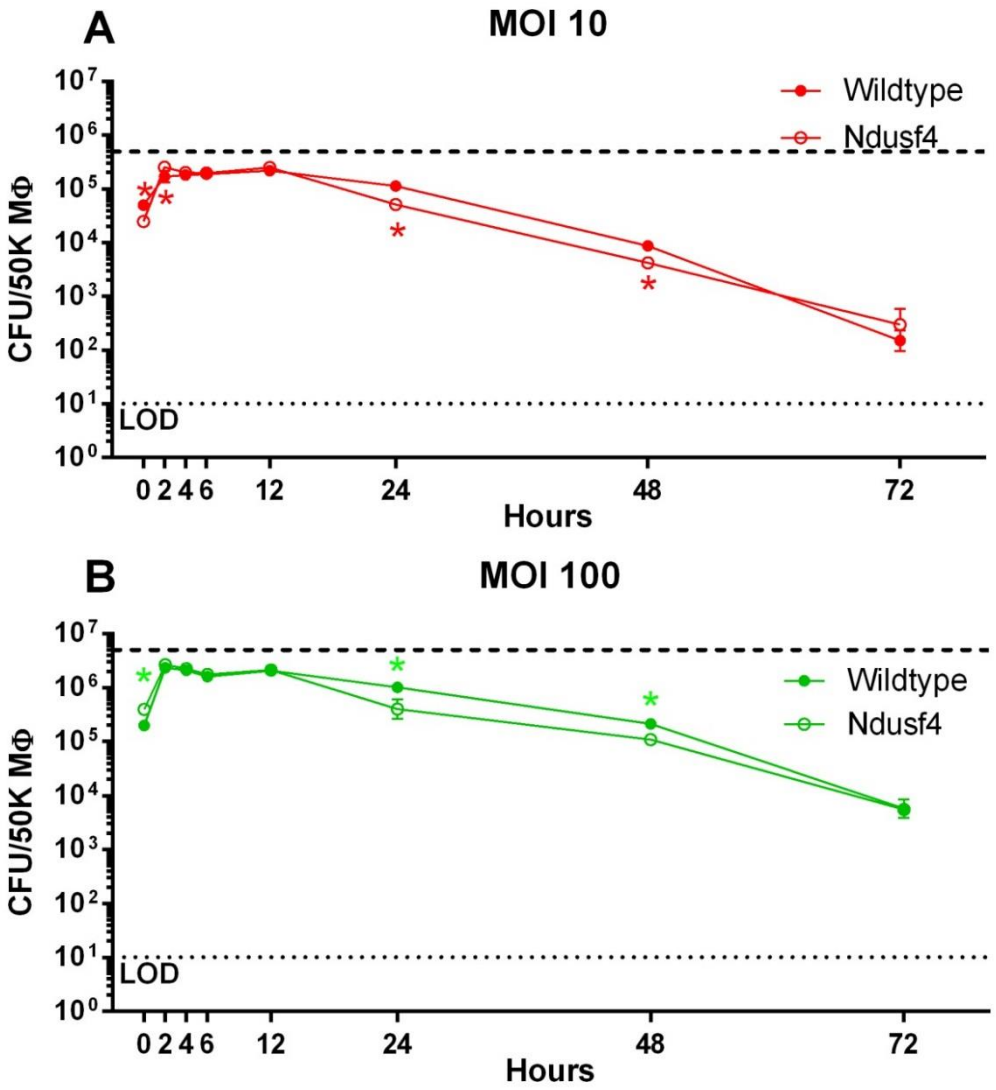

***Ndusf4*$^{fl/fl}$*;LysM*^{Cre} MΦs display increased *S. aureus* bactericidal activity.** Bone marrow-derived MΦs from *Ndusf4*$^{fl/fl}$;*LysM*^{null} and *Ndusf4*$^{fl/fl}$;*LysM*^{Cre} mice were plated in a 96-well plate at 5x10^4 MΦs per well for 24 h. MΦs were challenged with *S. aureus* at an MOI of (**A**) 10 or (**B**) 100 for 45 min and treated with 100μg/mL gentamicin to kill remaining extracellular bacteria. MΦs were maintained in medium supplemented with low dose gentamicin (20μg/mL) until the specified time points, whereupon lysates were plated to enumerate viable intracellular bacteria, which is reported as CFU/5x10^4 MΦs. Dashed and dotted lines represent the limit of detection

(LOD) and the inoculum, respectively. Data is presented as the mean (n=3). (*, $p < 0.05$; student's *t*-test.).

Figure 5.5

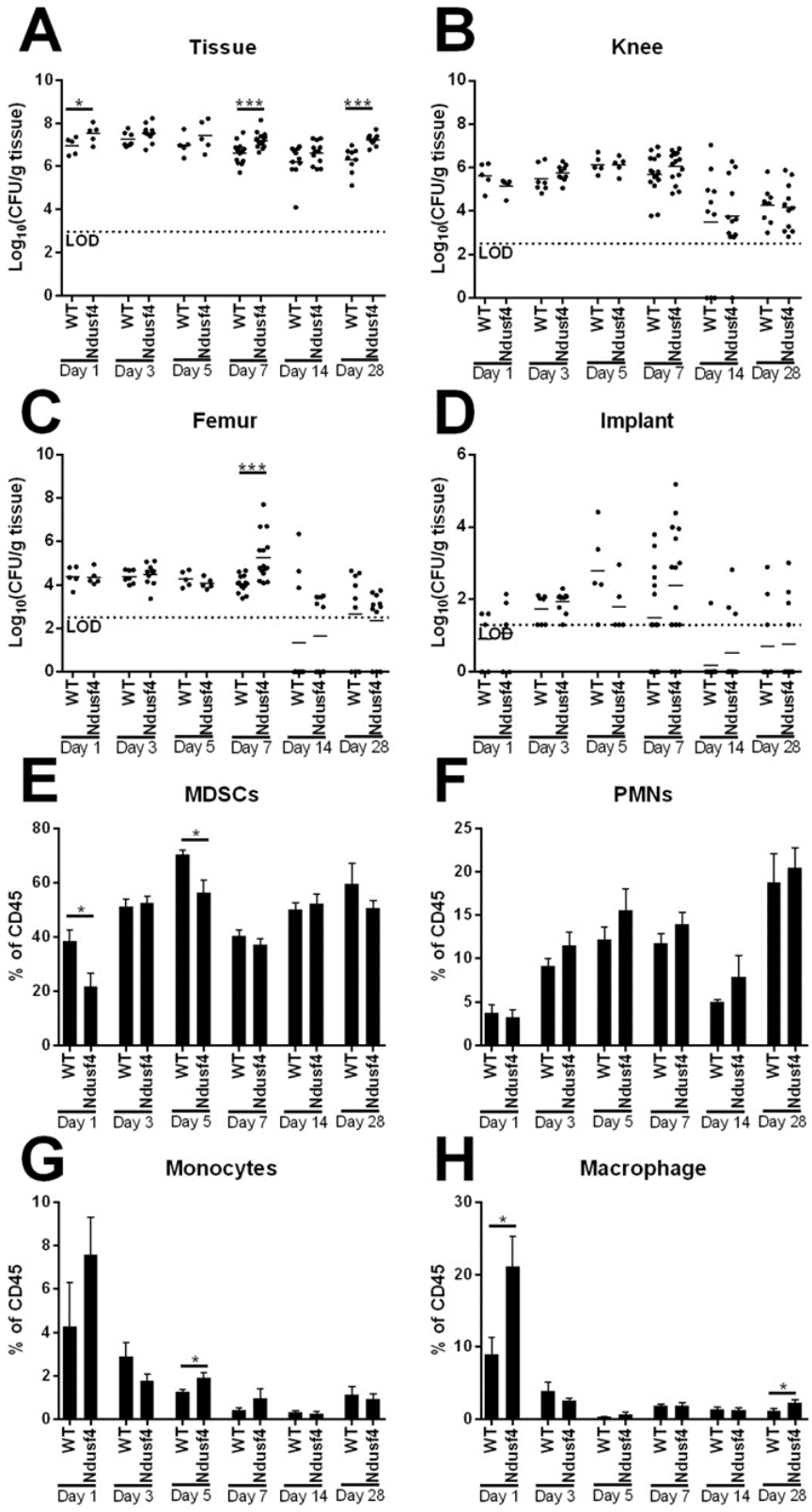
A
Tissue
B
Knee
C
Femur
D
Implant
E
MDSCs
F
PMNs
G
Monocytes
H
Macrophage
Log10(CFU/g tissue)
% of CD45
LOD
WT
Ndusf4
Day 1
Day 3
Day 5
Day 7
Day 14
Day 28

Myeloid deletion of *Ndusf4* leads to an increase in bacterial burdens during orthopedic implant infection. A titanium orthopedic implant was placed in the femur of *Ndusf4*$^{fl/fl}$;*LysM*^{null} (WT) and *Ndusf4*$^{fl/fl}$;*LysM*^{Cre} mice and inoculated with 10^3 CFU *S. aureus* LAC. (**A-D**)Tissue surrounding the infected implant, knee joint, femur, and implant were collected at the indicated intervals post-infection to quantify bacterial burdens. (**E-H**) Infiltrating leukocyte populations in implant-associated tissues were evaluated by flow cytometry. Results are representative of ≥ 2 independent experiments. (*, $p < 0.05$; ***, $p < 0.001$; unpaired 2-tailed Student's *t*-test.)

Figure 5.6

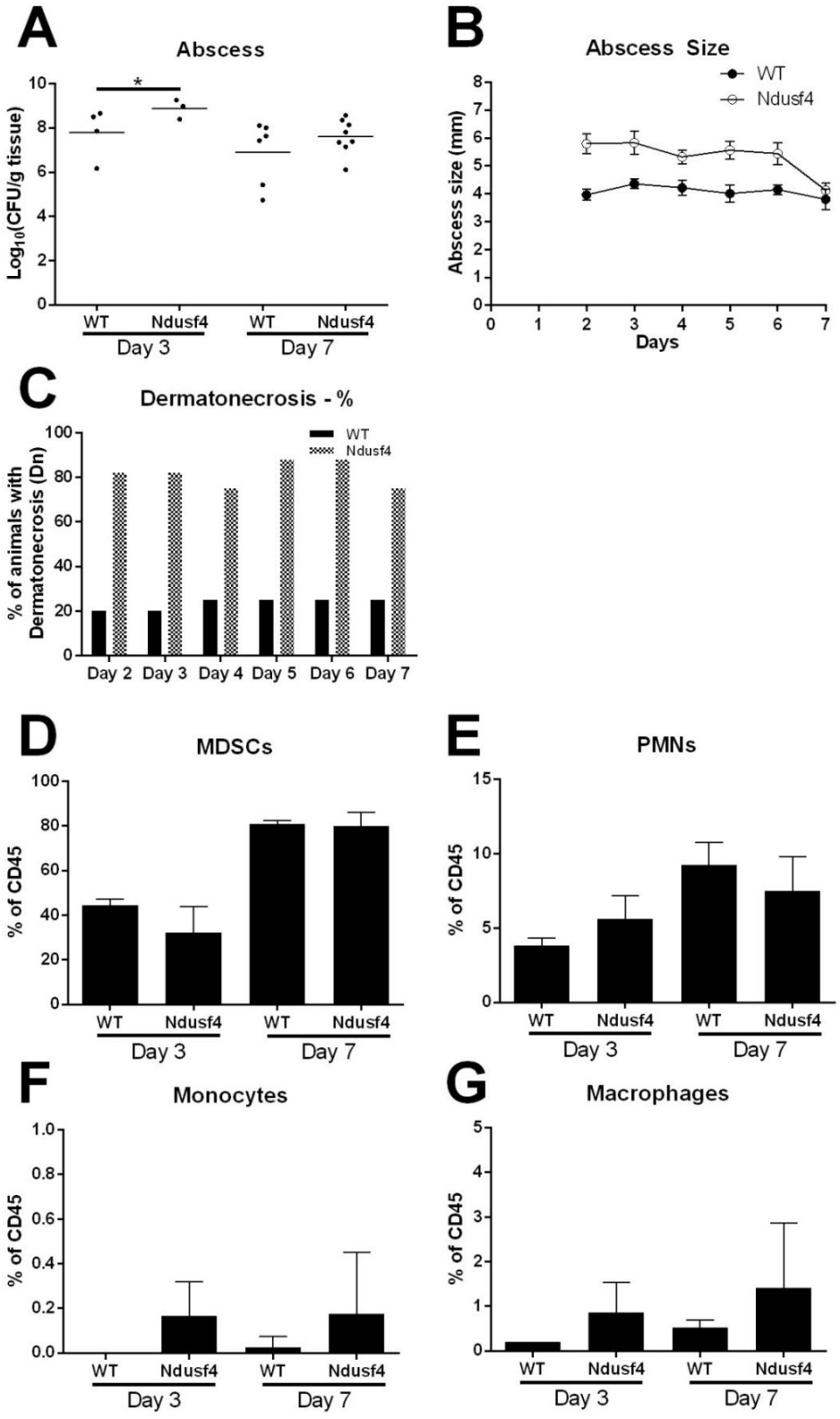
A
Abscess
Log10(CFU/g tissue)
WT
Ndusf4
Day 3
Day 7
B
Abscess Size
WT
Ndusf4
Abscess size (mm)
Days
C
Dermatonecrosis - %
% of animals with Dermatonecrosis (Dn)
Day 2
Day 3
Day 4
Day 5
Day 6
Day 7
D
MDSCs
% of CD45
E
PMNs
F
Monocytes
G
Macrophages

Myeloid deletion of *Ndusf4* leads to an increase in bacterial burdens during subcutaneous abscess infection. Subcutaneous abscesses were established in *Ndusf4*$^{fl/fl}$;*LysM*^{null} (WT) and *Ndusf4*$^{fl/fl}$;*LysM*^{Cre} mice following inoculation with 10^7 CFU *S. aureus* LAC. Animals were sacrificed at days 3 and 7 post-infection, whereupon abscess associated bacterial burdens (**A**) and leukocyte infiltrates (**D-G**) were determined. (**B**) Abscess sizes were monitored throughout the course of infection with calipers. (**C**) The presence of dermatonecrosis was noted daily. Results are from a single experiment. *, $p < 0.05$; unpaired 2-tailed Student's *t*-test.

Determine what MDSC- or biofilm-derived products mediate the shift in monocyte metabolism

Biofilm-associated monocytes process signals from a dynamic and complex milieu, receiving input from both surrounding host cells and the biofilm. Our laboratory has demonstrated that MDSCs are important for polarizing monocytes toward an anti-inflammatory state. This was evident following MDSC depletion using a Ly6G antibody, where FACS-purified $Ly6G^{-}Ly6C^{+}$ monocytes/MΦs exhibited increased iNOS, IL-12p40, and IL-6 expression, which translated into improved biofilm clearance (187). Meanwhile, the abundance of PAMPs at the site of infection likely influences monocyte metabolism. In addition, our laboratory has used proteomic analysis of biofilms to demonstrate the immune inhibitory role of *S. aureus* toxins, including Hla and LukAB (60). It is known that Hla facilitates immune evasion by preventing phagosome-mediated killing, but both Hla and LukAB are able to kill leukocytes by binding to ADAM10 and CD11b, respectively (60).

Since MDSCs are the primary source of IL-10 during *S. aureus* biofilm infection, which can block monocyte NF-κB activation and downregulate cytokine expression, IL-10 is likely a key mechanism whereby MDSCs polarize biofilm-associated monocytes to an anti-inflammatory state (148, 187). In addition, monocytes isolated from biofilm infected IL-10 KO mice, showed increased iNOS, IL-1α, and TNF-α expression, with a concomitant decrease in Arg-1, suggesting that these monocytes are now pro-inflammatory. IL-10 KO animals have significantly reduced bacterial burdens, and this is negated by adoptively transferring wildtype, *in vitro*-derived MDSCs (148). Therefore, since MDSC IL-10 production significantly influences the inflammatory phenotype of monocytes, IL-10 likely plays a role in shifting monocyte metabolism to favor OxPhos. While it is known that IL-10 affects metabolism through the induction of the mTOR inhibitor DDIT4, this has not yet been examined in the context of *S. aureus* biofilm infection (353). It would be interesting to see whether DDIT4-deficient animals would be able to clear a chronic biofilm infection. In addition, *in vivo* depletion studies in IL-10 KO animals and

co-culture experiments of IL-10 KO or WT MDSCs with WT MΦs on a biofilm can help to determine the role of IL-10 in metabolic skewing.

PAMPs and other bacterial products also likely influence monocyte metabolism and inflammatory phenotype. Despite the abundance of pro-inflammatory molecules that exist at the site of infection, the biofilm may produce, or possibly deplete, molecules to bias monocyte metabolism towards OxPhos to promote anti-inflammatory activity. Specific evidence from MΦ co-cultures with WT or ΔLuk-AB/Hla *S. aureus* biofilms show that these molecules kill leukocytes and affect their inflammatory activity. While MΦ death was mitigated, MΦ skewing was not completely relieved with the ΔLuk-AB/Hla strain, suggesting that other proteins act redundantly to alter leukocyte activity and metabolism (60). While the level of redundancy is unknown, proteomic studies of biofilms co-cultured with both MDSCs and MΦs may be necessary to fully elucidate the contributing mechanisms utilized by the biofilm vs MDSCs to shift monocyte metabolism. The *S. aureus* biofilm infection milieu is complex and dynamic, and should be studied further to elucidate the mechanism of metabolic-mediated immune polarization of monocytes, in order to develop novel therapeutics.

Effect of monocyte metabolism on leukocyte longevity

Leukocyte lifespan is tightly regulated to limit self-inflicted injury by activated leukocytes following the resolution of infection. Several studies have demonstrated that reliance on OxPhos supports cellular longevity. For example, anti-inflammatory MΦs that favor OxPhos have an increased life span, whereas pro-inflammatory MΦs, which rely more on glycolysis are shorter lived (255). While pro-inflammatory cytokines and PAMPs are abundant in the biofilm milieu, effector populations are sparse and exhibit anti-inflammatory activity. During biofilm infection, this suggests that elevated glycolysis-inducing cytokines possibly contribute to biofilm persistence by eliminating effector cells by glycolysis-induced apoptosis, in addition to biofilm-derived PAMPs. Following biofilm establishment and maturation, nutrient deprivation likely also

prevents glycolysis and monocyte activation. Therefore, we hypothesize that the biofilm takes advantage of the diminished longevity of glycolytic leukocytes in order to inhibit immune clearance. Measuring leukocyte metabolism throughout the course of infection will provide further insight into this aspect of monocyte metabolism, which can be correlated with leukocyte death.

To directly examine the dynamics of leukocyte OxPhos and glycolysis *in vivo*, fluorescent molecules indicative of both events can be used, i.e. JC-1 and 2-NBDG (2-(N-(7-Nitrobenz-2-oxa-1,3-diazol-4-yl)Amino)-2-Deoxyglucose). JC-1 is a bi-fluorescent cationic molecule that accumulates in mitochondria with larger membrane potentials. At low concentrations, it emits green fluorescence, while at high concentrations it forms J-aggregates that fluoresce at ~590nm. Cells with more OxPhos activity, will have a more active electron transport chain and lower mitochondrial membrane potential, which should manifest as a larger green:red ratio. 2-NBDG is a fluorescent glucose analog that cannot be metabolized, which is used to monitor glucose uptake and by extension, glycolytic activity. Together these two fluorescent dyes can be used to characterize the metabolic activity of leukocytes during *S. aureus* biofilm infections. Specifically, anti-inflammatory monocytes undergoing more OxPhos will show a heightened green:red ratio when incubated with JC-1, and decreased 2-NBDG uptake. Conversely, pro-inflammatory monocytes will show lower green:red ratios with JC-1 and increased 2-NBDG uptake. My preliminary studies with these dyes have shown that relative to animals receiving sterile implants at day 7, monocytes from infected animals undergo more OxPhos and less glycolysis (Figure 5.7). These studies were expanded to examine the metabolic profiles of leukocytes throughout the first week of infection to identify when monocyte metabolism becomes permissive to *S. aureus* biofilm.

Figure 5.7

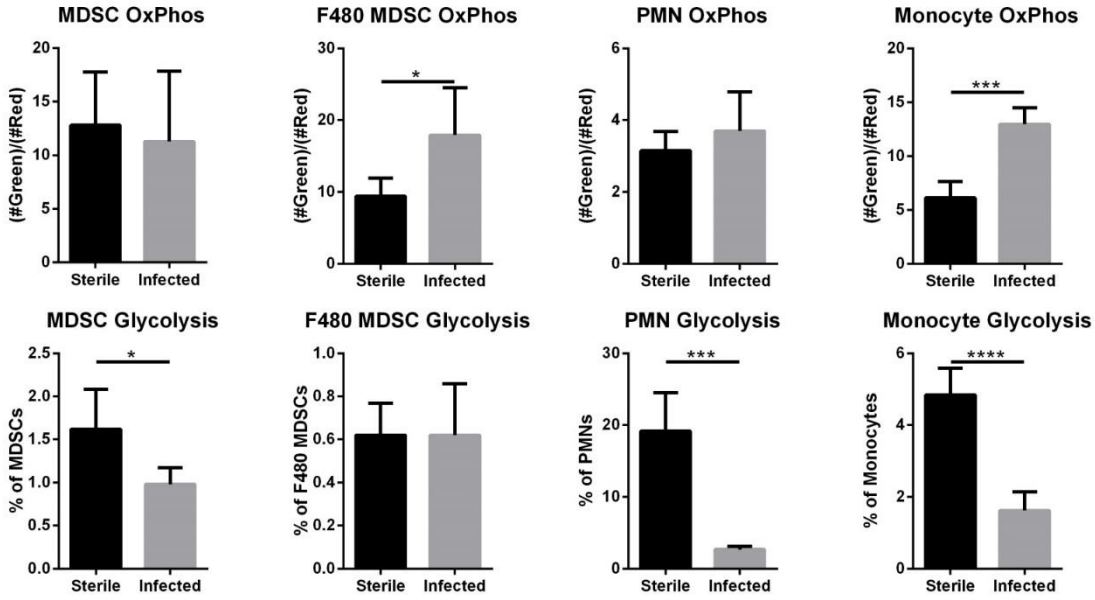

Leukocyte metabolism during *S. aureus* biofilm infection. Tissue homogenates from sterile and infected mice Day 7 post-orthopedic implant, were stained with JC-1 (**A-D**) and 2-NBDG (**E-H**) dyes for 30 minutes at 37°C. Cells were washed and stained with antibodies to cell markers and analyzed by flow cytometry. (**A-D**) OxPhos activity was determined in JC-1 stained cells by the Green:Red ratios. (**E-H**) Glycolytic activity was determined by the percentage of cells that stained positively for the fluorescent glucose analog. Results are from a single experiment. *, $p < 0.05$; ***, $p < 0.005$; ****, $p < 0.0005$; unpaired 2-tailed Student's *t*-test.

Role of tissue injury in promoting *S. aureus* biofilm establishment and persistence

Trauma and tissue injury has been shown to disrupt normal immune homeostasis, which could cause a host to be susceptible to infectious complications. This is due to the fact that the release of DAMPs are associated with immune suppression and increased susceptibility to infections (354). Circulating DAMPs released from injured tissues can lead to a decrease in MHC-II expression and suppression of pro-inflammatory activation (203). Preliminary studies from our laboratory have demonstrated that the tissue damage associated with orthopedic implant surgery promotes *S. aureus* biofilm infection. In particular, in animals receiving a sterile implant that was allowed to heal for one week prior to *S. aureus* challenge (i.e. DAMP resolution) had significantly less bacterial burdens and inflammatory mediator production concomitant with reduced MDSC and increased monocyte infiltrates compared to animals where infection occurred at the time of surgery (i.e. time of DAMP release). It would be interesting to determine the differences in leukocyte metabolism in response to injury using this paradigm. This could be investigated by complimentary approaches. *In vivo*, staining with JC-1 and 2-NBDG would determine how leukocyte metabolism changes following sterile surgery, or cells could be sorted for intracellular metabolomic analysis. *In vitro*, MΦs treated with homogenates from a sterile surgery could be subjected to Seahorse Assays to obtain a real-time measurement of their metabolic activity. In addition, determining whether specific DAMPs are driving susceptibility to *S. aureus* biofilm infection would allow for their targeting to prevent susceptibility to post-surgical infectious complications.

Relationship between myeloid metabolism and bone destruction/formation during *S. aureus* biofilm infection

S. aureus orthopedic implant biofilm infections elicit a large degree of osteomyelitis and bone loss. Prior studies have shown that *S. aureus* can induce receptor activator of nuclear factor kappa-B ligand (RANKL) expression and osteoclastogenesis from myeloid precursors (355-357).

Similar to monocytes and MΦs, osteoclast function and differentiation is intimately related to metabolic activity. Specifically, high rates of glycolysis are linked to osteoclastogenesis, while osteoclasts actively resorbing bone will increase the expression of TCA cycle enzymes and mitochondrial mass and activity (358-360). Furthermore, the reliance of osteoclast bone resorption activity on OxPhos is supported by the induction or inhibition of OxPhos by pyruvate or oligomycin, respectively (359). By extension, we hypothesize that bone resorption by osteoclasts is fueled by OxPhos during *S. aureus* biofilm infection. Understanding the mechanisms by which *S. aureus* can induce OxPhos activity in leukocytes to escape immune-mediated clearance may provide insights into how the pathogen regulates bone resorption and osteolysis. This is important to ultimately determine how to prevent and treat these infections, in addition to reducing bone-loss during infection.

FINAL CONCLUSIONS

S. aureus biofilms actively polarize a host's immune response towards an anti-inflammatory phenotype which allows for the establishment or chronic infection. The complex metabolic interactions between *S. aureus* biofilms and host leukocytes were a previously unexplored area of research. We have shown that biofilm associated anti-inflammatory monocytes are biased towards OxPhos metabolism, but can be actively reprogrammed to be pro-inflammatory and reduce bacterial burdens. However, the direct and indirect mechanisms by which *S. aureus* biofilms polarize monocyte metabolism will need to be determined. Furthermore, the consequences of metabolic polarization and pharmaceutical reprogramming are unknown and will be investigated with the studies discussed above. Together, these studies will allow for the development of novel therapeutic options for biofilm infections and other chronic diseases.

References

1. Brown AF, Leech JM, Rogers TR, McLoughlin RM. Staphylococcus aureus Colonization: Modulation of Host Immune Response and Impact on Human Vaccine Design. Frontiers in immunology. 2014;4:507.
2. Foster TJ. Staphylococci and staphylococcal infections. Expert review of anti-infective therapy. 2010;8(12):1337-8.
3. Otto M. Staphylococcal biofilms. Current topics in microbiology and immunology. 2008;322:207-28.
4. Park HY, Kim CR, Huh IS, Jung MY, Seo EY, Park JH, Lee DY, Yang JM. Staphylococcus aureus Colonization in Acute and Chronic Skin Lesions of Patients with Atopic Dermatitis. Annals of dermatology. 2013;25(4):410-6.
5. Rasigade JP, Dumitrescu O, Lina G. New epidemiology of Staphylococcus aureus infections. Clinical microbiology and infection : the official publication of the European Society of Clinical Microbiology and Infectious Diseases. 2014;20(7):587-8.
6. Stryjewski ME, Corey GR. Methicillin-resistant Staphylococcus aureus: an evolving pathogen. Clinical infectious diseases : an official publication of the Infectious Diseases Society of America. 2014;58 Suppl 1:S10-9.
7. Rodvold KA, McConeghy KW. Methicillin-resistant Staphylococcus aureus therapy: past, present, and future. Clinical infectious diseases : an official publication of the Infectious Diseases Society of America. 2014;58 Suppl 1:S20-7.
8. Brumfitt W, Hamilton-Miller J. Methicillin-resistant Staphylococcus aureus. The New England journal of medicine. 1989;320(18):1188-96.
9. Zecconi A, Scali F. Staphylococcus aureus virulence factors in evasion from innate immune defenses in human and animal diseases. Immunology letters. 2013;150(1-2):12-22.
10. Shorr AF. Epidemiology of staphylococcal resistance. Clinical infectious diseases : an official publication of the Infectious Diseases Society of America. 2007;45 Suppl 3:S171-6.
11. Lakhundi S, Zhang K. Methicillin-Resistant Staphylococcus aureus: Molecular Characterization, Evolution, and Epidemiology. Clinical microbiology reviews. 2018;31(4).
12. Holland TL, Raad I, Boucher HW, Anderson DJ, Cosgrove SE, Aycock PS, Baddley JW, Chaftari AM, Chow SC, Chu VH, Carugati M, Cook P, Corey GR, Crowley AL, Daly J, Gu J, Hachem R, Horton J, Jenkins TC, Levine D, Miro JM, Pericas JM, Riska P, Rubin Z, Rupp ME, Schrank J, Jr., Sims M, Wray D, Zervos M, Fowler VG, Jr., Staphylococcal Bacteremia I. Effect of Algorithm-Based Therapy vs Usual Care on Clinical Success and Serious Adverse Events in Patients with Staphylococcal Bacteremia: A Randomized Clinical Trial. Jama. 2018;320(12):1249-58.
13. Paterson GK, Harrison EM, Holmes MA. The emergence of mecC methicillin-resistant Staphylococcus aureus. Trends in microbiology. 2014;22(1):42-7.
14. Paterson GK, Morgan FJ, Harrison EM, Cartwright EJ, Torok ME, Zadoks RN, Parkhill J, Peacock SJ, Holmes MA. Prevalence and characterization of human mecC methicillin-resistant Staphylococcus aureus isolates in England. The Journal of antimicrobial chemotherapy. 2014;69(4):907-10.
15. International Working Group on the Classification of Staphylococcal Cassette Chromosome E. Classification of staphylococcal cassette chromosome mec (SCCmec): guidelines for reporting novel SCCmec elements. Antimicrobial agents and chemotherapy. 2009;53(12):4961-7.
16. Namvar AE, Afshar M, Asghari B, Rastegar Lari A. Characterisation of SCCmec elements in methicillin-resistant Staphylococcus aureus isolated from burn patients. Burns : journal of the International Society for Burn Injuries. 2014;40(4):708-12.

17. Ito T, Kuwahara-Arai K, Katayama Y, Uehara Y, Han X, Kondo Y, Hiramatsu K. Staphylococcal Cassette Chromosome mec (SCCmec) analysis of MRSA. Methods in molecular biology. 2014;1085:131-48.
18. Jimenez JN, Ocampo AM, Vanegas JM, Rodriguez EA, Mediavilla JR, Chen L, Muskus CE, Velez LA, Rojas C, Restrepo AV, Ospina S, Garces C, Franco L, Bifani P, Kreiswirth BN, Correa MM. CC8 MRSA strains harboring SCCmec type IVc are predominant in Colombian hospitals. PloS one. 2012;7(6):e38576.
19. Perovic O, Iyaloo S, Kularatne R, Lowman W, Bosman N, Wadula J, Seetharam S, Duse A, Mbelle N, Bamford C, Dawood H, Mahabeer Y, Bhola P, Abrahams S, Singh-Moodley A. Prevalence and Trends of Staphylococcus aureus Bacteraemia in Hospitalized Patients in South Africa, 2010 to 2012: Laboratory-Based Surveillance Mapping of Antimicrobial Resistance and Molecular Epidemiology. PloS one. 2015;10(12):e0145429.
20. Valsesia G, Rossi M, Bertschy S, Pfyffer GE. Emergence of SCCmec type IV and SCCmec type V methicillin-resistant Staphylococcus aureus containing the Panton-Valentine leukocidin genes in a large academic teaching hospital in central Switzerland: external invaders or persisting circulators? Journal of clinical microbiology. 2010;48(3):720-7.
21. Vossenkuhl B, Brandt J, Fetsch A, Kasbohrer A, Kraushaar B, Alt K, Tenhagen BA. Comparison of spa types, SCCmec types and antimicrobial resistance profiles of MRSA isolated from turkeys at farm, slaughter and from retail meat indicates transmission along the production chain. PloS one. 2014;9(5):e96308.
22. Drago L, De Vecchi E, Nicola L, Gismondo MR. In vitro evaluation of antibiotics' combinations for empirical therapy of suspected methicillin resistant Staphylococcus aureus severe respiratory infections. BMC infectious diseases. 2007;7:111.
23. Kennedy AD, Otto M, Braughton KR, Whitney AR, Chen L, Mathema B, Mediavilla JR, Byrne KA, Parkins LD, Tenover FC, Kreiswirth BN, Musser JM, DeLeo FR. Epidemic community-associated methicillin-resistant Staphylococcus aureus: recent clonal expansion and diversification. Proceedings of the National Academy of Sciences of the United States of America. 2008;105(4):1327-32.
24. Naber CK. Staphylococcus aureus bacteremia: epidemiology, pathophysiology, and management strategies. Clinical infectious diseases : an official publication of the Infectious Diseases Society of America. 2009;48 Suppl 4:S231-7.
25. David MZ, Rudolph KM, Hennessy TW, Boyle-Vavra S, Daum RS. Molecular epidemiology of methicillin-resistant Staphylococcus aureus, rural southwestern Alaska. Emerging infectious diseases. 2008;14(11):1693-9.
26. Cadena J, Sreeramoju P, Nair S, Henao-Martinez A, Jorgensen J, Patterson JE. Clindamycin-resistant methicillin-resistant Staphylococcus aureus: epidemiologic and molecular characteristics and associated clinical factors. Diagnostic microbiology and infectious disease. 2012;74(1):16-21.
27. Dalhoff A. Global fluoroquinolone resistance epidemiology and implictions for clinical use. Interdisciplinary perspectives on infectious diseases. 2012;2012:976273.
28. Benito D, Lozano C, Rezusta A, Ferrer I, Vasquez MA, Ceballos S, Zarazaga M, Revillo MJ, Torres C. Characterization of tetracycline and methicillin resistant Staphylococcus aureus strains in a Spanish hospital: is livestock-contact a risk factor in infections caused by MRSA CC398? International journal of medical microbiology : IJMM. 2014;304(8):1226-32.
29. Albrecht VS, Zervos MJ, Kaye KS, Tosh PK, Arshad S, Hayakawa K, Kallen AJ, McDougal LK, Limbago BM, Guh AY. Prevalence of and risk factors for vancomycin-resistant Staphylococcus aureus precursor organisms in Southeastern Michigan. Infection control and hospital epidemiology. 2014;35(12):1531-4.

30. Hasan R, Acharjee M, Noor R. Prevalence of vancomycin resistant Staphylococcus aureus (VRSA) in methicillin resistant S. aureus (MRSA) strains isolated from burn wound infections. Ci ji yi xue za zhi = Tzu-chi medical journal. 2016;28(2):49-53.
31. Zhang S, Sun X, Chang W, Dai Y, Ma X. Systematic Review and Meta-Analysis of the Epidemiology of Vancomycin-Intermediate and Heterogeneous Vancomycin-Intermediate Staphylococcus aureus Isolates. PloS one. 2015;10(8):e0136082.
32. Boucher H, Miller LG, Razonable RR. Serious infections caused by methicillin-resistant Staphylococcus aureus. Clinical infectious diseases : an official publication of the Infectious Diseases Society of America. 2010;51 Suppl 2:S183-97.
33. Alexander EL, Gardete S, Bar HY, Wells MT, Tomasz A, Rhee KY. Intermediate-type vancomycin resistance (VISA) in genetically-distinct Staphylococcus aureus isolates is linked to specific, reversible metabolic alterations. PloS one. 2014;9(5):e97137.
34. Gardete S, Tomasz A. Mechanisms of vancomycin resistance in Staphylococcus aureus. The Journal of clinical investigation. 2014;124(7):2836-40.
35. Bishara J, Goldberg E, Leibovici L, Samra Z, Shaked H, Mansur N, Paul M. Healthcare-associated vs. hospital-acquired Staphylococcus aureus bacteremia. International journal of infectious diseases : IJID : official publication of the International Society for Infectious Diseases. 2012;16(6):e457-63.
36. Fowler VG, Jr., Olsen MK, Corey GR, Woods CW, Cabell CH, Reller LB, Cheng AC, Dudley T, Oddone EZ. Clinical identifiers of complicated Staphylococcus aureus bacteremia. Archives of internal medicine. 2003;163(17):2066-72.
37. Morgenstern M, Erichsen C, Hackl S, Mily J, Militz M, Friederichs J, Hungerer S, Buhren V, Moriarty TF, Post V, Richards RG, Kates SL. Antibiotic Resistance of Commensal Staphylococcus aureus and Coagulase-Negative Staphylococci in an International Cohort of Surgeons: A Prospective Point-Prevalence Study. PloS one. 2016;11(2):e0148437.
38. Parry MC, Duncan CP. The challenge of methicillin resistant staphylococcal infection after total hip replacement: overlooked or overstated? The bone & joint journal. 2014;96-B(11 Supple A):60-5.
39. Naimi TS, LeDell KH, Como-Sabetti K, Borchardt SM, Boxrud DJ, Etienne J, Johnson SK, Vandenesch F, Fridkin S, O'Boyle C, Danila RN, Lynfield R. Comparison of community- and health care-associated methicillin-resistant Staphylococcus aureus infection. Jama. 2003;290(22):2976-84.
40. Hota B, Lyles R, Rim J, Popovich KJ, Rice T, Aroutcheva A, Weinstein RA, Epicenters CDCP. Predictors of clinical virulence in community-onset methicillin-resistant Staphylococcus aureus infections: the importance of USA300 and pneumonia. Clinical infectious diseases : an official publication of the Infectious Diseases Society of America. 2011;53(8):757-65.
41. Wang SH, Hines L, van Balen J, Mediavilla JR, Pan X, Hoet AE, Kreiswirth BN, Pancholi P, Stevenson KB. Molecular and clinical characteristics of hospital and community onset methicillin-resistant Staphylococcus aureus strains associated with bloodstream infections. Journal of clinical microbiology. 2015;53(5):1599-608.
42. David MZ, Daum RS. Community-associated methicillin-resistant Staphylococcus aureus: epidemiology and clinical consequences of an emerging epidemic. Clinical microbiology reviews. 2010;23(3):616-87.
43. Bukharie HA. A review of community-acquired methicillin-resistant Staphylococcus aureus for primary care physicians. Journal of family & community medicine. 2010;17(3):117-20.
44. Kluytmans-Vandenbergh MF, Kluytmans JA. Community-acquired methicillin-resistant Staphylococcus aureus: current perspectives. Clinical microbiology and infection : the official

publication of the European Society of Clinical Microbiology and Infectious Diseases. 2006;12 Suppl 1:9-15.
45. Diep BA, Otto M. The role of virulence determinants in community-associated MRSA pathogenesis. Trends in microbiology. 2008;16(8):361-9.
46. Nimmo GR. USA300 abroad: global spread of a virulent strain of community-associated methicillin-resistant Staphylococcus aureus. Clinical microbiology and infection : the official publication of the European Society of Clinical Microbiology and Infectious Diseases. 2012;18(8):725-34.
47. Rooijakkers SH, Ruyken M, Roos A, Daha MR, Presanis JS, Sim RB, van Wamel WJ, van Kessel KP, van Strijp JA. Immune evasion by a staphylococcal complement inhibitor that acts on C3 convertases. Nature immunology. 2005;6(9):920-7.
48. Rooijakkers SH, van Kessel KP, van Strijp JA. Staphylococcal innate immune evasion. Trends in microbiology. 2005;13(12):596-601.
49. Powers ME, Bubeck Wardenburg J. Igniting the fire: Staphylococcus aureus virulence factors in the pathogenesis of sepsis. PLoS pathogens. 2014;10(2):e1003871.
50. Pan ES, Diep BA, Carleton HA, Charlebois ED, Sensabaugh GF, Haller BL, Perdreau-Remington F. Increasing prevalence of methicillin-resistant Staphylococcus aureus infection in California jails. Clinical infectious diseases : an official publication of the Infectious Diseases Society of America. 2003;37(10):1384-8.
51. Kazakova SV, Hageman JC, Matava M, Srinivasan A, Phelan L, Garfinkel B, Boo T, McAllister S, Anderson J, Jensen B, Dodson D, Lonsway D, McDougal LK, Arduino M, Fraser VJ, Killgore G, Tenover FC, Cody S, Jernigan DB. A clone of methicillin-resistant Staphylococcus aureus among professional football players. The New England journal of medicine. 2005;352(5):468-75.
52. McDougal LK, Steward CD, Killgore GE, Chaitram JM, McAllister SK, Tenover FC. Pulsed-field gel electrophoresis typing of oxacillin-resistant Staphylococcus aureus isolates from the United States: establishing a national database. Journal of clinical microbiology. 2003;41(11):5113-20.
53. King JM, Kulhankova K, Stach CS, Vu BG, Salgado-Pabon W. Phenotypes and Virulence among Staphylococcus aureus USA100, USA200, USA300, USA400, and USA600 Clonal Lineages. mSphere. 2016;1(3).
54. Nienaber JJ, Sharma Kuinkel BK, Clarke-Pearson M, Lamlertthon S, Park L, Rude TH, Barriere S, Woods CW, Chu VH, Marin M, Bukovski S, Garcia P, Corey GR, Korman T, Doco-Lecompte T, Murdoch DR, Reller LB, Fowler VG, Jr., International Collaboration on Endocarditis-Microbiology I. Methicillin-susceptible Staphylococcus aureus endocarditis isolates are associated with clonal complex 30 genotype and a distinct repertoire of enterotoxins and adhesins. The Journal of infectious diseases. 2011;204(5):704-13.
55. Tristan A, Rasigade JP, Ruizendaal E, Laurent F, Bes M, Meugnier H, Lina G, Etienne J, Celard M, Tattevin P, Monecke S, Le Moing V, Vandenesch F, French AsGoIE. Rise of CC398 lineage of Staphylococcus aureus among Infective endocarditis isolates revealed by two consecutive population-based studies in France. PloS one. 2012;7(12):e51172.
56. Diep BA, Gill SR, Chang RF, Phan TH, Chen JH, Davidson MG, Lin F, Lin J, Carleton HA, Mongodin EF, Sensabaugh GF, Perdreau-Remington F. Complete genome sequence of USA300, an epidemic clone of community-acquired meticillin-resistant Staphylococcus aureus. Lancet. 2006;367(9512):731-9.
57. Tenover FC, McDougal LK, Goering RV, Killgore G, Projan SJ, Patel JB, Dunman PM. Characterization of a strain of community-associated methicillin-resistant Staphylococcus aureus widely disseminated in the United States. Journal of clinical microbiology. 2006;44(1):108-18.

58. Diep BA, Palazzolo-Ballance AM, Tattevin P, Basuino L, Braughton KR, Whitney AR, Chen L, Kreiswirth BN, Otto M, DeLeo FR, Chambers HF. Contribution of Panton-Valentine leukocidin in community-associated methicillin-resistant Staphylococcus aureus pathogenesis. PloS one. 2008;3(9):e3198.
59. Diep BA, Stone GG, Basuino L, Graber CJ, Miller A, des Etages SA, Jones A, Palazzolo-Ballance AM, Perdreau-Remington F, Sensabaugh GF, DeLeo FR, Chambers HF. The arginine catabolic mobile element and staphylococcal chromosomal cassette mec linkage: convergence of virulence and resistance in the USA300 clone of methicillin-resistant Staphylococcus aureus. The Journal of infectious diseases. 2008;197(11):1523-30.
60. Scherr TD, Hanke ML, Huang O, James DB, Horswill AR, Bayles KW, Fey PD, Torres VJ, Kielian T. Staphylococcus aureus Biofilms Induce Macrophage Dysfunction Through Leukocidin AB and Alpha-Toxin. mBio. 2015;6(4).
61. Voyich JM, Braughton KR, Sturdevant DE, Whitney AR, Said-Salim B, Porcella SF, Long RD, Dorward DW, Gardner DJ, Kreiswirth BN, Musser JM, DeLeo FR. Insights into mechanisms used by Staphylococcus aureus to avoid destruction by human neutrophils. Journal of immunology. 2005;175(6):3907-19.
62. Fey PD, Endres JL, Yajjala VK, Widhelm TJ, Boissy RJ, Bose JL, Bayles KW. A genetic resource for rapid and comprehensive phenotype screening of nonessential Staphylococcus aureus genes. mBio. 2013;4(1):e00537-12.
63. Kumar A, Alam A, Rani M, Ehtesham NZ, Hasnain SE. Biofilms: Survival and defense strategy for pathogens. International journal of medical microbiology : IJMM. 2017;307(8):481-9.
64. Costerton JW, Stewart PS, Greenberg EP. Bacterial biofilms: a common cause of persistent infections. Science. 1999;284(5418):1318-22.
65. Stewart PS. Multicellular resistance: biofilms. Trends in microbiology. 2001;9(5):204.
66. Stewart PS, Costerton JW. Antibiotic resistance of bacteria in biofilms. Lancet. 2001;358(9276):135-8.
67. Stewart PS, Franklin MJ. Physiological heterogeneity in biofilms. Nature reviews Microbiology. 2008;6(3):199-210.
68. Flemming HC, Wingender J, Szewzyk U, Steinberg P, Rice SA, Kjelleberg S. Biofilms: an emergent form of bacterial life. Nature reviews Microbiology. 2016;14(9):563-75.
69. Gries CM, Kielian T. Staphylococcal Biofilms and Immune Polarization During Prosthetic Joint Infection. The Journal of the American Academy of Orthopaedic Surgeons. 2017;25 Suppl 1:S20-S4.
70. Mulcahy LR, Isabella VM, Lewis K. Pseudomonas aeruginosa biofilms in disease. Microbial ecology. 2014;68(1):1-12.
71. Spoering AL, Lewis K. Biofilms and planktonic cells of Pseudomonas aeruginosa have similar resistance to killing by antimicrobials. Journal of bacteriology. 2001;183(23):6746-51.
72. Archer NK, Mazaitis MJ, Costerton JW, Leid JG, Powers ME, Shirtliff ME. Staphylococcus aureus biofilms: properties, regulation, and roles in human disease. Virulence. 2011;2(5):445-59.
73. Humphries J, Xiong L, Liu J, Prindle A, Yuan F, Arjes HA, Tsimring L, Suel GM. Species-Independent Attraction to Biofilms through Electrical Signaling. Cell. 2017;168(1-2):200-9 e12.
74. Southey-Pillig CJ, Davies DG, Sauer K. Characterization of temporal protein production in Pseudomonas aeruginosa biofilms. Journal of bacteriology. 2005;187(23):8114-26.
75. Rasamiravaka T, Labtani Q, Duez P, El Jaziri M. The formation of biofilms by Pseudomonas aeruginosa: a review of the natural and synthetic compounds interfering with control mechanisms. BioMed research international. 2015;2015:759348.

76. Davies D. Understanding biofilm resistance to antibacterial agents. Nature reviews Drug discovery. 2003;2(2):114-22.
77. del Pozo JL, Patel R. The challenge of treating biofilm-associated bacterial infections. Clinical pharmacology and therapeutics. 2007;82(2):204-9.
78. Stewart PS. Diffusion in biofilms. Journal of bacteriology. 2003;185(5):1485-91.
79. Stewart PS, Zhang T, Xu R, Pitts B, Walters MC, Roe F, Kikhney J, Moter A. Reaction-diffusion theory explains hypoxia and heterogeneous growth within microbial biofilms associated with chronic infections. NPJ biofilms and microbiomes. 2016;2:16012.
80. Lamotta EJ. Internal diffusion and reaction in biological films. Environmental science & technology. 1976;10(8):765-9.
81. Hall-Stoodley L, Stoodley P. Evolving concepts in biofilm infections. Cellular microbiology. 2009;11(7):1034-43.
82. Kiamco MM, Atci E, Mohamed A, Call DR, Beyenal H. Hyperosmotic Agents and Antibiotics Affect Dissolved Oxygen and pH Concentration Gradients in Staphylococcus aureus Biofilms. Applied and environmental microbiology. 2017;83(6).
83. Roberts ME, Stewart PS. Modelling protection from antimicrobial agents in biofilms through the formation of persister cells. Microbiology. 2005;151(Pt 1):75-80.
84. Le KY, Dastgheyb S, Ho TV, Otto M. Molecular determinants of staphylococcal biofilm dispersal and structuring. Frontiers in cellular and infection microbiology. 2014;4:167.
85. Leid JG, Willson CJ, Shirtliff ME, Hassett DJ, Parsek MR, Jeffers AK. The exopolysaccharide alginate protects Pseudomonas aeruginosa biofilm bacteria from IFN-gamma-mediated macrophage killing. Journal of immunology. 2005;175(11):7512-8.
86. Moormeier DE, Bayles KW. Staphylococcus aureus biofilm: a complex developmental organism. Molecular microbiology. 2017;104(3):365-76.
87. Periasamy S, Joo HS, Duong AC, Bach TH, Tan VY, Chatterjee SS, Cheung GY, Otto M. How Staphylococcus aureus biofilms develop their characteristic structure. Proceedings of the National Academy of Sciences of the United States of America. 2012;109(4):1281-6.
88. Moormeier DE, Bose JL, Horswill AR, Bayles KW. Temporal and stochastic control of Staphylococcus aureus biofilm development. mBio. 2014;5(5):e01341-14.
89. Gil C, Solano C, Burgui S, Latasa C, Garcia B, Toledo-Arana A, Lasa I, Valle J. Biofilm matrix exoproteins induce a protective immune response against Staphylococcus aureus biofilm infection. Infection and immunity. 2014;82(3):1017-29.
90. Solano C, Echeverz M, Lasa I. Biofilm dispersion and quorum sensing. Current opinion in microbiology. 2014;18:96-104.
91. Resch A, Rosenstein R, Nerz C, Gotz F. Differential gene expression profiling of Staphylococcus aureus cultivated under biofilm and planktonic conditions. Applied and environmental microbiology. 2005;71(5):2663-76.
92. Hengge R, Grundling A, Jenal U, Ryan R, Yildiz F. Bacterial Signal Transduction by Cyclic Di-GMP and Other Nucleotide Second Messengers. Journal of bacteriology. 2016;198(1):15-26.
93. Gries CM, Bruger EL, Moormeier DE, Scherr TD, Waters CM, Kielian T. Cyclic di-AMP Released from Staphylococcus aureus Biofilm Induces a Macrophage Type I Interferon Response. Infection and immunity. 2016;84(12):3564-74.
94. Booth SC, Workentine ML, Wen J, Shaykhutdinov R, Vogel HJ, Ceri H, Turner RJ, Weljie AM. Differences in metabolism between the biofilm and planktonic response to metal stress. Journal of proteome research. 2011;10(7):3190-9.
95. Kulkarni R, Antala S, Wang A, Amaral FE, Rampersaud R, Larussa SJ, Planet PJ, Ratner AJ. Cigarette smoke increases Staphylococcus aureus biofilm formation via oxidative stress. Infection and immunity. 2012;80(11):3804-11.

96. McEachern EK, Hwang JH, Sladewski KM, Nicatia S, Dewitz C, Mathew DP, Nizet V, Crotty Alexander LE. Analysis of the effects of cigarette smoke on staphylococcal virulence phenotypes. Infection and immunity. 2015;83(6):2443-52.
97. Dotsch A, Eckweiler D, Schniederjans M, Zimmermann A, Jensen V, Scharfe M, Geffers R, Haussler S. The Pseudomonas aeruginosa transcriptome in planktonic cultures and static biofilms using RNA sequencing. PloS one. 2012;7(2):e31092.
98. Wei Q, Ma LZ. Biofilm matrix and its regulation in Pseudomonas aeruginosa. International journal of molecular sciences. 2013;14(10):20983-1005.
99. Klausen M, Aaes-Jorgensen A, Molin S, Tolker-Nielsen T. Involvement of bacterial migration in the development of complex multicellular structures in Pseudomonas aeruginosa biofilms. Molecular microbiology. 2003;50(1):61-8.
100. Elchinger PH, Delattre C, Faure S, Roy O, Badel S, Bernardi T, Taillefumier C, Michaud P. Effect of proteases against biofilms of Staphylococcus aureus and Staphylococcus epidermidis. Letters in applied microbiology. 2014;59(5):507-13.
101. Gilan I, Sivan A. Effect of proteases on biofilm formation of the plastic-degrading actinomycete Rhodococcus ruber C208. FEMS microbiology letters. 2013;342(1):18-23.
102. Tetz GV, Artemenko NK, Tetz VV. Effect of DNase and antibiotics on biofilm characteristics. Antimicrobial agents and chemotherapy. 2009;53(3):1204-9.
103. Arrecubieta C, Toba FA, von Bayern M, Akashi H, Deng MC, Naka Y, Lowy FD. SdrF, a Staphylococcus epidermidis surface protein, contributes to the initiation of ventricular assist device driveline-related infections. PLoS pathogens. 2009;5(5):e1000411.
104. Rada B. Interactions between Neutrophils and Pseudomonas aeruginosa in Cystic Fibrosis. Pathogens. 2017;6(1).
105. Bernthal NM, Stavrakis AI, Billi F, Cho JS, Kremen TJ, Simon SI, Cheung AL, Finerman GA, Lieberman JR, Adams JS, Miller LS. A mouse model of post-arthroplasty Staphylococcus aureus joint infection to evaluate in vivo the efficacy of antimicrobial implant coatings. PloS one. 2010;5(9):e12580.
106. Heim CE, Vidlak D, Odvody J, Hartman CW, Garvin KL, Kielian T. Human prosthetic joint infections are associated with myeloid-derived suppressor cells (MDSCs): Implications for infection persistence. Journal of orthopaedic research : official publication of the Orthopaedic Research Society. 2017.
107. Moran E, Byren I, Atkins BL. The diagnosis and management of prosthetic joint infections. The Journal of antimicrobial chemotherapy. 2010;65 Suppl 3:iii45-54.
108. Pulido L, Ghanem E, Joshi A, Purtill JJ, Parvizi J. Periprosthetic joint infection: the incidence, timing, and predisposing factors. Clinical orthopaedics and related research. 2008;466(7):1710-5.
109. Scherr TD, Lindgren KE, Schaeffer CR, Hanke ML, Hartman CW, Kielian T. Mouse model of post-arthroplasty Staphylococcus epidermidis joint infection. Methods in molecular biology. 2014;1106:173-81.
110. Tande AJ, Osmon DR, Greenwood-Quaintance KE, Mabry TM, Hanssen AD, Patel R. Clinical characteristics and outcomes of prosthetic joint infection caused by small colony variant staphylococci. mBio. 2014;5(5):e01910-14.
111. Tande AJ, Patel R. Prosthetic joint infection. Clinical microbiology reviews. 2014;27(2):302-45.
112. Donlan RM. Biofilms: microbial life on surfaces. Emerging infectious diseases. 2002;8(9):881-90.
113. Donlan RM, Costerton JW. Biofilms: survival mechanisms of clinically relevant microorganisms. Clinical microbiology reviews. 2002;15(2):167-93.

114. Vidlak D, Kielian T. Infectious Dose Dictates the Host Response during Staphylococcus aureus Orthopedic-Implant Biofilm Infection. Infection and immunity. 2016;84(7):1957-65.
115. Angele MK, Faist E. Clinical review: immunodepression in the surgical patient and increased susceptibility to infection. Critical care. 2002;6(4):298-305.
116. Mody RM, Zapor M, Hartzell JD, Robben PM, Waterman P, Wood-Morris R, Trotta R, Andersen RC, Wortmann G. Infectious complications of damage control orthopedics in war trauma. The Journal of trauma. 2009;67(4):758-61.
117. Esposito S, Purrello SM, Bonnet E, Novelli A, Tripodi F, Pascale R, Unal S, Milkovich G. Central venous catheter-related biofilm infections: An up-to-date focus on meticillin-resistant Staphylococcus aureus. Journal of global antimicrobial resistance. 2013;1(2):71-8.
118. Hogan S, Zapotoczna M, Stevens NT, Humphreys H, O'Gara JP, O'Neill E. Eradication of Staphylococcus aureus Catheter-Related Biofilm Infections Using ML:8 and Citrox. Antimicrobial agents and chemotherapy. 2016;60(10):5968-75.
119. Stuart RL, Cameron DR, Scott C, Kotsanas D, Grayson ML, Korman TM, Gillespie EE, Johnson PD. Peripheral intravenous catheter-associated Staphylococcus aureus bacteraemia: more than 5 years of prospective data from two tertiary health services. The Medical journal of Australia. 2013;198(10):551-3.
120. Guggenbichler JP, Assadian O, Boeswald M, Kramer A. Incidence and clinical implication of nosocomial infections associated with implantable biomaterials - catheters, ventilator-associated pneumonia, urinary tract infections. GMS Krankenhaushygiene interdisziplinar. 2011;6(1):Doc18.
121. Klein E, Smith DL, Laxminarayan R. Hospitalizations and deaths caused by methicillin-resistant Staphylococcus aureus, United States, 1999-2005. Emerging infectious diseases. 2007;13(12):1840-6.
122. Arduino JM, Kaye KS, Reed SD, Peter SA, Sexton DJ, Chen LF, Hardy NC, Tong SY, Smugar SS, Fowler VG, Jr., Anderson DJ. Staphylococcus aureus infections following knee and hip prosthesis insertion procedures. Antimicrobial resistance and infection control. 2015;4:13.
123. Dapunt U, Radzuweit-Mihaljevic S, Lehner B, Haensch GM, Ewerbeck V. Bacterial Infection and Implant Loosening in Hip and Knee Arthroplasty: Evaluation of 209 Cases. Materials. 2016;9(11).
124. Dorota Teterycz, Tristan Ferry, Daniel Lew, Richard Stern, Mathieu Assal, Pierre Hoffmeyer, Louis Bernard, Uc¸kay I. Outcome of orthopedic implant infections due to different staphylococci. International Journal of Infectious Diseases. 2010;14(10):e913-e8.
125. Kurtz S, Ong K, Lau E, Mowat F, Halpern M. Projections of primary and revision hip and knee arthroplasty in the United States from 2005 to 2030. The Journal of bone and joint surgery American volume. 2007;89(4):780-5.
126. Kurtz SM, Ong KL, Schmier J, Mowat F, Saleh K, Dybvik E, Karrholm J, Garellick G, Havelin LI, Furnes O, Malchau H, Lau E. Future clinical and economic impact of revision total hip and knee arthroplasty. The Journal of bone and joint surgery American volume. 2007;89 Suppl 3:144-51.
127. Buchholz HW, Elson RA, Engelbrecht E, Lodenkamper H, Rottger J, Siegel A. Management of deep infection of total hip replacement. The Journal of bone and joint surgery British volume. 1981;63-B(3):342-53.
128. Lentino JR. Prosthetic joint infections: bane of orthopedists, challenge for infectious disease specialists. Clinical infectious diseases : an official publication of the Infectious Diseases Society of America. 2003;36(9):1157-61.
129. Robbins GM, Masri BA, Garbuz DS, Duncan CP. Primary total hip arthroplasty after infection. Instructional course lectures. 2001;50:317-33.

130. Wisplinghoff H, Bischoff T, Tallent SM, Seifert H, Wenzel RP, Edmond MB. Nosocomial bloodstream infections in US hospitals: analysis of 24,179 cases from a prospective nationwide surveillance study. Clinical infectious diseases : an official publication of the Infectious Diseases Society of America. 2004;39(3):309-17.
131. Lo E, Nicolle LE, Coffin SE, Gould C, Maragakis LL, Meddings J, Pegues DA, Pettis AM, Saint S, Yokoe DS. Strategies to prevent catheter-associated urinary tract infections in acute care hospitals: 2014 update. Infection control and hospital epidemiology. 2014;35(5):464-79.
132. Nicolle LE. Catheter associated urinary tract infections. Antimicrobial resistance and infection control. 2014;3:23.
133. Walker JN, Flores-Mireles AL, Pinkner CL, Schreiber HLt, Joens MS, Park AM, Potretzke AM, Bauman TM, Pinkner JS, Fitzpatrick JAJ, Desai A, Caparon MG, Hultgren SJ. Catheterization alters bladder ecology to potentiate Staphylococcus aureus infection of the urinary tract. Proceedings of the National Academy of Sciences of the United States of America. 2017;114(41):E8721-E30.
134. Muder RR, Brennen C, Rihs JD, Wagener MM, Obman A, Stout JE, Yu VL. Isolation of Staphylococcus aureus from the urinary tract: association of isolation with symptomatic urinary tract infection and subsequent staphylococcal bacteremia. Clinical infectious diseases : an official publication of the Infectious Diseases Society of America. 2006;42(1):46-50.
135. Scherr TD, Heim CE, Morrison JM, Kielian T. Hiding in Plain Sight: Interplay between Staphylococcal Biofilms and Host Immunity. Frontiers in immunology. 2014;5:37.
136. Ribeiro M, Monteiro FJ, Ferraz MP. Infection of orthopedic implants with emphasis on bacterial adhesion process and techniques used in studying bacterial-material interactions. Biomatter. 2012;2(4):176-94.
137. Del Pozo JL, Patel R. Clinical practice. Infection associated with prosthetic joints. The New England journal of medicine. 2009;361(8):787-94.
138. Hanke ML, Heim CE, Angle A, Sanderson SD, Kielian T. Targeting macrophage activation for the prevention and treatment of Staphylococcus aureus biofilm infections. Journal of immunology. 2013;190(5):2159-68.
139. Thurlow LR, Hanke ML, Fritz T, Angle A, Aldrich A, Williams SH, Engebretsen IL, Bayles KW, Horswill AR, Kielian T. Staphylococcus aureus biofilms prevent macrophage phagocytosis and attenuate inflammation in vivo. Journal of immunology. 2011;186(11):6585-96.
140. Ulphani JS, Rupp ME. Model of Staphylococcus aureus central venous catheter-associated infection in rats. Laboratory animal science. 1999;49(3):283-7.
141. Rupp ME, Ulphani JS, Fey PD, Bartscht K, Mack D. Characterization of the importance of polysaccharide intercellular adhesin/hemagglutinin of Staphylococcus epidermidis in the pathogenesis of biomaterial-based infection in a mouse foreign body infection model. Infection and immunity. 1999;67(5):2627-32.
142. Rupp ME, Ulphani JS, Fey PD, Mack D. Characterization of Staphylococcus epidermidis polysaccharide intercellular adhesin/hemagglutinin in the pathogenesis of intravascular catheter-associated infection in a rat model. Infection and immunity. 1999;67(5):2656-9.
143. Snowden JN, Beaver M, Beenken K, Smeltzer M, Horswill AR, Kielian T. Staphylococcus aureus sarA regulates inflammation and colonization during central nervous system biofilm formation. PloS one. 2013;8(12):e84089.
144. Wang ML, Zhang Y, Fan M, Guo YJ, Ren WD, Luo EJ. A rabbit model of right-sided Staphylococcus aureus endocarditis created with echocardiographic guidance. Cardiovasc Ultrasound. 2013;11:3.
145. Heim CE, Vidlak D, Odvody J, Hartman CW, Garvin KL, Kielian T. Human prosthetic joint infections are associated with myeloid-derived suppressor cells (MDSCs): Implications for

infection persistence. Journal of orthopaedic research : official publication of the Orthopaedic Research Society. 2018;36(6):1605-13.
146. Heim CE, Vidlak D, Scherr TD, Hartman CW, Garvin KL, Kielian T. IL-12 promotes myeloid-derived suppressor cell recruitment and bacterial persistence during Staphylococcus aureus orthopedic implant infection. Journal of immunology. 2015;194(8):3861-72.
147. Hanke ML, Angle A, Kielian T. MyD88-dependent signaling influences fibrosis and alternative macrophage activation during Staphylococcus aureus biofilm infection. PloS one. 2012;7(8):e42476.
148. Heim CE, Vidlak D, Kielian T. Interleukin-10 production by myeloid-derived suppressor cells contributes to bacterial persistence during Staphylococcus aureus orthopedic biofilm infection. Journal of leukocyte biology. 2015;98(6):1003-13.
149. Thurlow LR, Joshi GS, Clark JR, Spontak JS, Neely CJ, Maile R, Richardson AR. Functional modularity of the arginine catabolic mobile element contributes to the success of USA300 methicillin-resistant Staphylococcus aureus. Cell host & microbe. 2013;13(1):100-7.
150. Kim HK, Cheng AG, Kim HY, Missiakas DM, Schneewind O. Nontoxigenic protein A vaccine for methicillin-resistant Staphylococcus aureus infections in mice. The Journal of experimental medicine. 2010;207(9):1863-70.
151. Missiakas D, Schneewind O. Staphylococcus aureus vaccines: Deviating from the carol. The Journal of experimental medicine. 2016;213(9):1645-53.
152. Bubeck Wardenburg J, Schneewind O. Vaccine protection against Staphylococcus aureus pneumonia. The Journal of experimental medicine. 2008;205(2):287-94.
153. Kawai T, Akira S. Toll-like receptors and their crosstalk with other innate receptors in infection and immunity. Immunity. 2011;34(5):637-50.
154. Kopp E, Medzhitov R. Recognition of microbial infection by Toll-like receptors. Current opinion in immunology. 2003;15(4):396-401.
155. Esen N, Kielian T. Toll-like receptors in brain abscess. Current topics in microbiology and immunology. 2009;336:41-61.
156. Kielian T. Toll-like receptors in central nervous system glial inflammation and homeostasis. Journal of neuroscience research. 2006;83(5):711-30.
157. Kielian T. Overview of toll-like receptors in the CNS. Current topics in microbiology and immunology. 2009;336:1-14.
158. Konat GW, Kielian T, Marriott I. The role of Toll-like receptors in CNS response to microbial challenge. Journal of neurochemistry. 2006;99(1):1-12.
159. Takeda K, Akira S. Toll-like receptors in innate immunity. International immunology. 2005;17(1):1-14.
160. Mullaly SC, Kubes P. The role of TLR2 in vivo following challenge with Staphylococcus aureus and prototypic ligands. Journal of immunology. 2006;177(11):8154-63.
161. Strunk T, Power Coombs MR, Currie AJ, Richmond P, Golenbock DT, Stoler-Barak L, Gallington LC, Otto M, Burgner D, Levy O. TLR2 mediates recognition of live Staphylococcus epidermidis and clearance of bacteremia. PloS one. 2010;5(4):e10111.
162. Takeuchi O, Hoshino K, Akira S. Cutting edge: TLR2-deficient and MyD88-deficient mice are highly susceptible to Staphylococcus aureus infection. Journal of immunology. 2000;165(10):5392-6.
163. Mohamed W, Domann E, Chakraborty T, Mannala G, Lips KS, Heiss C, Schnettler R, Alt V. TLR9 mediates S. aureus killing inside osteoblasts via induction of oxidative stress. BMC microbiology. 2016;16(1):230.
164. Parker D, Prince A. Staphylococcus aureus induces type I IFN signaling in dendritic cells via TLR9. Journal of immunology. 2012;189(8):4040-6.

165. Bose JL, Lehman MK, Fey PD, Bayles KW. Contribution of the Staphylococcus aureus Atl AM and GL murein hydrolase activities in cell division, autolysis, and biofilm formation. PloS one. 2012;7(7):e42244.
166. Houston P, Rowe SE, Pozzi C, Waters EM, O'Gara JP. Essential role for the major autolysin in the fibronectin-binding protein-mediated Staphylococcus aureus biofilm phenotype. Infection and immunity. 2011;79(3):1153-65.
167. Rice KC, Mann EE, Endres JL, Weiss EC, Cassat JE, Smeltzer MS, Bayles KW. The cidA murein hydrolase regulator contributes to DNA release and biofilm development in Staphylococcus aureus. Proceedings of the National Academy of Sciences of the United States of America. 2007;104(19):8113-8.
168. Mann EE, Rice KC, Boles BR, Endres JL, Ranjit D, Chandramohan L, Tsang LH, Smeltzer MS, Horswill AR, Bayles KW. Modulation of eDNA release and degradation affects Staphylococcus aureus biofilm maturation. PloS one. 2009;4(6):e5822.
169. Bernthal NM, Pribaz JR, Stavrakis AI, Billi F, Cho JS, Ramos RI, Francis KP, Iwakura Y, Miller LS. Protective role of IL-1beta against post-arthroplasty Staphylococcus aureus infection. Journal of orthopaedic research : official publication of the Orthopaedic Research Society. 2011;29(10):1621-6.
170. Goodyear CS, Silverman GJ. Death by a B cell superantigen: In vivo VH-targeted apoptotic supraclonal B cell deletion by a Staphylococcal Toxin. The Journal of experimental medicine. 2003;197(9):1125-39.
171. Inoshima I, Inoshima N, Wilke GA, Powers ME, Frank KM, Wang Y, Bubeck Wardenburg J. A Staphylococcus aureus pore-forming toxin subverts the activity of ADAM10 to cause lethal infection in mice. Nature medicine. 2011;17(10):1310-4.
172. Koziel J, Chmiest D, Bryzek D, Kmiecik K, Mizgalska D, Maciag-Gudowska A, Shaw LN, Potempa J. The Janus face of alpha-toxin: a potent mediator of cytoprotection in staphylococci-infected macrophages. Journal of innate immunity. 2015;7(2):187-98.
173. Spaulding AR, Salgado-Pabon W, Kohler PL, Horswill AR, Leung DY, Schlievert PM. Staphylococcal and streptococcal superantigen exotoxins. Clinical microbiology reviews. 2013;26(3):422-47.
174. DuMont AL, Yoong P, Day CJ, Alonzo F, 3rd, McDonald WH, Jennings MP, Torres VJ. Staphylococcus aureus LukAB cytotoxin kills human neutrophils by targeting the CD11b subunit of the integrin Mac-1. Proceedings of the National Academy of Sciences of the United States of America. 2013;110(26):10794-9.
175. DuMont AL, Yoong P, Surewaard BG, Benson MA, Nijland R, van Strijp JA, Torres VJ. Staphylococcus aureus elaborates leukocidin AB to mediate escape from within human neutrophils. Infection and immunity. 2013;81(5):1830-41.
176. Huang SS, Diekema DJ, Warren DK, Zuccotti G, Winokur PL, Tendolkar S, Boyken L, Datta R, Jones RM, Ward MA, Aubrey T, Onderdonk AB, Garcia C, Platt R. Strain-relatedness of methicillin-resistant Staphylococcus aureus isolates recovered from patients with repeated infection. Clinical infectious diseases : an official publication of the Infectious Diseases Society of America. 2008;46(8):1241-7.
177. Huang SS, Platt R. Risk of methicillin-resistant Staphylococcus aureus infection after previous infection or colonization. Clinical infectious diseases : an official publication of the Infectious Diseases Society of America. 2003;36(3):281-5.
178. O'Seaghdha M, van Schooten CJ, Kerrigan SW, Emsley J, Silverman GJ, Cox D, Lenting PJ, Foster TJ. Staphylococcus aureus protein A binding to von Willebrand factor A1 domain is mediated by conserved IgG binding regions. The FEBS journal. 2006;273(21):4831-41.

179. Romagnani S, Giudizi MG, del Prete G, Maggi E, Biagiotti R, Almerigogna F, Ricci M. Demonstration on protein A of two distinct immunoglobulin-binding sites and their role in the mitogenic activity of Staphylococcus aureus Cowan I on human B cells. Journal of immunology. 1982;129(2):596-602.
180. Forsgren A. Significance of protein a production by staphylococci. Infection and immunity. 1970;2(5):672-3.
181. Cerca N, Jefferson KK, Oliveira R, Pier GB, Azeredo J. Comparative antibody-mediated phagocytosis of Staphylococcus epidermidis cells grown in a biofilm or in the planktonic state. Infection and immunity. 2006;74(8):4849-55.
182. Prabhakara R, Harro JM, Leid JG, Keegan AD, Prior ML, Shirtliff ME. Suppression of the inflammatory immune response prevents the development of chronic biofilm infection due to methicillin-resistant Staphylococcus aureus. Infection and immunity. 2011;79(12):5010-8.
183. Lee LY, Hook M, Haviland D, Wetsel RA, Yonter EO, Syribeys P, Vernachio J, Brown EL. Inhibition of complement activation by a secreted Staphylococcus aureus protein. The Journal of infectious diseases. 2004;190(3):571-9.
184. Yeaman MR, Yount NY. Mechanisms of antimicrobial peptide action and resistance. Pharmacological reviews. 2003;55(1):27-55.
185. Lopez-Leban F, Kiran MD, Wolcott R, Balaban N. Molecular mechanisms of RIP, an effective inhibitor of chronic infections. The International journal of artificial organs. 2010;33(9):582-9.
186. Dean SN, Bishop BM, van Hoek ML. Natural and synthetic cathelicidin peptides with anti-microbial and anti-biofilm activity against Staphylococcus aureus. BMC microbiology. 2011;11:114.
187. Heim CE, Vidlak D, Scherr TD, Kozel JA, Holzapfel M, Muirhead DE, Kielian T. Myeloid-derived suppressor cells contribute to Staphylococcus aureus orthopedic biofilm infection. Journal of immunology. 2014;192(8):3778-92.
188. Hanke ML, Kielian T. Deciphering mechanisms of staphylococcal biofilm evasion of host immunity. Frontiers in cellular and infection microbiology. 2012;2:62.
189. Heim CE, Hanke ML, Kielian T. A mouse model of Staphylococcus catheter-associated biofilm infection. Methods in molecular biology. 2014;1106:183-91.
190. Danilin S, Merkel AR, Johnson JR, Johnson RW, Edwards JR, Sterling JA. Myeloid-derived suppressor cells expand during breast cancer progression and promote tumor-induced bone destruction. Oncoimmunology. 2012;1(9):1484-94.
191. Kumar V, Patel S, Tcyganov E, Gabrilovich DI. The Nature of Myeloid-Derived Suppressor Cells in the Tumor Microenvironment. Trends in immunology. 2016;37(3):208-20.
192. Ost M, Singh A, Peschel A, Mehling R, Rieber N, Hartl D. Myeloid-Derived Suppressor Cells in Bacterial Infections. Frontiers in cellular and infection microbiology. 2016;6:37.
193. OuYang LY, Wu XJ, Ye SB, Zhang RX, Li ZL, Liao W, Pan ZZ, Zheng LM, Zhang XS, Wang Z, Li Q, Ma G, Li J. Tumor-induced myeloid-derived suppressor cells promote tumor progression through oxidative metabolism in human colorectal cancer. Journal of translational medicine. 2015;13:47.
194. Zhang H, Huang Y, Wang S, Fu R, Guo C, Wang H, Zhao J, Gaskin F, Chen J, Yang N, Fu SM. Myeloid-derived suppressor cells contribute to bone erosion in collagen-induced arthritis by differentiating to osteoclasts. Journal of autoimmunity. 2015;65:82-9.
195. Zhang H, Li ZL, Ye SB, Ouyang LY, Chen YS, He J, Huang HQ, Zeng YX, Zhang XS, Li J. Myeloid-derived suppressor cells inhibit T cell proliferation in human extranodal NK/T cell lymphoma: a novel prognostic indicator. Cancer immunology, immunotherapy : CII. 2015;64(12):1587-99.

196. Shadyab AH, Crum-Cianflone NF. Methicillin-resistant Staphylococcus aureus (MRSA) infections among HIV-infected persons in the era of highly active antiretroviral therapy: a review of the literature. HIV medicine. 2012;13(6):319-32.
197. Spellberg B, Ibrahim AS, Yeaman MR, Lin L, Fu Y, Avanesian V, Bayer AS, Filler SG, Lipke P, Otoo H, Edwards JE, Jr. The antifungal vaccine derived from the recombinant N terminus of Als3p protects mice against the bacterium Staphylococcus aureus. Infection and immunity. 2008;76(10):4574-80.
198. Bohach GA, Fast DJ, Nelson RD, Schlievert PM. Staphylococcal and streptococcal pyrogenic toxins involved in toxic shock syndrome and related illnesses. Critical reviews in microbiology. 1990;17(4):251-72.
199. Stach CS, Herrera A, Schlievert PM. Staphylococcal superantigens interact with multiple host receptors to cause serious diseases. Immunologic research. 2014;59(1-3):177-81.
200. Llewelyn M, Cohen J. Superantigens: microbial agents that corrupt immunity. The Lancet Infectious diseases. 2002;2(3):156-62.
201. Llewelyn M, Sriskandan S, Terrazzini N, Cohen J, Altmann DM. The TCR Vbeta signature of bacterial superantigens spreads with stimulus strength. International immunology. 2006;18(10):1433-41.
202. Xu SX, McCormick JK. Staphylococcal superantigens in colonization and disease. Frontiers in cellular and infection microbiology. 2012;2:52.
203. Muehlstedt SG, Lyte M, Rodriguez JL. Increased IL-10 production and HLA-DR suppression in the lungs of injured patients precede the development of nosocomial pneumonia. Shock. 2002;17(6):443-50.
204. Krakauer T. Update on staphylococcal superantigen-induced signaling pathways and therapeutic interventions. Toxins (Basel). 2013;5(9):1629-54.
205. DaSilva L, Welcher BC, Ulrich RG, Aman MJ, David CS, Bavari S. Humanlike immune response of human leukocyte antigen-DR3 transgenic mice to staphylococcal enterotoxins: a novel model for superantigen vaccines. The Journal of infectious diseases. 2002;185(12):1754-60.
206. Bogoslowski A, Butcher EC, Kubes P. Neutrophils recruited through high endothelial venules of the lymph nodes via PNAd intercept disseminating Staphylococcus aureus. Proceedings of the National Academy of Sciences of the United States of America. 2018;115(10):2449-54.
207. Greenlee-Wacker MC, Rigby KM, Kobayashi SD, Porter AR, DeLeo FR, Nauseef WM. Phagocytosis of Staphylococcus aureus by human neutrophils prevents macrophage efferocytosis and induces programmed necrosis. Journal of immunology. 2014;192(10):4709-17.
208. Guerra FE, Borgogna TR, Patel DM, Sward EW, Voyich JM. Epic Immune Battles of History: Neutrophils vs. Staphylococcus aureus. Frontiers in cellular and infection microbiology. 2017;7:286.
209. Rigby KM, DeLeo FR. Neutrophils in innate host defense against Staphylococcus aureus infections. Seminars in immunopathology. 2012;34(2):237-59.
210. Olaru F, Jensen LE. Staphylococcus aureus stimulates neutrophil targeting chemokine expression in keratinocytes through an autocrine IL-1alpha signaling loop. The Journal of investigative dermatology. 2010;130(7):1866-76.
211. Standiford TJ, Arenberg DA, Danforth JM, Kunkel SL, VanOtteren GM, Strieter RM. Lipoteichoic acid induces secretion of interleukin-8 from human blood monocytes: a cellular and molecular analysis. Infection and immunity. 1994;62(1):119-25.

212. Yagdiran Y, Tallkvist J, Artursson K, Oskarsson A. Staphylococcus aureus and Lipopolysaccharide Modulate Gene Expressions of Drug Transporters in Mouse Mammary Epithelial Cells Correlation to Inflammatory Biomarkers. PloS one. 2016;11(9):e0161346.
213. Krakauer T. Interleukin-8 production by human monocytic cells in response to staphylococcal exotoxins is direct and independent of interleukin-1 and tumor necrosis factor-alpha. The Journal of infectious diseases. 1998;178(2):573-7.
214. Cassatella MA. The production of cytokines by polymorphonuclear neutrophils. Immunology today. 1995;16(1):21-6.
215. Witko-Sarsat V, Rieu P, Descamps-Latscha B, Lesavre P, Halbwachs-Mecarelli L. Neutrophils: molecules, functions and pathophysiological aspects. Laboratory investigation; a journal of technical methods and pathology. 2000;80(5):617-53.
216. Grosser MR, Weiss A, Shaw LN, Richardson AR. Regulatory Requirements for Staphylococcus aureus Nitric Oxide Resistance. Journal of bacteriology. 2016;198(15):2043-55.
217. Wickersham M, Wachtel S, Wong Fok Lung T, Soong G, Jacquet R, Richardson A, Parker D, Prince A. Metabolic Stress Drives Keratinocyte Defenses against Staphylococcus aureus Infection. Cell reports. 2017;18(11):2742-51.
218. Faurschou M, Borregaard N. Neutrophil granules and secretory vesicles in inflammation. Microbes and infection. 2003;5(14):1317-27.
219. Wilke GA, Bubeck Wardenburg J. Role of a disintegrin and metalloprotease 10 in Staphylococcus aureus alpha-hemolysin-mediated cellular injury. Proceedings of the National Academy of Sciences of the United States of America. 2010;107(30):13473-8.
220. de Haas CJ, Veldkamp KE, Peschel A, Weerkamp F, Van Wamel WJ, Heezius EC, Poppelier MJ, Van Kessel KP, van Strijp JA. Chemotaxis inhibitory protein of Staphylococcus aureus, a bacterial antiinflammatory agent. The Journal of experimental medicine. 2004;199(5):687-95.
221. Postma B, Poppelier MJ, van Galen JC, Prossnitz ER, van Strijp JA, de Haas CJ, van Kessel KP. Chemotaxis inhibitory protein of Staphylococcus aureus binds specifically to the C5a and formylated peptide receptor. Journal of immunology. 2004;172(11):6994-7001.
222. Wright AJ, Higginbottom A, Philippe D, Upadhyay A, Bagby S, Read RC, Monk PN, Partridge LJ. Characterisation of receptor binding by the chemotaxis inhibitory protein of Staphylococcus aureus and the effects of the host immune response. Molecular immunology. 2007;44(10):2507-17.
223. Chavakis T, Hussain M, Kanse SM, Peters G, Bretzel RG, Flock JI, Herrmann M, Preissner KT. Staphylococcus aureus extracellular adherence protein serves as anti-inflammatory factor by inhibiting the recruitment of host leukocytes. Nature medicine. 2002;8(7):687-93.
224. Haggar A, Ehrnfelt C, Holgersson J, Flock JI. The extracellular adherence protein from Staphylococcus aureus inhibits neutrophil binding to endothelial cells. Infection and immunity. 2004;72(10):6164-7.
225. Kobayashi SD, Braughton KR, Palazzolo-Ballance AM, Kennedy AD, Sampaio E, Kristosturyan E, Whitney AR, Sturdevant DE, Dorward DW, Holland SM, Kreiswirth BN, Musser JM, DeLeo FR. Rapid neutrophil destruction following phagocytosis of Staphylococcus aureus. Journal of innate immunity. 2010;2(6):560-75.
226. Heim CE, West SC, Ali H, Kielian T. Heterogeneity of Ly6G(+)Ly6C(+) myeloid-derived suppressor cell (MDSC) infiltrates during S. aureus biofilm infection. Infection and immunity. 2018.
227. De Veirman K, Van Valckenborgh E, Lahmar Q, Geeraerts X, De Bruyne E, Menu E, Van Riet I, Vanderkerken K, Van Ginderachter JA. Myeloid-derived suppressor cells as therapeutic target in hematological malignancies. Frontiers in oncology. 2014;4:349.

228. Dilek N, van Rompaey N, Le Moine A, Vanhove B. Myeloid-derived suppressor cells in transplantation. Current opinion in organ transplantation. 2010;15(6):765-8.
229. Gabrilovich DI, Nagaraj S. Myeloid-derived suppressor cells as regulators of the immune system. Nature reviews Immunology. 2009;9(3):162-74.
230. Skabytska Y, Wolbing F, Gunther C, Koberle M, Kaesler S, Chen KM, Guenova E, Demircioglu D, Kempf WE, Volz T, Rammensee HG, Schaller M, Rocken M, Gotz F, Biedermann T. Cutaneous innate immune sensing of Toll-like receptor 2-6 ligands suppresses T cell immunity by inducing myeloid-derived suppressor cells. Immunity. 2014;41(5):762-75.
231. Tebartz C, Horst SA, Sparwasser T, Huehn J, Beineke A, Peters G, Medina E. A major role for myeloid-derived suppressor cells and a minor role for regulatory T cells in immunosuppression during Staphylococcus aureus infection. Journal of immunology. 2015;194(3):1100-11.
232. Gabrilovich DI, Ostrand-Rosenberg S, Bronte V. Coordinated regulation of myeloid cells by tumours. Nature reviews Immunology. 2012;12(4):253-68.
233. Bronte V, Serafini P, Mazzoni A, Segal DM, Zanovello P. L-arginine metabolism in myeloid cells controls T-lymphocyte functions. Trends in immunology. 2003;24(6):302-6.
234. Kusmartsev S, Cheng F, Yu B, Nefedova Y, Sotomayor E, Lush R, Gabrilovich D. All-trans-retinoic acid eliminates immature myeloid cells from tumor-bearing mice and improves the effect of vaccination. Cancer research. 2003;63(15):4441-9.
235. Kusmartsev S, Gabrilovich DI. Inhibition of myeloid cell differentiation in cancer: the role of reactive oxygen species. Journal of leukocyte biology. 2003;74(2):186-96.
236. Kusmartsev S, Nefedova Y, Yoder D, Gabrilovich DI. Antigen-specific inhibition of CD8+ T cell response by immature myeloid cells in cancer is mediated by reactive oxygen species. Journal of immunology. 2004;172(2):989-99.
237. Youn JI, Collazo M, Shalova IN, Biswas SK, Gabrilovich DI. Characterization of the nature of granulocytic myeloid-derived suppressor cells in tumor-bearing mice. Journal of leukocyte biology. 2012;91(1):167-81.
238. Youn JI, Gabrilovich DI. The biology of myeloid-derived suppressor cells: the blessing and the curse of morphological and functional heterogeneity. European journal of immunology. 2010;40(11):2969-75.
239. Srivastava MK, Sinha P, Clements VK, Rodriguez P, Ostrand-Rosenberg S. Myeloid-derived suppressor cells inhibit T-cell activation by depleting cystine and cysteine. Cancer research. 2010;70(1):68-77.
240. McInnes IB, Leung B, Wei XQ, Gemmell CC, Liew FY. Septic arthritis following Staphylococcus aureus infection in mice lacking inducible nitric oxide synthase. Journal of immunology. 1998;160(1):308-15.
241. Yamada KJ, Heim CE, Aldrich AL, Gries CM, Staudacher AG, Kielian T. Arginase-1 expression in myeloid cells regulates S. aureus planktonic but not biofilm infection. Infection and immunity. 2018.
242. Hirayama D, Iida T, Nakase H. The Phagocytic Function of Macrophage-Enforcing Innate Immunity and Tissue Homeostasis. International journal of molecular sciences. 2017;19(1).
243. Ruiz-Alcaraz AJ, Carmona-Martinez V, Tristan-Manzano M, Machado-Linde F, Sanchez-Ferrer ML, Garcia-Penarrubia P, Martinez-Esparza M. Characterization of human peritoneal monocyte/macrophage subsets in homeostasis: Phenotype, GATA6, phagocytic/oxidative activities and cytokines expression. Scientific reports. 2018;8(1):12794.
244. Jantsch J, Binger KJ, Muller DN, Titze J. Macrophages in homeostatic immune function. Frontiers in physiology. 2014;5:146.

245. Labonte AC, Tosello-Trampont AC, Hahn YS. The role of macrophage polarization in infectious and inflammatory diseases. Molecules and cells. 2014;37(4):275-85.
246. Silva MF, Napimoga MH, Rodrigues DB, Pereira SA, Silva CL. Phenotypic and functional characterization of pulmonary macrophages subpopulations after intratracheal injection of Paracoccidioides brasiliensis cell wall components. Immunobiology. 2011;216(7):821-31.
247. Silva MT. Neutrophils and macrophages work in concert as inducers and effectors of adaptive immunity against extracellular and intracellular microbial pathogens. Journal of leukocyte biology. 2010;87(5):805-13.
248. Silva RC, Landgraf MA, Hiyane MI, Pacheco-Silva A, Camara NO, Landgraf RG. Leukotrienes produced in allergic lung inflammation activate alveolar macrophages. Cellular physiology and biochemistry : international journal of experimental cellular physiology, biochemistry, and pharmacology. 2010;26(3):319-26.
249. Sica A, Mantovani A. Macrophage plasticity and polarization: in vivo veritas. The Journal of clinical investigation. 2012;122(3):787-95.
250. Biswas SK, Mantovani A. Macrophage plasticity and interaction with lymphocyte subsets: cancer as a paradigm. Nature immunology. 2010;11(10):889-96.
251. Jablonski KA, Amici SA, Webb LM, Ruiz-Rosado Jde D, Popovich PG, Partida-Sanchez S, Guerau-de-Arellano M. Novel Markers to Delineate Murine M1 and M2 Macrophages. PloS one. 2015;10(12):e0145342.
252. Mosser DM, Edwards JP. Exploring the full spectrum of macrophage activation. Nature reviews Immunology. 2008;8(12):958-69.
253. Laoui D, Van Overmeire E, De Baetselier P, Van Ginderachter JA, Raes G. Functional Relationship between Tumor-Associated Macrophages and Macrophage Colony-Stimulating Factor as Contributors to Cancer Progression. Frontiers in immunology. 2014;5:489.
254. Martinez FO, Gordon S. The M1 and M2 paradigm of macrophage activation: time for reassessment. F1000prime reports. 2014;6:13.
255. Loftus RM, Finlay DK. Immunometabolism: Cellular Metabolism Turns Immune Regulator. The Journal of biological chemistry. 2016;291(1):1-10.
256. O'Neill LA, Pearce EJ. Immunometabolism governs dendritic cell and macrophage function. The Journal of experimental medicine. 2016;213(1):15-23.
257. Torres A, Makowski L, Wellen KE. Immunometabolism: Metabolism fine-tunes macrophage activation. eLife. 2016;5.
258. Hsu PP, Sabatini DM. Cancer cell metabolism: Warburg and beyond. Cell. 2008;134(5):703-7.
259. Warburg O. On the origin of cancer cells. Science. 1956;123(3191):309-14.
260. Geeraerts X, Bolli E, Fendt SM, Van Ginderachter JA. Macrophage Metabolism As Therapeutic Target for Cancer, Atherosclerosis, and Obesity. Frontiers in immunology. 2017;8:289.
261. Wilde AD, Snyder DJ, Putnam NE, Valentino MD, Hammer ND, Lonergan ZR, Hinger SA, Aysanoa EE, Blanchard C, Dunman PM, Wasserman GA, Chen J, Shopsin B, Gilmore MS, Skaar EP, Cassat JE. Bacterial Hypoxic Responses Revealed as Critical Determinants of the Host-Pathogen Outcome by TnSeq Analysis of Staphylococcus aureus Invasive Infection. PLoS pathogens. 2015;11(12):e1005341.
262. Hirayama A, Kami K, Sugimoto M, Sugawara M, Toki N, Onozuka H, Kinoshita T, Saito N, Ochiai A, Tomita M, Esumi H, Soga T. Quantitative metabolome profiling of colon and stomach cancer microenvironment by capillary electrophoresis time-of-flight mass spectrometry. Cancer research. 2009;69(11):4918-25.

263. Friedman DB, Stauff DL, Pishchany G, Whitwell CW, Torres VJ, Skaar EP. Staphylococcus aureus redirects central metabolism to increase iron availability. PLoS pathogens. 2006;2(8):e87.
264. Grayczyk JP, Harvey CJ, Laczkovich I, Alonzo F, 3rd. A Lipoylated Metabolic Protein Released by Staphylococcus aureus Suppresses Macrophage Activation. Cell host & microbe. 2017;22(5):678-87 e9.
265. Johnson CH, Dejea CM, Edler D, Hoang LT, Santidrian AF, Felding BH, Ivanisevic J, Cho K, Wick EC, Hechenbleikner EM, Uritboonthai W, Goetz L, Casero RA, Jr., Pardoll DM, White JR, Patti GJ, Sears CL, Siuzdak G. Metabolism links bacterial biofilms and colon carcinogenesis. Cell metabolism. 2015;21(6):891-7.
266. Jin Z, Wei W, Yang M, Du Y, Wan Y. Mitochondrial complex I activity suppresses inflammation and enhances bone resorption by shifting macrophage-osteoclast polarization. Cell metabolism. 2014;20(3):483-98.
267. Kruse SE, Watt WC, Marcinek DJ, Kapur RP, Schenkman KA, Palmiter RD. Mice with mitochondrial complex I deficiency develop a fatal encephalomyopathy. Cell metabolism. 2008;7(4):312-20.
268. El Kasmi KC, Qualls JE, Pesce JT, Smith AM, Thompson RW, Henao-Tamayo M, Basaraba RJ, Konig T, Schleicher U, Koo MS, Kaplan G, Fitzgerald KA, Tuomanen EI, Orme IM, Kanneganti TD, Bogdan C, Wynn TA, Murray PJ. Toll-like receptor-induced arginase 1 in macrophages thwarts effective immunity against intracellular pathogens. Nature immunology. 2008;9(12):1399-406.
269. Clausen BE, Burkhardt C, Reith W, Renkawitz R, Forster I. Conditional gene targeting in macrophages and granulocytes using LysMcre mice. Transgenic research. 1999;8(4):265-77.
270. Murray PJ, Wynn TA. Obstacles and opportunities for understanding macrophage polarization. Journal of leukocyte biology. 2011;89(4):557-63.
271. Pang YY, Schwartz J, Thoendel M, Ackermann LW, Horswill AR, Nauseef WM. agr-Dependent interactions of Staphylococcus aureus USA300 with human polymorphonuclear neutrophils. Journal of innate immunity. 2010;2(6):546-59.
272. Rogers GW, Brand MD, Petrosyan S, Ashok D, Elorza AA, Ferrick DA, Murphy AN. High throughput microplate respiratory measurements using minimal quantities of isolated mitochondria. PLoS One. 2011;6(7):e21746.
273. Tan B, Xiao H, Li F, Zeng L, Yin Y. The profiles of mitochondrial respiration and glycolysis using extracellular flux analysis in porcine enterocyte IPEC-J2. Anim Nutr. 2015;1(3):239-43.
274. Desale SS, Soni KS, Romanova S, Cohen SM, Bronich TK. Targeted delivery of platinum-taxane combination therapy in ovarian cancer. Journal of controlled release : official journal of the Controlled Release Society. 2015;220(Pt B):651-9.
275. Kim JO, Oberoi HS, Desale S, Kabanov AV, Bronich TK. Polypeptide nanogels with hydrophobic moieties in the cross-linked ionic cores: synthesis, characterization and implications for anticancer drug delivery. Journal of drug targeting. 2013;21(10):981-93.
276. Zu Y, Zhao Q, Zhao X, Zu S, Meng L. Process optimization for the preparation of oligomycin-loaded folate-conjugated chitosan nanoparticles as a tumor-targeted drug delivery system using a two-level factorial design method. International journal of nanomedicine. 2011;6:3429-41.
277. Gunda V, Yu F, Singh PK. Validation of Metabolic Alterations in Microscale Cell Culture Lysates Using Hydrophilic Interaction Liquid Chromatography (HILIC)-Tandem Mass Spectrometry-Based Metabolomics. PloS one. 2016;11(4):e0154416.
278. Conlon BP, Rowe SE, Gandt AB, Nuxoll AS, Donegan NP, Zalis EA, Clair G, Adkins JN, Cheung AL, Lewis K. Persister formation in Staphylococcus aureus is associated with ATP depletion. Nature microbiology. 2016;1:16051.

279. Tavakoli S, Zamora D, Ullevig S, Asmis R. Bioenergetic profiles diverge during macrophage polarization: implications for the interpretation of 18F-FDG PET imaging of atherosclerosis. Journal of nuclear medicine : official publication, Society of Nuclear Medicine. 2013;54(9):1661-7.
280. Galvan-Pena S, O'Neill LA. Metabolic reprograming in macrophage polarization. Frontiers in immunology. 2014;5:420.
281. Odegaard JI, Chawla A. Alternative macrophage activation and metabolism. Annual review of pathology. 2011;6:275-97.
282. Feingold KR, Shigenaga JK, Cross AS, Moser A, Grunfeld C. Angiopoietin like protein 4 expression is decreased in activated macrophages. Biochemical and biophysical research communications. 2012;421(3):612-5.
283. Feingold KR, Shigenaga JK, Kazemi MR, McDonald CM, Patzek SM, Cross AS, Moser A, Grunfeld C. Mechanisms of triglyceride accumulation in activated macrophages. Journal of leukocyte biology. 2012;92(4):829-39.
284. Izquierdo E, Cuevas VD, Fernandez-Arroyo S, Riera-Borrull M, Orta-Zavalza E, Joven J, Rial E, Corbi AL, Escribese MM. Reshaping of Human Macrophage Polarization through Modulation of Glucose Catabolic Pathways. Journal of immunology. 2015;195(5):2442-51.
285. Jain S, Amiji M. Tuftsin-modified alginate nanoparticles as a noncondensing macrophage-targeted DNA delivery system. Biomacromolecules. 2012;13(4):1074-85.
286. Jain S, Tran TH, Amiji M. Macrophage repolarization with targeted alginate nanoparticles containing IL-10 plasmid DNA for the treatment of experimental arthritis. Biomaterials. 2015;61:162-77.
287. Zheng L, Sun X, Zhu X, Lv F, Zhong Z, Zhang F, Guo W, Cao W, Yang L, Tian Y. Apoptosis of THP-1 derived macrophages induced by sonodynamic therapy using a new sonosensitizer hydroxyl acetylated curcumin. PloS one. 2014;9(3):e93133.
288. Yamada K, Saito M, Matsuoka H, Inagaki N. A real-time method of imaging glucose uptake in single, living mammalian cells. Nat Protoc. 2007;2(3):753-62.
289. O'Neill LA. A broken krebs cycle in macrophages. Immunity. 2015;42(3):393-4.
290. O'Neill LA, Kishton RJ, Rathmell J. A guide to immunometabolism for immunologists. Nature reviews Immunology. 2016;16(9):553-65.
291. Hao W, Chang CP, Tsao CC, Xu J. Oligomycin-induced bioenergetic adaptation in cancer cells with heterogeneous bioenergetic organization. The Journal of biological chemistry. 2010;285(17):12647-54.
292. Kramar R, Hohenegger M, Srour AN, Khanakah G. Oligomycin toxicity in intact rats. Agents and actions. 1984;15(5-6):660-3.
293. Vaamonde-Garcia C, Loureiro J, Valcarcel-Ares MN, Riveiro-Naveira RR, Ramil-Gomez O, Hermida-Carballo L, Centeno A, Meijide-Failde R, Blanco FJ, Lopez-Armada MJ. The mitochondrial inhibitor oligomycin induces an inflammatory response in the rat knee joint. BMC musculoskeletal disorders. 2017;18(1):254.
294. Dutta T, Garg M, Jain NK. Targeting of efavirenz loaded tuftsin conjugated poly(propyleneimine) dendrimers to HIV infected macrophages in vitro. European journal of pharmaceutical sciences : official journal of the European Federation for Pharmaceutical Sciences. 2008;34(2-3):181-9.
295. Talekar M, Tran TH, Amiji M. Translational Nano-Medicines: Targeted Therapeutic Delivery for Cancer and Inflammatory Diseases. The AAPS journal. 2015;17(4):813-27.
296. Lobritz MA, Belenky P, Porter CB, Gutierrez A, Yang JH, Schwarz EG, Dwyer DJ, Khalil AS, Collins JJ. Antibiotic efficacy is linked to bacterial cellular respiration. Proceedings of the National Academy of Sciences of the United States of America. 2015;112(27):8173-80.

297. Vestergaard M, Nohr-Meldgaard K, Bojer MS, Krogsgard Nielsen C, Meyer RL, Slavetinsky C, Peschel A, Ingmer H. Inhibition of the ATP Synthase Eliminates the Intrinsic Resistance of Staphylococcus aureus towards Polymyxins. mBio. 2017;8(5).
298. Dietl K, Renner K, Dettmer K, Timischl B, Eberhart K, Dorn C, Hellerbrand C, Kastenberger M, Kunz-Schughart LA, Oefner PJ, Andreesen R, Gottfried E, Kreutz MP. Lactic acid and acidification inhibit TNF secretion and glycolysis of human monocytes. Journal of immunology. 2010;184(3):1200-9.
299. Sherer TB, Betarbet R, Testa CM, Seo BB, Richardson JR, Kim JH, Miller GW, Yagi T, Matsuno-Yagi A, Greenamyre JT. Mechanism of toxicity in rotenone models of Parkinson's disease. The Journal of neuroscience : the official journal of the Society for Neuroscience. 2003;23(34):10756-64.
300. Sherer TB, Kim JH, Betarbet R, Greenamyre JT. Subcutaneous rotenone exposure causes highly selective dopaminergic degeneration and alpha-synuclein aggregation. Experimental neurology. 2003;179(1):9-16.
301. Yamagishi SI, Edelstein D, Du XL, Kaneda Y, Guzman M, Brownlee M. Leptin induces mitochondrial superoxide production and monocyte chemoattractant protein-1 expression in aortic endothelial cells by increasing fatty acid oxidation via protein kinase A. The Journal of biological chemistry. 2001;276(27):25096-100.
302. Bronte V, Brandau S, Chen SH, Colombo MP, Frey AB, Greten TF, Mandruzzato S, Murray PJ, Ochoa A, Ostrand-Rosenberg S, Rodriguez PC, Sica A, Umansky V, Vonderheide RH, Gabrilovich DI. Recommendations for myeloid-derived suppressor cell nomenclature and characterization standards. Nature communications. 2016;7:12150.
303. Schwartz J, Leidal KG, Femling JK, Weiss JP, Nauseef WM. Neutrophil bleaching of GFP-expressing staphylococci: probing the intraphagosomal fate of individual bacteria. Journal of immunology. 2009;183(4):2632-41.
304. Yoon BR, Oh YJ, Kang SW, Lee EB, Lee WW. Role of SLC7A5 in Metabolic Reprogramming of Human Monocyte/Macrophage Immune Responses. Frontiers in immunology. 2018;9:53.
305. Infantino V, Castegna A, Iacobazzi F, Spera I, Scala I, Andria G, Iacobazzi V. Impairment of methyl cycle affects mitochondrial methyl availability and glutathione level in Down's syndrome. Molecular genetics and metabolism. 2011;102(3):378-82.
306. Phan AT, Goldrath AW, Glass CK. Metabolic and Epigenetic Coordination of T Cell and Macrophage Immunity. Immunity. 2017;46(5):714-29.
307. Jha AK, Huang SC, Sergushichev A, Lampropoulou V, Ivanova Y, Loginicheva E, Chmielewski K, Stewart KM, Ashall J, Everts B, Pearce EJ, Driggers EM, Artyomov MN. Network integration of parallel metabolic and transcriptional data reveals metabolic modules that regulate macrophage polarization. Immunity. 2015;42(3):419-30.
308. Cordes T, Michelucci A, Hiller K. Itaconic Acid: The Surprising Role of an Industrial Compound as a Mammalian Antimicrobial Metabolite. Annual review of nutrition. 2015;35:451-73.
309. Cordes T, Wallace M, Michelucci A, Divakaruni AS, Sapcariu SC, Sousa C, Koseki H, Cabrales P, Murphy AN, Hiller K, Metallo CM. Immunoresponsive Gene 1 and Itaconate Inhibit Succinate Dehydrogenase to Modulate Intracellular Succinate Levels. The Journal of biological chemistry. 2016;291(27):14274-84.
310. Intlekofer AM, Dematteo RG, Venneti S, Finley LW, Lu C, Judkins AR, Rustenburg AS, Grinaway PB, Chodera JD, Cross JR, Thompson CB. Hypoxia Induces Production of L-2-Hydroxyglutarate. Cell metabolism. 2015;22(2):304-11.

311. Orlowsky EW, Stabler TV, Montell E, Verges J, Kraus VB. Monosodium urate crystal induced macrophage inflammation is attenuated by chondroitin sulphate: pre-clinical model for gout prophylaxis? BMC musculoskeletal disorders. 2014;15:318.
312. Shi Y, Evans JE, Rock KL. Molecular identification of a danger signal that alerts the immune system to dying cells. Nature. 2003;425(6957):516-21.
313. Fei F, Lee KM, McCarry BE, Bowdish DM. Age-associated metabolic dysregulation in bone marrow-derived macrophages stimulated with lipopolysaccharide. Scientific reports. 2016;6:22637.
314. Rattigan KM, Pountain AW, Regnault C, Achcar F, Vincent IM, Goodyear CS, Barrett MP. Metabolomic profiling of macrophages determines the discrete metabolomic signature and metabolomic interactome triggered by polarising immune stimuli. PloS one. 2018;13(3):e0194126.
315. Nahrendorf M, Swirski FK. Abandoning M1/M2 for a Network Model of Macrophage Function. Circulation research. 2016;119(3):414-7.
316. Jastroch M, Divakaruni AS, Mookerjee S, Treberg JR, Brand MD. Mitochondrial proton and electron leaks. Essays in biochemistry. 2010;47:53-67.
317. Dobashi K, Aihara M, Araki T, Shimizu Y, Utsugi M, Iizuka K, Murata Y, Hamuro J, Nakazawa T, Mori M. Regulation of LPS induced IL-12 production by IFN-gamma and IL-4 through intracellular glutathione status in human alveolar macrophages. Clinical and experimental immunology. 2001;124(2):290-6.
318. Mak TW, Grusdat M, Duncan GS, Dostert C, Nonnenmacher Y, Cox M, Binsfeld C, Hao Z, Brustle A, Itsumi M, Jager C, Chen Y, Pinkenburg O, Camara B, Ollert M, Bindslev-Jensen C, Vasiliou V, Gorrini C, Lang PA, Lohoff M, Harris IS, Hiller K, Brenner D. Glutathione Primes T Cell Metabolism for Inflammation. Immunity. 2017;46(4):675-89.
319. Rovito HA, Oblong JE. Nicotinamide preferentially protects glycolysis in dermal fibroblasts under oxidative stress conditions. The British journal of dermatology. 2013;169 Suppl 2:15-24.
320. R. J. Walls, S. J. Roche, A. O'Rourke, McCabe JP. Surgical site infection with methicillinresistant Staphylococcus aureus after primary total hip replacement. The Bone and Joint Journal. 2008;90-B(3):292-8.
321. Self WH, Wunderink RG, Williams DJ, Zhu Y, Anderson EJ, Balk RA, Fakhran SS, Chappell JD, Casimir G, Courtney DM, Trabue C, Waterer GW, Bramley A, Magill S, Jain S, Edwards KM, Grijalva CG. Staphylococcus aureus Community-acquired Pneumonia: Prevalence, Clinical Characteristics, and Outcomes. Clinical infectious diseases : an official publication of the Infectious Diseases Society of America. 2016;63(3):300-9.
322. Munder M. Arginase: an emerging key player in the mammalian immune system. British journal of pharmacology. 2009;158(3):638-51.
323. Makarenkova VP, Bansal V, Matta BM, Perez LA, Ochoa JB. CD11b+/Gr-1+ myeloid suppressor cells cause T cell dysfunction after traumatic stress. Journal of immunology. 2006;176(4):2085-94.
324. Rodriguez PC, Quiceno DG, Ochoa AC. L-arginine availability regulates T-lymphocyte cell-cycle progression. Blood. 2007;109(4):1568-73.
325. Rodriguez PC, Zea AH, DeSalvo J, Culotta KS, Zabaleta J, Quiceno DG, Ochoa JB, Ochoa AC. L-arginine consumption by macrophages modulates the expression of CD3 zeta chain in T lymphocytes. Journal of immunology. 2003;171(3):1232-9.
326. Zhu X, Pribis JP, Rodriguez PC, Morris SM, Jr., Vodovotz Y, Billiar TR, Ochoa JB. The central role of arginine catabolism in T-cell dysfunction and increased susceptibility to infection after physical injury. Annals of surgery. 2014;259(1):171-8.

327. Bronte V, Serafini P, De Santo C, Marigo I, Tosello V, Mazzoni A, Segal DM, Staib C, Lowel M, Sutter G, Colombo MP, Zanovello P. IL-4-induced arginase 1 suppresses alloreactive T cells in tumor-bearing mice. Journal of immunology. 2003;170(1):270-8.
328. Modolell M, Choi BS, Ryan RO, Hancock M, Titus RG, Abebe T, Hailu A, Muller I, Rogers ME, Bangham CR, Munder M, Kropf P. Local suppression of T cell responses by arginase-induced L-arginine depletion in nonhealing leishmaniasis. PLoS neglected tropical diseases. 2009;3(7):e480.
329. Rodriguez PC, Quiceno DG, Zabaleta J, Ortiz B, Zea AH, Piazuelo MB, Delgado A, Correa P, Brayer J, Sotomayor EM, Antonia S, Ochoa JB, Ochoa AC. Arginase I production in the tumor microenvironment by mature myeloid cells inhibits T-cell receptor expression and antigen-specific T-cell responses. Cancer research. 2004;64(16):5839-49.
330. Wijnands KA, Hoeksema MA, Meesters DM, van den Akker NM, Molin DG, Briede JJ, Ghosh M, Kohler SE, van Zandvoort MA, de Winther MP, Buurman WA, Lamers WH, Poeze M. Arginase-1 deficiency regulates arginine concentrations and NOS2-mediated NO production during endotoxemia. PloS one. 2014;9(1):e86135.
331. Gaur U, Roberts SC, Dalvi RP, Corraliza I, Ullman B, Wilson ME. An effect of parasite-encoded arginase on the outcome of murine cutaneous leishmaniasis. Journal of immunology. 2007;179(12):8446-53.
332. Maarsingh H, Leusink J, Bos IS, Zaagsma J, Meurs H. Arginase strongly impairs neuronal nitric oxide-mediated airway smooth muscle relaxation in allergic asthma. Respiratory research. 2006;7:6.
333. Meurs H, McKay S, Maarsingh H, Hamer MA, Macic L, Molendijk N, Zaagsma J. Increased arginase activity underlies allergen-induced deficiency of cNOS-derived nitric oxide and airway hyperresponsiveness. British journal of pharmacology. 2002;136(3):391-8.
334. Zabaleta J, McGee DJ, Zea AH, Hernandez CP, Rodriguez PC, Sierra RA, Correa P, Ochoa AC. Helicobacter pylori arginase inhibits T cell proliferation and reduces the expression of the TCR zeta-chain (CD3zeta). Journal of immunology. 2004;173(1):586-93.
335. Bian Z, Abdelaal AM, Shi L, Liang H, Xiong L, Kidder K, Venkataramani M, Culpepper C, Zen K, Liu Y. Arginase-1 is neither constitutively expressed in nor required for myeloid-derived suppressor cell (MDSC)-mediated inhibition of T cell proliferation. European journal of immunology. 2018.
336. Deshane J, Zmijewski JW, Luther R, Gaggar A, Deshane R, Lai JF, Xu X, Spell M, Estell K, Weaver CT, Abraham E, Schwiebert LM, Chaplin DD. Free radical-producing myeloid-derived regulatory cells: potent activators and suppressors of lung inflammation and airway hyperresponsiveness. Mucosal immunology. 2011;4(5):503-18.
337. Kan MJ, Lee JE, Wilson JG, Everhart AL, Brown CM, Hoofnagle AN, Jansen M, Vitek MP, Gunn MD, Colton CA. Arginine deprivation and immune suppression in a mouse model of Alzheimer's disease. The Journal of neuroscience : the official journal of the Society for Neuroscience. 2015;35(15):5969-82.
338. Knippenberg S, Brumshagen C, Aschenbrenner F, Welte T, Maus UA. Arginase 1 activity worsens lung-protective immunity against Streptococcus pneumoniae infection. European journal of immunology. 2015;45(6):1716-26.
339. Kisanuki YY, Hammer RE, Miyazaki J, Williams SC, Richardson JA, Yanagisawa M. Tie2-Cre transgenic mice: a new model for endothelial cell-lineage analysis in vivo. Developmental biology. 2001;230(2):230-42.
340. Fletcher M, Ramirez ME, Sierra RA, Raber P, Thevenot P, Al-Khami AA, Sanchez-Pino D, Hernandez C, Wyczechowska DD, Ochoa AC, Rodriguez PC. l-Arginine depletion blunts antitumor

T-cell responses by inducing myeloid-derived suppressor cells. Cancer research. 2015;75(2):275-83.
341. Choi S, Park C, Ahn M, Lee JH, Shin T. Immunohistochemical study of arginase 1 and 2 in various tissues of rats. Acta histochemica. 2012;114(5):487-94.
342. Grant SK, Green BG, Stiffey-Wilusz J, Durette PL, Shah SK, Kozarich JW. Structural requirements for human inducible nitric oxide synthase substrates and substrate analogue inhibitors. Biochemistry. 1998;37(12):4174-80.
343. Sun K, Yajjala VK, Bauer C, Talmon GA, Fischer KJ, Kielian T, Metzger DW. Nox2-derived oxidative stress results in inefficacy of antibiotics against post-influenza S. aureus pneumonia. The Journal of experimental medicine. 2016;213(9):1851-64.
344. Nuxoll AS, Halouska SM, Sadykov MR, Hanke ML, Bayles KW, Kielian T, Powers R, Fey PD. CcpA regulates arginine biosynthesis in Staphylococcus aureus through repression of proline catabolism. PLoS pathogens. 2012;8(11):e1003033.
345. Zheng B, Zhang Z, Black CM, de Crombrugghe B, Denton CP. Ligand-dependent genetic recombination in fibroblasts : a potentially powerful technique for investigating gene function in fibrosis. The American journal of pathology. 2002;160(5):1609-17.
346. de Haas R, Russel FG, Smeitink JA. Gait analysis in a mouse model resembling Leigh disease. Behavioural brain research. 2016;296:191-8.
347. Quintana A, Zanella S, Koch H, Kruse SE, Lee D, Ramirez JM, Palmiter RD. Fatal breathing dysfunction in a mouse model of Leigh syndrome. The Journal of clinical investigation. 2012;122(7):2359-68.
348. Karamanlidis G, Lee CF, Garcia-Menendez L, Kolwicz SC, Jr., Suthammarak W, Gong G, Sedensky MM, Morgan PG, Wang W, Tian R. Mitochondrial complex I deficiency increases protein acetylation and accelerates heart failure. Cell metabolism. 2013;18(2):239-50.
349. Otto M. Staphylococcal infections: mechanisms of biofilm maturation and detachment as critical determinants of pathogenicity. Annual review of medicine. 2013;64:175-88.
350. Castleman MJ, Pokhrel S, Triplett KD, Kusewitt DF, Elmore BO, Joyner JA, Femling JK, Sharma G, Hathaway HJ, Prossnitz ER, Hall PR. Innate Sex Bias of Staphylococcus aureus Skin Infection Is Driven by alpha-Hemolysin. Journal of immunology. 2018;200(2):657-68.
351. Cai TT, Ye SB, Liu YN, He J, Chen QY, Mai HQ, Zhang CX, Cui J, Zhang XS, Busson P, Zeng YX, Li J. LMP1-mediated glycolysis induces myeloid-derived suppressor cell expansion in nasopharyngeal carcinoma. PLoS pathogens. 2017;13(7):e1006503.
352. Hamanaka RB, Glasauer A, Hoover P, Yang S, Blatt H, Mullen AR, Getsios S, Gottardi CJ, DeBerardinis RJ, Lavker RM, Chandel NS. Mitochondrial reactive oxygen species promote epidermal differentiation and hair follicle development. Science signaling. 2013;6(261):ra8.
353. Ip WKE, Hoshi N, Shouval DS, Snapper S, Medzhitov R. Anti-inflammatory effect of IL-10 mediated by metabolic reprogramming of macrophages. Science. 2017;356(6337):513-9.
354. Timmermans K, Kox M, Vaneker M, van den Berg M, John A, van Laarhoven A, van der Hoeven H, Scheffer GJ, Pickkers P. Plasma levels of danger-associated molecular patterns are associated with immune suppression in trauma patients. Intensive care medicine. 2016;42(4):551-61.
355. Cao F, Zhou W, Liu G, Xia T, Liu M, Mi B, Liu Y. Staphylococcus aureus peptidoglycan promotes osteoclastogenesis via TLR2-mediated activation of the NF-kappaB/NFATc1 signaling pathway. American journal of translational research. 2017;9(11):5022-30.
356. Lau YS, Wang W, Sabokbar A, Simpson H, Nair S, Henderson B, Berendt A, Athanasou NA. Staphylococcus aureus capsular material promotes osteoclast formation. Injury. 2006;37 Suppl 2:S41-8.

357. Verdrengh M, Bokarewa M, Ohlsson C, Stolina M, Tarkowski A. RANKL-targeted therapy inhibits bone resorption in experimental Staphylococcus aureus-induced arthritis. Bone. 2010;46(3):752-8.
358. Indo Y, Takeshita S, Ishii KA, Hoshii T, Aburatani H, Hirao A, Ikeda K. Metabolic regulation of osteoclast differentiation and function. Journal of bone and mineral research : the official journal of the American Society for Bone and Mineral Research. 2013;28(11):2392-9.
359. Kim JM, Jeong D, Kang HK, Jung SY, Kang SS, Min BM. Osteoclast precursors display dynamic metabolic shifts toward accelerated glucose metabolism at an early stage of RANKL-stimulated osteoclast differentiation. Cellular physiology and biochemistry : international journal of experimental cellular physiology, biochemistry, and pharmacology. 2007;20(6):935-46.
360. Lemma S, Sboarina M, Porporato PE, Zini N, Sonveaux P, Di Pompo G, Baldini N, Avnet S. Energy metabolism in osteoclast formation and activity. The international journal of biochemistry & cell biology. 2016;79:168-80.